Conditional Moment Closures For Turbulent Reacting Flows

Robert Michael Woolley

Submitted in accordance with the requirements for the degree of Doctor of Philosophy

The University of Leeds
Department of Chemical Engineering

Submitted July 2003

Acknowledgements

A number of people have given me a great deal of support and advice throughout the course of this work, and it is the greatest of pleasures to have the opportunity for acknowledgement of such in these pages.

I am greatly indebted for the efforts, advice, and patience of my supervisor Dr. Michael Fairweather, whose enthusiasm for his work has perhaps carried me at times when mine has waned. I would also care to thank Professor Robert Bilger, Dr. Andreas Kronenburg, and Dr. Cecile Devaud for a number of informative discussions over my period of study.

I would care to express a great gratitude to my parents for standing beside me over these long years. Thanks must go to my Father for late-night deliberations, and to my Mother whose tireless support, patience, and words of wisdom made all my achievements possible. For her tolerance and rosy outlook on life I would also like to show my appreciation to Madeleine, my future wife.

Thanks to the EPSRC must be given also for the funding of the project through a quota award.

Finally, I would care to dedicate this thesis to those who are loved and much thought of, but unfortunately not here to see its completion. Their words I still heed every day, and make me the man that I am.

Abstract

Mathematical modelling of the turbulent combustion process is becoming increasingly applied in calculations to assist in the design and analysis of practical combustion devices for efficiency-improvement and emission reduction. The current requirement to accurately predict pollutant emissions in many applications has increased the need for linking turbulent flow calculations and finite-rate chemistry effects in a rigorous way. Several methodologies are available for modelling such interactions, including the transported probability density function (PDF) approach and the conditional moment closure (CMC) method.

Although in the early stages of its development, the CMC method has been shown to be a promising technique for predicting a wide range of practical problems. These include both premixed and non-premixed combustion, relatively slow chemistry effects, and ignition and extinction phenomena. This study concerns the CMC approach, and addresses the application of a number of models to a wide range of flows displaying varied compositions and geometries, including hydrogen and methane, and rim-stable and lifted jets. The impact of the choice of chemistry mechanism is considered for all the flows, and a higher-order CMC chemistry closure is investigated for the hydrogen flames. Analysis is made as to the ability of a parabolic CMC model to predict such flows, and the performance of the sub-model interactions is also reported on. The method of

coupling the turbulent mixing field and the chemical kinetics is also investigated, and the effects of Reynolds stress and $k-\varepsilon$ turbulence closures upon subsequent CMC calculations are compared in all the flows considered.

Overall, the results shown and conclusions drawn are very promising with respect to the possible future development of CMC. Requirements essential for this step forward of CMC methodologies for use in modelling practical geometries are specified, and an outline for the continuation of these studies is presented.

Contents

List of Tables

List of Figures

Nomenclature

a	absorption coefficient
b	Arrhenius equation temperature exponent
c	square-root of local sound velocity
c_p	heat capacity at constant pressure
d	nozzle/pipe diameter
f	arbitrary function
g	gravitational acceleration
h	enthalpy
j	diffusive flux
k	reaction rate constant
l	length scale
p	pressure
q	arbitrary scalar variable
r	radial axisymmetric cylindrical coordinate
s	oxygen to fuel stoichiometric value
t	time
u	velocity vector
v	velocity vector
w	chemical source term
w_h	enthalpy source term
x	axial Cartesian or axisymmetric cylindrical coordinate
y	radial Cartesian coordinate
A	pre-exponential factor in Arrhenius equation
C	constant
D	molecular diffusivity
E	activation energy
G	conditional variance
H	lift-off height
K	variance
L	visible flame length
M	third body coefficient
M_t	turbulent Mach number
P	probability density function
Q	conditional reactive scalar variable
Q_h	conditional enthalpy
R	universal gas constant
S	source term

T	temperature
W	molecular weight
Y	reactive scalar variable
$\boldsymbol{Y}$	composition vector of scalar variable
Z	mixture fraction

Greek letters

β	conserved property
χ	scalar dissipation
δ	Kronecker delta
ε	dissipation of turbulence kinetic energy
ϕ	random variable vector
φ	independent sample space variable
η	independent sample space variable
κ	turbulence kinetic energy
λ	thermal conductivity
μ	dynamic viscosity
μ_t	turbulent viscosity
ρ	density
σ_t	turbulent Prandtl number
σ	Stefan-Boltzmann constant
τ	stress tensor
υ	kinematic viscosity
υ_t	eddy viscosity
ϑ	stream function
ω	Patankar-Spalding coordinate
ξ	conserved scalar
ψ	independent sample space variable
Φ	transported property
Γ	number of moles
Θ	diffusive exchange coefficient
Ψ	independent sample space variable vector

Subscripts

axis	value established at centreline
c	of chemistry
cl	centreline value
cg	value established at constant gradient boundary
corr	correction term
eff	effective value
f	of fuel
for	of formation
i	vector component
inni	initial value

j	vector component
k	of turbulence kinetic energy equation
l	tensor notation
lb	laminar burning
m	tensor notation
mm	of molecular mixing
o	of oxidiser
p	of products
r	of reaction
s	stoichiometry
t	total
D	downstream locale
K	Kolmogorov scale
R	cross-stream average
TM	Taylor microscale
U	upstream locale
α	scalar index
β	scalar index

Superscripts

pe	partial equilibrium assumption
$'$	fluctuation with respect to the conventional mean
$''$	fluctuation with respect to the Favre or conditional mean

Overbars

–	conventional average
~	Favre average

Other symbols

$\langle\ \rangle$	ensemble averaging
$\langle \alpha \vert \beta \rangle$	conditional expectation of α at some value β

Non-dimensional Groups

Da	Damköhler number
Fr	Froud number
Le	Lewis number
Re	Reynolds number

1: Introduction

1.i Relevance of The Study

'The presence in the atmosphere of substances or energy in such quantities and of such duration resulting from the activity of man or from natural processes liable to cause harm to human, plant, animal life, or the environment, or changes in the weather and climate.'

There are many differing views as to what constitutes atmospheric pollution, but the above description is a most succinct, and yet still punctilious one. The wide scope of this definition has not always been supported, and until well into the last century, atmospheric pollutants were synonymous with suspended particulate matter such as soot or smoke, and also with sulphur dioxide emissions. More recently, with the advent and wider availability of petroleum-powered machinery such as motorised vehicles, several new emissions are recognised as pollutants. These, along with toxic chemical releases from developing industries, and the problems associated with ionising radiation liberated from nuclear-power projects or weapons testing, prove to be the greatest challenge to the continuing survival of modern-day man.

The pollutants of greatest concern formed during combustion processes include the oxides of sulphur (SO_x), the oxides of nitrogen (NO_x), the oxides of carbon (CO_x), volatile organic compounds (VOCs), unburned hydrocarbons (UHCs), and soot.

The combustion of gaseous fuels such as natural gas does not contribute greatly to the increase in atmospheric concentration of sulphur oxides, but nevertheless do have input. The greatest sole major source is from the utilisation of coal and oil-fired power stations due to the fuel-stock's very high natural content of sulphur compounds. Although anthropogenic contribution only accounts for about half of global emissions (natural oxide sources include sea-spray, forest fires, and volcanoes), these tend to be very concentrated, and are the largest contributors to the acid-rain problem.

The oxides of nitrogen are formed during all combustion processes involving atmospheric air as the oxidising medium, and their emission has two major implications with respect to environmental issues. Firstly, as with sulphur compounds, they increase the acidity of rain by the production of nitric acid and associated species. Secondly, in the presence of sunlight, they are precursors to the production of the irritating oxidant pollutants, ozone and peroxyacetylnitrate (PAN), which cause eye, nose, and respiratory irritation in humans, in addition to damaging vegetation. VOCs such as reactive hydrocarbons are also major originators of photochemical oxidants.

Carbon dioxide and carbon monoxide, in addition to contributing to the acidity of atmospheric precipitation, are the major causes of the greenhouse effect. Along with nitrous oxide, UHCs, chlorofluorocarbons (CFCs), low-level ozone, and water vapour, they are virtually transparent to incoming short-wave solar radiation, but are strong absorbers of outgoing long-wave terrestrial radiation. This causes a proportion of the energy that should normally dissipate to outer space to be trapped within the atmosphere, and its subsequent reradiation to the planet surface. The natural greenhouse effect is essential to our survival as a

species, raising the planet's temperature by thirty-two to thirty-four degrees Celsius. However, the ecological effects of raising this temperature by anthropological means have far-reaching consequences. For example, an increase of average global temperature of several degrees over the next fifty years would be expected to cause a sea-level rise between 0.5 and 1.5 metres. The effects of this on coastal areas around the world could be catastrophic.

The control of these polluting emissions has been a concern of industrialised nations as far back as the thirteenth century. During the reign of Edward I in Great Britain, a royal proclamation was issued which prohibited the use of sea-coal in open furnaces. Conviction of three offences of this type was punishable by death. More recently, the Stockholm Declaration of 1972 (UNEP 2000) laid the foundation for modern environmental policy, and in 1990, the United Nations General Assembly launched negotiations on what was to become the United Nations Framework Convention on Climate Change (UNFCCC). This was later adopted in 1992, and opened for signature shortly after at the United Nations Conference on Environment And Development on Rio de Janeiro, Brazil. Entering into force in 1994, the convention now has one hundred and eighty-six parties, all of which have continued to negotiate on matters that will advance its implementation. The negotiations lead to the adoption of the Kyoto Protocol (UNFCCC 2002) in December 1997 that contained new emissions targets for the post-2000 period. Collective emissions of the six greenhouse gases, CO_2, CH_4, N_2O, hydrofluorocarbons (HFCs), perfluorocarbons (PFCs), and SF_6 by the developed countries, are required to be reduced by at least five percent on their 1990 levels by the period 2008-2012.

The preceding text serves to highlight the importance assigned to regulation of toxic emissions from anthropogenic sources. One major aim of combustion research is to provide insight into the complex interactions between chemical and physical processes required to further the understanding of flame structure, pollutant formation, and other phenomena. An increased understanding of these processes is essential in the design and production of more efficient and cleaner technologies, required to comply with increasingly more stringent environmental control strategies. In addition to addressing environmental issues, combustion research aims to provide suitable computational models for the numerical prediction of combustion processes. This aid in the design and optimisation of engineering equipment reduces production costs by eliminating the need for prolonged and expensive prototype development and analysis. Also, an overall increased understanding of combustion phenomena, and the ability to mathematically represent them, inevitably leads to the safer and more effective applications of existing technologies.

1.ii Objectives And Scope of The Study

The aim of this doctoral submission was originally intended to be an investigation and evaluation of the Conditional Moment Closure (CMC) combustion model in its application to various turbulent jet diffusion flames. The improvement of efficiency and the reduction of emissions are primary considerations in the design and analysis of modern practical combustion devices, and hence tools such as those under investigation here are increasingly in demand. The development of calculation procedures which offer a high degree of universality with respect to the flows and geometries they can represent are therefore the ultimate goal of developmental work such as that to be subsequently discussed. The focus throughout this study therefore, was not so much a detailed analysis of specific models and their behaviour, but more a study of the overall abilities of a number of models to predict experimental observations, and the effect their differing interactions have upon the collective abilities. From the outset, intentions lay in the investigation of the effect of the chosen turbulence closure upon CMC calculations, in addition to the sensitivity of predictions to the type of chemistry closure applied.

Overall, the goal of these works was to shorten the distance between the research and developmental stages for the inclusion and application of CMC calculations in the design of practical combusting systems. Although the end-goal was not expected to be achieved in the limited time available, it was intended to leave the studies in a form which another could continue expanding upon the findings.

2: Literature Review

The intention of this chapter is to provide an overview of current thinking and practices concerning the structure and modelling of the diffusion flame. Section 2.i discusses the physical phenomena that represent such flames of both burner-stable and lifted type. Section 2.ii broaches the subject of turbulence modelling, and section 2.iii the subject of combustion modelling, including a comprehensive review of current CMC development.

2.i The Diffusion Flame

Gaseous flames can be classified into three regimes of combustion: Partially premixed; premixed; and nonpremixed. The object of scrutiny in this study is the nonpremixed flame, otherwise referred to as the diffusion flame, due to the reaction-rate controlling step being that of diffusion in mixing processes. Their application is widespread throughout industry, being found in such equipment as turbo-machinery, jet engines, and gas-fired boilers. Their use is often preferable to premixed flames due to a greater tolerance to variation in flame conditions, and a greater degree of safety due to no premixing of fuels and oxidisers prior to combustion. For published theory regarding the properties of diffusion flames, Burke and Schumann (1928a) can be considered amongst the first, proposing mathematical theory concerning the flame-front in a coflowing arrangement. This they historically reported, as the first article in the First Symposium on Combustion.

2.i.i The Laminar Diffusion Flame

The simplest form of the diffusion flame can be described as a steady flame, stabilised at the boundary between two laminar streams of oxidant rich and fuel rich composition. If the chemistry at the interface of the two streams is assumed to be one step and very fast, an infinitely thin reaction sheet separates the fuel

and products on one side from the oxidant and products on the other. The structure of jet flames with these configurations is well known, being composed of diffusion-convection zones on either side of the flame-sheet, which provide the only molecular mixing mechanisms in the flame. Both fuel and oxidant diffuse to the reaction sheet due to gradients imposed by the chemical reaction, and hence the flame cannot propagate into the fuel in the absence of oxidant, or vice-versa.

2.i.ii The Turbulent Diffusion Flame

Continually raising the velocity of flow at a jet nozzle will increase a laminar diffusion-flame length to a point at which turbulent structure begins to form. After surpassing a degree of turbulence being referred to as transitional, and usually indicated by a value of Reynolds number (see below), this is now defined as a turbulent jet diffusion flame. The main observable property of the turbulent flame in comparison to its laminar counterpart is its length. Being defined by any suitable means, the length is almost independent of the jet velocity, as opposed to a proportional relationship observed in the laminar case (Lewis and Von Elbe 1951). With reference to Burke and Schumann (1928b) and Hawthorne et al (1949), a simple correlation can be established for the length of a diffusion flame, *id est*:

$$L \approx \frac{d^2 u}{D}$$

which in the case of laminar flames, D is found to be independent of the velocity and nozzle diameter. Hence:

$$L \propto d^2 u$$

which concurs Lewis and Von Elbe's observations (1951). In the case of the turbulent diffusion flame, D represents the eddy diffusivity rather than a molecular diffusivity, and is proposed as being proportional to the product of the characteristic dimensions of the flame, *videlicet*:

$$L \approx \frac{d^2 u}{du} \propto d$$

which again is concurrent with earlier observation.

The turbulent flame is characterised by continuous fluctuations in velocity, and hence fluctuations in scalars such as composition, density, and temperature. These fluctuations are brought about by the action of shear-generated vortices within the flow, the growth of which being controlled by competition between the generation and the destruction processes due to viscous dissipation. A certain flow may be considered to have made the transition from a laminar to a turbulent condition once the generation rate surpasses that of the dissipation.

The physical nature of these flames may be described by a number of means, but the most common is by reference to a set of length scales describing the eddies within the fluid (Warnatz et al 2001). The Kolmogorov microscale is the smallest length scale, and thus represents the dimension at which turbulence kinetic energy dissipates to fluid internal energy. This is defined as:

$$l_K = \left(\frac{\upsilon^3}{\varepsilon} \right)^{1/4} \tag{2.1}$$

The next in ascending order of size is the Taylor microscale, and can be defined as the distance over which velocity differences are of the same order as the deviations of the local velocity from the mean value, *videlicet*:

$$l_{TM} = \frac{\sqrt{u'^2}}{\sqrt{\frac{\partial u'^2}{\partial x}}} \tag{2.2}$$

The largest length scale is the Integral scale, otherwise known as the Taylor macroscale, and represented as:

$$l_I = \frac{\left(\sqrt{u'^2}\right)^3}{\varepsilon} \tag{2.3}$$

The largest possible eddy can be defined by a characteristic width of the flow, and hence for flow in a pipe, the largest eddy permissible would be equal to the pipe diameter.

Many regions of turbulence can be investigated on the basis of values representative of length and time scales in the form of non-dimensional groups such as Reynolds number and Froude number, *id est*:

$$Re = \frac{\rho u d}{\mu} \tag{2.4}$$

$$Fr = \frac{u^2}{gd} \tag{2.5}$$

which represent the ratios of destabilising inertial forces to the stabilising viscous forces and gravitational forces respectively. Also, by making use of molecular mixing and chemical time-scales, the Damköhler number can be defined as:

$$Da = \frac{t_{mm}}{t_c} \tag{2.6}$$

which describes the competition between turbulent mixing and chemical reaction. These are very useful descriptors of turbulent reacting flow, and both Re and Da shall be subsequently implemented in discussion throughout this study. The Froude number however, is more often employed in the discussion of

flows with large buoyancy contributions due to it being an indication of the competition between momentum and buoyancy terms.

2.i.iii The Lifted Diffusion Flame

At sufficiently high fluid-flow velocities, a diffusion flame forms an entirely turbulent one, which has its origins at the mouth of the issuing pipe. This is referred to as an attached flame, and exists for a range of pipe-exit velocities. A critical velocity (lift-off velocity) exists for each fuel and burner arrangement at which the flame will detach from the pipe exit, and travel further downstream with increasing fuel velocity. A flame stabilised at a distance from the nozzle in the mixing region, and at a constant fuel velocity, is described as a lifted flame. A continuous increase in velocity will cause the flame stabilisation plane to progressively move downstream until blow-off occurs. This is the point at which no stabilisation is observed, and the flame is completely extinguished. The associated critical fuel velocity is termed the blow-off velocity.

Lifted diffusion flames have been a subject of study for over fifty years (Wohl et al 1949) and are currently of interest as they include many of the mechanisms controlling physical phenomena such as ignition and extinction encountered in practical industrial applications. Much experimental work has been undertaken over the years in an attempt to elucidate the stabilisation mechanisms in such flames. Schefer et al (1988) present results based on CH radical, methane, and temperature planar imaging, that demonstrate heat release having a significant effect on turbulence and mixing in lifted jets. Here they make comparisons between a non-reacting methane jet, and a lifted methane jet flame. The primary

observable differences in terms of the lifted flame were the lower centreline decay-rate of methane, and higher instantaneous gradients and fluctuations of concentration. In terms of heat release, this lower centreline decay is shown to be due to a reduction in mass entrainment by the central fuel jet as a result of the lower density of surrounding gases in the combusting case. The higher fluctuations in concentration is attributed to the effects of heat release on the volumetric expansion of turbulent scales in the mixing region, in addition to the steeper gradients of methane concentration along the jet boundaries.

However, the physical mechanisms of lifted flame stabilisation are still not well understood, and at present, theory can be divided into three categories as follows:

2.i.iii.i Premixed Flame Propagation

The earliest attempt at contriving a hypothesis for a stabilisation mechanism can be accredited to Vanquickenbourne and van Tiggelen (1966). In their work, they study a number of methane/air flames, and suggest that the fuel and the oxidiser are fully premixed at the base of the lifted diffusion flame, and that this stabilisation occurs where the mean flow velocity at stoichiometric mixture equals the burning velocity of a stoichiometric premixed turbulent flame. Experimental investigations of lift-off of natural gas and hydrogen jet mixtures by Hall et al (1980) and Günther et al (1981) follow this concept, and suggest that the most likely location for combustion at the flame base is along the mixture-fraction isopleth at which the fuel and oxidiser mixture displays its maximum laminar flame speed. Kalghatgi (1984) presents extensive data of lifted flames with respect to blowout and lift-off for a range of fuels and burner

dimensions. By assuming the premixed model of Vanquickenbourne and van Tiggelen (1966), the author successfully correlates his results using dimensional analysis, and approximates lift-off height as:

$$H = C_H \left[\frac{u\upsilon}{(u_{lb})^2_{\max}} \right] \left(\frac{\rho_f}{\rho_o} \right)^{3/2} \qquad (2.7)$$

Eickhoff et al (1984) can be referred to for further investigation of lift-off and associated phenomena in diffusion flames of natural gas, where once again, Vanquickenbourne and van Tiggelen's (1966) premixed combustion hypothesis is supported. They deduce that forty to fifty percent of the fuel stream is already mixed at the molecular level, upstream from the stabilisation zone, which subsequently reacts over a very short distance. They conclude that molecular diffusion occurs through the large eddies in the non-reacting flow, thus providing a premixed combustion region.

2.i.iii.ii Flamelet Quenching And Large Scale Re-entrainment

The premixed flame model has been challenged by a number of more recent theories. Peters and Williams (1983) argue that in axisymmetric turbulent jets, the degree to which molecular mixing occurs is insufficient to support the premixed concept, and present a model that assumes stabilisation to be controlled by laminar diffusion flamelets which are extinguished when a strain rate of critical value is imposed upon them. Stabilisation is hence expected to occur at the point where the extinction and the propagation rates balance.

For further reading, and variation of combustion extinction hypothesis, Miake-Lye and Hammer (1988), Byggstoyl and Magnussen (1983), and Broadwell et al (1984) also propose theory. In application of the flamelet quenching hypothesis, Miake-Lye and Hammer (1988) derive a model by determining a stability criterion from the strain of large-scale structures being imposed upon the flow field. This model is seen to perform well for pure fuels of methane, ethylene, and natural gas. Byggstoyl and Magnussen (1983) also display good agreement between predicted lift-off height and experimental data using a model developed from the suggestion that extinction occurs, but in the smallest vortices of the flow, under premixed conditions. Broadwell et al (1984) apply their model to the prediction of dependency of lift-off height on jet exit velocity with perhaps less success. They propose that hot combustion products are transported to the jet periphery by large-scale structures, where they are re-entrained, and ignite the combustible mixture. Here, they introduce a parameter referred to as the 'ratio of two times', being defined by a characteristic chemical reaction time and a mixing time of re-entrained products. Lift-off and blowout can hence be associated with critical parameter values when re-entrained products are mixed so rapidly that reaction cannot be initiated before radical values drop below their critical concentrations.

2.i.iii.iii Triple Flame

Triple flames have attracted a great deal of attention in recent years, the theory constituting both premixed and diffusion-flame stabilisation concepts (Müller et al 1994). They occur when a flame propagates across a fuel concentration

gradient such as a mixing layer, resulting in a stoichiometric flame at the fuel and oxidiser interface, and two curved branches to either side, consisting of fuel-lean and fuel-rich partially-premixed flames. A diffusion flame remains the constituent of the main reaction zone, lying along the stoichiometric line downstream of the premixed branches. This is supported by excess air and fuel from the lean and rich partially-premixed flames respectively.

The study of Ruetsch et al (1995) shows the reaction-rate profiles of triple flames resemble in form the premixed and nonpremixed zones previously defined. Imagery of a lifted methane flame base (Schefer et al 1988, 1994) does not however display all of these characteristics. As a means of explanation, Veyante et al (1994) and Favier and Vervisch (1998) demonstrate that triple flames are able to survive strong interaction with vortices by adjusting their structure in respect to their environment. Vortical motion can distort the flame so that the characteristic branching does not always exist, which goes some way to explaining experimental observations.

2.i.iii.iv Comments on Lifted-flame Theory

A number of additional works exist relevant to stabilisation theory of lifted diffusion flames and associated phenomena. Reviews by Pitts (1988) and Schefer (1994) are recommended sources of informative material for further investigation. Pitts (1988) concludes that neither the premixed or extinction hypothesis are adequate to predict lift-off or blowout behaviour, and that the inclusion of effects due to large-scale structures must be included if improvements are to be made. Schefer (1994) concludes that the previously

discussed concepts introduced by Broadwell et al (1984) should be incorporated with premixed propagation theories in development of improved models. More recent investigations include that of Chen et al (2000), in which a flamelet model for partially premixed combustion based on the premixed flame propagation mechanism is proposed, that takes the triple-flame structure into account. Good agreement with experimental data is observed for lift-off heights of methane/air and propane/air jet flames.

Laminar lifted flames have also been used to improve the understanding of stabilisation mechanisms within their turbulent counterparts, and recent works concerning reattachment and blowout in laminar flames include that of Lee and Chung (2001) regarding lifted partially-premixed propane jets. Using the similarity solutions for jets, flame reattachment is explained based upon the balance between the propagation speed of a tribrachial flame, and flow velocity. Chung and co-workers have undertaken extensive analytical and experimental work of laminar lifted flames in fuel injectors, and more recent works can be found cited in Won et al (2000).

2.ii Turbulence And Chemistry Interaction

To successfully model turbulent combusting flows, three important facets must be identified and addressed. Firstly, a knowledge of the turbulent flow-field; secondly, a knowledge of the chemical kinetics involved; and thirdly, a knowledge of how these phenomena interact.

Generally, conservation equations applicable to fluid-flow properties are solved alongside species transport equations when modelling turbulent combustion. Many methodologies of modelling, and procedures for solution have been developed over the years, and the following text outlines some of the more rigorously investigated and applied.

2.ii.i Turbulence Modelling

The continuity equations of mass and momentum are the starting point of turbulence modelling theory, and are defined below. Their derivation is well known, and the reader is directed to any one of numerous texts available outlining this procedure. One such example can be found in that written by Bird, Stuart, and Lightfoot (1960).

Mass conservation:
$$\frac{\partial \rho}{\partial t} + \frac{\partial}{\partial x_i}(\rho u_i) = 0 \qquad (2.1)$$

Momentum conservation: $$\rho\frac{\partial u_i}{\partial t}+\rho u_l\frac{\partial u_i}{\partial x_l}=-\frac{\partial p}{\partial x_i}\frac{\partial \tau_{il}}{\partial x_l}+\rho g_i \qquad (2.2)$$

Newtonian stress tensor: $$\tau_{ij}=-\mu\left(\frac{\partial u_i}{\partial x_j}+\frac{\partial u_j}{\partial x_i}-\frac{2}{3}\frac{\partial u_l}{\partial x_l}\delta_{ij}\right) \qquad (2.3)$$

Due to the turbulent nature of the flows investigated in this study, it is desirable to be able to predict mean variable values. To proceed, the equations characterising the turbulence must be solved. Initially, the dependent variables must be decomposed into their mean and fluctuating parts, *id est*:

$$Y=\overline{Y}+Y' \qquad (2.4)$$

Substitution of equation (2.4) into equations (2.1) and (2.2), followed by subsequent averaging, provides the turbulent flow equations. The consequence of this averaging being that the mean values of variables can be obtained without the requirement of resolving all the smaller temporal and spatial length scales of flow.

Two types of averaging are commonly applied; Reynolds averaging described as unweighted averaging, and Favre averaging described as density-weighted averaging (Bilger 1975). Favre averaging is more often than not employed, as the resulting equations do not contain correlation terms involving density fluctuations. This makes their subsequent solution less demanding than their Reynolds counterparts. The common feature of these averaging processes is the transformation of a set of closed equations into one containing unclosed terms that require modelling. This is referred to as the closure problem, and representation of these quantities by suitable models defines turbulence modelling.

When applying Favre averaging, the dependent variables barring density and pressure are decomposed according to:

$$Y(x,t) = \tilde{Y}(x,t) + Y''(x,t) \tag{2.5}$$

where:
$$\tilde{Y}(x,t) = \frac{\overline{\rho Y(x,t)}}{\overline{\rho(x,t)}} \tag{2.6}$$

The subsequent substitution into, and averaging of the conservation equations leads to:

$$\frac{\partial \overline{\rho}}{\partial t} + \frac{\partial}{\partial x_l}(\overline{\rho}\tilde{u}_l) = 0 \tag{2.7}$$

$$\overline{\rho}\frac{\partial \tilde{u}_i}{\partial t} + \overline{\rho}\tilde{u}_l\frac{\partial \tilde{u}_i}{\partial x_l} = -\frac{\partial \overline{p}}{\partial x_i} - \frac{\partial}{\partial x_l}(\overline{\rho}\widetilde{u_i''u_l''}) + \overline{\rho}g_i \tag{2.8}$$

Equation (2.8) has been simplified here by considering flows of high Reynolds number. In this case, the molecular viscous and diffusive transport terms are neglected as being of negligible importance in comparison with the turbulent transport terms.

This new unclosed set of equations now contains a number of terms that require modelling; these being the mean density observable in equations (2.7) and (2.8), and the Reynolds stress terms observable in equation (2.8). Methods employed to represent these Reynolds stress terms are covered in the following review.

2.ii.i.i Zero Equation Turbulence Model

As the name of this concept implies, partial differential equations are solved only for the mean velocity components, and not the turbulence properties. The eddy viscosity model, originally proposed by Boussinesq in 1877 and given as equation (2.9), is implemented with equation (2.10), being Prandtl's mixing length model.

$$\tau_{ij} = -\bar{\rho}\widetilde{u_i''u_j''} = \mu_t\left(\frac{\partial \tilde{u}_i}{\partial x_j} + \frac{\partial \tilde{u}_j}{\partial x_i}\right) \tag{2.9}$$

$$\upsilon_t = l^2\left|\frac{\partial \tilde{u}}{\partial y}\right| \tag{2.10}$$

Noting that the gradient term in equation (2.10) is the only significant mean velocity gradient in a two-dimensional thin shear layer, the Reynolds stresses may be represented as:

$$-\rho\widetilde{u_i''u_j''} = \bar{\rho}\upsilon_t\left|\frac{\partial \tilde{u}}{\partial y}\right| \tag{2.11}$$

The model does however have its drawbacks. The length scale must be varied with the problem being addressed, which in the case of simple free turbulent flows and boundary layers, can be obtained with the use of simple algebraic formulae. Also, convection and diffusion of turbulence energy are ignored due to the assumption of isotropy of energy generation and dissipation.

2.ii.i.ii Two Equation Turbulence Model

The $k-\varepsilon$ model of Jones and Launder (1972) is widely used in many of today's applications. It requires the solution of two additional partial differential equations in conjunction with the mass and momentum conservation equations, and is widely favoured for its simplicity and relatively low computational costs. However, its performance is questionable when applied to flows with strong streamline curvature, recirculation, swirl, or buoyancy. This is again due to the assumption of turbulence isotropy. These two equations represent the transport of

turbulence kinetic energy (k) and its rate of dissipation (ε), being equations (2.12) and (2.13) respectively.

$$\bar{\rho}\frac{\partial k}{\partial t}+\bar{\rho}\tilde{u}_l\frac{\partial k}{\partial x_l}=\frac{\partial}{\partial x_l}\left[\left(\frac{\mu_t}{\sigma_\kappa}+\mu\right)\frac{\partial k}{\partial x_i}\right]-\bar{\rho}\widetilde{u_l''u_m''}\frac{\partial \tilde{u}_m}{\partial x_l}-\frac{\mu_t}{\bar{\rho}^2}\frac{\partial \bar{\rho}}{\partial x_l}\frac{\partial \bar{p}}{\partial x_l}-\bar{\rho}\varepsilon \tag{2.12}$$

$$\bar{\rho}\frac{\partial \varepsilon}{\partial t}+\bar{\rho}\tilde{u}_l\frac{\partial \varepsilon}{\partial x_l}=\frac{\partial}{\partial x_l}\left[\left(\frac{\mu_t}{\sigma_\varepsilon}\right)+\mu\frac{\partial \varepsilon}{\partial x_l}\right]\ -C_{\varepsilon 1}\frac{\varepsilon}{k}\left(\bar{\rho}\widetilde{u_l''u_m''}\frac{\partial \tilde{u}_m}{\partial x_l}+\frac{\mu_t}{\bar{\rho}^2}\frac{\partial \bar{\rho}}{\partial x_l}\frac{\partial \bar{p}}{\partial x_l}\right)-C_{\varepsilon 2}\bar{\rho}\frac{\varepsilon^2}{k} \tag{2.13}$$

The solutions of these equations yield values for k and ε, and applying the same approach as used in the mixing length model, the eddy viscosity can be defined as equation (2.14). The Reynolds stresses are then derived from an extended eddy-viscosity model, and defined as equation (2.15).

$$\mu_t=C_\mu\bar{\rho}\frac{k^2}{\varepsilon} \tag{2.14}$$

$$\bar{\rho}\widetilde{u_i''u_j''}=-\mu_t\left|\frac{\partial \tilde{u}_i}{\partial x_j}+\frac{\partial \tilde{u}_j}{\partial x_i}\right|-\frac{2}{3}\bar{\rho}k\delta_{ij} \tag{2.15}$$

2.ii.i.iii Second Moment Closure Turbulence Model

Due to the shortcomings of eddy-viscosity models, it may be desirable for certain flow situations to use a set of transport equations to represent the individual Reynolds stresses. These transport equations are complex, and less robust than the $k-\varepsilon$ system, but are better suited for more complex flow situations; the $k-\varepsilon$ model originally being developed for thin shear layers. Among the first papers to address the derivation of the second moment closures were those of Hanjalic and Launder (1972, 1976), and Launder, Reece, and Rodi (1975). The transport equation takes the form:

$$\frac{\partial}{\partial t}\overline{\rho}\widetilde{u_i''u_j''}+\frac{\partial}{\partial x_l}\overline{\rho}\tilde{u}_i\widetilde{u_i''u_l''}+\frac{\partial}{\partial x_l}\overline{\rho}\tilde{u}_j\widetilde{u_j''u_l''}=-\left(\widetilde{u_i''\frac{\partial\overline{p}}{\partial x_j}}+\widetilde{u_j''\frac{\partial\overline{p}}{\partial x_i}}-\frac{2}{3}\delta_{ij}\widetilde{u_l''\frac{\partial\overline{p}}{\partial x_l}}\right)$$
$$-2\mu_t\widetilde{\frac{\partial u_i''}{\partial x_l}\frac{\partial u_j''}{\partial x_l}}-\frac{\partial}{\partial x_l}\left(\overline{\rho}\widetilde{u_i''u_j''u_l''}+\frac{2}{3}\delta_{ij}\widetilde{u_l''\overline{p}}\right) \tag{2.16}$$

Additional modelling is required of the terms on the right-hand side of this equation. The first term is the pressure-strain term, and is responsible for the redistribution of the Reynolds stresses. This can be separated into two parts for modelling purposes; the return-to-isotropy part containing only turbulent quantities, and the other being proportional to the mean rate of strain. With the assumption of local isotropy, the destruction rate due to viscous effects can by represented as equation (2.17).

$$2\mu_t\widetilde{\frac{\partial u_i''}{\partial x_l}\frac{\partial u_j''}{\partial x_l}}=\frac{2}{3}\delta_{ij}\overline{\rho}\varepsilon \tag{2.17}$$

The diffusive transport term can be modelled using a simple gradient model, *videlicet*:

$$\widetilde{u_i''u_j''u_l''}+\frac{2}{3}\delta_{ij}\widetilde{u_l''\overline{p}}=-C_s\frac{k^2}{2\varepsilon}\widetilde{u_l''u_m''}\frac{\partial}{\partial x_l}\widetilde{u_i''u_j''} \tag{2.18}$$

This method provides a system of nine equations, one representing each of the Reynolds and normal stresses. Due to the equality of shear stresses, this reduces to a system of six. It is evident from equation (2.17) and (2.18) however, a transport equation for ε must be also be implemented, bringing the total number of additional partial differential equations to seven.

Lumley (1978) covers in great detail how these above terms can be modelled. Many systems of terms and constants exist; one such well-known set being those of Jones and Musonge (1988).

2.ii.ii Combustion Modelling

The intention of this review is to highlight certain aspects of combustion modelling which provide grounding to the theory and motivation for the present research. It is not intended to provide a comprehensive assessment of current practices, and the interested reader is encouraged to draw their attention to works such as that of Peters (2000) and Turns (2000).

In order to incorporate chemical reaction into turbulence calculations, the mass conservation equation (2.1) must be supplemented by the transport equations for each species mass-fraction to be considered. These take the form:

$$\rho \frac{\partial Y_\alpha}{\partial t} + \rho u_l \frac{\partial Y_\alpha}{\partial x_l} = -\frac{\partial j_\alpha}{\partial x_l} + w_\alpha \tag{2.19}$$

The term denoted by j_α describes the diffusive flux of species α, and can be most simply approximated using the binary flux representation, *videlicet*:

$$j_\alpha = -\rho D_\alpha \frac{\partial Y_\alpha}{\partial x_l} \tag{2.20}$$

This is only valid under the simplifying assumption of equal diffusivities of the system components, and otherwise violates mass conservation. A widely employed approximation, its implications in combustion calculations are becoming increasingly more investigated, and the topic is raised throughout latter parts of this study.

The last term in the right hand side of equation (2.19) is the production or destruction rate of the scalar Y_α. This source term contains the contribution of many reactions, depending upon the kinetic scheme employed, and leads to a system of stiff non-linear equations that the solution of does not prove to be a

straightforward integration problem. The source term is also temperature dependent, due to the Arrhenius expression representing the reaction rate constants. Hence, in addition to transport equations for the species mass fractions, we also require the solution of an enthalpy equation to model the energy content of the fluid. This takes the Favre-averaged form:

$$\bar{\rho}\frac{\partial \tilde{h}}{\partial t}+\bar{\rho}\tilde{u}_l\frac{\partial \tilde{h}}{\partial x_l}=\frac{\partial \bar{p}}{\partial t}+\frac{\partial}{\partial x_l}\left(\frac{\lambda}{c_p}\frac{\partial \tilde{h}}{\partial x_l}\right)+q_R-\sum_{\alpha=1}^{n}\tilde{h}_\alpha\frac{\partial}{\partial x_l}\left[\left(\frac{\lambda}{c_p}-\rho D_\alpha\right)\frac{\partial \tilde{Y}_\alpha}{\partial x_l}\right] \qquad (2.21)$$

As is usually the case for simplicity, all mass diffusivities (D_α) are assumed proportional to the thermal diffusivity, such that the Lewis numbers defined as equation (2.22) are constant and unity.

$$Le_\alpha=\frac{\lambda}{\rho c_p D_\alpha}=\frac{D}{D_\alpha}=1 \qquad (2.22)$$

As can be seen, this approximation causes the last term on the right hand side of equation (2.21) to equate with zero. This leaves the transient pressure term, the diffusive heat flux term, and the radiant source term. The modelling of the radiant source is an important issue where NO_x chemistry is involved, and this shall be addressed later in this study. Derivation of, and further discussion on equations (2.19) and (2.21) can be found in the texts of Turns (2000) or Kuo (1986).

To include these additional equations for species and enthalpy conservation into the framework of turbulent combustion modelling, they must be treated in a similar fashion to mass and momentum, as discussed in (2.iii.i). Decomposing the reactive scalars into their Favre mean and fluctuating components as in equation (2.5), and subsequent substitution into, and averaging of equation (2.19), provides the turbulent transport equation, *id est*:

$$\bar{\rho}\frac{\partial \tilde{Y}_\alpha}{\partial t}+\bar{\rho}\tilde{u}_l\frac{\partial \tilde{Y}_\alpha}{\partial x_l}=\frac{\partial}{\partial x_l}\left(\rho D_\alpha \frac{\tilde{Y}_\alpha}{\partial x_l}\right)-\frac{\partial}{\partial x_l}\left(\bar{\rho}\widetilde{u_l''Y_\alpha''}\right)+\tilde{w}_\alpha \qquad (2.23)$$

The last term on the right hand side of this equation is the mean chemical source term, and its evaluation has long been considered the main problem when using moment methods in turbulent combustion. As discussed earlier, this source is coupled with the Favre-mean temperature, and w_α can fluctuate significantly about its mean value evaluated at the Favre-mean temperature. This requires the evaluation of a number of higher moments involving temperature fluctuations so as to incorporate the effects into the source term. In addition, terms involving turbulence and scalar fluctuation correlations have now arisen, which require modelling, and invariably the solution of additional transport equations. This proves impractical for turbulent flame calculations, and solutions to this problem are termed as 'combustion models'.

2.ii.ii.i Eddy Dissipation Model

One solution of the previously discussed problem is to remove the influence of chemistry altogether, eliminating the need to solve for any fluctuating quantities. Proposed by Magnussen and Hjertager (1976), the Eddy Dissipation Model is an adaptation of the Eddy Break-up Model of Spalding (1971), and formulated primarily for premixed combustion. Here, a transport equation is solved for the mass fraction of fuel, the source term being implemented as the minimum of three reaction rates defined using the mass fraction of fuel, oxidiser, and the products, such that:

$$\tilde{w}_f = A\frac{\varepsilon}{k}\min\left(\tilde{Y}_f, \frac{\tilde{Y}_o}{s}, \frac{B\tilde{Y}_p}{1+s}\right) \tag{2.24}$$

where the value of constants A and B are problem dependent. Although a valiant attempt at closure, it is not always desirable to remove the influence of chemistry and associated fluctuating properties completely, and loss in accuracy of predictions is inevitable. Hence, other solutions to this problem have been sought.

2.ii.ii.ii Transported Probability Density Function Model

The transported probability density function (pdf) model, alongside CMC methods, represents one of the most promising developments in combustion modelling theory to date. A number of forms of this model exist, but common to all is the derivation and solution of a joint transported pdf of a set of reactive scalars by means of a Monte Carlo simulation. Techniques such as that suggested by Dopazo (1994), where joint statistics of the velocity, velocity gradients, and the scalar gradients are included into the pdf, are used to overcome certain closure problems. Dopazo (1994) may be referred to for a more comprehensive review of current transported pdf methods.

With reference to Pope (1985), the transport equation for the pdf (P) as a function of species mass fraction and energy can be derived from the respective conservation equations. To avoid the explicit appearance of correlations with density, the Favre-averaged formulation is often implemented, and takes the form:

$$\overline{\rho}\frac{\partial \tilde{P}}{\partial t}+\overline{\rho}\tilde{u}_l\frac{\partial \tilde{P}}{\partial x_l}+\overline{\rho}\frac{\partial}{\partial x_l}\left\langle u_l''\middle|\Psi\right\rangle\tilde{P}-\frac{\partial}{\partial x_l}\overline{\rho}D\frac{\partial \tilde{P}}{\partial x_l}=$$

$$-\overline{\rho}\frac{\partial}{\partial \psi_\alpha}\frac{\partial}{\partial \psi_\beta}\left(\left\langle D\frac{\partial \phi_\alpha}{\partial x_l}\frac{\partial \phi_\beta}{\partial x_l}\middle|\Psi\right\rangle\tilde{P}\right)-\overline{\rho}\frac{\partial}{\partial \psi_\alpha}\left(\frac{w_\alpha}{\overline{\rho}}\tilde{P}\right) \qquad (2.25)$$

$$-\overline{\rho}\frac{\partial}{\partial \psi_h}\left\langle\frac{\partial \overline{p}}{\partial t}+u_l\frac{\partial \overline{p}}{\partial x_l}+\phi_D\middle|\Psi\right\rangle\frac{1}{\overline{\rho}}\tilde{P}$$

The terms on the left hand side of the equation denote spatial exchange of $\tilde{P}$ due to convection and diffusion. The terms on the right sequentially represent turbulent mixing, reaction, and the last comprising compressibility effects and dissipation.

In contrast to moment methods, the non-linear source term in equation (2.25) appears in a closed form, which is of particular interest when considering the modelling of turbulent reacting flows. However, a number of terms (those in angular brackets) do remain unclosed, and the predictive capabilities of this method depend upon the ability of the models employed. These terms vary with the approach applied. For example, the turbulent convection term remains unclosed on the left hand side of equation (2.25), as velocity is not included in the formulation of this particular pdf conservation equation. Modelling of this turbulent flux is commonly achieved using a conventional gradient diffusion assumption as proposed by Pope (1981a). Other modelling techniques are utilised, such as the Linear Mean Square Estimation (LMSE) model proposed by Dopazo (1975). For chemically reacting flows however, the greatest challenge lies in the modelling of the molecular mixing term. By far the simplest and most widely applied model is the Interaction by Exchange with the Mean (IEM) model, introduced by Villermaux and Devillon (1972), and also known as the LMSE as discussed in Dopazo (1975). An example of its application, in addition

to an interesting comparative study of combustion models, can be founds in Obieglo, Gass, and Poulikakos (2000). Others, such as the Coalescence-Dispersion (CD) models are widely implemented. One such example is that of the modified Curl model of Janicka, Kolbe, and Kollmann (1979), developed from the original work of Curl (1963). Examples of application of this approach can be found in Pope (1981b), and Smith et al (1995). Again, Dopazo (1994), or Peters (2000) may be consulted for a comprehensive review on current practice and developments in this field.

Due to the exceptional high dimensionality of the transported pdf equation, the application of finite-volume and finite-difference techniques as a solution procedure is not suitable. Hence, Monte Carlo methods have been developed, such as that of Pope and co-workers (Pope 1990), to efficiently integrate equation (2.25). Here, the physical domain is subdivided by a computational grid, the pdf of each cell being represented by a large number of stochastic particles of the order of 50,000. In this Lagrangian approach, the particles are not bound to nodes, but each has its own position within the domain, and moves with its own instantaneous velocity. The particles are thus operated upon by decoupled computational functions simulating instantaneous convective mixing, diffusion, and chemical reaction. The form of the pdf is then established from the particle distribution in composition space, and the single-point statistics of the scalar variables subsequently obtained by convolution of the sample space variable with the pdf over the sample domain.

It is found that the solution of the Lagrangian equations requires properties of the flow, namely k and ε, which are obtained by the application of a finite-volume method over the computational grid. This often leads to a hybrid Eulerian-

Lagrangian Monte Carlo method for the representation of transported scalars being implemented.

2.ii.ii.iii Laminar Flamelet Models

The laminar flamelet concept views a turbulent diffusion flame as an ensemble of wrinkled, laminar, diffusion flame sheets, known as flamelets (Williams 1975, Bilger 1976). The primary assumption applied, being that the reaction zone is very thin in comparison with the turbulence length scales. This zone hence forms a flame sheet thin enough so that the local structure is unaffected by the turbulence excepting a strain induced on the flamelet plane.

Flamelet models, along with the Fast Chemistry Limit (FCL) and CMC models, belong to a group of nonpremixed combustion models that implement the concept of a conserved scalar and its dissipation. The conserved scalar of choice is typically the mixture fraction, defined as (Bilger 1976):

$$Z = \frac{(\beta - \beta_O)}{(\beta_F - \beta_O)} \tag{2.26}$$

where β can be any conserved property such as mass fraction, and the subscripts O and F refer to the oxidiser and fuel streams respectively.

One of the main advantages of laminar flamelet models, and indeed the CMC model, is that detailed chemical reaction calculations are not required within the framework of the turbulent flow field, as the chemistry is embedded into laminar flamelet library profiles of the species mass fractions as functions of Z and its dissipation rate χ, obtained from the solution of the laminar flamelet equations, *videlicet*:

$$\rho\frac{\partial Y_\alpha}{\partial t}=\frac{\rho}{Le_\alpha}\frac{\chi}{2}\frac{\partial^2 Y_\alpha}{\partial Z^2}+w_\alpha \tag{2.27}$$

Shown here in its unsteady form, the Lewis numbers are taken as unity for all α, and the instantaneous dissipation rate is defined as:

$$\chi=2D\left|\frac{\partial Z}{\partial x_l}\frac{\partial Z}{\partial x_l}\right| \tag{2.28}$$

Favre averaged mass fractions at any spatial location may then be established by convolution of the flamelet profile, and a pdf constructed using the moments of the Favre mean mixture fraction and its variance. It is now evident that additional transport equations for these conserved scalars must be solved simultaneously, within the turbulent field calculation. These take the form:

$$\bar{\rho}\frac{\partial\tilde{Z}}{\partial t}+\bar{\rho}\tilde{u}_l\frac{\partial\tilde{Z}}{\partial x_l}=\frac{\partial}{\partial x_l}\left(-\bar{\rho}\widetilde{u_l''Z''}\right) \tag{2.29}$$

$$\bar{\rho}\frac{\partial\widetilde{Z''^2}}{\partial t}+\bar{\rho}\tilde{u}_l\frac{\partial\widetilde{Z''^2}}{\partial x_l}=-\bar{\rho}\frac{\partial}{\partial x_l}\widetilde{u_l''Z''^2}-2\bar{\rho}\widetilde{u_l''Z''}\frac{\partial\tilde{Z}}{\partial x_l}-\bar{\rho}\tilde{\chi} \tag{2.30}$$

where the mean scalar dissipation may be modelled as:

$$\tilde{\chi}=C_{\tilde{\chi}}\frac{\varepsilon}{k}\widetilde{Z''^2} \tag{2.31}$$

with a model constant $C_{\tilde{\chi}}=2.0$. The turbulent fluxes can be modelled by the usual gradient flux approximation, or by implementation of a scalar flux transport equation set as is often applied in conjunction with Reynolds stress models. Now, if the Favre average over all $\chi(Z)$ is taken, conditioned at a fixed Z and t, the scalar dissipation rate in equation (2.27) can be replaced by the conditional Favre mean scalar dissipation rate, given by:

$$\langle\tilde{\chi}|Z\rangle=\frac{\langle\rho\chi|Z\rangle}{\langle\rho|Z\rangle} \tag{2.32}$$

and the Favre averaged mass fractions are then obtained by:

$$\tilde{Y}_\alpha(x,t) = \int_0^1 Y_\alpha\left(Z, \langle \tilde{\chi} | Z \rangle, t\right) \tilde{P}(Z;x,t) dZ \tag{2.33}$$

This formulation is the same as that used in the CMC concept, which shall be discussed presently. One of the great advantages of using laminar flamelet theory however, is the incorporation of the mean scalar dissipation term in the equation. As opposed to taking the conditional mean value as just described, the steady state flamelet equations can be solved, retaining the instantaneous values, and subsequent convolution with a joint pdf of $\tilde{Z}$ and $\tilde{\chi}_{st}$ will provide the Favre mean values, *id est*:

$$\tilde{Y}_\alpha(x,t) = \int_0^1 \int_0^\infty Y_\alpha(Z, \tilde{\chi}_{st}) \tilde{P}(Z, \tilde{\chi}_{st}; x, t) \, d\tilde{\chi}_{st} dZ \tag{2.34}$$

The benefits here lie in the ability of the model to account for ignition and extinction events, which are triggered by large and small values of χ. This approach is referred to as the Stretched Laminar Flamelet Model (SLFM), and is further presented by Liew, Bray, and Moss (1984).

Recent applications of flamelet models to turbulent jet diffusion flames can be found in works by Chen, Herrmann, and Peters (2000); Pitsch, Riesmeier, and Peters (2000); and Lentini and Puri (1995). For the more interested reader, a comprehensive review of the laminar flamelet concept can be found in Bray and Peters (1994). Barths et al (2000), and Coelho and Peters (2001b) can be referred to for interesting recent developments in flamelet techniques, namely the Eulerian Particle Flamelet Model (EPFM).

2.ii.ii.iv Conditional Moment Closure Model

The conditional moment closure equations have been independently developed by Bilger (1993a) and Klimenko (1993), using two differing methods of derivation, but yielding the same equation formulation. The theory central to CMC modelling is that most of the fluctuations in the transported scalar quantities (mass fractions and temperature) that make closure of the chemical production terms difficult can be associated with the fluctuations of one scalar variable (Klimenko and Bilger 1999). For nonpremixed combustion processes without local extinction, this is usually taken as the mixture fraction. This implies that in most cases, the fluctuation around the conditional means of the scalars conditionally averaged upon the mixture fraction, will be small in comparison to the mean quantities.

The following text outlines the derivation of the CMC equations, as defined by Klimenko and Bilger (1999), using both the decomposition and the joint pdf methods. Reference should be made to this aforementioned article for a comprehensive step-by-step analysis of the theory. It should be noted that although differing closure hypothesis are used, both methods utilise the instantaneous conservation equations of the reactive scalar (Y) and the conserved scalar (ξ), given by equations (2.19) and (2.35) respectively.

$$\rho\frac{\partial\xi}{\partial t}+\rho u_l\frac{\partial\xi}{\partial x_l}=-\rho D_\xi\frac{\partial^2\xi}{\partial x_l^2} \tag{2.35}$$

Decomposition Method:

Bilger begins his derivation by defining the conditional expectation of the mass fraction of a reactive scalar at a given value of the sample space variable associated with ξ as:

$$\langle Y|\eta\rangle = Q(x,\eta) = \langle Y(x,t)|\xi(x,t)=\eta\rangle \tag{2.36}$$

where the angular brackets denote an ensemble average over a number of realisations of the flow. The vertical bar indicates the condition of only the values on the left hand side of the ensemble, which meet the condition on the right hand side, shall be included into the average. Next, considering the scalar Y, it can be decomposed in a similar manner to equation (2.4) to obtain:

$$Y(x,t) = Q(\eta=\xi(x,t),x,t)+Y''(x,t) \tag{2.37}$$

Differentiating this equation yields:

$$\frac{\partial Y}{\partial t} = \frac{\partial Q(\xi)}{\partial t}+\frac{\partial Q(\xi)}{\partial \eta}\frac{\partial \xi}{\partial t}+\frac{\partial Y''}{\partial t} \tag{2.38}$$

and

$$\frac{\partial Y}{\partial x_l} = \frac{\partial Q(\xi)}{\partial x_l}+\frac{\partial Q(\xi)}{\partial \eta}\frac{\partial \xi}{\partial x_l}+\frac{\partial Y''}{\partial x_l} \tag{2.39}$$

where the bracketed expressions have been reduced or omitted for brevity. Applying the same decomposition method to the molecular diffusion term, equation (2.40) can be developed; and with subsequent substitution of equations

$$\begin{aligned}\frac{\partial}{\partial x_l}\left(\rho D\frac{\partial Y}{\partial x_l}\right) = \frac{\partial}{\partial x_l}\left(\rho D\frac{\partial Q(\xi)}{\partial x_l}\right)+\rho D\frac{\partial \xi}{\partial x_l}\frac{\partial^2 Q(\xi)}{\partial \eta \partial x_l} \\ +\rho D\frac{\partial^2 \xi}{\partial x_l^2}\frac{\partial^2 Q(\xi)}{\partial \eta^2}+\frac{\partial}{\partial x_l}\left(\rho D\frac{\partial Y''}{\partial x_l}\right)+\frac{\partial Q(\xi)}{\partial \eta}\frac{\partial}{\partial x_l}\left(\rho D\frac{\partial \xi}{\partial x_l}\right)\end{aligned} \tag{2.40}$$

(2.38), (2.39), and (2.40) into the transport equation for scalar Y (2.19), we obtain:

$$\rho w = \rho \frac{\partial Q(\xi)}{\partial t} + \rho u_l \frac{\partial Q(\xi)}{\partial x_l} - \rho\chi \frac{\partial^2 Q(\xi)}{\partial \eta^2} - \frac{\partial}{\partial x_l}\left(\rho D \frac{\partial Q(\xi)}{\partial x_l}\right) - \rho D \frac{\partial \xi}{\partial x_l}\frac{\partial^2 Q(\xi)}{\partial \eta \partial x_l} + \rho \frac{\partial Y''}{\partial t} + \rho u_l \frac{\partial Y''}{\partial x_l} - \frac{\partial}{\partial x_l}\left(\rho D \frac{\partial Y''}{\partial x_l}\right) \tag{2.41}$$

Taking the conditional expectation of equation (2.41), as defined by equation (2.36), the following three equations may be derived, representing the unclosed form of the CMC formulation.

$$\langle \rho | \eta \rangle \frac{\partial Q}{\partial t} + \langle \rho u_l | \eta \rangle \frac{\partial Q}{\partial x_l} = \langle \rho w | \eta \rangle + \frac{\partial^2 Q}{\partial \eta^2} \langle \rho\chi | \eta \rangle + e_Q + e_Y \tag{2.42}$$

where:
$$e_Q = \left\langle \frac{\partial}{\partial x_l}\left(\rho D \frac{\partial Q}{\partial x_l}\right) + \rho D \frac{\partial \xi}{\partial x_l}\frac{\partial^2 Q}{\partial \eta \partial x_l} \middle| \eta \right\rangle \tag{2.43}$$

and:
$$e_Y = -\left\langle \left(\rho \frac{\partial Y''}{\partial t}\right) + \rho u_l \left(\frac{\partial Y''}{\partial x_l}\right) - \frac{\partial}{\partial x_l}\left(\rho D \frac{\partial Y''}{\partial x_l}\right) \middle| \eta \right\rangle \tag{2.44}$$

Here, modelling strategies are required for equations (2.43), (2.44), and also the conditional expectations $\langle \rho u_l | \eta \rangle$, $\langle \rho w | \eta \rangle$, and $\langle \rho\chi | \eta \rangle$. Klimenko and Bilger's analysis (1999) states that e_Q can be neglected when the Reynolds number is large and the effects of differential diffusion are absent, due to it being of the order Re^{-1}. The main closure hypothesis employed in the decomposition method is for the term e_Y, which is modelled as:

$$e_Y = \frac{\frac{\partial}{\partial x_l}\left(\langle \rho | \eta \rangle \langle u_l'' Y'' | \eta \rangle P(\eta)\right)}{P(\eta)} \tag{2.45}$$

The chemical source term is closed under the assumption that fluctuations around the conditional mean mass fractions are small, hence detailed chemical mechanisms may be incorporated into calculations via the Arrhenius law. The representation of this term, and also of the conditionally averaged scalar

dissipation and velocity, may be undertaken by a number of approaches. These issues shall be further considered in Chapter 3.

Finally, the density weighted conditional moment closure equation takes the form:

$$\langle \rho|\eta\rangle \frac{\partial Q}{\partial t} + \langle \rho u_l|\eta\rangle \frac{\partial Q}{\partial x_l} + \frac{\frac{\partial}{\partial x_l}\left(\langle \rho|\eta\rangle \langle u_l'' Y''|\eta\rangle P(\eta)\right)}{P(\eta)} - \langle \rho\chi|\eta\rangle \frac{\partial^2 Q}{\partial \eta^2} = \langle \rho w|\eta\rangle \tag{2.46}$$

where the first term represents the transient contribution, and the following two terms the effects of convection, the latter being due to conditional fluctuations. The last term on the left hand side reflects diffusion in conserved scalar space, and the right hand side term the chemical source.

For the case of identical diffusion coefficients and low Mach number flow, the governing enthalpy equation takes the form of the conditional scalar conservation equation. Further simplification of assuming no radiative heat loss, leads to the following form of the CMC equation for enthalpy Q_h:

$$\langle \rho|\eta\rangle \frac{\partial Q_h}{\partial t} + \langle \rho u_l|\eta\rangle \frac{\partial Q_h}{\partial x_l} + \frac{\frac{\partial}{\partial x_l}\left(\langle \rho|\eta\rangle \langle u_l'' h''|\eta\rangle P(\eta)\right)}{P(\eta)} - \langle \rho\chi|\eta\rangle \frac{\partial^2 Q_h}{\partial \eta^2} = 0 \tag{2.47}$$

Derivation From The Transported pdf Equation:

Klimenko begins his derivation under the assumption of high Reynolds number flow, where a simplified form of the joint pdf equation (2.25) may be defined for P as a function of φ and η, as equation (2.48). Here, φ represents the sample-

$$\frac{\partial}{\partial t}\left(\langle\rho|\eta\rangle P\right)+\frac{\partial}{\partial x_l}\left(\langle\rho u_l|\varphi,\eta\rangle P\right)+ \frac{\partial^2}{\partial\varphi\partial\eta}\left(\left\langle\rho D\frac{\partial Y}{\partial x_l}\frac{\partial\xi}{\partial x_l}\middle|\varphi,\eta\right\rangle P\right)=-\frac{\partial}{\partial\varphi}\left(\langle\rho w|\varphi,\eta\rangle P\right) \tag{2.48}$$

space variable of the reactive scalar Y. Multiplication of this equation by φ, and integrating over all φ results in equation (2.49), where j_Y represents the net

$$\frac{\partial}{\partial t}\left(\langle\rho|\eta\rangle QP(\eta)\right)+\frac{\partial}{\partial x_l}\left(\langle\rho u_l Y|\eta\rangle P(\eta)\right)=\langle\rho w|\eta\rangle P(\eta)+\frac{\partial j_Y}{\partial\eta} \tag{2.49}$$

diffusive flux of the reactive scalar Y due to small scale diffusion processes in conserved scalar space, as given by equation (2.50). This term is unclosed, and to

$$j_Y\equiv 2\left\langle\rho D\left(\frac{\partial Y}{\partial x_l}\frac{\partial\xi}{\partial x_l}\right)\middle|\eta\right\rangle P(\eta)-\frac{\partial}{\partial\eta}\left(\langle\rho\chi Y|\eta\rangle P(\eta)\right) \tag{2.50}$$

proceed, requires modelling. Klimenko achieves this by establishing a diffusion approximation for the term under the assumption that particle diffusion in conserved scalar space can be considered a Markov process, *videlicet*:

$$j_Y=-\langle\rho\chi|\eta\rangle\frac{\partial P(\eta)}{\partial\eta}Q+\langle\rho\chi|\eta\rangle\frac{\partial Q}{\partial\eta}P(\eta) \tag{2.51}$$

Substitution of equation (2.51) into the unclosed equation (2.49) yields the basic CMC equation. A subsequent manipulation of the pdf equation (2.48) and substitution into this form provides the CMC equation as defined earlier in Bilger's derivation as equation (2.46).

The reader may notice similarities between the unsteady flamelet model and the CMC model. These manifest themselves mainly in appearance alone, a major observation being the flamelet model having originally been derived asymptotically for a thin reaction zone, and the CMC method being constructed as a set of global equations. A recent informative work, discussing this and other

relationships between the approaches can be found in Klimenko (2001) where in addition, the author suggests a new co-ordinate invariant form of the flamelet model, drawing comparisons with the CMC derivation in the process.

Application of CMC:

Turbulent Jet Diffusion And Bluff-body Flames: The greatest proportion of work involving CMC was initially concerned with turbulent jet diffusion flames, whether it be an attempt at numerical simulation, or their use for verification during model and sub-model development. One of the first applications can be found in Smith et al (1992), being focussed on the prediction of NO_x emission levels in H_2 flames to demonstrate the model's abilities to make accurate predictions in flames far from extinction. Smith et al (1992) apply the simplified parabolic form of the CMC equation (see Chapter 3.i) and use the PDF predictions of Chen and Driscoll (1991) as a comparison, concluding that the former was in better agreement with experimental findings due to the incorporation of a much more comprehensive reaction mechanism. Smith (1994) furthers this discussion in his doctoral thesis, and Bilger (1993b) concludes that in flames far from extinction such as those discussed, closure of the conditional moments of the chemical source can be made with first-order approximations without a great loss of accuracy. Smith et al (1995) further the work of Smith et al (1992) by the implementation of density-coupled calculations, and an optically thin radiation model. The overprediction of NO emission levels lead to a suggestion for the need of a second-order closure (see Chapter 4) of the chemical production terms. The issue of second order closure is addressed by Kronenburg

et al (1998), and applied to the H_2/He flames of Barlow and Carter (1994, 1996). Although improvement in predictive ability is found in the far-field locale, discrepancy with experimental data is not entirely accounted for. In a further comparative study of CMC and PDF performance, Barlow et al (1999) attribute the underprediction of NO by both models in the lower portion of the aforementioned flames to differential diffusion effects. This issue is addressed by Kronenburg and Bilger (1997, 2000a, 2000b), and subsequent improvements are made to the predictive ability of CMC.

As a means of model evaluation, H_2 flames provide excellent subject matter due to their relatively simple H_2/O_2 chemistry. An intermediate level of chemistry is provided in the combustion of oxygenated carbon compounds such as CO and CO_2. Using an identical approach to his H_2 jet modelling, Smith (1994) extends his study to $CO/H_2/N_2$ flames with notable success. Piloted jets of H_2/CO_2 have also been simulated in this manner by Roomina (1998) in his doctoral thesis. In all reported predictions of oxygenated carbon compound flames, major species are found to be well represented although discrepancies are found on the fuel-rich side of stoichiometric. Similar but more pronounced observations are made for minor and intermediate species, and lack of consideration of conditional fluctuations is generally accredited with being the cause.

A much more complex combustion chemistry is involved in the oxidation of hydrocarbons, and that of methane provides the simplest in this category (see Chapter 5). Roomina and Bilger (2001) present CMC calculations of the piloted methane flame of Barlow and Frank (1998) in which they investigate three chemical mechanisms, and their effects upon NO prediction. The importance of prompt NO representation in the mechanism used is noted, but a similar

overprediction of NO in far-field locale with earlier studies leads to the suggestion that second-order chemical effects require representation. Roomina (1998), and Roomina and Bilger (1999) extend their application of the parabolic CMC formulation to the chemistry of methanol diffusion flames with limited success. Once again, their observations of scatter data indicate a possible requirement for the inclusion of chemical conditional fluctuations, in addition to the introduction of differential diffusion and radial dependence to the calculations (see Chapter 3.i). Further discussion of the latter modelling issue can be found with reference to the elliptic regions of flow behind a bluff-body burner by Swaminathan and Dally (1998), and with reference to a hydrogen jet flame by Barlow and Carter (1996).

The elliptic form of the CMC equation is applied to a bluff-body stabilised methanol flame with more success by Kim et al (2000a). Discrepancies do still arise in calculations, and are attributed to similar phenomena as previously mentioned. Overall however, the elliptic calculations provide good agreement with experimental data, and outperform the stationary laminar flamelet model used as a comparison. Kim and Huh (2002a) also apply this methodology to the representation of a CH_4/H_2 bluff-body flame using three comprehensive chemical mechanisms with an emphasis on the prediction of NO formation. Again, they achieve notable success although fuel-rich side discrepancies are observable which are accounted for as uncertainties in with the chemical mechanisms. Kim et al (2000b) once again utilise the elliptic modelling technique for the prediction of autoignition of a turbulent methane jet, and find that major trends such as the dependence of ignition delay upon initial temperature observed in experimental

data are well reproduced by the CMC. It is once again suggested however, that a higher-order closure may be implemented to improve upon predictions.

Imperfectly Stirred Reactor: The possible applications of CMC do not lie solely in the realm of turbulent flames. Little work has been done to date regarding these possibilities, but some investigation has been undertaken. The imperfectly stirred reactor (ISR) is one such application, and is a generalisation of the perfectly stirred reactor. It is defined as a region of flow with simple boundaries, within which, the conditional average of species and temperature show little spatial variation, and the conditional variances of these means are shown to be small. For the modelling, all terms in the CMC equation are set to zero excepting the scalar dissipation and production-rate terms. Mobini (1998) modelled the head-end of a combustor using this technique but results were observed to be poor. The reasons for this however, were concluded as being a poorly predicted mixing field realised from an applied $k-\varepsilon$ model. Prior to this, Mobini et al (1995) also investigated the effect of pdf shape upon ISR modelling predictions, and found it had significant influence upon the results obtained. This research does perhaps indicate that a more elaborate modelling methodology should be adopted for the representation of such complex flows and geometries. Research regarding fully elliptic, three-dimensional solutions of similar burners is currently being undertaken by the author at the University of Leeds, in addition to the studies of Brizuela (2000) at the University of Buenos Aires.

Turbulent Reacting Plume: The main distinguishing feature of fire-plumes over turbulent jet flames is that they are driven by buoyancy rather than

momentum. Scalar dissipation rates are also observed to be small, and radiation levels can result in relatively large temperature decreases with height. Further to the study of Lee and Bilger (1995), Brown and Bilger (1996, 1998) studied a turbulent reactive plume of NO doped with O_3, using both experimental and calculated results to derive conclusions. NO enters at a point source three grid mesh lengths downstream of a turbulence grid, and has the same mean velocity as the flow, which contains about one part per million O_3. The CMC equations solved in the modelling of this arrangement omit the term for conditional turbulent flux. It was found that the predictions were relatively insensitive to values taken for the conditional scalar dissipation, and it was thus confirmed that the mixing term is less significant than the convection term in this type of flow. Importantly, it was verified that there is only a small variation in conditional averages across the flow, the range for the fluctuation of the conditional mean of NO concentration being around ±5%.

Considering the practical application of fire-plume modelling, Cleary et al (2002) recently present results of the elliptic CMC modelling of a buoyant, turbulent diffusion flame, burning under a hood. Here they address the issue of safety and the production of carbon monoxide in a situation such as a building or compartment fire. The geometry employed for the computational domain is a complex one, and the CMC model is seen to perform very well, displaying excellent predictive ability in conditions where reaction rates change considerably.

Modelling of Internal Combustion Engines: Autoignition of a hydrocarbon spray is one of the many important physical processes involved in the running of the

Internal Combustion (IC) engine. The accurate modelling of such is then quite evidently a much sought-after ability. With respect to CMC, relatively little work has been undertaken to date regarding this practical problem, although some works involving higher-order and double conditioning modelling of autoignition phenomena is described in the next section. However, a step closer to a realistic calculation of an IC chamber is made by Kim and Huh (2002b) in which a first-order CMC is applied to the autoignition of an n-heptane spray. Here, a number of approaches are investigated to represent the evaporation terms in the conditional species and scalar variance equations. The authors obtain reasonable agreement between the calculated and the measured ignition delay times under differing initial temperatures, and show that they are dependent upon the accumulation of effects of spray development, and chemical reactions combined with turbulence.

Higher Order And Double Conditioning Modelling: Using a reduced two-step mechanism for hydrocarbon combustion, Swaminathan and Bilger (1999a) conduct direct numerical simulations, and find that first-order CMC overestimates the rate of the fuel-consuming step in flows with non-negligible fluctuations of temperature and species mass fractions. Further discrepancies are found in a similar study of a fully compressible direct numerical simulation by Bushe et al (1999). This, along with previous evidence, has lead to second-order CMC studies being undertaken by Kronenburg et al (1998) as discussed earlier, and more recently, application to extinction and reignition phenomena in hydrocarbon fuel by Kim et al (2002b). Here, they observe improved predictions over the first-order model, primarily on the fuel-rich side of sample space, which

is to be expected with reference to the results obtained from the aforementioned direct numerical simulations. Second-order CMC for autoignition is developed by Mastorakos and Bilger (1998) alongside the study of the balance equations for conditional variance and covariance (Swaminathan and Bilger 1998, 1999b), and Chapter 4 should be consulted for further discussion regarding this topic. Cha and Pitsch (2002) can be referred to for an informative paper in which direct numerical simulation data is used to evaluate performance of higher-order CMC approaches, including third-order representation in the case of higher moment models in addition to the presumed conditional pdf approach. It is noted that first and second-order modelling is insufficient to describe conditional means in the presence of moderate levels of extinction, and third moments are required. However, second moment information is sufficient to describe extinction and reignition effects if the presumed beta-pdf model is used, and is in fact the approach applied in the later chapters of this present work. In addition, an interesting approach is proposed in Bradley et al (2002), who apply a hybrid of flamelet modelling and second-order CMC closure with some success to the piloted CH_4/air jet flames of Barlow and Frank (1998) which display significant extinction and re-ignition phenomena.

Doubly-conditional moment closure has perhaps received the least attention in recent studies of CMC modelling strategies. In his doctoral thesis, Bushe (1995) implements both single and doubly-conditional methods in the investigation of n-heptane/air mixtures. He demonstrates that autoignition is better represented by the introduction of a second conditioning variable, in this instance being the rate of strain, and effects solution of the species equations in three-dimensional (t,η,χ) space. More recently, Cha et al (2001) apply a doubly-conditional

strategy to represent extinction and reignition phenomena in the piloted methane/air flame of Barlow and Frank (1998). In this comparative study of singly and doubly-conditional approaches, the former method is observed as being inadequate to describe the combustion phenomena. The consideration of the effects of a second conditioning variable, once again being the scalar dissipation, describes extinction well but predicts the onset of reignition too early. Weakness in the new model is once again predictably attributed to non-insignificant fluctuations around the doubly-conditional mean scalar values, but an overall improvement in results is observed.

2.ii.iii Direct Numerical Simulation And Large Eddy Simulation

Direct Numerical Simulation (DNS), in contrast to the averaging methods implemented in turbulence modelling, attempts to resolve all time and spatial scales of the flow in question. This is of particular interest when investigating transient flows where the averaging process may obscure most of the important characteristics of the solution. Also, the DNS of the governing equations offers an alternative to expensive methods for the acquisition of data for model validation. Examples of DNS being used in the validation of CMC techniques can be found in a number of texts such as those of Mell et all (1993), Brethouwer and Nieuwstadt (2001), and Sreedhara and Laksmisha (2002). The drawback lies, however, with the large computational expense. The solutions this method provides are very accurate, but the method is not practical for the majority of

computational fluid dynamic applications due to high Reynolds number being a restrictive parameter. That said, with the advent of increasingly superior computing facilities, DNS is becoming a more investigated tool, and has featured in a number of recent articles. As far back as eight years ago, Baum et al. (1994) carried out a successful demonstration of DNS calculations of $H_2/O_2/N_2$ flames with complex chemistry in two-dimensional turbulent flow. More recently, Montgomery, Kosály, and Riley (1997) reported three-dimensional calculations of turbulent nonpremixed combustion using multistep H_2/O_2 kinetics. The progression in complexity of calculation is the DNS of hydrocarbon combustion and Bédat, Fokion, and Poinsot (1999) demonstrate DNS calculations of methane-air flames using four-step chemistry in both two-dimensional and three-dimensional flow.

A compromise of these two *modus operandi* is Large Eddy Simulation (LES). For a more detailed appraisal of this technique than is offered here, the reader is referred to the review paper of Lesieur and Métais (1996). Originally implemented in the nineteen-seventies for the purpose of atmospheric modelling, LES seeks to directly solve for the larger energy-containing scales, whilst modelling the smaller scales that contain only a small fraction of the turbulence kinetic energy. An eddy-viscosity model is commonly employed for this purpose. This resulting hybrid methodology involves the filtering of the Navier-Stokes equations so as to separate the scales into two groups, and then the subsequent relevant solution procedure.

To date, there have been few documented large eddy simulations of turbulent nonpremixed flames, and even less of their premixed counterparts. Recently, Pitsch and Steiner (2000) showed very good agreement with experimental data

for temperature and species predictions, including OH and NO, in a piloted turbulent methane diffusion flame (Sandia flame D). Here, the conservation equations for mass, momentum, and mixture fraction were solved using LES, and the transport of reactive scalars modelled using a Lagrangian Flamelet Model (LFM). A recent study of Steiner and Bushe (2001) is also of particular interest to this thesis. In their paper, a turbulent methane-air flame is investigated using LES, the notable feature being the implementation of Conditional Source-term Estimation (CSE) (Bushe and Steiner, 1999) to close the chemical source terms occurring in the species and enthalpy equations. This method is based on the CMC theory, and furthers validation of the feasibility of CMC for LES.

Jones (2002) presents results of LES calculations, applying the 'fast-chemistry' approximation to the modelling of a jet diffusion flame of hydrogen, and reports results of good agreement with experimental data. The author also takes a step forward with respect to furthering the practical application of LES by describing a calculation of a gas-turbine combustor using 1.25 million grid nodes, with a laminar flamelet assumption invoked to model the combustion. Blin et al (2003) may also be consulted for a recent application of LES to practical systems. Here, the authors consider LES over curved surfaces in their elucidation of turbulent behaviour within thrust-reversers for aircraft design applications. A detailed study of LES approaches applied to turbulent non-premixed hydrogen flames can also be consulted in Branley and Jones (2001), in which is presented a comprehensive investigation of sub-grid scale models and their interactions.

3: First Order Conditional Moment Closure Modelling of Hydrogen Jet Diffusion Flames

In this, the first part of an in-depth study of the performance of Conditional Moment Closure Models, the simplest form of the CMC equation is implemented in the prediction of three turbulent jet diffusion flames of hydrogen with varying degrees of helium dilution. For each flame, studies are carried out using both the $k-\varepsilon$ and Reynolds stress closures for the non-reacting field predictions. In addition, three kinetics schemes of varying degrees of complexity are implemented to analyse the effect upon reactive scalar predictions.

In addition to a description of how the flow field is represented and hence how the turbulence-chemistry interaction described, the following text defines the CMC equations utilised, the models used for unclosed terms, and the methods of solution applied. These methods have been developed for application to turbulent non-premixed jet flames of varying composition, geometries, and vector quantities. The treatment of premixed jet flames in the case of CMC modelling has not been considered in this study, but preliminary investigation can be found by the authors Swaminathan and Bilger (2001). They conclude in their work that CMC is well suited application to such problems, and their study additionally

includes an analysis of sub-models, using a direct numerical simulation database for validation purposes.

Later chapters extend the complexity of the CMC model, by investigating higher-order representation of conditional species production terms, and subsequently its application to flows displaying more complex flow patterns and physical phenomena.

3.i Experimental Data And Description of The Flames

The three flames used for model evaluations have been well documented by Barlow and Carter (1994, 1996). Using simultaneous Raman scattering, Rayleigh scattering, and Laser Induced Fluorescence (LIF), experimental data have been collated representing point values of O_2, N_2, H_2, H_2O, OH, NO mass fractions, temperature, mixture fraction, and corresponding root-mean-square values of fluctuations. In addition to this, conditional and Favre averaged data have also been made available. Also, works by Schlatter et al (1996) have produced complimentary velocity measurements by means of Laser Doppler Velocimetry (LDV), thus providing a comprehensive set of experimental data archives (Combustion Research Facility, Sandia National Laboratories 2002).

The three flames' parameters are highlighted in Table (3.1), where A represents a 100:0 H_2:He flame, B an 80:20 H_2:He flame, and C a 60:40 H_2:He flame. From here onwards, each flame shall be referenced respectively. This set of progressively diluted hydrogen flames proves to be an interesting test case, and subsequently, results shall be discussed in light of physical phenomena encountered in these instances. As can be seen from Table (3.1), flame C is operated at a reduced Reynolds number. This is to avoid the occurrence of lift-off, and associated phenomena.

Experimental Setup:

The experimental rig used at the Turbulent Diffusion Flame Laboratory is pictorially represented as Figure (3.1). The Raman/Rayleigh scattering measurement system consists of two doubled Nd:YAG lasers, and the LIF system of three Nd:YAG-pumped dye lasers. For investigation of the hydrogen flames in question, a 532nm flashlamp-pumped dye laser was employed for the Raman/Rayleigh measurements, and two Nd:YAG-pumped dye laser systems (285nm and 226nm) for the OH and NO fluorescence measurements. The three laser beams are combined on to a common axis via two dichroic mirrors, and focussed into the test section.

The burner itself consists of a straight tube of inner diameter 3.75mm, seated at the exit plane of a vertical wind tunnel, providing a constant coflow of air at a velocity of $1ms^{-1}$. A more detailed description of the apparatus, detection methods, and analytical treatment of the data can be found in references Barlow and Carter (1994, 1996).

3.ii Prediction of Flow-field And Turbulence Quantities

It can be seen from the CMC derivations in Chapter 2, the velocity field and the scalar dissipation are important parameters in the equation formulation. The scalar dissipation represents the turbulent mixing through k and ε, which are derived from flow-field calculations, in addition to velocity data. Also, as discussed previously, predictions of a conserved scalar (the mixture fraction) and its variance are also required to construct a statistical description of the flow at any defined location.

The flow and mixing fields in the subsequent calculations are resolved separately from the chemistry, using a version of the GENMIX code (Spalding 1977) modified for this purpose by the author. By proceeding in this manner, it is implied that turbulence will affect the chemistry, but heat release due to the combustion reactions has none or little effect upon the flow-field. This method of calculation is adopted due to its ease of use and speed during evaluation procedures. Sample calculations have been conducted in which density coupling is used between the flow-field and chemistry calculations, and are subsequently described in Chapter 5. It can be observed that no notable bss in accuracy is effected due to the aforementioned methodology. Closure of the mean density term is still required however, and is achieved using a prescribed beta-pdf and instantaneous values of density as a function of mixture fraction, derived from

adiabatic equilibrium calculations based on the three kinetics schemes described later in this chapter. The beta-pdf is a two-parameter distribution, and a standard model used to describe a random variable (Ross 1984). With respect to mixture fraction and its variance, the pdf can be defined by equation (3.1).

$$\tilde{P}(\eta) = \frac{\eta^{\alpha-1}(1-\eta)^{\beta-1}}{\int_0^1 \eta^{\alpha-1}(1-\eta)^{\beta-1}\,d\eta} \tag{3.1}$$

where: $\alpha = \tilde{Z}\left(\frac{\tilde{Z}(1-\tilde{Z})}{\widetilde{Z''^2}} - 1\right)$ $\beta = \frac{(1-\tilde{Z})}{\tilde{Z}}\alpha$

This model is widely used in the fields of turbulence and combustion modelling, and also throughout this present work. Further discussion shall be made regarding issues surrounding this model in later chapters. In all cases, predicted flow fields are founds to be insensitive to the particular kinetics scheme employed, with the influence of radiation heat loss on prescribed densities also having negligible effect on the flow field calculations.

Resolution of the fields is achieved via the solution of the two-dimensional axisymmetric forms of the density-weighted, fluid-flow equations, supplemented with the $k-\varepsilon$ model in the first instance, and with a second-moment Reynolds stress/scalar flux closure (RSSF) in the second. The reader is referred to the Appendix for the formulation of the equations solved in Cartesian tensor notation. The constants employed in the $k-\varepsilon$ model are standard (Jones and Launder 1972), excepting the instance of $C_{\varepsilon 1}$ which is modified according to the expression suggested by Morse (1977), and defined as equation (3.2), to improve prediction of spreading rate for flame A.

$$C_{\varepsilon 1} = 1.4 - 3.4\left(\frac{k}{\varepsilon}\frac{\partial \tilde{u}}{\partial x}\right)_{cl}^{3} \tag{3.2}$$

For flames B and C, the standard value of $C_{\varepsilon 1}$ is modified to 1.6 (Roekaerts and Teerling 2000). The Reynolds stress model employed is that reported by Jones and Musonge (1988), with the value of $C_{\varepsilon 1}$ again modified in line with the values employed in the eddy-viscosity based approach for all three flames. For the mixture fraction field, an improved version of the scalar flux closure is implemented, as described by Fairweather et al (1992). Equation sets for both the $k-\varepsilon$ and RSSF models are modified to account for buoyancy contributions, although such effects were found to be negligible in the high Reynolds-number flows considered. In both cases, equations are solved in conjunction with the conservation equations for the mean and variance of mixture fraction, as given by equations (1.29) and (1.30).

3.ii.i Mathematical Procedure

The GENMIX code applies a marching integration approach to simulate the parabolic flow-field of interest, in which the conservation equations are cast in the $x \sim \vartheta$ or Von Mises coordinate system. This in effect scales the y spatial coordinates to account for the width of the boundary layer being modelled. The variable ϑ is referred to as a stream function, and is related to the axial velocity of the fluid, the distance separating two streamlines, and the fluid density, *id est*:

$$\vartheta - \vartheta_{axis} = \int_0^y r\bar{\rho}\tilde{u}dy \tag{3.3}$$

where $y = 0$ at the symmetry axis. The equation set is further transformed onto the $x \sim \omega$ or Patankar-Spalding coordinate system. The relation between ϑ and ω can be described as:

$$\omega = \left(\vartheta - \vartheta_{axis}\right) \Big/ \left(\vartheta_{cg} - \vartheta_{axis}\right) \tag{3.4}$$

which has the effect of normalising the cross-stream variables over the width of the boundary layer. This method produces a computational grid system, which is restricted in size to the width of the flow, and is hence a very economical approach. Also, unlike Cartesian systems, it permits a higher density of grid points to be evaluated in the thinner parts of the boundary layer. Figure (3.2) depicts the form of the computational mesh described by these procedures.

The general form of the differential equations solved now takes the form:

$$\frac{\partial \Phi}{\partial x} = \frac{\partial}{\partial \vartheta}\left(r^2 \bar{\rho} \tilde{u} \Theta_{\Phi,eff} \frac{\partial \Phi}{\partial \vartheta} \right) + \frac{1}{\bar{\rho}\tilde{u}} S_{\Phi} \tag{3.5}$$

with the subsequent Patankar-Spalding transformation leading to:

$$\frac{\partial \Phi}{\partial x} + \left(a + b\omega\right)\frac{\partial \Phi}{\partial \omega} = \frac{\partial}{\partial \omega}\left(c \frac{\partial \Phi}{\partial \omega} \right) + d \tag{3.6}$$

where: $$a = \frac{-1}{\left(\vartheta_{cg} - \vartheta_{axis}\right)} \frac{\partial \vartheta_{axis}}{\partial x} \quad b = \frac{-1}{\left(\vartheta_{cg} - \vartheta_{axis}\right)} \frac{\partial}{\partial x}\left(\vartheta_{cg} - \vartheta_{axis}\right)$$

$$c = \frac{r^2 \bar{\rho} \tilde{u} \Theta_{\Phi,eff}}{\left(\vartheta_{cg} - \vartheta_{axis}\right)^2} \qquad d = \frac{1}{\bar{\rho}\tilde{u}} S_{\Phi}$$

Numbering the terms of equation (3.6) consecutively from left to right, term 1 represents the effect of longitudinal convection, term 2 that of lateral convection, term 3 the effect of viscous action or diffusion, and term 4 the effect of generation or destruction.

Here, another benefit of the coordinate system reveals itself; the simplicity of the term $\left(a + b\omega\right) \partial\Phi / \partial\omega$ being a major advantage of the method. In this form, $\left(a + b\omega\right)$ is a function of ω alone, but had another normalising transformation

been applied, such as $\omega \sim y/y_{cg}$, it would have involved an integral over ω of the forward velocity. In addition to computational expense, it comes to light that this velocity would have to be guessed before it could be calculated, thus creating the need for further mathematical procedure.

For further reading, a detailed description of the Patankar-Spalding methodology and equation derivation can be found in Spalding (1977).

3.ii.ii Numerical Methods

GENMIX applies an implicit formula in the stream-wise direction and a hybrid-differencing scheme in the cross-stream direction for its marching integration procedure. The hybrid scheme results in a central-differencing scheme if diffusive processes are overwhelming, and an upwind scheme if convection dominates. The implicit method allows free choice of the integration step without having to be overly concerned with numerical stability of the system. This is a major advantage over explicit methods, which can require very many forward steps to cover large grid spacing, as to avoid instability, the ratio of ∂x to ∂y must remain below a critical value. The implemented method provides more troublesome equations to solve, but the aforementioned advantage far outweighs this. The following describes the numerical integration procedure implemented in the GENMIX code.

Considering the general dependent variable Φ at stream-node i, the linear four-node implicit formula implemented within the code takes the form:

$$D_i\Phi_{i,D} = A_i\Phi_{i+1,D} + B_i\Phi_{i-1,D} + C_i\Phi_{i,U} + S_{i,D} \qquad (3.7)$$

where the terms $C_i\Phi_{i,U}$ and $S_{i,D}$ are already known, and A_i, B_i, C_i, and D_i are constants evaluated from the integration of the differential equations over the control volume surrounding the point defining Φ_i. Figure (3.3) illustrates the derivation of this formula. These constants can be represented by quantities that are known at the upstream stations, thus providing a system of coupled linear equations. An initial profile of scalar values is required to begin this procedure, and subsequently, values at the two boundaries (free and axisymmetric), which are not specified from the forward march. Outflow boundary values are not required as they are produced as the solution of the integration process itself.

This set of equations can now be converted by manipulation, and solved by implementation of the tri-diagonal matrix algorithm (TDMA), being a form of the well-known Gaussian-elimination technique. Further discussion regarding the TDMA and its application can be found in Roache (1972).

3.ii.iii Solution Domain And Initial Conditions

Numerical solutions are obtained using expanding finite-difference meshes, and in all cases grid-independent solutions are established using resolutions in excess of one million nodes. The distribution of these nodes is 300 in the radial direction, and upward of 3500 in the streamwise direction. The precise number of nodes in the streamwise direction varies for each flame studied due to the differing visible flame lengths being specified as a dimension of the computational domain. For flows A, B, and C, these are 180, 150, and 100 nozzle diameters respectively. The highest concentration of nodes is located at the

inflow of the domain, with grid spacings of the order of 0.01 mm, and the lowest at the outflow boundary with spacings of the order of 0.5 mm. Initial boundary conditions are prescribed as follows:

Inflow Boundary:

All fluid flow and turbulence quantities must be known and prescribed along this boundary as initial conditions, and are defined as:

Mixture fraction: Assigned a value of 1 for the fuel stream, and 0 for the oxidiser stream.

Mixture fraction variance: Assigned a value of 0 for all inflow locations.

Pressure: Assumed to be one standard atmosphere.

Axial velocity: Flat mean velocity profiles are prescribed for both the nozzle exit and the co-flowing stream. The validity of this approach was verified by running sample calculations using profiles derived from the Blasius one-seventh power law, *id est*:

$$\frac{u}{u_{cl}} = \left(\frac{r}{0.5d} \right)^{1/7} \tag{3.8}$$

It was found that results obtained from the application of these two methods were comparable.

Turbulence kinetic energy: Profiles are defined using a relationship based upon the experimental data of Hinze (1975), *videlicet*:

$$k = 0.0027u^2 \tag{3.9}$$

Turbulence kinetic energy dissipation: Assuming the turbulence length-scale in a pipe to be equivalent to the pipe diameter, then the kinetic energy dissipation can be prescribed as:

$$\varepsilon = \frac{k^{3/2}}{0.5d} \tag{3.10}$$

Reynolds Stresses: Application of the Reynolds stress model requires specification of the individual stresses to perform calculations. Both normal stresses $\widetilde{u''u''}$ and $\widetilde{v''v''}$ can be approximated from their defining relationship, *id est*:

$$k = \frac{1}{2}\left(\widetilde{u_i''u_i''}\right) \tag{3.11}$$

and the shear stress $\widetilde{u''v''}$ is prescribed a value of zero.

Symmetry Boundary:

Boundary conditions of scalar and vector components at the axis of symmetry are obtained via the setting of gradients to zero across this region, and hence prescribed profiles are not a requirement of initialisation. In addition, the value of the velocity component normal to the axis is assigned a value of zero.

Free Boundary:

Values of variables in this region of the domain are prescribed by the code via entrainment calculation and the definition of the co-flowing oxidising stream obtained from the inlet conditions.

3.ii.iv Results And Discussion

The following text presents the results of the mixing and flow-field calculations of the three H_2/He turbulent jet diffusion flames using two forms of turbulence model. All calculations were performed on an SGI workstation with a CPU clock-speed of 220 MHz, and took not in excess of four hours.

Figures (3.4-3.6) depict the predicted mixture fraction radial profiles at several locations within the respective flames A, B, and C. As mentioned earlier, the flow field is calibrated to obtain the best spreading rate along the flame length. This method of radially fitting the data has been chosen in preference to that of fitting the axial centreline profile as employed by Barlow et al (1999), in order to optimise the turbulent flow-field predictions to permit a more direct evaluation of the CMC model. These two methods provide a comparable set of results, although the radially fitted data do display slightly better agreement with experimental observations. With reference to Figure (3.4), the RSSF model is seen to over-predict the near-axis mixture fraction at the first two measuring stations, although results further downstream are in good agreement with the data. Results derived from the eddy-viscosity based approach are in good agreement with data at all axial locations. Figures (3.5, 3.6) display similar results for the flames B and C, although in these cases, improved agreement between the RSSF model and experiment is observed close to the nozzle. Mixture fraction predictions of the RSSF model are comparable to those made using a second-order turbulence closure with standard constants by Lindstedt and Vaos (2001) in their consideration of flame A with a transported-pdf combustion model. It may be observed by comparison, that the adjustments to constants

made in the present work, although improving the centreline decay prediction, has effected a slight increase in the spread of the profile over the experimental data values. Also, their approach shows improved near-field mixture fraction predictions, but accuracy in the regions further away from the nozzle is sacrificed by its application. Figures (3.7-3.9) show the root-mean-squared mixture-fraction predictions for the respective three flames. Both turbulence models proffer a similar level of agreement with experimental data, the RSSF model generally displaying a slight over-prediction, and the k-ε a slight under-prediction. Trends in the calculated values are however observed to be in concordance with the deviations from experimental evidence seen in the mixture-fraction fields.

Results for the velocity field were found to be comparable with those of previous investigations (Barlow et al 1999) for both turbulence closures, and are depicted in Figures (3.10-3.12) for the respective calculations. The RSSF model however, is seen to provide qualitatively and quantitatively superior results in determination of the $\widetilde{u''u''}$ and $\widetilde{v''v''}$ normal-stresses in all three flames, over its k-ε counterpart as indicated by Figures (3.13-3.18). This observation is further compounded by Figure (3.19), depicting radial profiles of turbulence kinetic energy of flame A. The RSSF model does overpredict this quantity at the measuring station closest the nozzle exit, but this is still in agreement with the previously made observations. Prediction of the $\widetilde{u''v''}$ shear stress in flames B and C are shown in Figures (3.20, 3.21). A similar level of qualitative agreement between the models is noted, with an over-prediction recorded at all measuring stations in the near-field and quantitatively accurate results being obtained at axial locations in excess of fifty nozzle diameters. In Obieglo et al's (2000) study of flame A, the authors apply the k-ε model for the mixing-field resolution,

making use of the Pope correction (Pope 1978) to account for the axisymmetric round-jet anomaly, and keeping all other constants standard. Interestingly, at near nozzle locale, they report very similar qualitative results in the prediction of turbulence quantities as observed in the present study made using the $C_{\varepsilon 1}$ modification, verifying the common characteristics of the model employed.

3.iii Prediction of Species: First Order, One Dimensional, CMC Model

The derivation of the CMC equations defining the production and transport of the conditionally averaged scalars and enthalpy has previously been presented in Chapter 2, and equation (2.42) represents the unclosed, elliptic form. Considering the hydrogen jet flames to be modelled, which are parabolic flows in nature, simplifying assumptions can be applied to this equation as outlined by Klimenko and Bilger (1999). Firstly, terms corresponding to macro-transport by molecular diffusion can be neglected in the case of large Re as the diffusion coefficient can be assumed to be small. Secondly, in flows without stabilisation regimes, the turbulent flux contribution may be neglected. Assuming the flow to be axisymmetric in the mean, the dependence of Q and Q_h on radial location can thus be assumed negligible, and the dimensionality of the problem reduced. The parabolic, one-dimensional transport equations for species mass-fraction and enthalpy then respectively become:

$$\langle \rho u | \eta \rangle \frac{\partial Q}{\partial x} - \langle \rho \chi | \eta \rangle \frac{\partial^2 Q}{\partial \eta^2} = \langle \rho w | \eta \rangle \tag{3.12}$$

$$\langle \rho u | \eta \rangle \frac{\partial Q_h}{\partial x} - \langle \rho \chi | \eta \rangle \frac{\partial^2 Q_h}{\partial \eta^2} = \langle \rho w_h | \eta \rangle \tag{3.13}$$

However, it has been shown experimentally (Barlow and Carter 1996), and further supported by the asymptotic analysis of Klimenko (1995), that a certain degree of radial dependence is displayed in the jet flames considered. Hence, the

method of cross-stream averaging for conditional velocity and scalar dissipation is applied as defined by Klimenko (1990). To obtain these values, an averaging operator is defined for cylindrical coordinates, using an arbitrary function f, with R defined as a characteristic radius *id est*:

$$(f)_R \equiv \frac{2}{R^2}\int_0^R f(r) r dr \tag{3.14}$$

its application being subsequently described.

3.iii.i Closure of The CMC Equation

Inspection of equations (3.12, 3.13) reveals three common terms that require an approach to closure. Enclosed in angular brackets, these are the conditional axial velocity $\langle u|\eta \rangle$, the conditional scalar dissipation $\langle \chi|\eta \rangle$, and the conditional source term $\langle w|\eta \rangle$. The approach used to represent these terms in subsequent calculations is discussed, along with some other common formulations, in the following text. It should be noted however, that consideration could be given to these issues in the form an individual doctoral thesis, and so is out of the scope of these present works to provide an in depth analysis of said methodologies.

3.iii.i.i Conditional Axial Velocity

A number of approaches to the modelling of conditional axial velocity have been implemented in previous CMC studies. In the present study, three such methods

were investigated, with the observation being made that the impact upon final results of model variation is negligible.

In early works, such as that of Smith et al (1992), the conditional averages are approximated as being the unconditional averages at the same axial location, but at the radial position to which the mixture fraction equals the value of the conditioning variable (η). Further works (Smith et al 1995, Kronenburg et al 1998, Barlow et al 1999) apply the assumption that there exists only a very weak conditional correlation of velocity-density fluctuations about the unconditional mean, and employ the approximation:

$$\langle u|\eta\rangle_R = \frac{\left(\tilde{u}(r)\tilde{P}(\eta,r)\right)_R}{\left(\tilde{P}(\eta,r)\right)_R} \tag{3.15}$$

to establish the cross-stream averaged conditional values. This is the method of calculation employed in the present works, being selected for its ease of incorporation into the current parabolic calculation procedure, in addition to its relative stability. A third method currently employed involves the development of a linear model of the form:

$$\langle u|\eta\rangle = \tilde{u} + \frac{\widetilde{u''Z''}}{\widetilde{Z''^2}}\left(\eta - \tilde{Z}\right) \tag{3.16}$$

which is approximated for example by Roomina and Bilger (2001) as:

$$\langle u|\eta\rangle \approx \tilde{u} + \left(\frac{k}{6\widetilde{Z''^2}}\right)^{1/2}\left(\eta - \tilde{Z}\right) \tag{3.17}$$

This model is valid as long as the velocity and the conserved scalar proffer a jointly Gaussian pdf; effectively meaning that their fluctuations are totally decorrelated. Equation (3.16) has been experimentally verified by Li and Bilger

(1994) and holds near the centreline of a turbulent jet, but fails near the shear-layer boundaries where the deviation $\left(\eta - \tilde{Z}\right)$ is large.

3.iii.i.ii Conditional Scalar Dissipation

Again, a wide range of strategies has been used in the modelling of the conditional scalar dissipation in previous studies. Its accurate modelling is however considered crucial to obtaining reliable predictions. The scalar dissipation has been previously defined in equation (2.28), and the simplest model previously applied to obtain its conditional values is employed by Smith et al (1992), and more recently by Cleary et al (2002) in the prediction of fires. In these works, the conditional values are approximated as the unconditional averages as described previously in the derivation of conditional velocity. This method is also implemented in Roomina (1998), where good agreement is shown with Girimaji's model (Girimaji 1992), which is discussed presently.

A rigorous method of evaluating $\langle \chi | \eta \rangle$ is implemented by Barlow et al (1999) and Roomina and Bilger (2001), where the conservation of mass within the conditionally averaged system of equations is ensured by the implementation of the steady-state cross-stream averaged mixture-fraction pdf transport equation. It is assumed that the mixture-fraction pdf at each radial location can be represented by a presumed form from its mean and variance. Barlow et al (1999) apply both a clipped Gaussian and a beta-pdf formulation to their calculations, and indicate that the differences between the resulting profiles are small. Further

extensive discussion regarding the use of this method can be found in Smith (1994).

An even more rigorous method of evaluation is prescribed by Girimaji (1992) in which consideration is made of possible radial dependencies throughout his derivation. Similarly to the previously described method, this relies on a double integration of the balance scalar transport equation in its formulation, and hence, although the pdf equation is not solved alongside the CMC equations, conservation of mass is achieved. It is in fact beneficial not to solve the transported pdf equation simultaneously due to complications arising from numerical difficulties in its integration. In his derivation, Girimaji (1992) uses the observation that over all stages of two-scalar, constant-density mixing in statistically stationary isotropic turbulence, the scalar pdf can be characterised by the presumed β-pdf. This observation being validated by earlier works of the same author (Girimaji 1991). From the pdf transport equation, Girimaji thus obtains equation (3.18) for

$$\langle \chi | \eta \rangle = -2\tilde{\chi} \frac{\tilde{Z}\left(1-\tilde{Z}\right)}{\widetilde{Z''^2}} \frac{I(\eta)}{\tilde{P}(\eta)} \tag{3.18}$$

where:

$$I(\eta) = \int_0^{\eta} \left\{ \tilde{Z}\left[\ln\varphi - \langle \ln\eta \rangle\right] + \left(1-\tilde{Z}\right)\left[\ln\left(1-\varphi\right) - \left\langle \ln\left(1-\eta\right)\right\rangle\right] \right\} \tilde{P}(\varphi)(\eta-\varphi)\,d\varphi$$

conditional scalar dissipation, where the mean scalar dissipation rate is defined from the traditional assumption of equality of times scales as equation (2.31), and the pdf term as equation (3.1).

Due to its elaborate evaluation and validation, this method of determination is implemented in subsequent calculations. Observing that the model is developed for isotropic turbulence, work was undertaken to validate its implementation for

the jet flows of interest. With reference to Table (3.2), which displays sample results obtained for flame A, comparisons were made between the values of the cross-stream averaged mean scalar dissipation (χ_1) and the integral of the cross-stream averaged product of the conditional scalar dissipation and pdf (χ_2) at several axial locations, *videlicet*:

$$\left(\tilde{\chi}(x,r)\right)_R = \int_0^1 \left(\chi(x,r,\eta)\tilde{P}\right)_R d\eta \tag{3.19}$$

and between the integral of the product of the conditional scalar dissipation and pdf (χ_3) and the mean scalar dissipation (χ_4) at several spatial locations, *id est*:

$$\int_0^1 \chi(x,r,\eta)\tilde{P}(x,r,\eta)\,d\eta = \tilde{\chi}(x,r) \tag{3.20}$$

As can be seen, although discrepancies in predictions occur close to the nozzle exit, predictions throughout the flow-field are generally very good.

In addition, this model has been successfully implemented in a number of publications, including those of Kim et al (2000b) and Swaminathan and Mahalingam (1996).

Another method is commonly employed for the evaluation of conditional scalar dissipation which is derived from the Amplitude Mapping Closure (AMC) (O'Brien and Jiang 1991) in homogeneous turbulence, or from the solution of the governing mixture fraction equation (Peters 1984), and takes the functional form:

$$\langle \chi | \eta \rangle = C \exp\left\{-2\left[erf^{-1}(2\eta - 1)\right]^2\right\} \tag{3.21}$$

where:

$$C = \frac{\tilde{\chi}}{\int_0^1 \exp\left\{-2\left[erf^{-1}(2\eta-1)\right]^2\right\}\tilde{P}(\eta)\,d\eta}$$

Again, this function has been widely applied; such examples being found in Swaminathan and Bilger (1999a), Kim et al (2000a), and more recently in Kim

and Huh (2002b) in the application of CMC to spray autoignition problems. Assessment of the AMC-derived model's performance has been conducted by both Mell et al (1994) and Swaminathan and Mahalingam (1996). Mell et al (1994) find the model performs better than the simple unconditional/conditional value equality assumption, but Swaminathan and Mahalingam (1996) find the converse. The authors in the latter paper do however find that Girimaji's model performs generally better than the AMC derived approach.

3.iii.i.iii Conditional Source Term

The non-linear conditional source term in the scalar transport equations is approximated as for first-order closure, assuming the fluctuation of the species production rates around the mean to be negligible. Mean rates are hence obtained by the direct implementation of chemical kinetic schemes via the CHEMKIN package (Kee et al 1996). The package consists of over one hundred FORTRAN subroutines which, when provided with a reaction scheme and respective Arrhenius rate-equation terms, can relay not only species production rates, but quantities such as specific heat, density, and enthalpies of a gas-phase composition. Thermodynamic property data is also required to accomplish these calculations, and such was taken from McBride et al (1993), Burcat and McBride (1993), and Burcat (2001). As previously discussed, three kinetics schemes of varying complexity are utilised in the flame calculations, and are defined as schemes (i), (ii), and (iii) henceforth.

With reference to Table (3.3), scheme (i) is the five-step reduced mechanism of Chen et al (1995). No Arrhenius parameters are listed for this mechanism as its

application is via the introduction of an additional FORTRAN routine to the CHEMKIN package, which has all the information contained within its algorithms. This scheme has been validated against the forty-eight step starting mechanism from which it is derived by Barlow et al (1999). Here, the authors demonstrate that as far as departure from equilibrium and NO production are concerned, there is very little difference between the reduced and starting mechanisms, with said difference in NO predictions being less than one percent. The scheme describes the production of eight species involved in the five reduced steps; these being H, H_2, H_2O, NO, N_2, O, OH, and O_2. The lesser species concentrations of HNO, HO_2, N, and NO_2 are approximated by steady-state assumptions.

Scheme (ii), as illustrated in Table (3.4), describes the production of twelve species carried by the twenty-four step mechanism; the species being H, HO_2, H_2, H_2O, H_2O_2, N, NO, NO_2, N_2, O, OH and O_2. The reaction steps are extracted from the mechanism described by Miller and Bowman (1989), with the exception of the two body shuffle reactions governing production of the radicals H, O and OH which are drawn from the skeletal mechanism described by Smooke and Giovangigli (1990). Previous studies of CMC methods using this scheme by Smith et al (1992, 1995) have shown good agreement of species predictions with experimental data.

Scheme (iii), as defined in Table (3.5), describes the production of eighteen species carried by a sixty-two step mechanism; the species being H, HNO, HO_2, H_2, H_2O, H_2O_2, N, NH, NH_2, NH_3, NO, NNH, N_2, N_2H_2, N_2O, O, OH and O_2. This scheme is a sub-mechanism of the comprehensive C_1-C_2 mechanism developed and validated by Lindstedt and co-workers (Lindstedt and Selim 1994,

Leung and Lindstedt 1995, Lindstedt and Skevis 1997, Sick et al 1998). The sub-mechanism itself has shown good agreement with experimental data when applied using a transported pdf technique (Lindstedt and Vaos 2001), although the latter work employed a truncated version involving solution for ten species, with the remaining eight species assumed to be in steady state.

The source term in the equation for conditional enthalpy also requires modelling, and is taken to be the conditional radiation heat loss. This latter term is represented using the optically thin assumption, as outlined by Marracino and Lentini (1997), and represented by:

$$\langle w_h | \eta \rangle = -4.0\sigma p \langle T | \eta \rangle^4 \sum_{\alpha} a_{\alpha} \langle T | \eta \rangle \langle Q_{\alpha} \tag{3.22}$$

where Q is the conditional reactive scalar α expressed in terms of mole fraction. For flames of hydrogen and helium mixtures burning in air, H_2O can be considered the dominating radiating species and is hence the only species considered in these present calculations. The absorption coefficient is derived as (Marracino and Lentini 1997):

$$\log_{10} a_{H_2O} = 0.93567 - 5.5258 \times 10^{-4} T \tag{3.23}$$

It is to be expected that this model may overestimate the radiation as the gas-phase is assumed only to give up heat with no re-absorption. It was found in calculations that the model effected an improvement in predictions of the temperature field in the order of one to two percent over the non-radiating case in these present works.

3.iii.ii Mathematical Procedure

Flow and mixing-field data from the turbulent flow calculations are passed to the CMC model, where the set of species mass-fraction equations plus the enthalpy equation are constructed and solved in mixture-fraction space. Comparison between densities obtained from the CMC solution and prescribed equilibrium values showed little variation and so coupling of the flow field and CMC calculations was therefore judged unnecessary at this stage of development, and for these flames. Species calculations are carried out at the respective physical-space locations prescribed by those at which the turbulence-field data is derived. The data essential for CMC calculation purposes include the mixture fraction and its variance to be used in the implementation of the presumed-form pdf methods, the turbulence quantities k and ε for the formulation of mean scalar dissipation, and the axial velocity.

As applied in the mixing-field calculations, a parabolic approach is taken to the solution of the species and enthalpy equations, and the system is solved by a marching integration procedure from the prescribed upstream conditions, along the length of the flame. Each solution in turn becomes the initial values at the start of the next calculation, thus providing profiles of conditional mean species and enthalpies throughout the flow in question. The presumed form pdf once again comes into play in the evaluation of physical-space data, which can be obtained by convolution of the conditional species predictions and the pdf at any spatial location (x,r) *videlicet*:

$$\tilde{Y}(x,r)=\int_0^1 Q\tilde{P}(x,r,\eta)d\eta \qquad (3.24)$$

3.iii.iii Numerical Methods

Cross-stream averaging and integrations of the pdf such as equations (3.14, 3.18, 3.24) are common to the closures employed in the CMC equation, and these calculations are undertaken by the implementation of the NAG routine D01AJF (NAG 2002) which is an adaptive routine using the Gauss ten-point and the Kronrod twenty-one-point rules in a one-dimensional quadrature, finite interval strategy due to Piessens et al (1983), which allows for badly behaved integrands. The system of first-order Ordinary Differential Equations (ODEs) defined by equations (3.12, 3.13) are solved via the application of the Variable coefficient ODE solver VODE (Brown et al 1989), which has been developed with the solution of initial-value stiff problems in mind. The kind of problem under scrutiny here is typical of a stiff-system, being one in which two or more scales of the independent variable upon which the dependent variable is changing, display relatively large differences. The general representation of the initial-value problem addressed by VODE is given as:

$$\frac{\partial y}{\partial t} = f(t, y), \quad y(t_0) = y_0, \qquad y \in \mathbb{R}^N$$

and:

$$\frac{\partial y_\alpha}{\partial t} = f(y) = f\left(\alpha, t, y_1, y_2, \ldots, y_{neq}\right) \quad \alpha = 1 \ldots neq \tag{3.25}$$

Written as a FORTRAN package, SVODE applies a backward differentiation formula in its solution method, and being a mutistep technique, applies the linear step formula:

$$\sum_{i=0}^{C_1} \iota_{\alpha,i} y_{\alpha-i} + \sum_{i=0}^{C_2} \gamma_{\alpha,i} y_{\alpha-i} = 0 \tag{3.26}$$

where the order C_1 varies between one and five, C_2 is zero, and the coefficients ι and γ are computed as functions of the current and past step-sizes. As with any implicit method, an iterative scheme must be implemented at each step to solve the system, and in this case is conducted using a modified Newton method utilising an internally generated Jacobian matrix.

VODE is also called by the CHEMKIN set of subroutines during the evaluation of the mean species production rate term, for which the latter requires a system temperature in addition to composition. The determination of this conditional temperature is effected by the use of the species composition and enthalpy at each node in composition space by an iterative linear interpolation.

The only remaining term requiring assessment is the second-order differential of the diffusion term in the CMC equations. In this instance, a second-order central differencing scheme is implemented.

3.iii.iv Solution Domain And Initial Conditions

Table (3.1) displays the specifications for the three flames (Barlow and Carter 1994, 1996) under investigation, and give indication as to the make-up of the fuel in each case. The conditional mean profiles of species and enthalpy are unknown at the nozzle exit plane, excepting the bounding mixture fractions being pure fuel and pure air, and defined as follows.

$$Q_\alpha(x=0,\eta=0)=Y_{\alpha,o}(x=0) \tag{3.27}$$

$$Q_h(x=0,\eta=0)=h_o(x=0) \tag{3.28}$$

$$Q_\alpha(x=0,\eta=1)=Y_{\alpha,f}(x=0) \tag{3.29}$$

$$Q_h(x=0,\eta=1)=h_{\alpha,f}(x=0) \tag{3.30}$$

These profiles are required however as initial conditions for the parabolic CMC sweep. The initial temperature of the reacting streams is ambient, and the pressure is taken to be atmospheric. These conditions do not suggest autoignition would occur, so the flame has to be 'ignited' by some other means. In contrast to specifying simple pure-mixing species profiles, an adiabatic equilibrium calculation is employed to impose a combusting state upon the system. This is calculated for each η value over composition space, which consists of sixty-eight unevenly spaced nodes, concentrated around the stoichiometric mixture fraction. Subroutines provided with the CHEMKIN package are once again called upon to carry out these calculations, and subsequently provide initial conditional values of enthalpy also. Calculations in physical space are initiated at a distance of two nozzle diameters downstream from the exit plane to ensure that the flame does not strain to extinction. This is also a finding of other CMC investigations (Klimenko and Bilger 1999, Devaud 1999). The spatial resolution of the physical domain over which the CMC equations are integrated is in excess of 3000 nodes in all cases.

3.iii.v Results And Discussion

All calculations were performed on an SGI workstation with a CPU clock-speed of 220 MHz, and took not in excess of eight hours, twelve hours, and sixteen hours respectively for the three kinetics schemes employed. Figures (3.22-3.24) present conditional predictions of the major species H_2, H_2O, N_2, and O_2, and

mean temperature, for flame A at six axial locations. Plotted against experimentally derived conditional data are predictions obtained using the three respective kinetics schemes, with results derived using both turbulence models being shown in each plot. No significant difference is observed between results derived using the k-ε and RSSF turbulence models at all downstream locations, with good agreement with data being obtained. Negligible differences between the three kinetic schemes are also noted. The only exception is an under-prediction of temperature by all the kinetic schemes and turbulence models at 22.5d, this being particularly the case for the Re stress model. The latter finding is in line with the previously mentioned under-prediction of the spreading rate of this flame by the RSSF model. Similar discrepancies at near-nozzle locations have been noted in the work of Barlow et al (1999) and in predictions of methanol flames (Roomina 1998, Roomina and Bilger 1999). This may be attributed to the inability of first-order CMC models to capture the effects of two phenomena for which experimental evidence exists; *videlicet*, differential diffusion and the effects of heat release. Differential diffusion effects are known (Meier et al 1996) to increase thermal NO production rates by increasing temperature and radical concentrations near to the stoichiometric mixture fraction. Heat release in close proximity to the nozzle can also promote laminarisation of the reaction zone near to the base of the flame that in turn promotes differential diffusion, and also increases residence times for NO production (Clemens and Paul 1995). Conversely, conditional temperatures away from the jet exit plane show a tendency to be high on the rich side of stoichiometric in comparison with experimental data for kinetic schemes (i) and (ii). Similar results were obtained for flames B and C. Figures (3.25, 3.26)

compare data and predictions for these flames obtained using the sixty-two step mechanism devised by Lindstedt and co-workers (Lindsted and Vaos 2001). These figures demonstrate that increasing helium dilution of the flames generally leads to reduced differential diffusion effects close to the nozzle and an improvement in the accuracy with which peak temperatures are predicted. Away from the nozzle, agreement with data in fuel-rich regions is generally decreased slightly for flame B, but increased for flame C. Similar results were also observed in the application of kinetics schemes (i) and (ii).

Figures (3.27-3.29) present conditional predictions of minor species OH and NO mass fractions in flame A for the three respective kinetics schemes. Because experimental uncertainties associated with the measurement of minor species are more significant than for the major species given in Figure (3.22) (Barlow and Carter 1994, Combustion Research Facility, Sandia National Laboratories 2002), these data are plotted as conditional means with uncertainties (Barlow and Carter 1994, Combustion Research Facility, Sandia National Laboratories 2002) indicted by error bars. Once again, very little difference is observable over the three sets of predictions for OH, with the results being in good agreement with the data. Results obtained from the k-ε model do, however, show slightly lower values of OH mass fraction. The previously noted effect of temperature depression is observed to cause considerable underprediction of conditional NO mass fraction at the near-nozzle station, with all three schemes then tending to ultimately over-predict conditional NO further downstream. The RSSF model in this instance is seen to provide notably better agreement with the data. These observations are in line with those obtained from previous studies of this flame using a Reynolds stress turbulence model and a twenty-four step reduced scheme

(Smith et al 1995). Similar results were also found for flames B and C, with comparisons between predictions based upon kinetic scheme (iii) and experimental data for these two flames being given respectively in Figures (3.30, 3.31). In line with earlier findings, agreement with data generally decreased slightly for flame B, but improved for flame C. Once again, similar results were obtained with the application of kinetic schemes (i) and (ii).

Turning to predictions in real space, Figures (3.32-3.34) give radial profiles of mean temperature in flame A obtained using both the k-ε and RSSF models, and the three kinetics schemes respectively. Again, there are no significant differences between results derived using the various kinetic schemes. The RSSF model predictions for the first two measurement stations are less accurate than those obtained from the k-ε closure, which are in good agreement with data. This is to be expected given the effects observed in Figures (3.4-3.6), and results in the significant under-prediction of NO levels at these stations by the former model, illustrated by Figures (3.37-3.39). Further from the nozzle, radial temperatures obtained from the RSSF model improve over k-ε model-based predictions due to the superior representation of mixing quantities required by the CMC approach. It is observable for both models, however, that the temperature profile decays too rapidly over the radius of flame A, with this effect being accentuated with downstream distance. However, high predicted values of conditional NO concentrations at these stations (Figures (3.27-3.29)) then lead to good agreement of real space NO levels in the outer regions of the flame for the RSSF-based results. Overall, predictions of NO levels within this flame show good agreement with data when based on the second-moment turbulence closure, apart from at the first two axial locations, although results based on the eddy

viscosity approach tend to significantly over-predict NO data within the main body of the flame. Similar results were observed for flames B and C, with predictions obtained using kinetic scheme (iii) for mean temperatures and NO levels being given, respectively, in Figures (3.35, 3.36) and Figures (3.40, 3.41). These results, in line with those obtained using the two simpler kinetic prescriptions, do indicate some slight qualitative improvement with increasing He dilution of the flames.

The results given in this chapter demonstrate that CMC model predictions based on the RSSF turbulence model are, in general, both qualitatively and quantitatively superior to those based on the k-ε model. As far as could be tested using the data available, this was due to the better representation by the former model of the quantities required in the CMC approach, and used in the representation of mean scalar dissipation rates and their conditional counterparts. The use of these two turbulence models also leads to the largest difference between the results obtained, indicating that accurate representation of the mixing field is of paramount importance to the accuracy of subsequent CMC calculations. A similar level of agreement is obtained between predictions based on the three kinetics schemes employed, indicating that the level of kinetic representation is not of paramount importance to the modelling of hydrogen flames far from extinction. Over all the flames examined, the performance of kinetic scheme (ii), the twenty-four-step scheme used in previous CMC investigations (Smith et al 1992 1995, Kronenburg et al 1998) was slightly superior, although this may be considered to some extent fortuitous and subject to results to be generated through the further work described below.

Overall, the results obtained compare favourably with earlier investigations of the flames studied by Barlow and Carter (1994) that employed both CMC (Barlow et al 1999) and pdf (Barlow et al 1999, Lindstedt and Vaos 2001) methods. In terms of earlier (Barlow et al 1999) CMC results in particular, derived using a Reynolds stress turbulence closure, predictions obtained by the latter authors for OH and NO levels in mixture fraction space are comparable, whilst differences between real space predictions of mixture fraction, mean temperature and NO levels in all three flames are explicable in terms of the way flow field predictions were optimised in the two studies. Barlow et al (1999) therefore optimised predictions against axial profiles, to allow a direct comparison between results from CMC and pdf methods, rather than the radial profiles employed in the present work. The approach of the latter authors led to an over-prediction of radial mixture fraction profiles in regions away from the nozzle in all three flames that, in contrast to the present findings, resulted in the slight over-prediction of mean temperatures at all radial locations. Resultant NO levels in real space were then, however, in broad agreement with the results described herein.

Further work remains to be performed. In particular, results derived using the RSSF turbulence model under-predict mixing close to the nozzle, despite slightly over-predicting mean velocities and fluctuating mixture fraction in this region, with the influence of these effects being observable in subsequent scalar predictions in both real and mixture fraction space. Radial profiles of temperature also under-predict data at distances away from the centre-line. The investigation of alternative Reynolds stress closures is therefore warranted, although it may be noted that the above effects are not apparent in predictions of methane flames

being studied as part of the International Workshop on Measurement and Computation of Turbulent Nonpremixed Flames Combustion Research Facility, Sandia National Laboratories 2002) and presented in Chapter 5, using the same RSSF closure as employed in the present work.

Additionally, all results exhibit an under-prediction of NO mole fraction close to the nozzle that, for the case of k-ε based results, occurs despite the reasonable prediction of mean temperatures within this region. There is also a general trend for NO levels to be over-predicted at downstream locations. Further work is therefore required to establish the reasons for these inaccuracies. This should include an analysis of the applicability of the presumed form of the probability density function used within the CMC method, as well as the applicability of cross-stream averaged quantities for these flames, particularly with respect to the temperature predictions. Second-order chemistry effects also need to be addressed, and Chapter 4 can be referred to for further discussion. Kronenburg et al (1998) observe a significant reduction in NO predictions within the main body of all three flames with the application of a more rigorous treatment of the kinetic representation, the application of which results in excellent agreement with observed NO levels. Requirement for a higher-order chemistry closure has also been identified by Desjardin and Frankel (1997) in turbulent reacting flows of non-premixed reactants. Here, they compare a Linear-Eddy Modelling (LEM) approach with CMC predictions in their consideration of systems near extinction. Kronenburg and Bilger (2001a, 2001b) have also investigated the effects of differential diffusion of H and H_2 on the prediction of NO levels, and demonstrate an increase in the accuracy of near-field predictions of NO when such effects are incorporated. Differential diffusion effects were, however, found

to be not solely responsible for the under-prediction of NO levels close to the nozzle, with improved modelling of scalar diffusion being suggested as one means of further improving results (Kronenburg and Bilger 2001a). All these results were, however, obtained using an eddy viscosity-based turbulence modelling approach, with the changes in NO levels as a consequence of accommodating both second-order and differential diffusion effects being comparable to the differences observed between k-ε and RSSF model predictions in the present work. Further investigation of all these effects using Reynolds stress closures is therefore warranted.

3.iv Conclusions

A first-order CMC model has been applied to the calculation of three H_2 and H_2/He non-premixed jet flames, with predictions based on three different chemical kinetic schemes and both k-ε and Reynolds stress/scalar flux turbulence closures. The results obtained demonstrate that CMC model predictions based on the RSSF turbulence model are, in general, superior to those obtained using the simpler eddy viscosity-based approach. A similar level of agreement is, however, obtained between predictions derived from all three kinetics schemes.

Overall, predictions of major and minor species, and flame temperatures, in all three flames are in reasonable agreement with experimental data, and compare favourably with the results of earlier investigations of these flames that employed both CMC and PDF methods. Results do, however, tend to under-predict radial temperatures away from the flame centre-line, with the RSSF closure also under-predicting mixing close to the nozzle. Additionally, all results exhibit an under-prediction of NO levels close to the nozzle, with an over-prediction occurring within the main body of the flame. All these results point to the requirement for further work to refine the presumed form of the probability density function used within the present CMC method, and to investigate the applicability of cross-stream averaged quantities for these flames. Further investigations using a second-order closure for the chemical reaction rate term, including an assessment of the effects of differential diffusion, are also warranted. The present results do, however, emphasise that accurate representation of the mixing field is of

significant importance to the accuracy of subsequent CMC calculations, particularly in terms of NO results, such that any further study of the above effects should be conducted in conjunction with Reynolds stress turbulence closures.

The following chapter discusses the implementation of a second-order chemistry model to the three flames studied here, in addition to a lifted hydrogen diffusion flame. The intention for future study is the development of higher-order CMC models for calculation of hydrocarbon flames, so work is carried out in this area as a logical step forward. Investigation of differential diffusion effects has previously been conducted (Kronenburg and Bilger 2001a, 2001b) in these flames and future results have and will be analysed bearing in mind their observations. The effects of differential diffusion are not considered to be of primary concern in the modelling of hydrocarbon or mono-constituent high Mach number flames such as the lifted hydrogen jet to be discussed forthwith. Hence, also considering limitations imposed by time, the next direction of this work is that concerning higher-order kinetic representation.

3.v Tables

Flame	H_2:He by volume	Re	Axial Velocity (ms^{-1})	L / d	Stoic Z
A	100:0	10,000	296	180	0.028
B	80:20	9,800	294	150	0.042
C	60:40	8,300	256	100	0.064

Table 3.1 – Hydrogen:Helium Jet Flame Parameters

Axial Location (m x 10^2)	χ_1	χ_2	χ_3 r = 0.07031 m x 10^2	χ_4 r = 0.07031 m x 10^2
0.07031	1211.698	1371.615	0	0.171
0.1641	1343.488	1364.076	1.764	0.863
0.4189	1018.919	1011.603	29.299	15.237
0.7114	705.64	700.66	214.908	178.154
0.9763	488.0926	483.878	737.36	744.017
1.272	338.725	335.612	1545.421	1564.689
1.433	251.066	248.771	1748.202	1766.454
1.691	206.281	204.438	1477.29	1492.019
1.876	142.423	141.167	1126.821	1138.065
2.172	86.329	85.612	645.168	651.607
2.384	68.345	67.82	423.419	427.643
2.607	45.246	44.9	273.162	275.884
2.724	40.059	39.757	218.887	221.067
2.967	26.726	26.547	140.763	142.168
3.094	23.694	23.533	113.14	114.271
3.358	16.014	15.923	73.558	74.294
3.496	14.242	14.162	59.577	60.169
3.782	9.77	9.731	39.398	39.787
4.745	3.373	3.369	12.185	12.304
4.921	3.035	3.032	10.106	10.205

Table 3.2 – Sample Validation Results For The Application of Girimaji's Model

Reaction
O2 + H = OH + O
H + O = OH
H2 + O = OH + H
O2 + N2 = 2NO
H2 + OH = H2O + H

Table 3.3 – Hydrogen/Air Combustion Mechanism Scheme (i)

Reaction	A	b	E
O2 + H = OH + O	2.00E+14	0	16800
OH + O = H + O2	1.57E+13	0	841.3
H2 + O = OH + H	5.06E+04	2.67	6286
H + OH = O + H2	2.22E+04	2.67	4371
H2 + OH = H2O + H	1.00E+08	1.6	3298
H2O + H = H2 + OH	4.31E+08	1.6	18274
O + H2O = OH + OH	1.47E+10	1.14	16991
OH + OH = H2O + O	1.59E+09	1.14	100.4
H + O2 + M = HO2 + M	2.30E+18	-0.8	0
H + HO2 = OH + OH	1.50E+14	0	1004
H + HO2 = H2 + O2	2.50E+13	0	693.1
H + HO2 = H2O + O	3.00E+13	0	1721
OH + HO2 = H2O + O2	6.00E+13	0	0
O + HO2 = OH + O2	1.80E+13	0	-406.3
HO2 + HO2 = H2O2 + O2	2.00E+12	0	0
HO2 + H2O = H2O2 + OH	2.86E+13	0	32790
H2O2 + OH = HO2 + H2O	1.00E+13	0	1800
H2O2 + M = OH + OH + M	1.30E+17	0	45500
OH + OH + M = H2O2 + M	9.86E+14	0	-5070
OH + H + M = H2O + M	2.20E+22	-2	0
H + H + M = H2 + M	1.80E+18	-1	0
O + N2 = NO + N	1.40E+14	0	75800
N + O2 = NO + O	6.40E+09	1	6280
OH + N = NO + H	4.00E+13	0	0
NO + HO2 = NO2 + OH	2.11E+12	0	-480
NO2 + H = NO + OH	3.50E+14	0	1500

Table 3.4 – Hydrogen/Air Combustion Mechanism Scheme (ii)
(Units: mole, m^3, s, K, cal)

Reaction	A	B	E
O2 + H = OH + O	2.00E+14	0	70300
H2 + O = OH + H	5.12E+04	2.67	26300
H2 + OH = H2O + H	1.00E+08	1.6	13800
OH + OH = H2O + O	1.50E+09	1.14	420
H + O2 + M = HO2 + M	2.30E+18	-0.8	0
H + HO2 = OH + OH	1.68E+14	0	3660
H + HO2 = H2 + O2	4.27E+13	0	5900
OH + HO2 = H2O + O2	2.89E+13	0	-2080
H + HO2 = H2O + O	3.00E+13	0	7200
O + HO2 = OH + O2	3.19E+13	0	0
H2O2 + OH = HO2 + H2O	7.83E+12	0	5570
H2O2 + M = OH + OH + M	1.20E+17	0	190000
OH + H + M = H2O + M	2.20E+22	-2	0
NH3 + M = NH2 + H + M	1.40E+16	0.06	379070
NH3 + H = NH2 + H2	6.36E+05	2.39	42555
NH3 + OH = NH2 + H2O	2.04E+06	2.04	2368
NH3 + O = NH2 + OH	2.10E+13	0	37656
NH2 + H = NH + H2	5.75E+11	0.59	15262
NH2 + OH = NH + H2O	9.00E+07	1.5	-1912
NH2 + O = NH + OH	7.00E+12	0	0
NH2 + O = HNO + H	9.90E+14	-0.5	0
NH2 + N = N2 + H + H	7.20E+13	0	0
NH2 + NO = N2 + H2O	3.00E+20	-2.6	3866
NH + H = N + H2	1.00E+13	0	0
NH + O = NO + H	7.00E+13	0	0
NH + OH = N + H2O	2.00E+09	1.2	25
NH + OH = HNO + H	4.00E+13	0	0
NH + O2 = NO + OH	1.00E+13	-0.2	20080
NH + NO (+M) = N2O + H (+M)	2.94E+14	-0.4	0
NH + NH = N2 + H + H	2.54E+13	0	0
N + O2 = NO + O	6.40E+09	1	26275
N + OH = NO + H	3.80E+13	0	0
N + NO = N2 + O	3.30E+12	0.3	0
N2H2 + M = NNH + H + M	1.17E+17	0	209200
N2H2 + H = NNH + H2	5.00E+13	0	4184
N2H2 + NO = NH2 + N2O	3.00E+12	0	0
N2H2 + NH2 = NNH + NH3	1.00E+13	0	4184
NNH + M = N2 + H + M	1.70E+12	0	59860
NNH + OH = N2 + H2O	5.00E+13	0	0
NNH + NH2 = N2 + NH3	5.00E+13	0	0
NO + NNH = N2 + HNO	2.00E+12	0	0
NH2 + NH = N2H2 + H	1.00E+15	-0.5	0
NH2 + NH2 = N2H2 + H2	4.00E+13	0	49551
NH2 + NO = NNH + OH	1.39E+12	0	0
N2O + H (+M) = N2 + OH (+M)	2.53E+10	0	19037
N2O + OH = N2 + HO2	2.00E+12	0	41840
HNO + M = H + NO + M	2.35E+16	0	203677
HNO + H = H2 + NO	5.00E+12	0	0
HNO + OH = H2O + NO	7.20E+13	0	0
HNO + O = OH + NO	3.60E+13	0	0
HNO + NH2 = NH3 + NO	2.00E+13	0	4184
HNO + NO = N2O + OH	2.00E+12	0	108784
NH + O2 = HNO + O	4.61E+05	2	27196
HNO + O2 = NO + HO2	3.16E+12	0	12552
NH2 + HO2 = NH3 + O2	4.52E+13	0	0
NNH + NH = N2 + NH2	5.00E+10	0	0
NH + NO = N2 + OH	2.16E+10	-0.23	0
NNH + O = NO + NH	1.00E+13	0	0
NH2 + NH2 = NH + NH3	5.00E+13	0	41570
NH2 + NO = N2O + H2	5.00E+13	0	102428
NH + O = N + OH	7.00E+12	0	0
NH2 + O = NO + H2	5.00E+12	0	0

Table 3.5 – Hydrogen/Air Combustion Mechanism Scheme (iii)
(Units: mole, m^3, s, K, J)

3.vi Figures

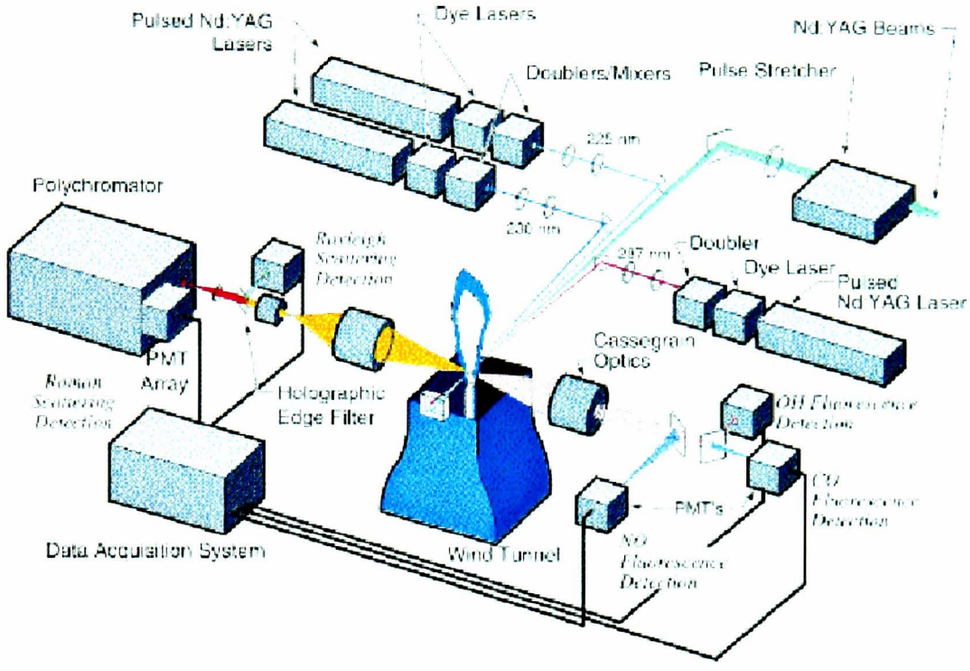

Figure 3.1 – Experimental Setup Used at Sandia National Laboratories.

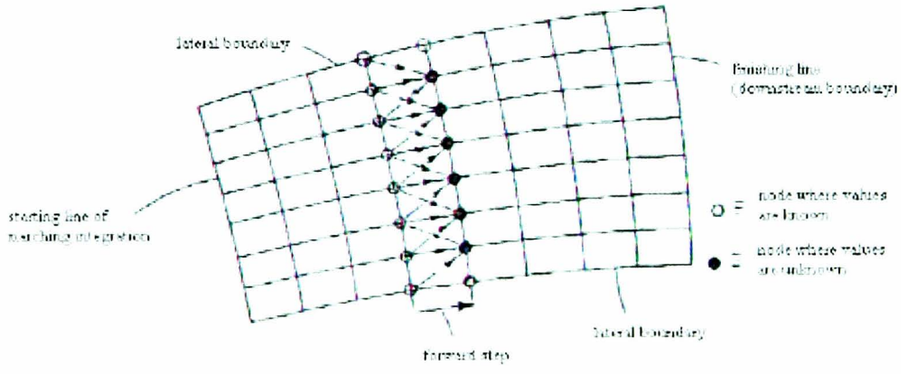

Figure 3.2 – Form of GENMIX computational mesh.

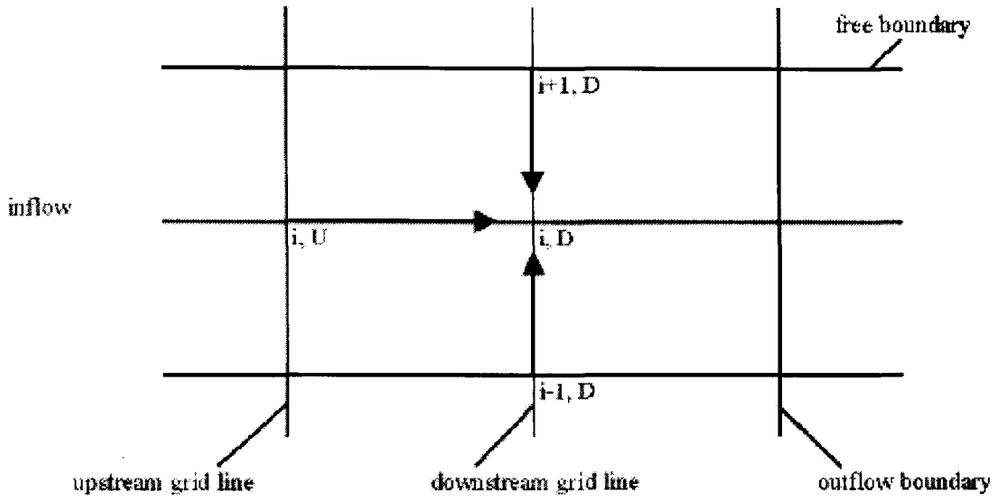

Figure 3.3 – Implementation of four-node implicit discretisation scheme.

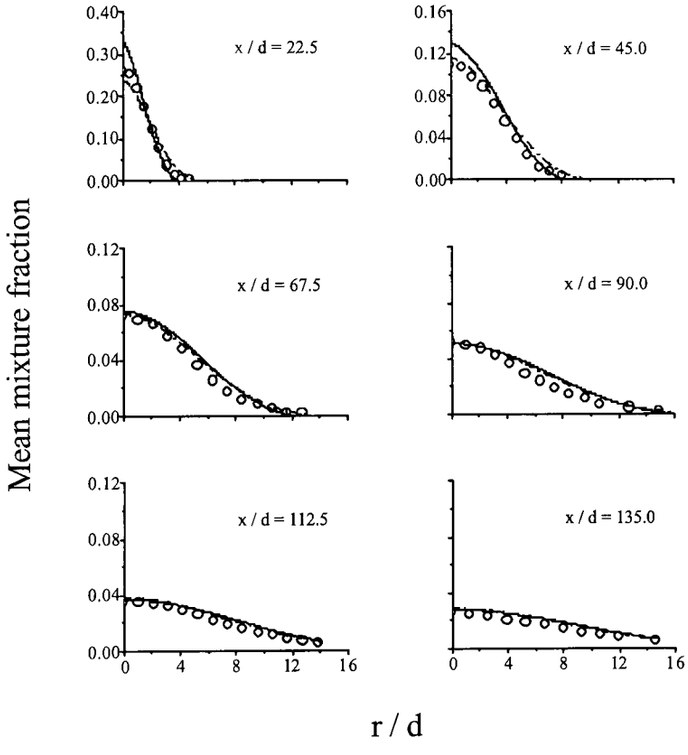

Figure 3.4 – Comparison of measured and predicted radial mean mixture-fraction profiles at six axial stations for hydrogen flame A (o measured, — predicted Re stress, - - predicted k-ε).

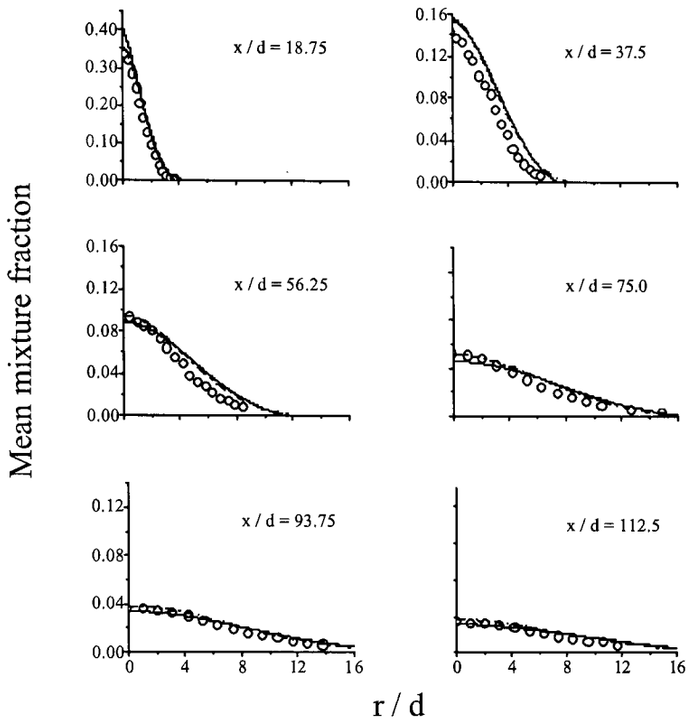

Figure 3.5 – Comparison of measured and predicted radial mean mixture-fraction profiles at six axial stations for hydrogen flame B (o measured, —predicted Re stress, - - predicted k-ε).

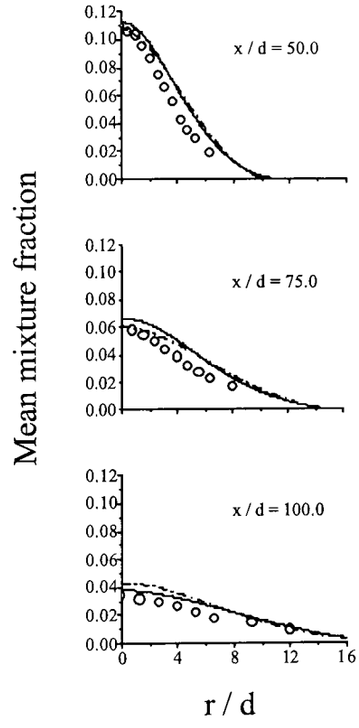

Figure 3.6 – Comparison of measured and predicted radial mean mixture-fraction profiles at three axial stations for hydrogen flame C (o measured, —predicted Re stress, - - predicted k-ε).

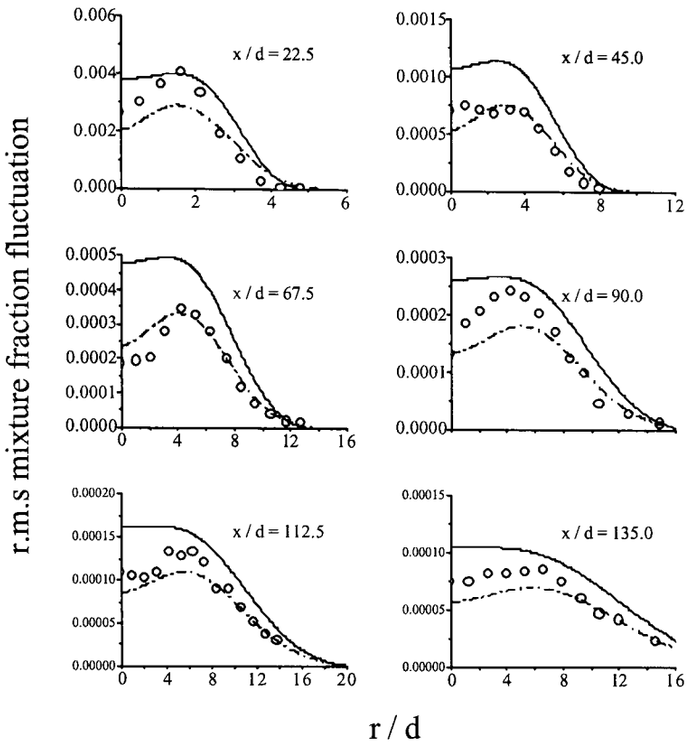

Figure 3.7 – Comparison of measured and predicted radial root-mean-squared mixture-fraction fluctuation profiles at six axial stations for hydrogen flame A (o measured, — predicted Re stress, - - predicted k-ε).

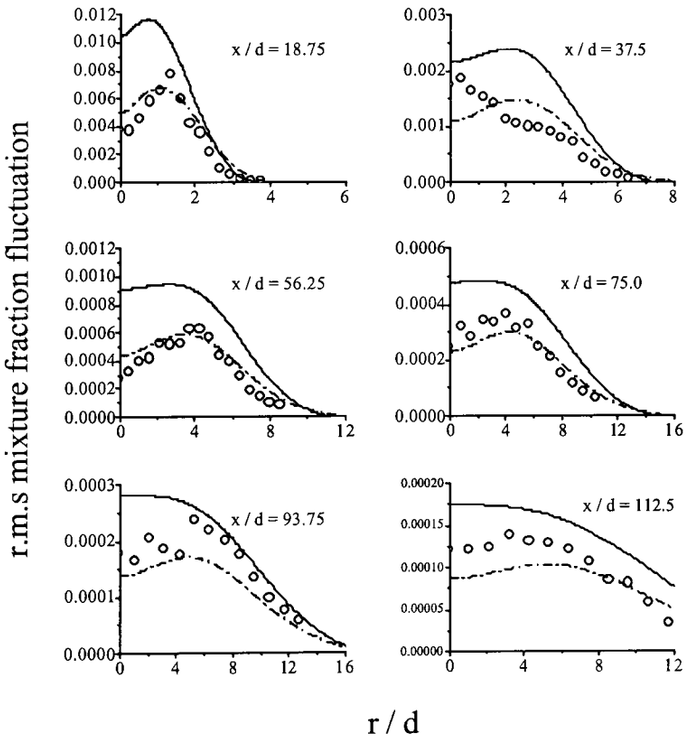

Figure 3.8 – Comparison of measured and predicted radial root-mean-squared mixture-fraction fluctuation profiles at six axial stations for hydrogen flame B (o measured, — predicted Re stress, - - predicted k-ε).

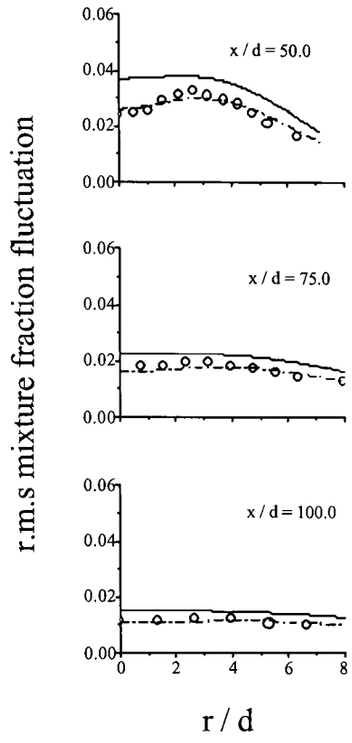

Figure 3.9 – Comparison of measured and predicted radial root-mean-squared mixture-fraction fluctuation profiles at six axial stations for hydrogen flame C (o measured, — predicted Re stress, - - predicted k-ε).

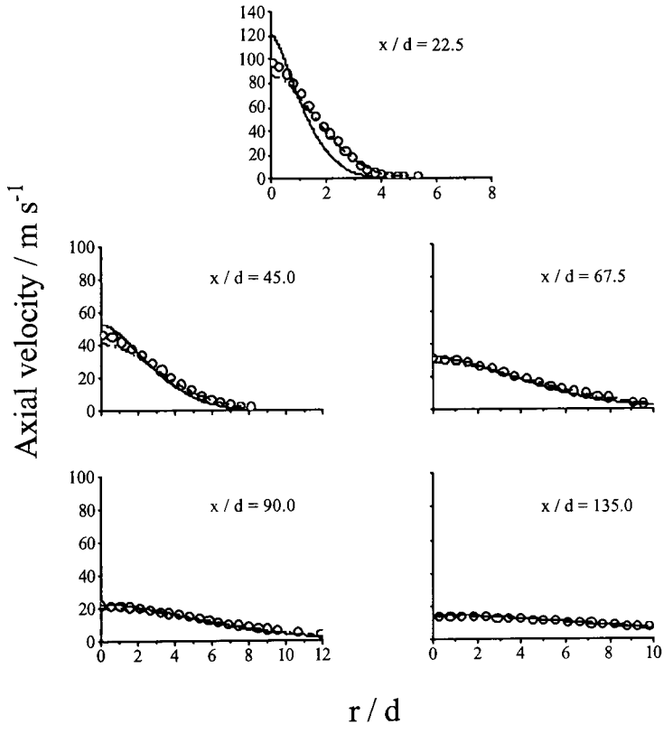

Figure 3.10 – Comparison of measured and predicted radial axial-velocity profiles at six axial stations for hydrogen flame A (o measured, — predicted Re stress, - - predicted k-ε).

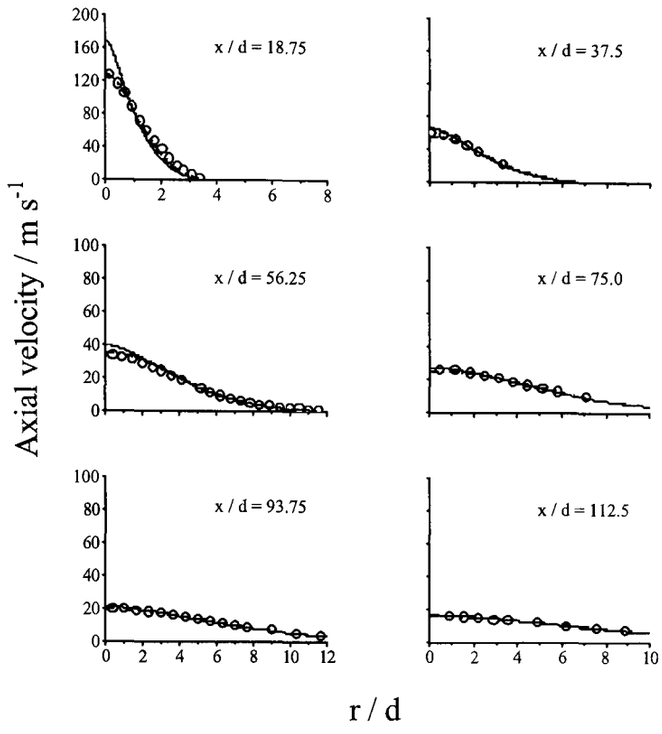

Figure 3.11 – Comparison of measured and predicted radial axial-velocity profiles at six axial stations for hydrogen flame B (o measured, — predicted Re stress, - - predicted k-ε).

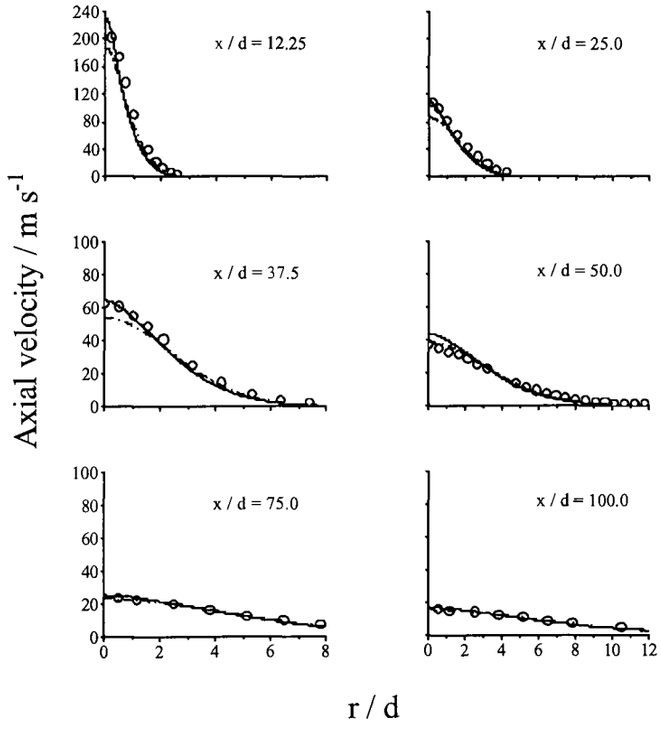

Figure 3.12 – Comparison of measured and predicted radial axial-velocity profiles at six axial stations for hydrogen flame C (o measured, — predicted Re stress, - - predicted k-ε).

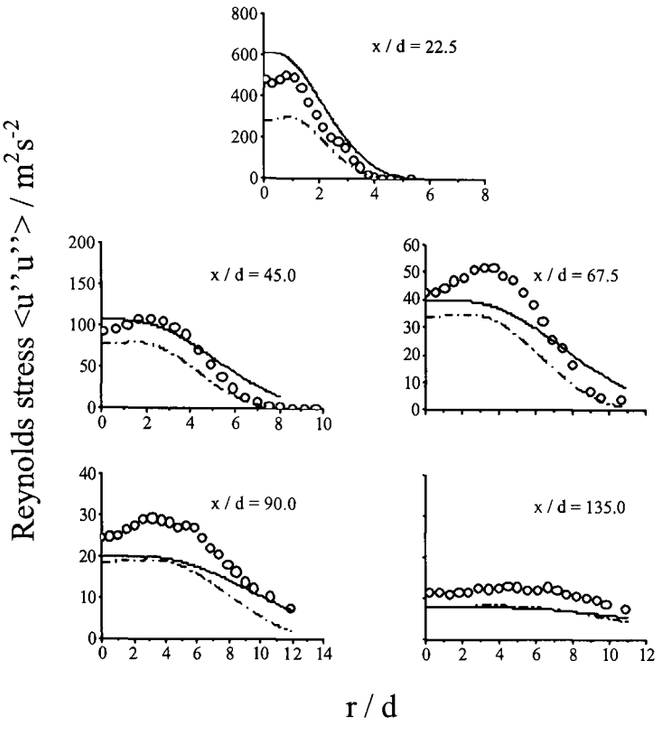

Figure 3.13 – Comparison of measured and predicted radial Reynolds-stress profiles at six axial stations for hydrogen flame A (o measured, — predicted Re stress, -- predicted k-ε).

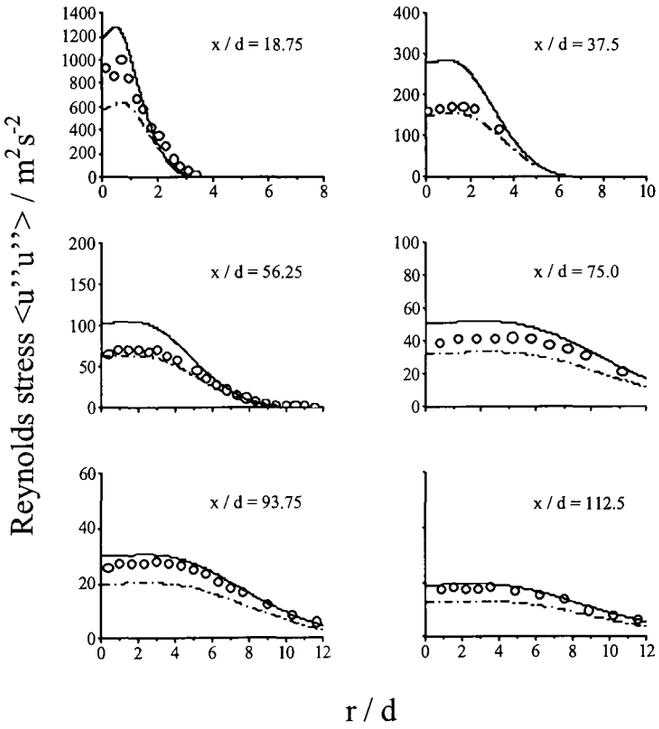

Figure 3.14 – Comparison of measured and predicted radial Reynolds-stress profiles at six axial stations for hydrogen flame B (o measured, — predicted Re stress, -- predicted k-ε).

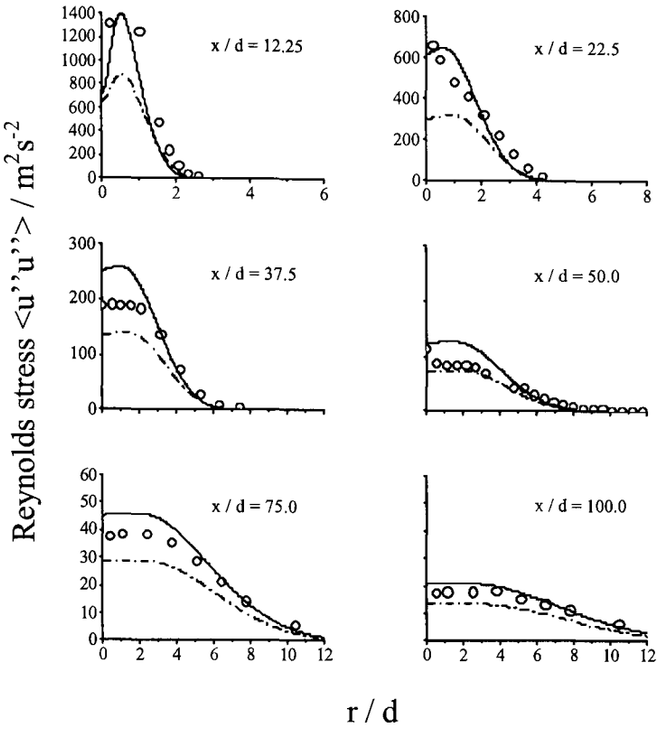

Figure 3.15 – Comparison of measured and predicted radial Reynolds-stress profiles at six axial stations for hydrogen flame C (o measured, — predicted Re stress, -- predicted k-ε).

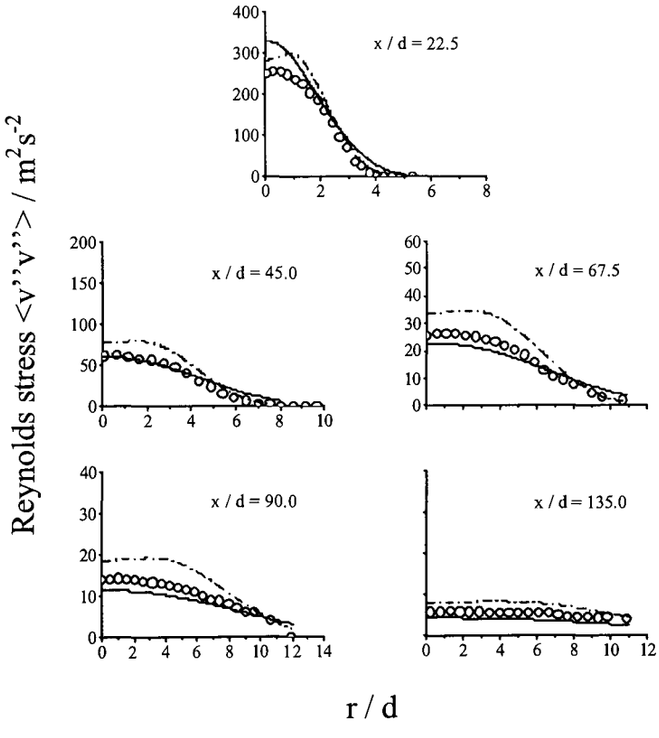

Figure 3.16 – Comparison of measured and predicted radial Reynolds-stress profiles at six axial stations for hydrogen flame A (o measured, — predicted Re stress, -- predicted k-ε).

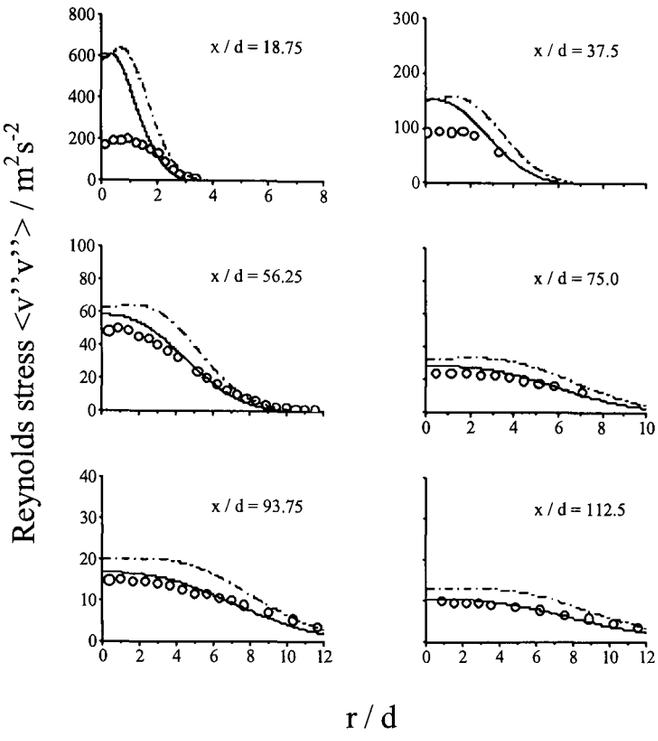

Figure 3.17 – Comparison of measured and predicted radial Reynolds-stress profiles at six axial stations for hydrogen flame B (o measured, — predicted Re stress, - - predicted k-ε).

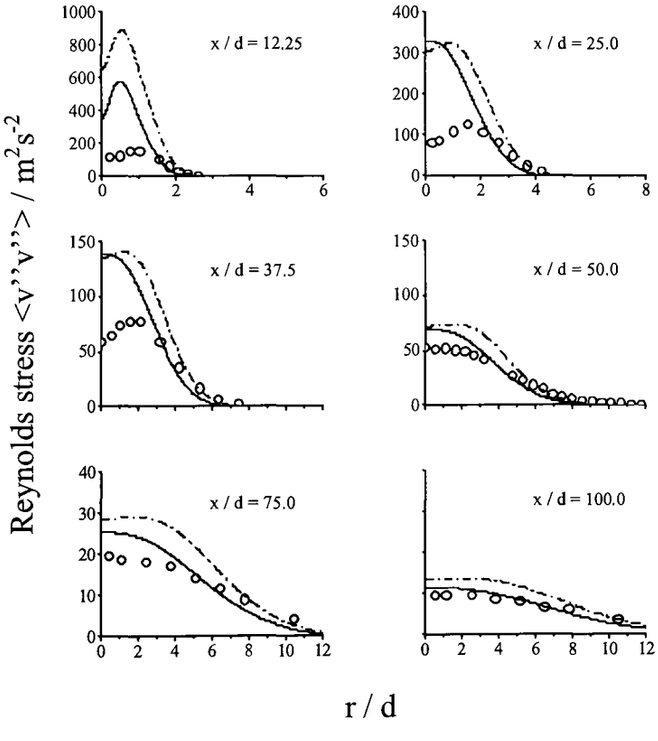

Figure 3.18 – Comparison of measured and predicted radial Reynolds-stress profiles at six axial stations for hydrogen flame C (o measured, — predicted Re stress, - - predicted k-ε).

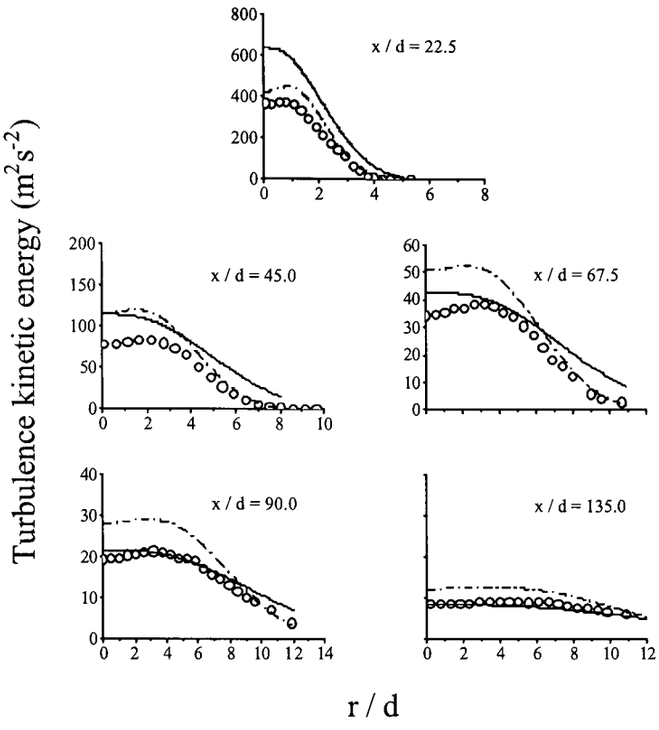

Figure 3.19 – Comparison of measured and predicted radial turbulence kinetic energy profiles at six axial stations for hydrogen flame A (o measured, — predicted Re stress, - - predicted k-ε).

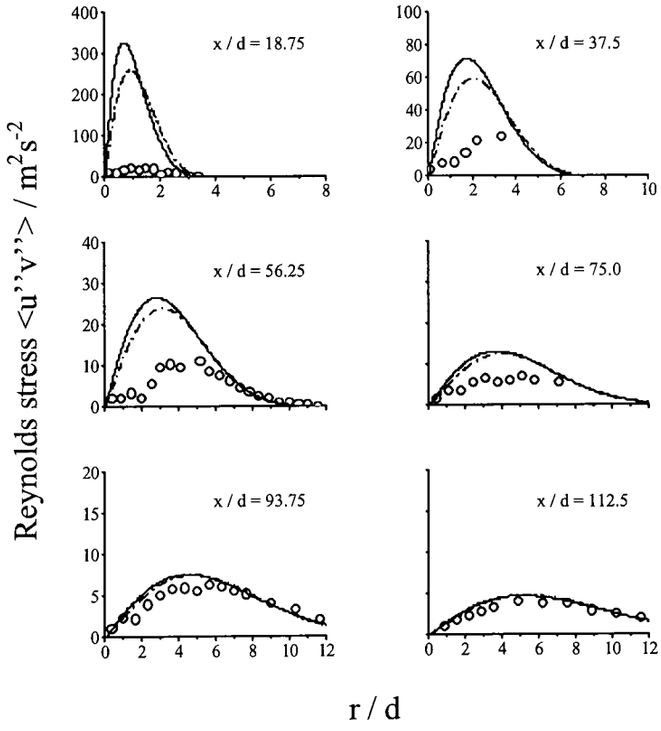

Figure 3.20 – Comparison of measured and predicted radial Reynolds-stress profiles at six axial stations for hydrogen flame B (o measured, — predicted Re stress, - - predicted k-ε).

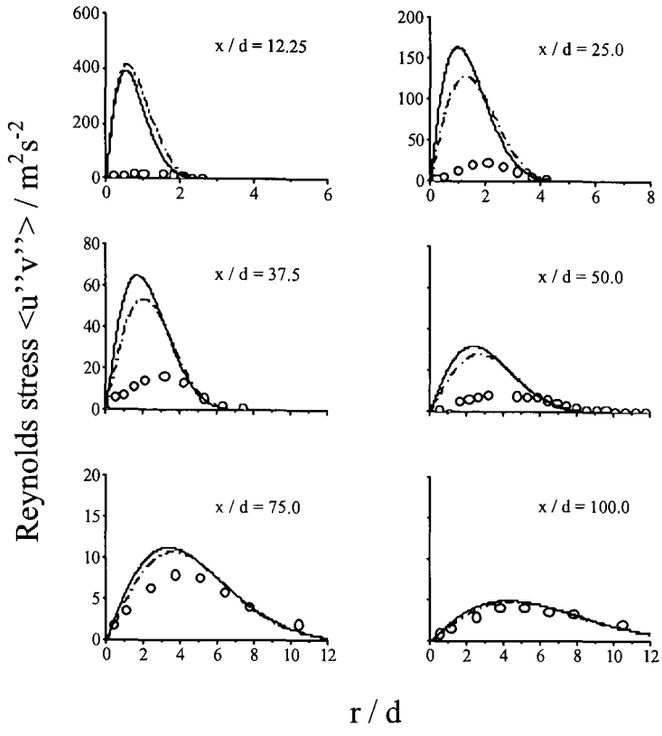

Figure 3.21 – Comparison of measured and predicted radial Reynolds-stress profiles at six axial stations for hydrogen flame C (o measured, —predicted Re stress, - - predicted k-ε).

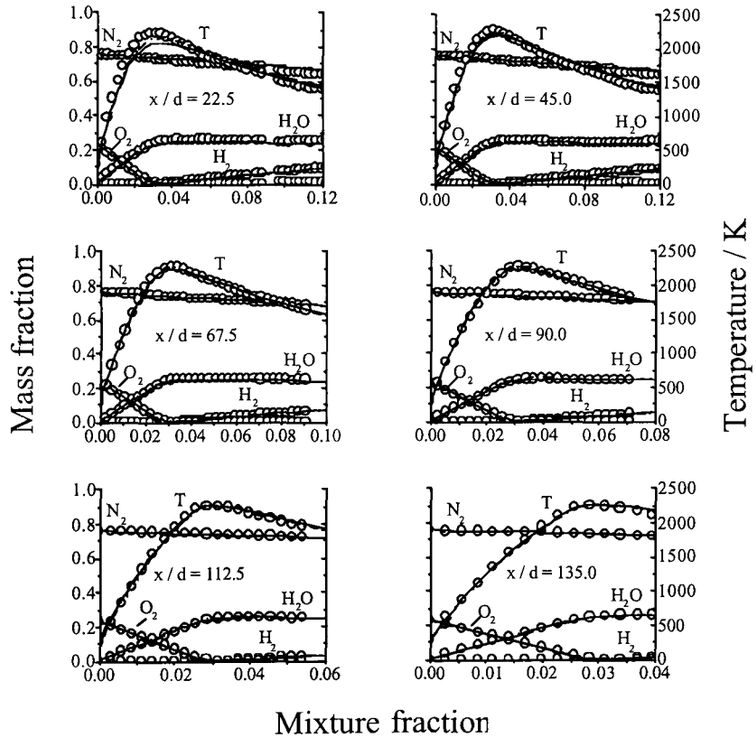

Figure 3.22 – Comparison of measured and predicted conditional species mass-fractions and temperature at six axial stations for hydrogen flame A, derived using kinetics scheme (i) (o measured, —predicted Re stress, - - predicted k-ε).

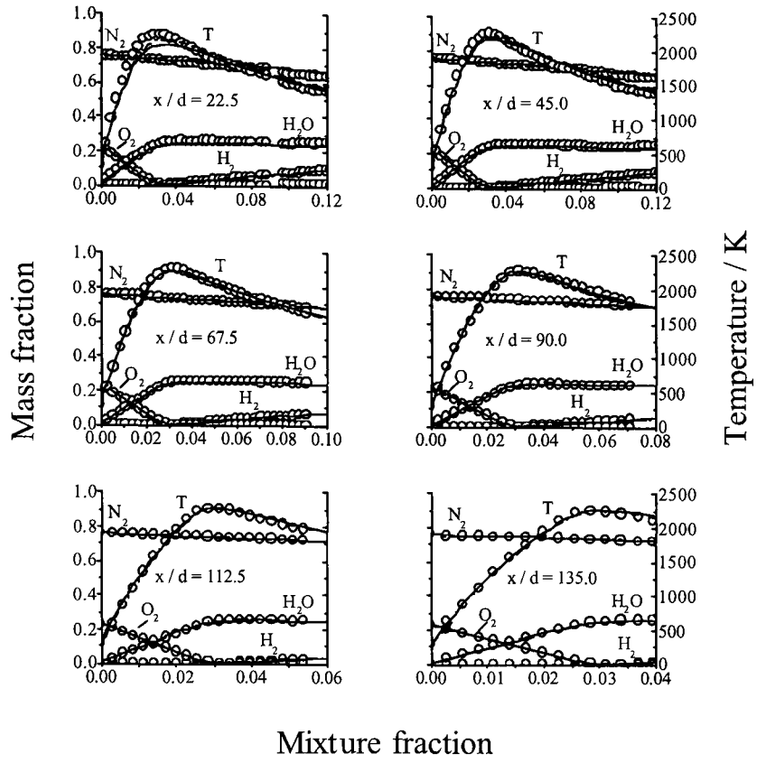

Figure 3.23 – Comparison of measured and predicted conditional species mass-fractions and temperature at six axial stations for hydrogen flame A, derived using kinetics scheme (ii) (o measured, —predicted Re stress, - - predicted k-ε).

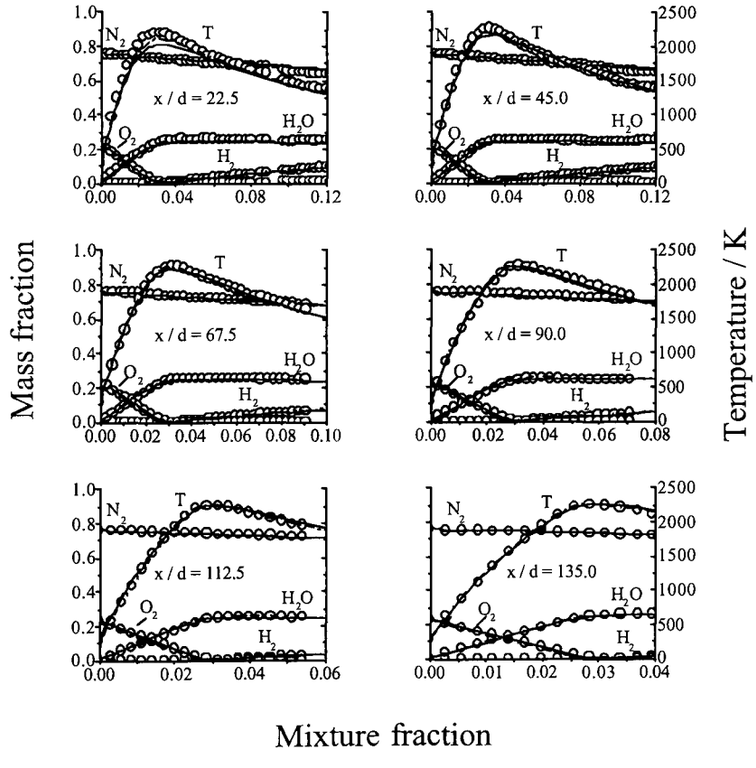

Figure 3.24 – Comparison of measured and predicted conditional species mass-fractions and temperature at six axial stations for hydrogen flame A, derived using kinetics scheme (iii) (o measured, —predicted Re stress, - - predicted k-ε).

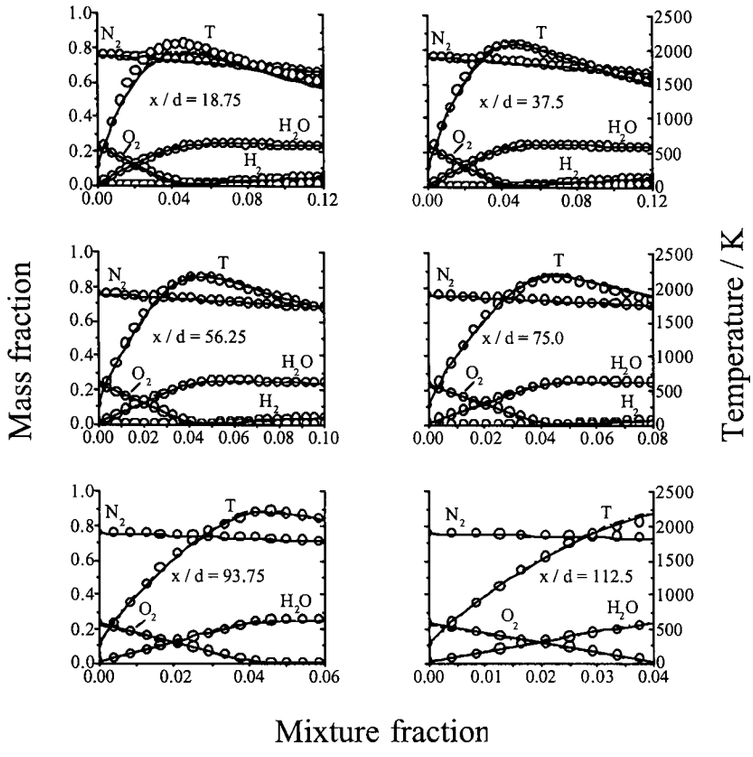

Figure 3.25 – Comparison of measured and predicted conditional species mass-fractions and temperature at six axial stations for hydrogen flame B, derived using kinetics scheme (iii) (o measured, —predicted Re stress, -·- predicted k-ε).

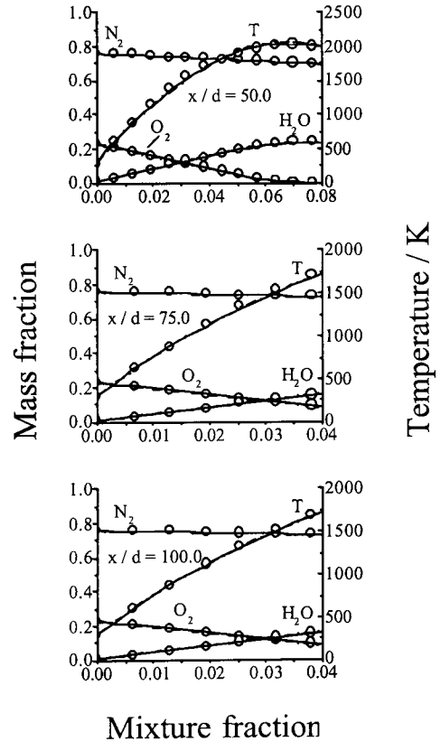

Figure 3.26 – Comparison of measured and predicted conditional species mass-fractions and temperature at six axial stations for hydrogen flame C, derived using kinetics scheme (iii) (o measured, —predicted Re stress, -·- predicted k-ε).

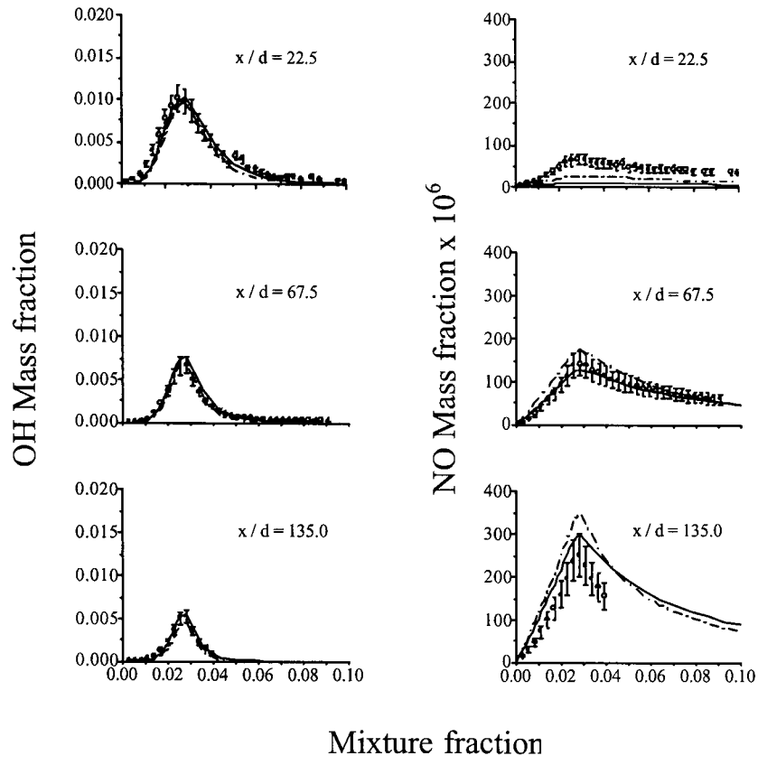

Figure 3.27 – Comparison of measured and predicted conditional OH and NO mass-fractions at three axial stations for hydrogen flame A, derived using kinetics scheme (i) (o measured, — predicted Re stress, - - predicted k-ε).

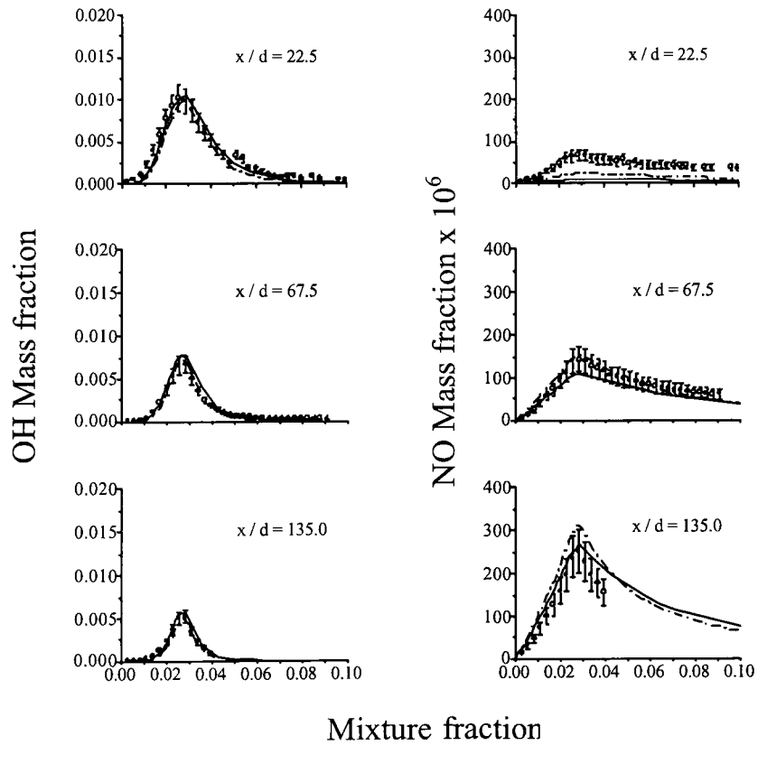

Figure 3.28 – Comparison of measured and predicted conditional OH and NO mass-fractions at three axial stations for hydrogen flame A, derived using kinetics scheme (ii) (o measured, — predicted Re stress, - - predicted k-ε).

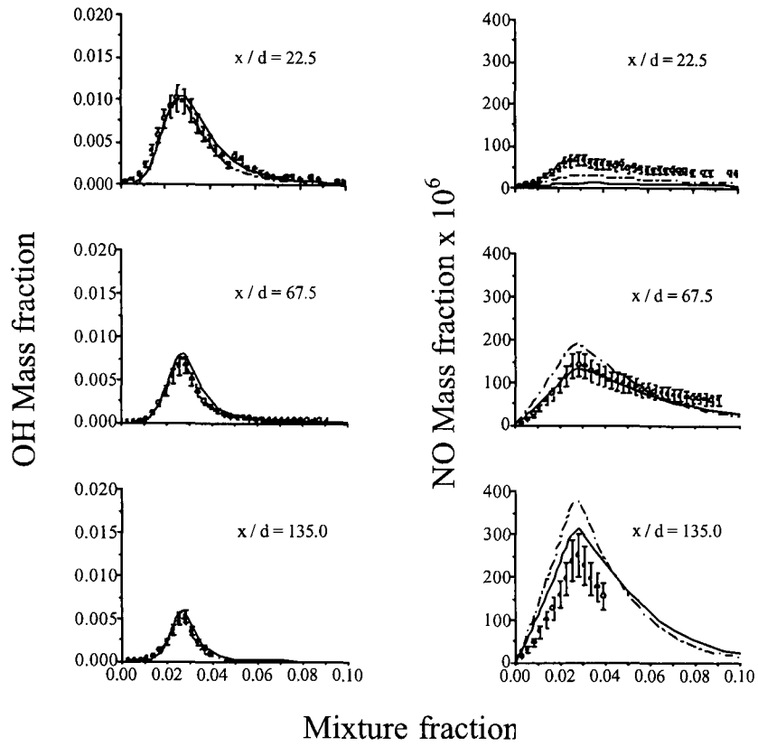

Figure 3.29 – Comparison of measured and predicted conditional OH and NO mass-fractions at three axial stations for hydrogen flame A, derived using kinetics scheme (iii) (o measured, —predicted Re stress, - - predicted k-ε).

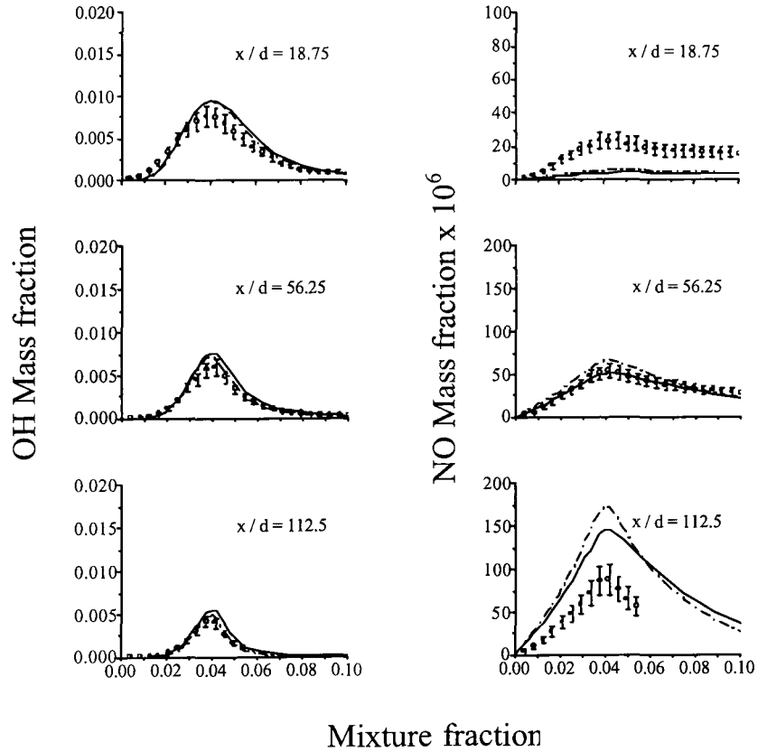

Figure 3.30 – Comparison of measured and predicted conditional OH and NO mass-fractions at three axial stations for hydrogen flame B, derived using kinetics scheme (iii) (o measured, —predicted Re stress, - - predicted k-ε).

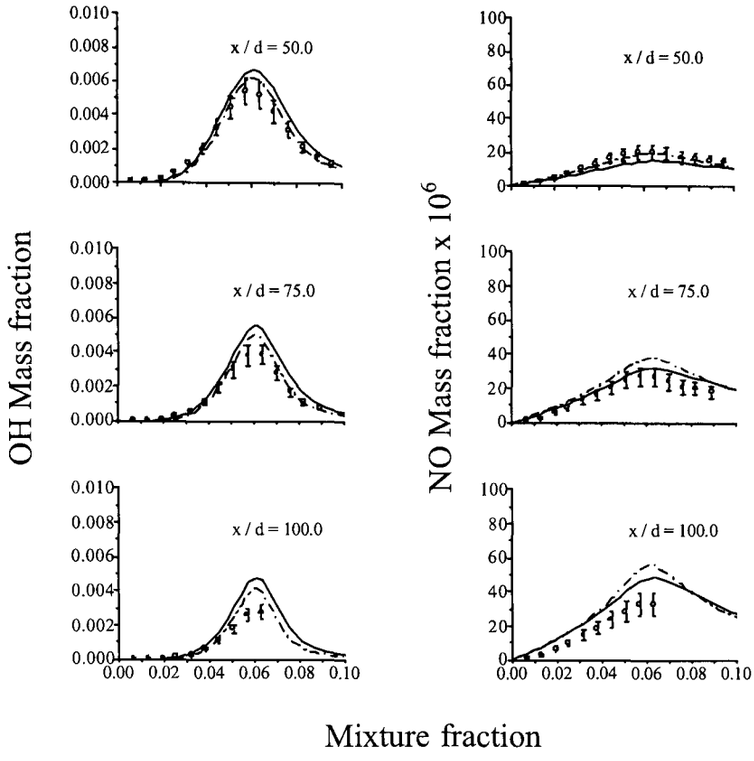

Figure 3.31 – Comparison of measured and predicted conditional OH and NO mass-fractions at three axial stations for hydrogen flame C, derived using kinetics scheme (iii) (o measured, — predicted Re stress, - - predicted k-ε).

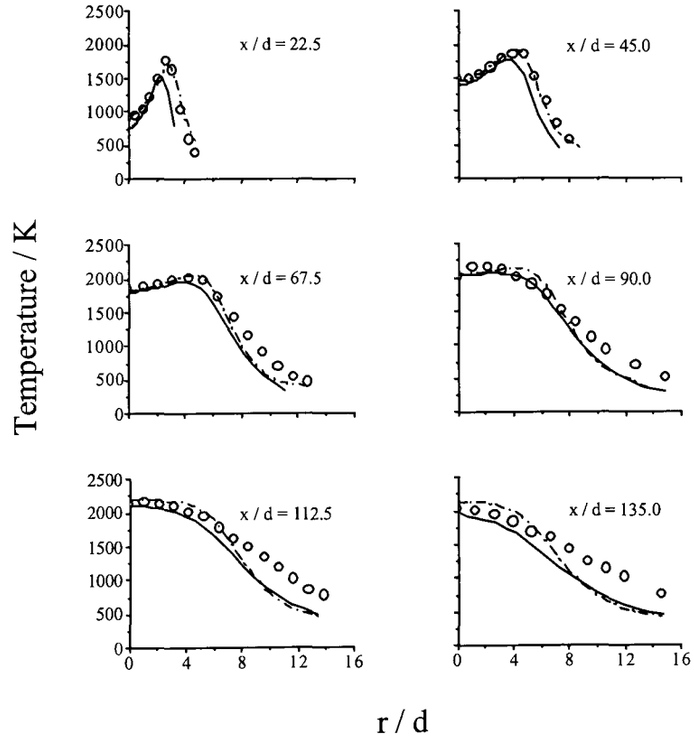

Figure 3.32 – Comparison of measured and predicted radial temperature profiles at six axial stations for hydrogen flame A, derived using kinetics scheme (i)
(o measured, — predicted Re stress, - - predicted k-ε).

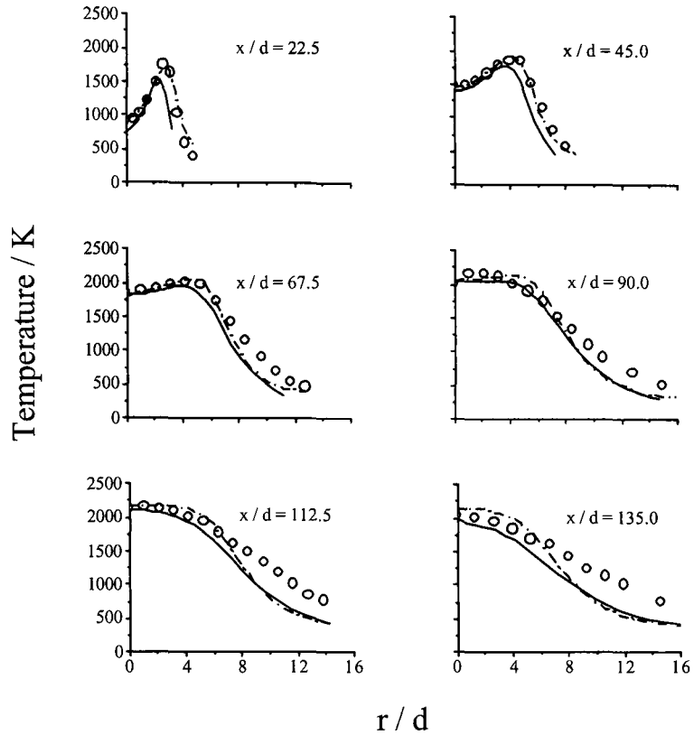

Figure 3.33 – Comparison of measured and predicted radial temperature profiles at six axial stations for hydrogen flame A, derived using kinetics scheme (ii)
(o measured, —predicted Re stress, - - predicted k-ε).

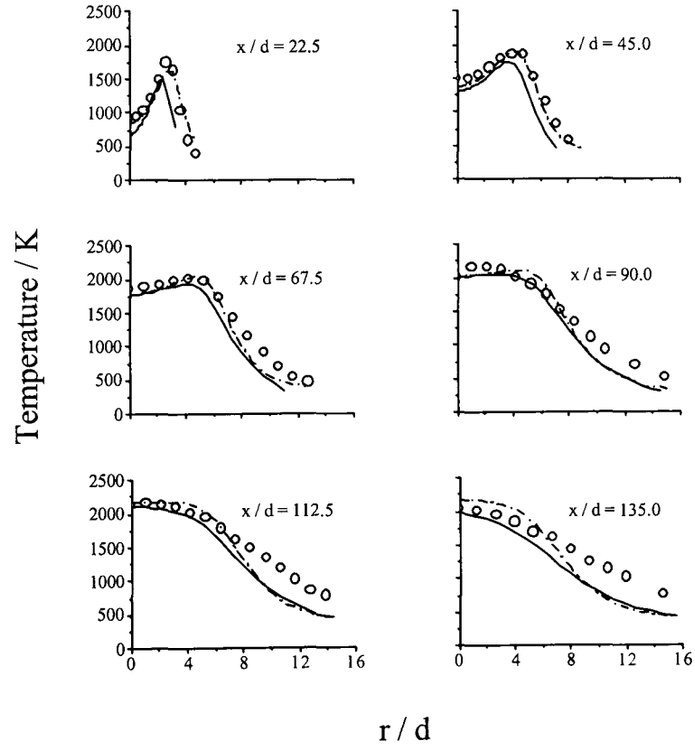

Figure 3.34 – Comparison of measured and predicted radial temperature profiles at six axial stations for hydrogen flame A, derived using kinetics scheme (iii)
(o measured, —predicted Re stress, - - predicted k-ε).

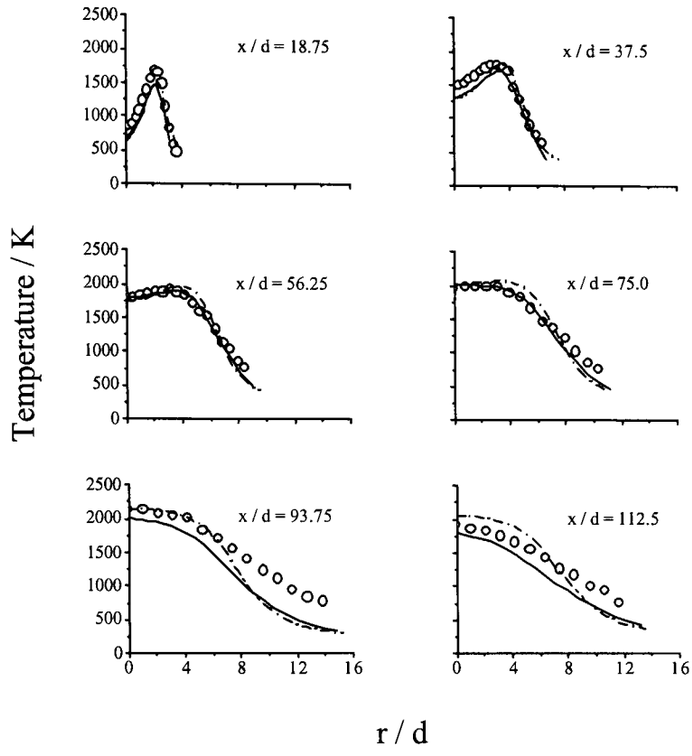

Figure 3.35 – Comparison of measured and predicted radial temperature profiles at six axial stations for hydrogen flame B, derived using kinetics scheme (iii)
(o measured, — predicted Re stress, - - predicted k-ε).

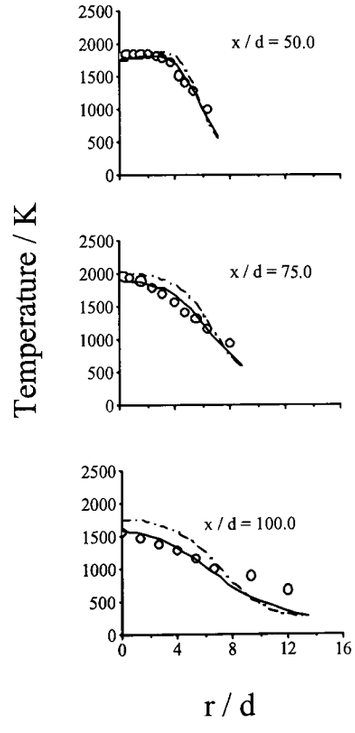

Figure 3.36 – Comparison of measured and predicted radial temperature profiles at six axial stations for hydrogen flame C, derived using kinetics scheme (iii)
(o measured, — predicted Re stress, - - predicted k-ε).

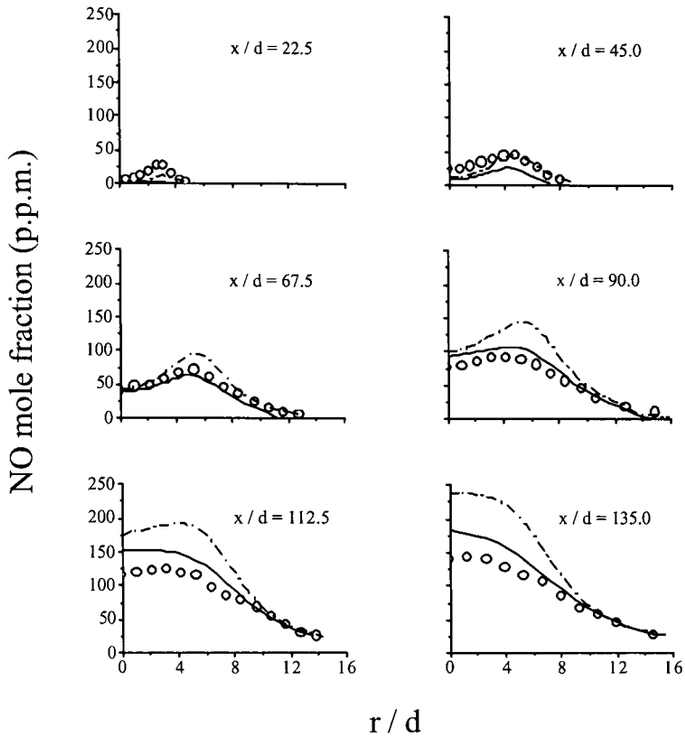

Figure 3.37 – Comparison of measured and predicted radial NO mole-fraction profiles at six axial stations for hydrogen flame A, derived using kinetics scheme (i) (o measured, — predicted Re stress, - - predicted k-ε).

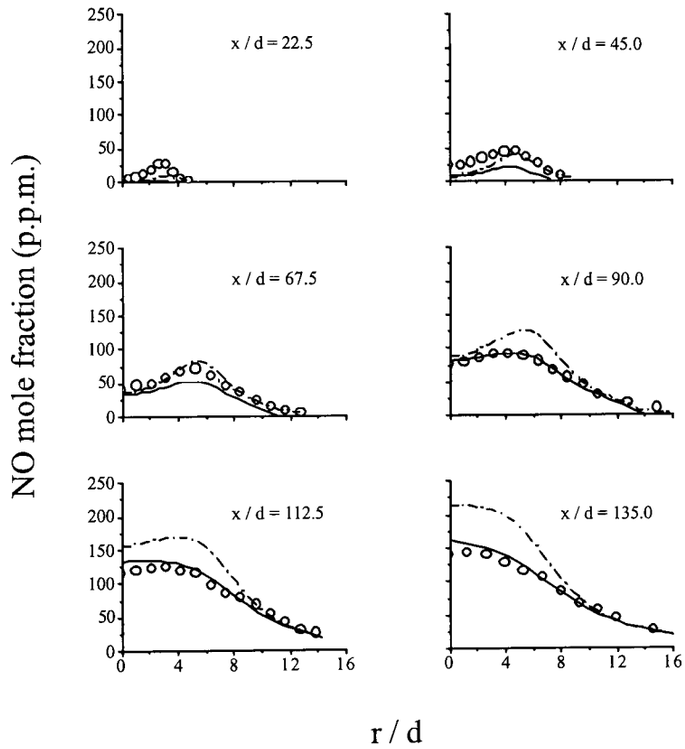

Figure 3.38 – Comparison of measured and predicted radial NO mole-fraction profiles at six axial stations for hydrogen flame A, derived using kinetics scheme (ii) (o measured, — predicted Re stress, - - predicted k-ε).

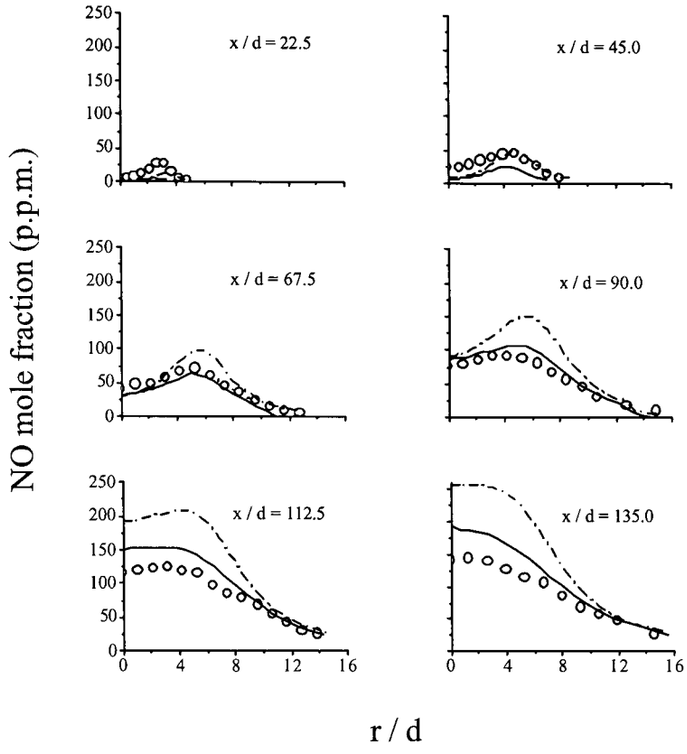

Figure 3.39 – Comparison of measured and predicted radial NO mole-fraction profiles at six axial stations for hydrogen flame A, derived using kinetics scheme (iii) (o measured, —predicted Re stress, - - predicted k-ε).

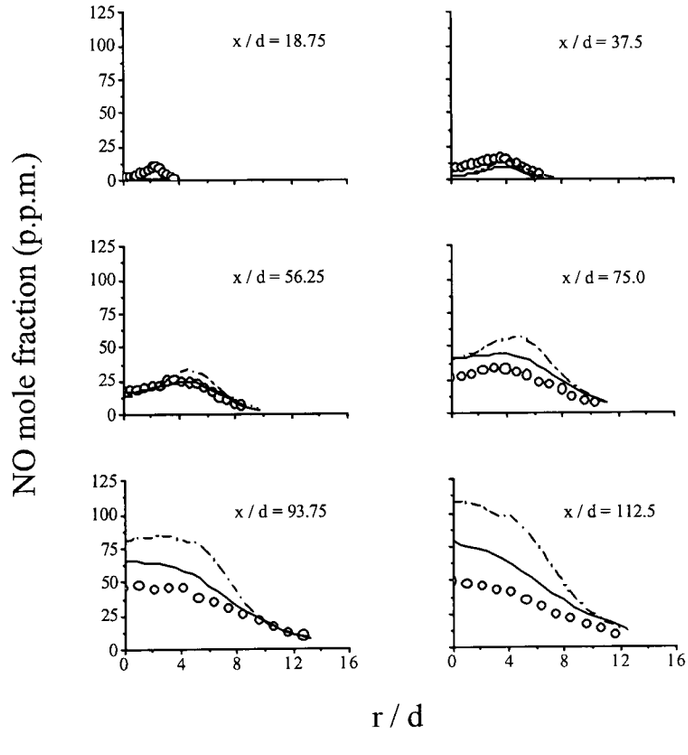

Figure 3.40 – Comparison of measured and predicted radial NO mole-fraction profiles at six axial stations for hydrogen flame B, derived using kinetics scheme (iii) (o measured, —predicted Re stress, - - predicted k-ε).

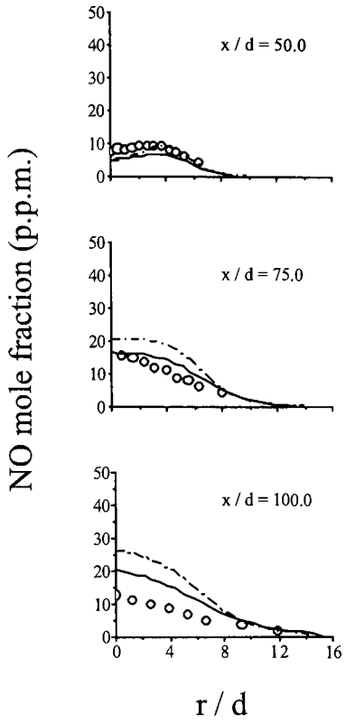

Figure 3.41 – Comparison of measured and predicted radial NO mole-fraction profiles at six axial stations for hydrogen flame C, derived using kinetics scheme (iii) (o measured, — predicted Re stress, - - predicted k-ε).

4: Second Order Conditional Moment Closure Modelling of Turbulent Hydrogen Jet Diffusion Flames

In the previous works discussed, a simple first-order closure of the conditional reaction-rate term $\langle w|\eta\rangle$ has been considered, based on the assumption that fluctuations of reactive scalars and temperature about the conditional mean are negligible. The validity of this assumption is questioned by Kronenburg et al (1998) after making an estimate of the influence of the fluctuation correlations as follows: Taking a Taylor expansion around the conditional mean of the reaction rate, and neglecting moments of third and higher order, it is found that:

$$\langle \rho w_r|\eta\rangle = k(Q_T)Q_\alpha Q_\beta\left(1+\frac{\langle Y_\alpha'' Y_\beta''|\eta\rangle}{Q_\alpha Q_\beta}+\left[b+\frac{T_a}{Q_T}\right]\left[\frac{\langle Y_\alpha'' T''|\eta\rangle}{Q_\alpha Q_T}+\frac{\langle Y_\beta'' T''|\eta\rangle}{Q_\beta Q_T}\right]+\frac{1}{2}\left[b\{b-1\}+\frac{2\{b-1\}T_a}{Q_T}+\frac{T_a^2}{Q_T^2}\right]\frac{\langle [T'']^2|\eta\rangle}{Q_T^2}\right) \tag{4.1}$$

where the chemical source term for the one-step irreversible reaction:

$$A+B=products$$

is given by:

$$w=\rho k Y_\alpha Y_\beta \tag{4.2}$$

where:
$$k = AT^{b} \exp\left(\frac{-T_a}{T}\right) \tag{4.3}$$

and
$$T_a = E/R \tag{4.4}$$

As can be seen from equation (4.1), the errors involved with first-order closure will be small if the conditional fluctuations of the reactive scalars and temperature are relatively small in comparison to the square of their respective means. However, Kronenburg et al (1998) use the derivation (4.1) to estimate a possible increase in the conditional reaction rate for NO to be a factor of 1.5 in a hydrogen jet diffusion flame, considering an activation temperature of 36,000K for thermal NO production, and a conditional temperature of 2000K, with conditional root-mean-square fluctuations of 124K. This estimate is a good indication that second-order closure may be required to represent the effects of conditional fluctuations on the reaction-rate term. In their experimental work, Barlow and Carter (1996) show that significant fluctuations of conditional mean values do occur at the base of rim-stable turbulent hydrogen diffusion flames, furthering the evidence for the requirement of second-order representation. It is evident from equation (4.1) that this expression contains a number of conditional variances and covariances, as defined by equations (4.5, 4.6) respectively, which if to be implemented, would require closure either by modelling or from their respective transport equations.

$$\left(Y''\right)^2 = K \quad ; \quad G = \left\langle K \middle| \eta \right\rangle \tag{4.5}$$

$$Y''_{\alpha} Y''_{\beta} = K_{\alpha\beta} \quad ; \quad G_{\alpha\beta} = \left\langle K_{\alpha\beta} \middle| \eta \right\rangle \tag{4.6}$$

Presently, investigation into these closures has not been conducted, and is out of the scope of this present study. This is markedly a too greater task to undertake, and another representation of these terms is sought. The following text outlines

the derivation of the transport equation for G, its application to second-order CMC modelling, and its subsequent application to calculations of turbulent jet diffusion flames. Results are then presented and evaluated for a number of test cases.

4.i Derivation of $G_{\alpha\beta}$ And G Transport Equations

Once again, the derivation of these conditional moment equations may be achieved via the joint pdf equation, or the decomposition method. The pdf route may be followed in Klimenko and Bilger (1999), but the decomposition method of Li and Bilger (1993) is that described below.

Firstly, using equation (2.41), an expression for $Y_\alpha'' Y_\beta''$ can be derived as follows. Multiplying (2.41) written for species α by Y_β'', and then summing with (2.41) written for species β and multiplied by Y_α'' yields:

$$\rho\frac{\partial K_{\alpha\beta}}{\partial t}+\rho u_l\frac{\partial K_{\alpha\beta}}{\partial x_l}-\frac{\partial}{\partial x_l}\left(\rho D\frac{\partial K_{\alpha\beta}}{\partial x_l}\right)+2\rho D\left(\frac{\partial Y_\alpha''}{\partial x_l}\frac{\partial Y_\beta''}{\partial x_l}\right)= \rho\left(w_\alpha Y_\beta''+w_\beta Y_\alpha''\right)+E_{D_{\alpha\beta}}+E_{D_{\beta\alpha}}-E_{Q_{\alpha\beta}}-E_{Q_{\beta\alpha}} \tag{4.7}$$

where: $$E_{D_{\alpha\beta}}=Y_\alpha''\rho D\frac{\partial\xi}{\partial x_l}\frac{\partial^2 Q_\beta}{\partial x_l\partial\eta}+Y_\alpha''\frac{\partial}{\partial x_l}\left(\rho D\frac{\partial Q_\beta}{\partial x_l}\right) \tag{4.8}$$

and $$E_{Q_{\alpha\beta}}=Y_\alpha''\left(\rho\frac{\partial Q_\beta}{\partial t}+\rho u_l\frac{\partial Q_\beta}{\partial x_l}-\rho\chi\frac{\partial^2 Q_\beta}{\partial\eta^2}\right) \tag{4.9}$$

Decomposing the correlation $Y_\alpha'' Y_\beta''$ in a similar manner to equation (2.4) and differentiating, equations (4.10) and (4.11) are realised.

$$\frac{\partial K_{\alpha\beta}}{\partial t}=\frac{\partial G_{\alpha\beta}}{\partial t}+\frac{\partial G_{\alpha\beta}}{\partial\eta}\frac{\partial\xi}{\partial t}+\frac{\partial K_{\alpha\beta}''}{\partial t} \tag{4.10}$$

$$\frac{\partial K_{\alpha\beta}}{\partial x_l}=\frac{\partial G_{\alpha\beta}}{\partial x_l}+\frac{\partial G_{\alpha\beta}}{\partial\eta}\frac{\partial\xi}{\partial x_l}+\frac{\partial K_{\alpha\beta}''}{\partial x_l} \tag{4.11}$$

Substitution of the preceding two equations into equation (4.7) provides the following:

$$\rho\frac{\partial G_{\alpha\beta}}{\partial t}+\rho u_l\frac{\partial G_{\alpha\beta}}{\partial x_l}-\rho\chi\frac{\partial^2 G_{\alpha\beta}}{\partial\eta^2}+2\rho D\left(\frac{\partial Y_\alpha''}{\partial x_l}\frac{\partial Y_\beta''}{\partial x_l}\right)= \rho\left(w_\alpha Y_\beta''+w_\beta Y_\alpha''\right)+E_{D_{\alpha\beta}}+E_{D_{\beta\alpha}}-E_{Q_{\alpha\beta}}-E_{Q_{\beta\alpha}}+E_G-E_K \tag{4.12}$$

where:
$$E_G=\frac{\partial}{\partial x_l}\left(\rho D\frac{\partial G_{\alpha\beta}}{\partial x_l}\right)+\rho D\frac{\partial\xi}{\partial x_l}\frac{\partial}{\partial x_l}\left(\frac{\partial G_{\alpha\beta}}{\partial\eta}\right) \tag{4.13}$$

and
$$E_K=\rho\frac{K_{\alpha\beta}''}{\partial t}+\rho u_l\frac{\partial K_{\alpha\beta}''}{\partial x_l}-\frac{\partial}{\partial x_l}\left(\rho D\frac{\partial K_{\alpha\beta}''}{\partial x_l}\right) \tag{4.14}$$

In a similar manner to the formulation of equation (2.42), taking the conditional expectation of the above expression gives:

$$\frac{\partial G_{\alpha\beta}}{\partial t}+\langle u_l|\eta\rangle\frac{\partial G_{\alpha\beta}}{\partial x_l}-\langle\chi|\eta\rangle\frac{\partial^2 G_{\alpha\beta}}{\partial\eta^2}+ \frac{\frac{\partial}{\partial x_l}\left(\langle\rho|\eta\rangle\langle u_l''K_{\alpha\beta}''|\eta\rangle P(\eta)\right)}{P(\eta)\langle\rho|\eta\rangle}=\langle w_\alpha''Y_\beta''+w_\beta''Y_\alpha''|\eta\rangle- 2\left\langle D\left(\frac{\partial Y_\alpha''}{\partial x_l}\frac{\partial Y_\beta''}{\partial x_l}\right)\middle|\eta\right\rangle-\frac{\partial Q_\alpha}{\partial x_l}\langle u_l''Y_\beta''|\eta\rangle-\frac{\partial Q_\beta}{\partial x_l}\langle u_l''Y_\alpha''|\eta\rangle+ \frac{\partial^2 Q_\alpha}{\partial\eta^2}\langle\chi''Y_\beta''|\eta\rangle+\frac{\partial^2 Q_\beta}{\partial\eta^2}\langle\chi''Y_\alpha''|\eta\rangle \tag{4.15}$$

This represents the unclosed equation for the conditional scalar covariance. In its derivation, a similar approach is taken for the representation of E_K as used for the term e_Y in equation (2.42). In addition, the terms $\langle E_{D_{\alpha\beta}}|\eta\rangle$ and $\langle E_G|\eta\rangle$ are deemed small for high Reynolds number flows, and omitted as negligible from equation (4.15)

Finally, a transport equation for the conditional scalar variance can be established by setting $\alpha = \beta$, *videlicet*:

$$\frac{\partial G}{\partial t} + \langle u_l | \eta \rangle \frac{\partial G}{\partial x_l} - \langle \chi | \eta \rangle \frac{\partial^2 G}{\partial \eta^2} + \frac{\frac{\partial}{\partial x_l}\left(\langle \rho | \eta \rangle \langle u_l'' K'' | \eta \rangle P(\eta)\right)}{P(\eta)\langle \rho | \eta \rangle} = 2\langle w'' Y'' | \eta \rangle - 2\left\langle D\left(\frac{\partial Y''}{\partial x_l}\right)^2 \middle| \eta \right\rangle - 2\frac{\partial Q}{\partial x_l}\langle u_l'' Y'' | \eta \rangle + 2\frac{\partial^2 Q}{\partial \eta^2}\langle \chi'' Y'' | \eta \rangle \tag{4.16}$$

We now have a number of terms that require modelling, and the approaches are discussed further in Chapter 4.iii.ii.

4.ii Application of The Conditional Variance Equation in Second Order CMC Modelling

The observations made at the beginning of Chapter 4, alongside the results presented in Chapter 3, and in addition to those of previous investigations described in Chapter 2.ii.ii.iv, invariably indicate the requirement of a second-order or higher-order closure of the reaction rate term in the CMC equation. It is evident that this is the case when considering thermally sensitive reactions such as NO pathways, and also for the representation of extinction phenomena.

The following text defines the approach taken in the implementation of second-order CMC to a turbulent jet diffusion flame, and subsequently its performance is discussed in light of earlier first-order calculations. Using this study as a validation of the model, a modelling strategy is presented, and its applicability to a lifted turbulent jet diffusion flame investigated.

Conditional second-order moments of a conditional reaction rate may be incorporated by either the evaluation of an approximation such as the Taylor expansion given in equation (4.1), or in an exact form as defined in equation (4.17)

$$\langle w_r | \eta \rangle = \int_Y \int_h w_r(\boldsymbol{Y}, h) P(\boldsymbol{Y}, h | \eta) \, d\boldsymbol{Y} dh \qquad (4.17)$$

where $\boldsymbol{Y}$ is the composition vector of the scalar variable Y. Here, $P(\boldsymbol{Y}, h|\eta)$ is the joint pdf of $\boldsymbol{Y}$ and h, and unknown. However, presumed shape pdfs such as a clipped Gaussian or beta-function may be implemented to represent the

distribution. Variances and covariances may be used for this task, but once again, the problem of equation number and closure comes to the fore. It is evident that another approach to this issue is required.

The following methodology is similar to that employed by Kronenburg (1998) and Devaud (1999) in their attempts to elucidate second-order chemistry effects in turbulent jet diffusion flames. The methods do differ, and the implications are subsequently discussed.

The modelling approach implemented in this study has a basis in the systematic reduction of a full reaction mechanism to a one-step global reaction. Following the method of Chen (1998), and ignoring nitrogen-carrying species, this single step can be defined for hydrogen oxidation as equation (4.18).

$$2H_2 + O_2 \rightarrow 2H_2O \tag{4.18}$$

With the introduction of a reaction progress variable (Γ_t, the total number of moles per unit mass as defined by equation (4.19)), the system can be fully described by the mixture fraction, the enthalpy, and the new variable.

$$\Gamma_t = \sum_{\alpha=1}^{i} \frac{Y_\alpha}{W_\alpha} \tag{4.19}$$

With reference to Table (3.4), Janicka and Kollmann (1979) discuss the four pairs of bi-molecular reactions (first eight), describing them as fast 'shuffle' reactions in comparison to the slower three-body recombination reactions. The progress of the global reaction (4.18) can thus be expressed in terms of the recombinations, *id est*:

$$w_{\Gamma_t} = w_9 + w_{20} - w_{21} \tag{4.20}$$

For any value of mixture fraction, this system will evolve within the limits of a minima and maxima value of Γ_t. An inspection of (4.18) indicates, hydrogen

oxidation reduces the total number of moles in the system, and hence the maximum value of Γ_t at any value of Z can be defined as when the fuel and the oxidiser are mixed without reaction. This can be simply transcribed as:

$$\Gamma_{t\max} = \frac{ZY_{H_2,f}}{W_{H_2}} + \frac{ZY_{He,f}}{W_{He}} + \frac{(1-Z)(1+\zeta)}{\left(W_{N_2} + \zeta W_{O_2}\right)} \tag{4.21}$$

where:

$$\zeta = \frac{0.228}{0.772}$$

Conversely, the minima occur when equilibrium is reached, and for any value of Z this can be obtained from equilibrium calculations.

Using these definitions, and further assumptions described in the preceding text, the molar concentrations of a simplified seven-species system consisting of O_2, H_2O, H_2, OH, H, O, and HO_2 can be defined. Elements of this reduced mechanism model were first suggested by Dixon-Lewis et al (1975), and implemented by Janicka and Kollmann (1979). More recent works involving its usage include that of Chen and Kollmann (1990) with reference to presumed-pdf modelling, and Montgomery et al (1979), being incorporated into DNS.

Major Species: O_2, H_2, H_2O

The concentrations of the atomic species are linearly related to the mixture fraction, and hence, for the H_2/Air combustion system, the following balances can be easily formulated considering the species in question. A balance on the O atom provides:

$$2\frac{0.228\left(1-\left[\eta\left\{Y_{H_2}+Y_{He}\right\}\right]\right)}{W_{O_2}} = 2\Gamma_{O_2} + \Gamma_{H_2O} + \Gamma_O + \Gamma_{OH} \tag{4.22}$$

and the concentration of O_2 can be defined as:

$$\Gamma_{O_2} = \frac{0.228\left(1-\left[\eta\left\{Y_{H_2}+Y_{He}\right\}\right]\right)}{W_{O_2}} - 0.5\left(\Gamma_{H_2O}+\Gamma_O+\Gamma_{OH}\right) \tag{4.23}$$

where Y_{H_2} is the mass fraction of H_2 originating in the fuel stream. Similarly, a balance on H atom reveals:

$$\Gamma_{H_2} = \frac{\eta Y_{H_2}}{W_{H_2}} - \Gamma_{H_2O} - 0.5\left(\Gamma_H+\Gamma_{OH}\right) \tag{4.24}$$

Using the definition of the progress variable Γ_t (equation 4.19), a balance over the number of moles in the system enables the derivation of an expression for Γ_{H_2O}, *videlicet*:

$$\Gamma_{H_2O} = \Gamma_t - \Gamma_{O_2} - \Gamma_{N_2} - \Gamma_{H_2} - \Gamma_H - \Gamma_O - \Gamma_{OH} \tag{4.25}$$

Minor Species: H, O, OH, HO_2

The previously imposed partial equilibrium assumption leads to the definition of the three equilibrium equations (4.26, 4.27, 4.28) for the radicals H, O, and OH.

$$\Gamma_H = k_{1f}^{e\,1/2} k_{3f}^{e} \frac{\Gamma_{O_2}^{1/2}\Gamma_{H_2}^{3/2}}{\Gamma_{H_2O}} \tag{4.26}$$

$$\Gamma_O = k_{1f}^{e} k_{3f}^{e} \frac{\Gamma_{O_2}\Gamma_{H_2}}{\Gamma_{H_2O}} \tag{4.27}$$

$$\Gamma_{OH} = \left(k_{1f}^{e} k_{2f}^{e} \Gamma_{O_2}\Gamma_{H_2}\right)^{1/2} \tag{4.28}$$

where k_α^e is the equilibrium constant of reaction α evaluated at a given system temperature.

Assuming HO_2 to be in steady state, Montgomery et al (1997) obtain an expression for the number of moles, *id est*:

$$\Gamma_{HO_2} = \frac{k_5 \Gamma_H \Gamma_{O_2} M}{(k_6 + k_7)\Gamma_H + k_9 \Gamma_{OH}} \tag{4.29}$$

Enthalpy of the system: h

In addition to the seven balance equations for species, the equation for the system enthalpy must be solved so as to ensure its conservation at any given (η, Γ). This balance equation takes the form:

$$\sum_{\alpha=1}^{i} \Gamma_\alpha c_{p,\alpha} (T - 298) = \sum_{\alpha=1}^{i} h_\alpha (T_{ini}) - \sum_{\alpha=1}^{i} h_{\alpha,form} \tag{4.30}$$

where: $$\sum_{\alpha=1}^{i} h_\alpha (T_{ini}) = \eta h_f (T_{ini}) + (1-\eta) h_o (T_{ini}) \tag{4.31}$$

and thermodynamic data required for the calculations is taken from McBride et al (1993), Burcat and McBride (1993), and Burcat (2001).

Eight balance equations are thus defined for the respective reactive species and enthalpy, forming a highly non-linear set. Their simultaneous solution will define the system at any given value of (η, Γ_t, h). With this system information, the instantaneous progress rate of any reaction can be defined as:

$$w_r^{pe} = w_r^{pe} (\eta, \Gamma_t, h) \tag{4.32}$$

where the superscript pe indicates the variable's derivation under partial equilibrium assumptions.

The assumption that the conditional average enthalpy remains constant and only a function of mixture fraction, allows a simplification of equation (4.17) which

leads to an expression for the conditional reaction progress rate in terms of the progress variable Γ_t and η only, *videlicet*:

$$\left\langle w_r^{pe} \middle| \eta \right\rangle = \int_{\Gamma_t} w_r^{pe}(\eta, \Gamma_t) P(\eta, \Gamma_t) d\Gamma_t \tag{4.33}$$

Now, once again considering the mean conditional reaction rate, it can be expressed in a form which takes higher-order effects into consideration, *id est*:

$$\left\langle w_r \middle| \eta \right\rangle_{2ord} = \left\langle w_r \middle| \eta \right\rangle + \left\langle w_{r,corr}^{pe} \middle| \eta \right\rangle \tag{4.34}$$

where the subscript *corr* indicates a correction to the first-order term. Evidently, this correction term requires defining, and such a derivation can be achieved with use of equation (4.33) to give:

$$\left\langle w_{r,corr}^{pe} \middle| \eta \right\rangle = \left\langle w_r^{pe} \middle| \eta \right\rangle - w_r^{pe}\left(\left\langle \Gamma_t \middle| \eta \right\rangle, \eta\right) \tag{4.35}$$

where the final term in the equation describes the reaction rate as a function of η, and of Γ_t conditionally established at said η, which is easily obtained from subsequent calculations. The remaining term requiring elucidation in this method is the pdf of Γ_t and η in equation (4.33). Γ_t is the progress variable as previously discussed, and construction of the pdf is possible through use of this variable, its variance (Γ''^2), and a presumed form. In this study, a β-pdf is applied throughout, and the required value of $\left\langle \Gamma''^2 \middle| \eta \right\rangle$ is obtained from the solution of its transport equation, alongside the conditional moment equations outlined in the procedures of Chapter 3.iii.

4.iii Implementation of Second Order Conditional Moment Closure to The Modelling of H_2/He Turbulent Jet Diffusion Flames Far From Extinction

Here follows discussion regarding the implementation of the procedures defined in Chapter 4.ii as applied to the same flame configurations investigated in Chapter 3. A subsequent analysis of results is presented in context of those obtained in Chapter 3, and conclusions drawn as to the implications of this work. In this investigation, the same FORTRAN coding is used as that of Chapter 3. That used to describe the turbulence quantities remains unchanged, and modifications are made solely to the CMC code. These modifications can essentially be split into two tasks for the purpose of this discussion. The initial is the evaluation of a corrected set of species production rates, used to modify the first-order CMC transport equations. The second is to solve a conservation equation for the transport of scalar variance alongside the first-order equations.

4.iii.i Realisation of Corrected Species Production Rates

To obtain the correction term for the species production rates, it is required initially to evaluate equation (4.35) for each reaction r, at each value of η. As discussed, it is therefore necessary to establish a system composition over Γ_t space at each η, in addition to the pdf of Γ_t at the same location. Hence, the eight equations defining the molar concentrations of the seven species, and that of the enthalpy, must be simultaneously solved at each spatial location. Due to the nonlinearity of this equation set, a Newton-Raphson method is applied to their solution. This method is very efficient for multidimensional root finding, and is utilised via the FORTRAN code described by Press at al (1992). Although the Newton-Raphson method displays poor global convergence qualities, a sufficient initial condition for the solver can be supplied from equilibrium calculations, and so it proves to be an ideal method in this instance.

Γ_t space is represented by forty-five nodes, lying between the limits $\Gamma_{t\min}$ and $\Gamma_{t\max}$ as previously defined. The number of nodes was chosen after carrying out calculations using lesser and greater concentrations. It was found that this number provided grid-independent solutions whilst not being overly demanding upon computational resources. The progress rates for each reaction are obtained using the results of calculations by the CHEMKIN set of subroutines in a similar manner to their implementation for the first-order case. The term $\left\langle w_r^{pe} \middle| \eta \right\rangle$ may now be generated by the solution of equation (4.33), involving a convolution

with a presumed form β-pdf of the conditional variables Γ_t and $\Gamma_t''^2$, and subsequent integration over Γ_t space. It is now trivial to evaluate $w_r^{pe}\left(\langle\Gamma_t|\eta\rangle,\eta\right)$ of equation (4.35) from the data generated, and hence obtain the correction term for the conditional reaction progress rates defined by the aforementioned equation. To utilise this information in CMC calculations of species concentrations, corrections to the scalar production rates are established. With reference to table (3.4), these terms can be described as functions of the slower and the recombination reaction-rate corrections, *id est*:

$$w_{O_2,corr}^{pe} = w_{11,corr}^{pe} + w_{13,corr}^{pe} + w_{14,corr}^{pe} + w_{15,corr}^{pe} - w_{9,corr}^{pe} \tag{4.36}$$

$$w_{H_2O,corr}^{pe} = w_{12,corr}^{pe} + w_{13,corr}^{pe} + w_{17,corr}^{pe} + w_{20,corr}^{pe} - w_{16,corr}^{pe} \tag{4.37}$$

$$w_{H_2,corr}^{pe} = w_{11,corr}^{pe} + w_{21,corr}^{pe} \tag{4.38}$$

$$w_{OH,corr}^{pe} = 2\times w_{10,corr}^{pe} + w_{14,corr}^{pe} + w_{16,corr}^{pe} + 2\times w_{18,corr}^{pe} - \left(w_{13,corr}^{pe} + w_{17,corr}^{pe} + 2\times w_{19,corr}^{pe} + w_{20,corr}^{pe}\right) \tag{4.39}$$

$$w_{H,corr}^{pe} = -\left(w_{9,corr}^{pe} + w_{10,corr}^{pe} + w_{11,corr}^{pe} + w_{12,corr}^{pe} + w_{20,corr}^{pe} + 2\times w_{21,corr}^{pe}\right) \tag{4.40}$$

$$w_{O,corr}^{pe} = w_{12,corr}^{pe} - w_{14,corr}^{pe} \tag{4.41}$$

$$w_{HO_2,corr}^{pe} = 0 \tag{4.42}$$

where the subscripted numbers refer sequentially to the reactions of the table. These corrections may now be applied to the appropriate mean species production rate terms in the CMC source terms. For the purpose of practicality, the corrections are calculated only once per axial step, and the assumption is hence made that the change in the magnitude of the reaction-rate fluctuations over one integration step is negligible.

4.iii.ii Evaluation And Solution of The Transport Equation For The Conditional Variance $\Gamma_t''^2$

For the implementation of equation (4.33), the conditional variance of Γ_t is required at each location (η,Γ_t) for the construction of the presumed form pdf in addition to the reaction rates. This is effected by the solution of the transport equation for $\Gamma_t''^2$ alongside the existing CMC scalar equations. Rewriting equation (4.16) in terms of the progress variable Γ_t and its fluctuation Γ_t'', provides such an equation, *videlicet*:

$$\frac{\partial \Gamma_t''^2}{\partial t}+\langle u_l|\eta\rangle\frac{\partial \Gamma_t''^2}{\partial x_l}-\langle\chi|\eta\rangle\frac{\partial^2\Gamma_t''^2}{\partial\eta^2}+\frac{\frac{\partial}{\partial x_l}\left(\langle\rho|\eta\rangle\left\langle u_l''(\Gamma_t'')^2\middle|\eta\right\rangle P(\eta)\right)}{P(\eta)\langle\rho|\eta\rangle}= \\ 2\left\langle w_{\Gamma_t}''\Gamma_t''\middle|\eta\right\rangle-2\left\langle D\left(\frac{\partial\Gamma_t''}{\partial x_l}\right)^2\middle|\eta\right\rangle-2\frac{\partial\Gamma_t}{\partial x_l}\langle u_l''\Gamma_t''|\eta\rangle+2\frac{\partial^2\Gamma_t}{\partial\eta^2}\langle\chi''\Gamma_t''|\eta\rangle \tag{4.43}$$

where $\Gamma_t''^2$ represents a conditional value. Ordered sequentially, the terms requiring modelling are defined below.

$$T_i=\langle u_l|\eta\rangle\frac{\partial\Gamma_t''^2}{\partial x_l}$$

$$T_{ii}=\langle\chi|\eta\rangle\frac{\partial^2\Gamma_t''^2}{\partial\eta^2}$$

$$T_{iii}=\frac{\frac{\partial}{\partial x_l}\left(\langle\rho|\eta\rangle\left\langle u_l''(\Gamma_t'')^2\middle|\eta\right\rangle P(\eta)\right)}{P(\eta)\langle\rho|\eta\rangle}$$

$$T_{iv}=2\left\langle w_{\Gamma_t}''\Gamma_t''\middle|\eta\right\rangle$$

$$T_v = 2\left\langle D\left(\frac{\partial \Gamma_t''}{\partial x_l}\right)^2 \middle| \eta \right\rangle$$

$$T_{vi} = 2\frac{\partial \Gamma_t}{\partial x_l}\langle u_l'' \Gamma_t'' | \eta \rangle$$

$$T_{vii} = 2\frac{\partial^2 \Gamma_t}{\partial \eta^2}\langle \chi'' \Gamma_t'' | \eta \rangle$$

Each of these terms requires closing in a manner consistent with the other scalar transport equations, and the type of the flow situation considered in this investigation. Terms T_i and T_{ii} pose no new modelling difficulties as $\langle u_l | \eta \rangle$ and $\langle \chi | \eta \rangle$ have been evaluated previously, and applied in equation (2.42). Term T_{iii}, representing convective transport due to conditional fluctuations, is assumed negligible in comparison to term T_{iv}, as observed by Li and Bilger (1993) in light of experimental data for a turbulent reactive-scalar mixing layer. Hence, this term is not modelled in the final form of the equation. Term T_{iv} itself, being the chemical source term of the equation, requires careful consideration in its modelling, being specific to the application. It can be expanded as equation (4.44),

$$\langle w_{\Gamma_t}'' \Gamma_t'' | \eta \rangle = \langle w_{\Gamma_t} \Gamma_t | \eta \rangle - \langle w_{\Gamma_t} | \eta \rangle \langle \Gamma_t | \eta \rangle \tag{4.44}$$

and subsequently modelled as:

$$\begin{aligned} \langle w_{\Gamma_t} \Gamma_t | \eta \rangle - \langle w_{\Gamma_t} | \eta \rangle \langle \Gamma_t | \eta \rangle \approx & \int_{\Gamma_t} w_{\Gamma_t}^{pe}(\eta, \Gamma_t) \Gamma_t P(\eta, \Gamma_t) d\Gamma_t \\ & - \langle \Gamma_t | \eta \rangle \int_{\Gamma_t} w_{\Gamma_t}^{pe}(\eta, \Gamma_t) P(\eta, \Gamma_t) d\Gamma_t \end{aligned} \tag{4.45}$$

where $w_{\Gamma_t}^{pe}$ is defined by equation (4.20). Term T_v, being the reactive-scalar dissipation, can be modelled as described by Li and Bilger (1993), *id est*:

$$2\left\langle D\left(\frac{\partial\Gamma_t''}{\partial x_l}\right)^2\middle|\eta\right\rangle = C_{T_v}\left(\frac{\varepsilon}{k}\right)\Gamma_t''^2 \tag{4.46}$$

where in general, from experimental deliberation, $C_{T_v} \approx 2.0$. This form echoes that used for unconditional scalar dissipation modelling, although no real justification for this has yet been found. Using the same hypothesis as applied to the omission of the term T_{iii}, term T_{vi} may be neglected due to transverse gradients of Γ_t being small in most instances of shear flows. Once again referring to Li and Bilger (1993), the generation term due to the conditional scalar dissipation fluctuation (T_{vii}) can be represented by:

$$2\frac{\partial^2\Gamma_t}{\partial\eta^2}\langle\chi''\Gamma_t''|\eta\rangle = C_{T_{vii}}\langle\chi|\eta\rangle\left(\Gamma_t''^2\right)^{1/2}\frac{\partial^2\Gamma_t}{\partial\eta^2} \tag{4.47}$$

Kronenburg (1998) investigates the effects of constants C_{T_v} and $C_{T_{vii}}$ on both the prediction of unconditional variance, and root-mean-square (rms) temperature fluctuations. He observes that good agreement of temperature fluctuations with experimental data is achieved with constants these constants set to 1.82 and 1.1 respectively. These are in line with observations made by Li and Bilger (1993) in their mixing-layer investigations, and are hence employed in this study. With the exception of the term involving chemical influence, the closed transport equation for conditional variance hence takes the form:

$$\begin{aligned}\frac{\partial\Gamma_t''^2}{\partial t} + \langle u_l|\eta\rangle\frac{\partial\Gamma_t''^2}{\partial x_l} - \langle\chi|\eta\rangle\frac{\partial^2\Gamma_t''^2}{\partial\eta^2} = \\ 2\langle w''\Gamma_t''|\eta\rangle - C_{T_v}\left(\frac{\varepsilon}{k}\right)\Gamma_t''^2 + C_{T_{vii}}\langle\chi|\eta\rangle\left(\Gamma_t''^2\right)^{1/2}\frac{\partial^2\Gamma_t}{\partial\eta^2}\end{aligned} \tag{4.48}$$

Due to the assumptions made during the construction of the partial equilibrium model, this equation only holds near to the stoichiometric value of mixture

fraction, and at temperatures above 1,200K. The accuracy of $\Gamma_t''^2$ outside these parameters is not considered to be of great concern as the magnitude of the fluctuation in these regions of composition space is found to be negligible. and hence equation (4.48) is applied throughout the solution domain, with the data lying outside the allowable range being obtained via an extrapolation technique. For this, a rational function scheme was found to be the most suitable, and the FORTRAN coding was that provided in Press et al (1991). As with the calculations of species production rate corrections, the variance source term is also calculated only once per CMC axial step, bearing in mind similar assumptions.

4.iii.iii Results And Discussion

As previously mentioned, the three flames under investigation here are those of Barlow and Carter (1994,1996), and previously studied using a first-order chemistry closure in Chapter 3. All calculations subsequently discussed have been conducted using the same turbulence and flow-field data as used in the aforementioned study, and hence no further study shall be entered into regarding the mixing-field statistics. The same combustion code was also applied, with the exception of the modification discussed above being carried out. All calculations have however been carried out using data obtained from the application of kinetics scheme (ii) as defined in Chapter 3. Discussion regarding the implementation of differing kinetics schemes has already been made in said chapter, and no further analysis is considered necessary. Scheme (ii) is chosen

for application here for no more a reason than it produced marginally superior predictions, although possibly fortuitous, over the other two schemes applied. As with the first-order calculations, density coupling between the flow-field and chemistry is not conducted, but an analysis of such calculations can be read in Chapter 5. It should be noted that the ordering of the related figures in this chapter has been made so as to keep the data collected into that of individual flames. The discussion that follows however requires various analysis of data, and so the ordering of figures may appear not to be sequentially presented.

Figure (4.1) depicts first- and second-order predictions of major species and temperature in flame A, plotted in composition space, and obtained in conjunction with kinetics scheme (ii) with the Reynolds-stress/Scalar Flux (RSSF) (Jones and Musonge 1988) turbulence closure. It can be seen that at all locations, predictions are in good agreement with data, excepting an under-prediction of temperature at the first measuring station around stoichiometric, as noted in Chapter 3. Differences observed between the first- and second-order schemes are minimal, though a slight decrease in temperature and H_2O formation is seen at, and on the fuel-rich side of, stoichiometric for the higher-order case. As previously mentioned, the effects of second-order closure mainly act upon the reactions concerning the recombination of radicals, and effect an enhancement of these reactions. This radical depletion is the primary cause of these observations made. With downstream progression, these minor effects become lesser in magnitude, and at later measuring-stations at far-field locale, differences between the results of the first- and second-order schemes are negligible. Figure (4.2) and Figure (4.3) show predictions for flames B and C, plotted against experimental data, and obtained using the same modelling strategies as applied to flame A.

The same observations can be made of these two flames, although the difference between the first- and second-order chemistry predictions is now seen to become fractionally more enhanced with increased helium dilution. This trend is discussed with respect to those observed of the conditional variance in relation to minor species predictions production in the subsequent text. The $k-\varepsilon$ based predictions of the three flames, shown as Figures (4.4-4.6), are also subsequently discussed.

Figures (4.7-4.9) depict OH and NO mass fraction predictions in composition space, plotted against experimental data for flames A, B, and C respectively. Both first- and second-order results are shown, having been derived in conjunction with the RSSF turbulence model. With respect to NO predictions, the second-order corrections can be seen to decrease the peak quantities at all locations, effecting a shift across both fuel-lean and fuel-rich data. The magnitude of this adjusted value, relative to the first-order predictions, can be seen to decrease with axial distance, in-line with the evolution of the conditional variance which displays its maxima prior to reaching the first measuring station in the region of thirteen nozzle diameters. The respective plots of said data can be seen depicted by Figures (4.25-4.27) for the three flames, which all display maxima in their profiles at the relevant stoichiometric mixture fraction values. In addition, the relative magnitude of the correction is seen to increase from flame A to B to C, although it is difficult to draw comparisons with the scalar variance profiles on this point. From observation, the conditional variance prediction for each of the flames is quantitatively similar at respective locations. The resultant of the second-order chemistry application can be considered comparable to that observed by Kronenburg et al (1998) in a qualitative sense, excepting data at the

first measuring station. The present study shows a greater deviation of second-order results from the experimental data than the respective first-order calculations where Kronenburg et al (1998) show a relatively smaller difference. The same observations can be extended to predictions of the OH radical for all three flames, although the greatest influence of second-order chemistry appears upon the rich-side of stoichiometry in all cases. With attention drawn to quantitative analysis, the higher-order model is generally not seen to improve NO predictions across the three flames, but does display an expected trend in results. The correction terms enhance the slower three-body recombination reactions, resulting in lower rates of NO formation at upstream locations. However, in the majority of cases, the first-order predictions can be seen to be of a good level of agreement with experimental data, or indeed display an under-prediction, and hence a second-order correction only acts to worsen estimations. The exception can be seen in Figure (4.8) of flame B, where at 112.5 nozzle diameters, the second-order data is a marked improvement, and falls into agreement with experiment for lean stoichiometries and peak value, although still slightly over-predicting in fuel-rich regions. This however is not the case with respect to OH predictions, which all display a considerable improvement, although relatively minor in magnitude. In the majority of cases, first-order estimations notably over-predict OH peak levels and data on the fuel-rich side of stoichiometric, and the second-order effect upon the recombination reactions can be seen to bring these levels into line with experimental findings; corrections being more evident in the fuel-rich regions.

The effect on rich mixtures is noted in previous works (Devaud 1999, Kronenburg et al 1998), and means of explanation is not proffered until more

recent work regarding the modelling of differential diffusion in these flows (Kronenburg and Bilger 2001a). With the inclusion of such effects, Kronenburg and Bilger (2001a) establish the non-unity of the H ion Lewis number is responsible for the super-equilibrium temperatures on the lean side of stoichiometric, and hence improve OH predictions in this region. They also establish an improvement in NO at the near-field measurement station by an increase of around sixty percent of the equal-diffusivity counterparts. Also observed is the negligible effect of differential diffusion on results for further downstream regions.

Figures (4.4-4.6) display results for the respective flows, obtained using first- and second-order chemistry, but derived using data supplied from the application of the $k-\varepsilon$ turbulence model. Similar observations can be made as were of the RSSF derived computations with respect to fuel-rich region temperatures and H_2O prediction. What is now noticeable is a lesser effect of the higher-order closure on results in comparison to the RSSF closure approach. In fact, on inspection of far-field predictions in flames A and B, almost no discernment can be made between the two data sets. Figures (4.10-4.12) show predictions for flames A, B, and C of OH and NO in composition space, and again derived using the eddy-viscosity based turbulence closure. Again it is noted that second-order effects are less pronounced in this instance, with reference to both species at all measurement stations, although qualitatively the results display a degree of similitude. They also show a greater level of agreement with the results obtained by Kronenburg et al (1998) who also based their predictions on an eddy-viscosity model, which is most evident at the near-nozzle measuring stations. Comparisons made between Figures (4.28-4.30), depicting conditional variance

predictions for the three flames derived using the $k-\varepsilon$ model, and Figures (4.25-4.27), indicate reasons for the aforementioned differences in results. The $k-\varepsilon$ based predictions are notably numerically smaller, in most cases by approximately a factor of two. Although qualitatively the same, this is an important observation to be made between the effects of the two turbulence closures. With reference to Figures (3.7-3.21), being results of flow-field and turbulence quantities in Chapter 3, the source of this effect can perhaps be located in the differences observed in the predictions based on the two closures. Namely, the RSSF model has a tendency to over-predict the quantities provided by its $k-\varepsilon$ counterpart, certainly observable in plots of root-mean-square mixture-fraction fluctuation, axial velocity, and the $\widetilde{u_i''u_i''}$ normal Reynolds stress. Turning to physical space predictions, discussion regarding results from first-order calculations for NO and temperature can be found in Chapter 3, so the focus of the following text is with comparison of the performance of the first- and second-order closures. Figures (4.13-4.15) demonstrate the models' overall predictive ability in terms of NO parts-per-million (p.p.m.) predictions of the three respective flames. Derived from the RSSF closure approach, an excellent level of agreement is observed from the two models. The second-order results can be seen to generally negligibly differ from the first-order at upstream locale, and further downstream bring the predictions into line with experimental observations across all the flames. Similar comments can be made of the $k-\varepsilon$ derived predictions, being represented in Figures (4.16-4.18), although along with results presented in Chapter 3, the performance of this turbulence model in conjunction with both chemistry representations is not as satisfactory as its RSSF counterpart at all axial locations in each flame. Figures (4.19-4.21) display

temperature predictions plotted against experimental data, and derived using the second-moment turbulence closure. Little difference is observed between the two chemistry models, but the behaviour seen is as to be expected after analysis of the predictions in composition space. In all these flames, a small decrement over the first-order data is observable in the higher-order predictions, this being most notable near to the centreline of the flow. The reduction in temperature predictions observed in the fuel-rich areas of mixture-fraction space lead to a similar effect in these locations of physical space that are more likely to display regions of a similar composition. Little effect can be seen in the main body of the flames, but a small increase in temperatures is noted at the radial extremities of measurement, especially at down-stream locale. Although relatively small in terms of magnitude, this correction does demonstrate an improvement on the first-order data, which display an under-prediction at these locations in all the flames. The respective predictions of temperature in these flows, derived from the eddy-viscosity closure model are given as Figure (4.22-4.24). These display very similar results to the RSSF derived data, and the same observations can be made. As discussed in Chapter 3, the RSSF model does however proffer superior results of temperature predictions over the $k-\varepsilon$ approach in both a qualitative and a quantitative frame of reference for all the flames considered.

4.iv Implementation of First And Second Order Conditional Moment Closure to The Modelling of a Lifted H_2 Turbulent Jet Diffusion Flame

4.iv.i Experimental Data And Description of The Flame

The lifted flame to be examined in this chapter is the pure hydrogen jet diffusion flame as reported by Cheng et al (1992). The authors form such a flame by injecting fuel through a straight tube into still atmospheric air, producing a velocity of 680 m s^{-1} at the pipe exit, measured to be 2 mm in diameter. The exit temperature was recorded to be 280 K, the flow having a Reynolds number of 13,600 and a Mach number of 0.54. These flow parameters prescribe a flame that cannot maintain attachment to the pipe exit, and so a lifted height is established, there being approximately seven nozzle diameters between the visible flame base and the pipe mouth.

Experimental Setup:

The authors apply a UV KrF narrowband excimer-laser Raman system which provides a high repetition rate of approximately 100 Hz, and high spatial and temporal resolutions. This one laser is capable of not only measuring instantaneously and simultaneously major species of O_2, H_2, H_2O, N_2 and temperature, but also OH. KrF excimer-laser induced predissociative fluorescence (LIPF), due to the signal not being sensitive to collisional quenching in an atmospheric flame (Andresen et al 1990), allows for this quantitative assessment of the proliferation of the OH radical. Figure (4.31) shows a schematic of the UV Raman system implemented in the study of Cheng et al (1992), and a more detailed discussion regarding its implementation can be found in this said reference. As mentioned, a single KrF excimer laser is used, and tuned to 248.623 nm to minimise fluorescence interference from OH and O_2. Emitted light, scattered using a 200 mm quartz lens is focussed on the jet. The subsequent Stokes-Raman signals are collected and focussed by a Cassegrain mirror into a single-grating spectrometer. Mounted along the exit plane of the spectrometer are six Hamamatsu photomultiplier tubes (PMTs), each applied to the individual identification of O_2, N_2, H_2, OH, O_2, and H_2O fluorescence signals. Again, the aforementioned reference should be consulted for a detailed discussion regarding the calibration of equipment, treatment of data, results of species and temperature observations in both mixture-fraction and physical space, and a restricted amount of mixing-field data.

4.iv.ii Prediction of Flow Field And Turbulence Quantities

The approach taken to the elucidation of the turbulence and mixing field of the flame was that applied to the previous studies, with the implementation of a version of the parabolic GENMIX code (Spalding 1977). Again, the calculations were closed upon the mean density term, itself being derived from the implementation of a beta-pdf (Equation 3.1) and an instantaneous value of density as a function of mixture fraction; this data having been obtained from adiabatic equilibrium calculations. The first, and important point to note about this approach is that the parabolic nature of the calculations is not able to describe the complexities of such a flow, displaying high-turbulence effects such as considerable local extinction and subsequently lift-off. The lift-off phenomena is discussed further, in light of current and previously proposed theories which have been presented in an attempt to qualify the complex physics of such flows, in Chapter 2.i.iii. Although the parabolic model is seen to display this inherent inability to predict lift-off, the intention of this work is to display the methods' suitability for describing such a high-velocity jet-flow, and suggest levels of accuracy of which more elaborate calculations may be expected to provide. Hence, in an attempt to reasonably represent the mixture-fraction field, as a method of calibration, the flame was calculated using a non-reacting, pure-mixing density, up to a height of six nozzle diameters, at which the combusting density was gradually introduced over the following two diameters distance. Although only an approximation to the flame structure, this method provided

improved predictions, and the results obtained using both a $k-\varepsilon$ and a Reynolds stress/scalar flux (RSSF) closure are depicted in Figure (4.32). As can be seen, centreline values are reasonably well represented, but both models fail to capture the mixing effects, and tend to under-predict this in the outer extremities of the flow profile. In an attempt to improve the modelling of these profiles, and considering the high-velocity and Mach number of the flow, compressibility modifications to the $k-\varepsilon$ model were considered. Sarkar et al (1991) suggest that the eddy-viscosity turbulence model could be modified to include these effects by the algebraic modelling of the pressure-dilation term. This they achieved by the addition of a source term accounting for the compressible dissipation in the k equation, and a modification to the turbulent viscosity based upon a turbulent Mach number. These two modifications are described as equations (4.49) and (4.50) respectively.

$$S_k = -\overline{\rho} M_t^2 \varepsilon \tag{4.49}$$

where $M_t^2 = 2k/c^2$

and $c^2 = p/\overline{\rho}$

$$\mu_t = C_\mu \overline{\rho} k^2 / \left(1+M_t^2\right)\varepsilon \tag{4.50}$$

It was found that this modification had the desired effect upon the predictions obtained, but was left out of the final calculations reported due to the complex interactions observed between physical phenomena in the flame. Essentially, the application of additional models within the parabolic form of numerics lead to further complications with other approximations introduced, such as the specification of densities. Although shown to be a valid and functional model,

this exercise lead only to further highlight the need for an elliptic modelling approach.

4.iv.ii Results And Discussion

Figures (4.33, 4.34) depict first- and second-order major species and temperature predictions in composition space for the lifted hydrogen flame, plotted against experimentally derived data, and respectively derived using results obtained from the second-moment and the eddy-viscosity turbulence closures. Differences between the two sets of calculations are seen to be negligible at all measuring stations, and in both cases, predictions of scalars and temperature at the near lift-off heights of 7.0 and 9.5 nozzle diameters do not show great conformity with experimental data. The reason for this inaccuracy lies in the nature of the modelling approach used. As discussed in Chapter 3, the method of 'igniting' the flow on the computational grid is the application of an equilibrium profile to the initialisation. At these lift-off regions, the composition of the flow is far from equilibrium and hence increasingly accurate predictions are noted with downstream progression. Differences between calculations performed by the two different CMC schemes are minimal, although a slight reduction in temperature, and hence H_2O levels is noted in those obtained from the higher-order method. This is in concordance with the calculations of the rim-stable hydrogen jets, in addition to the RSSF model effecting a slight, but observably larger second-order chemistry correction.

Figures (4.35, 4.36) show NO predictions in conserved-scalar space, obtained using both first- and second-order chemistry models and RSSF and $k-\varepsilon$

closures respectively. Although no experimental data is available for this scalar, comment can be made with regard to the models' behaviour in this instance. The Reynolds stress model predictions appear generally to be lesser in magnitude than the $k-\varepsilon$ derived, and the effect of the second-order chemistry reduces the level of NO at all stoichiometries and all axial locations, more so in the fuel-rich regions. The effect of the conditional variance is seen to take form in causing the largest corrections at the near-nozzle and near lift-off locations, which with reference to Figure (4.45), coincides with its peak in the axial profile of evolution at the stoichiometric mixture fraction. This figure also demonstrates the difference in predictions obtained using the two turbulence closures. The RSSF model is seen to predict larger values than the eddy-viscosity approach up to the region associated with lift-off, and then decays at a greater rate than its counterpart, before levelling to a similar gradient. The difference in magnitude between the two is noted as being less than that observed in the previous study of the rim-stable flames. This is subsequently reflected in the prediction of species, and a comparison of Figure (4.35) and Figure (4.36) show little difference in the relative size of the higher-order corrections for the two models. Moreover, it can be seen that second-order effects have lesser an impact on the lifted flame calculations than on the others studied. Inspection of the conditional variance once again provides exposition, as it is found to be at some locations almost an order of magnitude smaller in the lifted flame's case. This observation falls in line with works of previous authors (Kronenburg et al 1998, Devaud 1999).

All the preceding observations can be made of the OH radical predictions, which are displayed as Figures (4.37, 4.38), being Reynolds stress and $k-\varepsilon$ closure derived data respectively. The first-order calculations are certainly less affected

by the second-order application, but conform to previous comments and observation. A limited amount of experimental data is available for the radical, and what is available is plotted at the three locations furthest downstream. As is to be expected, predictions are becoming increasingly conforming to data on increasing axial distance, again the nature of the combustion model implementation being held responsible for the near-nozzle deviations.

Turning to real-space predictions, Figures (4.39, 4.40) depict radial profiles of species obtained using a RSSF closure, and both CMC models. Following in form of the composition-space predictions, the second-order correction is not seen to affect the major species, excepting perhaps a small decrease in H_2O levels and subsequent H_2 over-prediction at near-axis locations. In contrast to results depicted in Figures (4.37, 4.38), the OH radical is now seen to be notably under-predicted at the far-field stations, but in good agreement with experiment at those closer to the nozzle. Generally, predictions are in reasonable agreement with data, although an under-prediction of O_2, N_2, and H_2O becomes more evident with downstream progression, particularly towards the radial limits of the flame measurement. This is due to an under-prediction of the mixing by the turbulence model at these locations, similar effects being present in first-order chemistry calculations of hydrogen flames (Fairweather and Woolley 2003) reported in Chapter 3. Figure (4.41) confirms these observations by demonstrating a general under-prediction of temperature across the radius of the flame. Again, little difference can be seen with respect to the first- and second-order chemistry applied, excepting a small reduction in prescription at near-axis locale. Comparing these results with those obtained using the eddy-viscosity closure (Figures (4.42-4.44)) reveals little difference in relation to the first-order

predictions. In previous calculations (Fairweather and Woolley 2003) however, it is shown that the second-moment closure approach does outperform its $k-\varepsilon$ counterpart in real-space predictions of NO and temperature. Lack of experimental data of NO profiles unfortunately prevents a similar analysis being made of the lifted flame, but as discussed earlier, a comparison of NO composition-space data reveals quantitatively smaller predicted values obtained using the Reynolds-stress model, being in line with the conserved scalar-space observations of the three rim-stable hydrogen jets examined earlier in the chapter. An important observation can be made however, with regard to the effect of the turbulence model on the second-order predictions. Here, the RSSF model is seen to produce a notably more prominent correction, especially affecting OH predictions.

4.v Conclusions

A second-order chemistry CMC has been successfully applied to three hydrogen diffusion flames of varying helium dilution. Results obtained using a k-e turbulence closure compare favourably with those of an earlier investigation (Kronenburg et al 1998). A Reynolds-stress model has for the first time been implemented with second-order calculation, and observable differences in minor species predictions between the two models recorded. The variation in relative magnitude of the second-order closure between the two turbulence models is indicative of the importance played in the accuracy to, and the method by, which the turbulence quantities are predicted.

Second-order predictions of NO would at first glance appear disappointing. However, in light of Kronenburg and Bilger's work (2001a), implementing differential diffusion effects on these flames, results are perhaps better than initial observations may lead to believe. The aforementioned authors report the greatest increase in NO production due to the effects at the near-nozzle locale, gradually decreasing along the length of the flame. It is hence suggested that the present calculations, under this influence, may fall more into line with experimentally obtained data, and further work is required in this area to support this supposition.

The actions of second-order corrections upon results are observed to be greatest on the rich side of stoichiometric, being most evident in OH predictions where over-estimation is corrected in most cases. Again, the effects of differential

diffusion upon the kinetics observed for lean mixtures (Kronenburg and Bilger 2001a) suggest that the inclusion of such will have a positive action upon agreement of results and experiment. The implication that the combined effects of differential diffusion and second-order kinetics should be investigated is once again brought to the fore.

Overall, unanswered questions remain, and in addition to the work suggested, other factors may have to be considered to explain anomalous near-nozzle NO predictions in these flames. In other applications of the same turbulence closure and CMC model described in Chapter 5, greater success in NO prediction has been achieved in CH_4 flames, leading to the suggestion that further investigation of kinetic schemes for NO pathways be undertaken. Also, the behaviour of models for scalar dissipation is highlighted for additional study. The application of Girimaji's model in the present study, although having been demonstrated to perform well (Fairweather and Woolley 2003) in these flames, may be brought under scrutiny at near-nozzle stations, and more accurate modelling may be required in these regions.

A Reynolds stress/scalar flux model has also for the first time been applied in conjunction with a higher-order CMC chemistry scheme in the calculation of a lifted hydrogen jet. Comparison of these results with those derived from the eddy-viscosity derived data show little variation, with the most notable differences seen in NO and temperature prediction. The observed effect of the turbulence closure upon the magnitude of the second-order chemistry correction is highlighted in these results however, indicating the importance of its selection. Lack of experimental data for NO prevents further analysis, but comparisons drawn with the calculations of rim-stable flames indicate an improvement in

minor species predictions may be expected. This noted lesser effect of second-order correction in the lifted jet leads to the conclusion that the next developmental step in the modelling of such flows should involve an elliptic flow-field and chemistry formulation, prior to further work on CMC sub-model closures. Experience of modelling the flow field also indicates a need to conduct density coupled and compressibility modified calculations to obtain a realistic representation of the mixing quantities. Both turbulence models' inability to accurately predict the rate of mixing, as echoed in the real-space profiles of predicted species and temperature, leads to this conclusion.

Overall, important observations have been made with regard to turbulence model choice, and its effect upon the second-order correction magnitude due to its influence upon the evolution of the conditional variance through prescription of turbulence quantities. This consideration should therefore be incorporated in the undertaking of future works.

4.v Figures

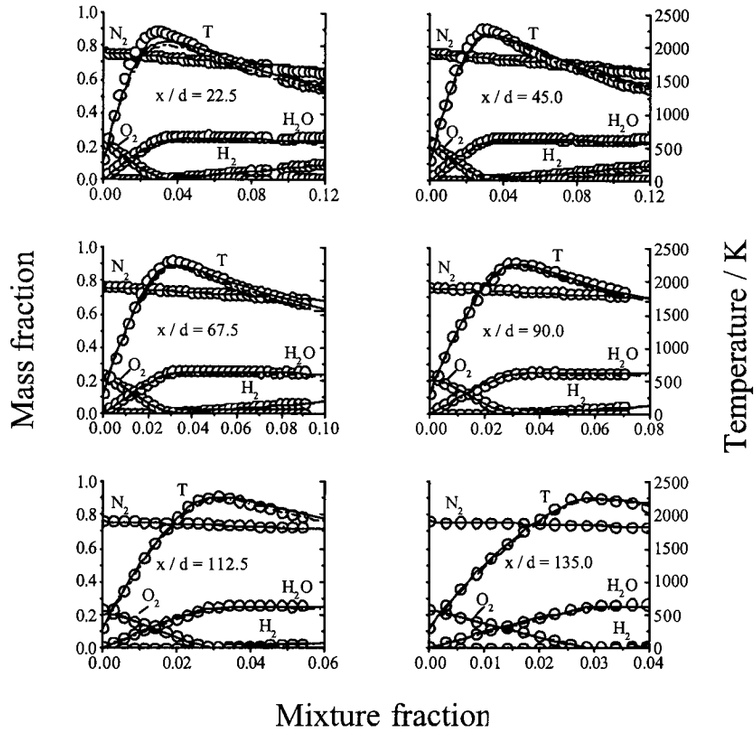

Figure 4.1 – Comparison of measured and predicted conditional species mass-fractions and temperature at six axial stations for hydrogen flame A, derived using kinetics scheme (ii) (o measured, —predicted Re stress 1st order, - - predicted Re stress 2nd order).

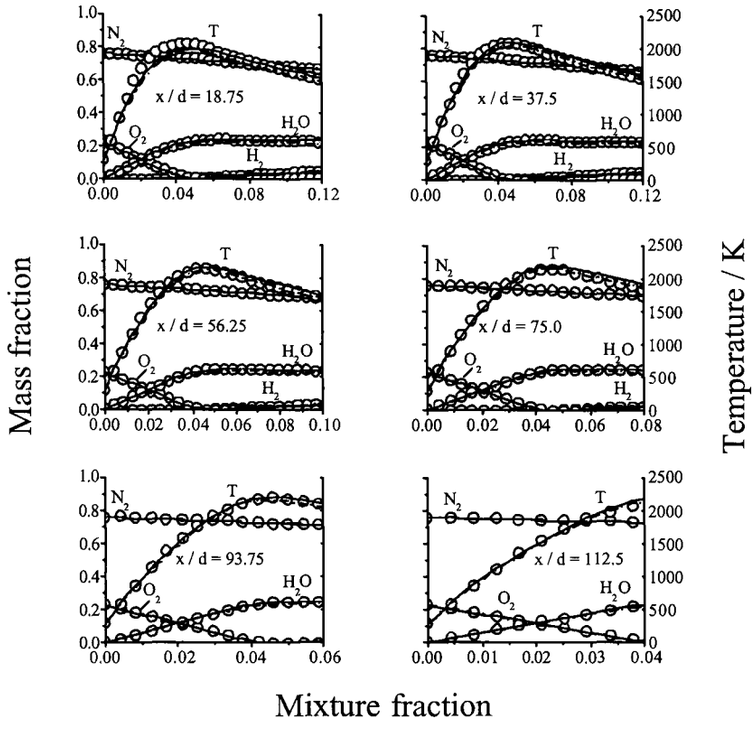

Figure 4.2 – Comparison of measured and predicted conditional species mass-fractions and temperature at six axial stations for hydrogen flame B, derived using kinetics scheme (ii) (o measured, —predicted Re stress 1st order, - - predicted Re stress 2nd order).

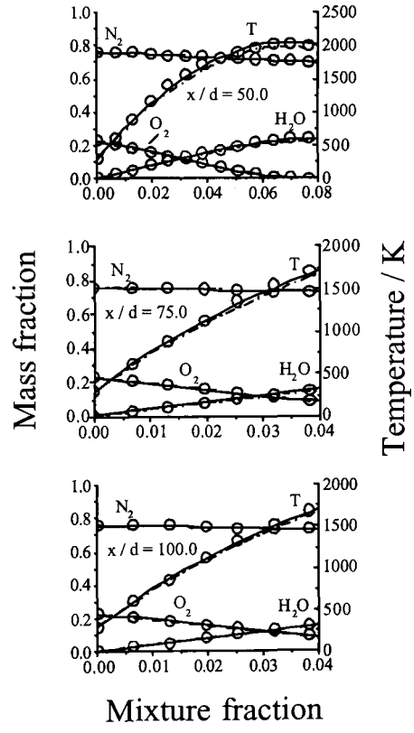

Figure 4.3 – Comparison of measured and predicted conditional species mass-fractions and temperature at three axial stations for hydrogen flame C, derived using kinetics scheme (ii) (o measured, —predicted Re stress 1st order, - - predicted Re stress 2nd order).

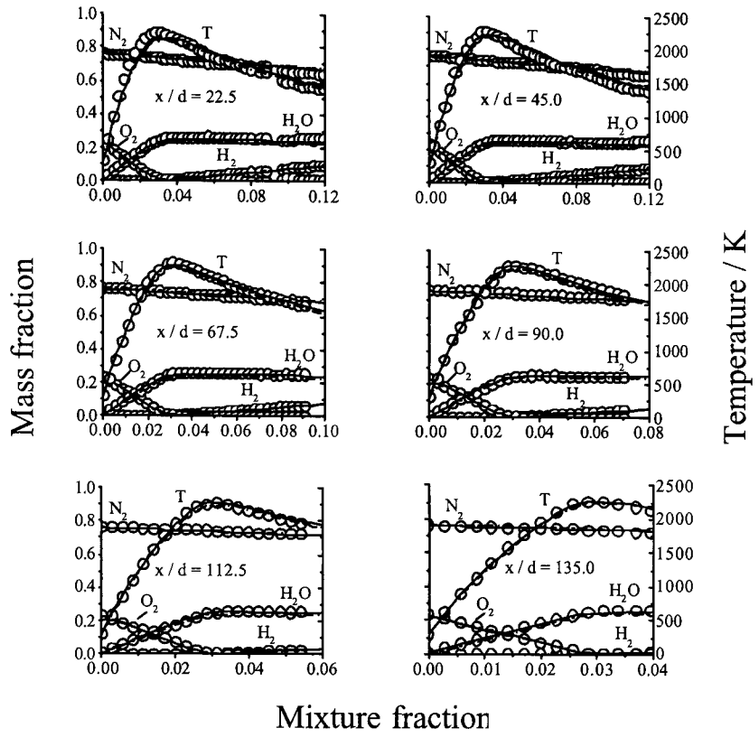

Figure 4.4 – Comparison of measured and predicted conditional species mass-fractions and temperature at six axial stations for hydrogen flame A, derived using kinetics scheme (ii) (o measured, —predicted k-ε 1st order, - - predicted k-ε 2nd order).

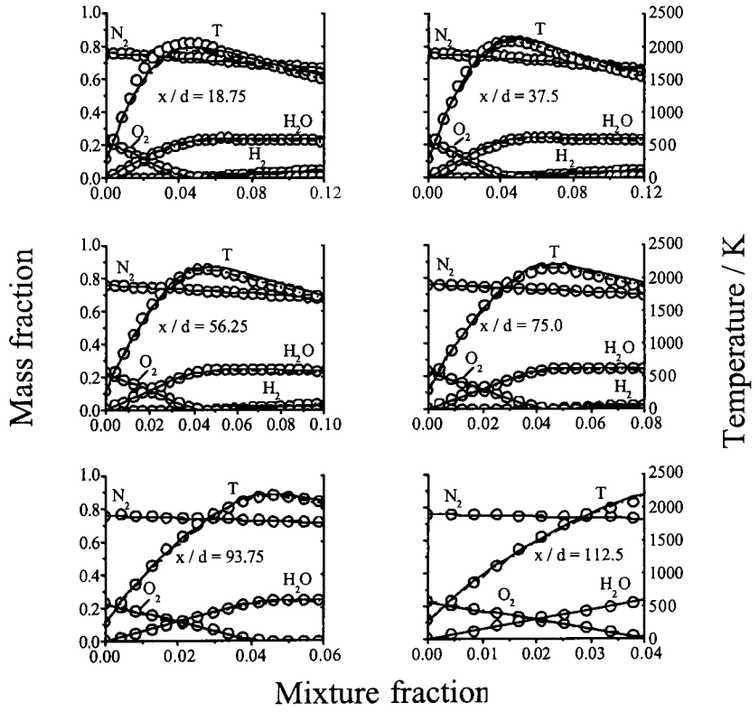

Figure 4.5 – Comparison of measured and predicted conditional species mass-fractions and temperature at six axial stations for hydrogen flame B, derived using kinetics scheme (ii) (o measured, —predicted k-ε 1st order, - - predicted k-ε 2nd order).

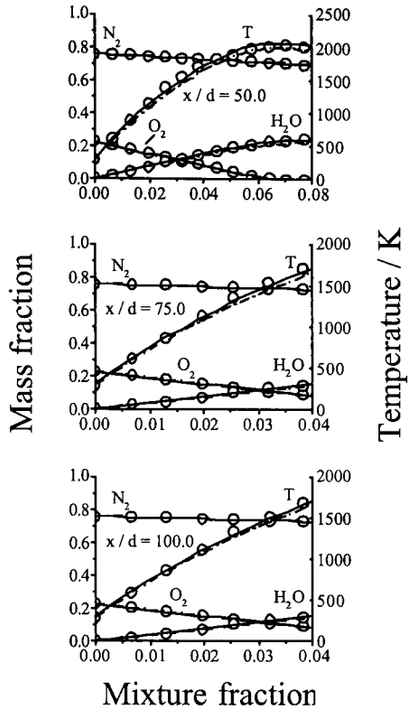

Figure 4.6 – Comparison of measured and predicted conditional species mass-fractions and temperature at three axial stations for hydrogen flame C, derived using kinetics scheme (ii) (o measured, —predicted k-e 1st order, - - predicted k-ε 2nd order).

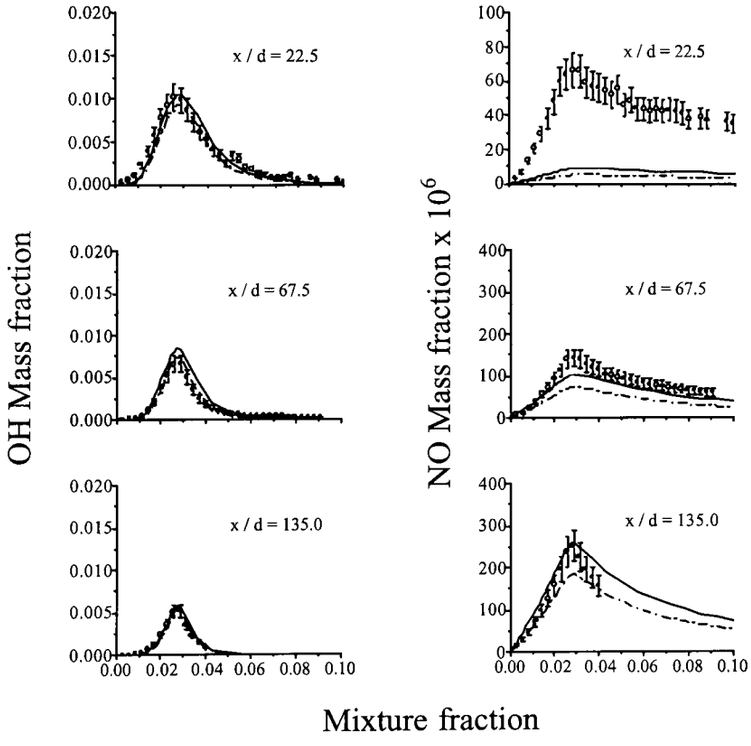

Figure 4.7 – Comparison of measured and predicted conditional OH and NO mass-fractions at three axial stations for hydrogen flame A, derived using kinetics scheme (ii) (o measured, —predicted Re stress 1st order, - - predicted Re stress 2nd order).

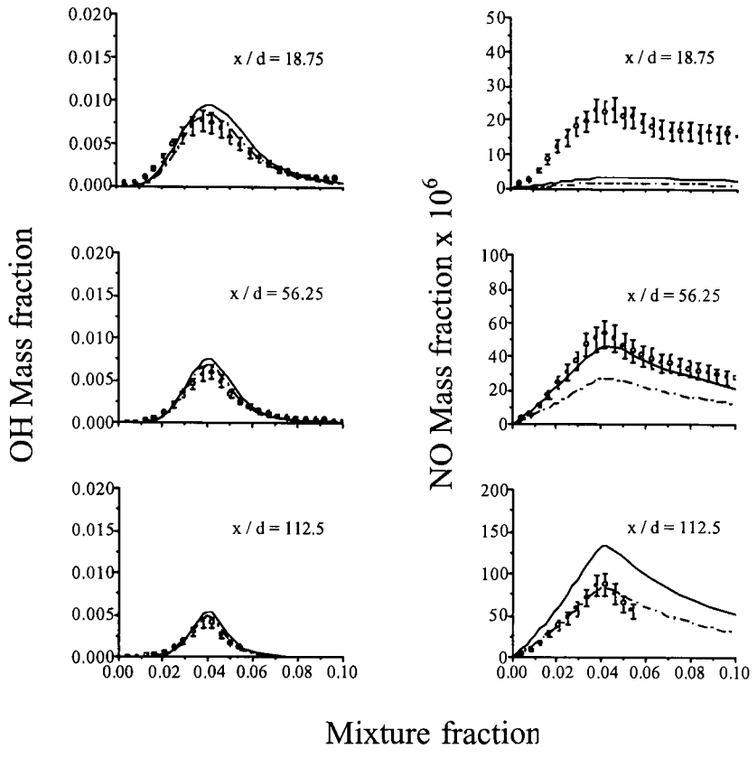

Figure 4.8 – Comparison of measured and predicted conditional OH and NO mass-fractions at three axial stations for hydrogen flame B, derived using kinetics scheme (ii) (o measured, —predicted Re stress 1st order, - - predicted Re stress 2nd order).

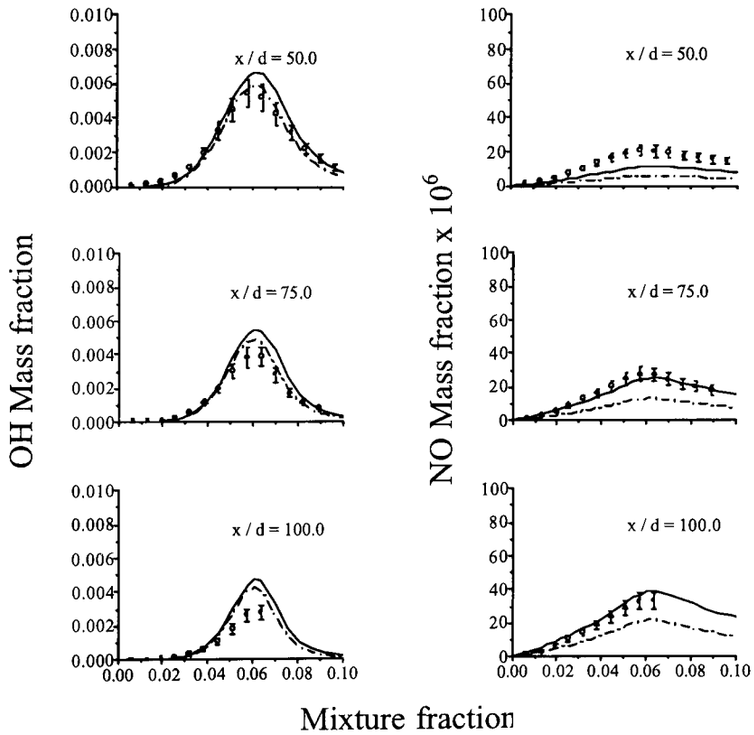

Figure 4.9 – Comparison of measured and predicted conditional OH and NO mass-fractions at three axial stations for hydrogen flame C, derived using kinetics scheme (ii) (o measured, —predicted Re stress 1st order, - - predicted Re stress 2nd order).

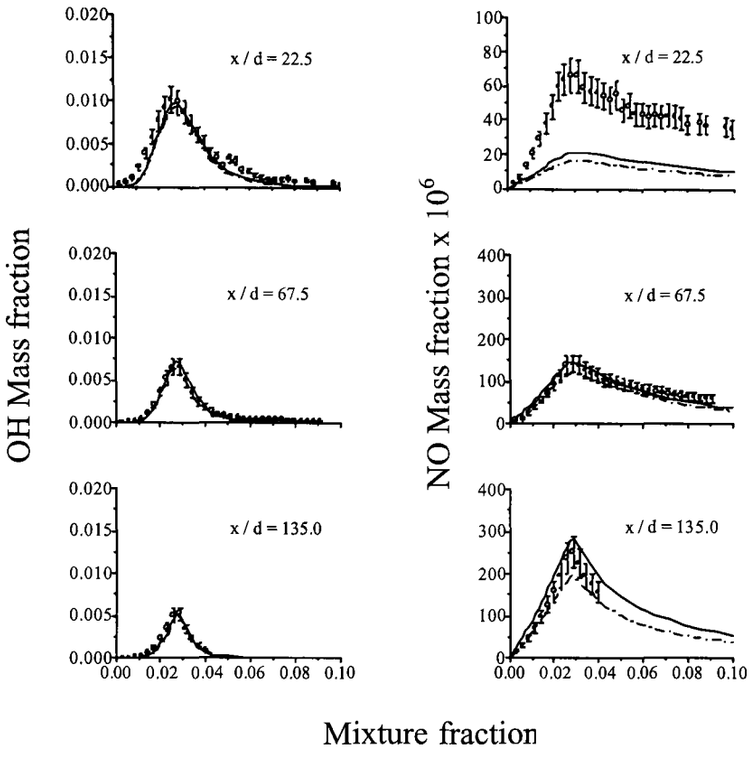

Figure 4.10 – Comparison of measured and predicted conditional OH and NO mass-fractions at three axial stations for hydrogen flame A, derived using kinetics scheme (ii) (o measured, —predicted k-e 1st order, - · - predicted k-ε 2nd order).

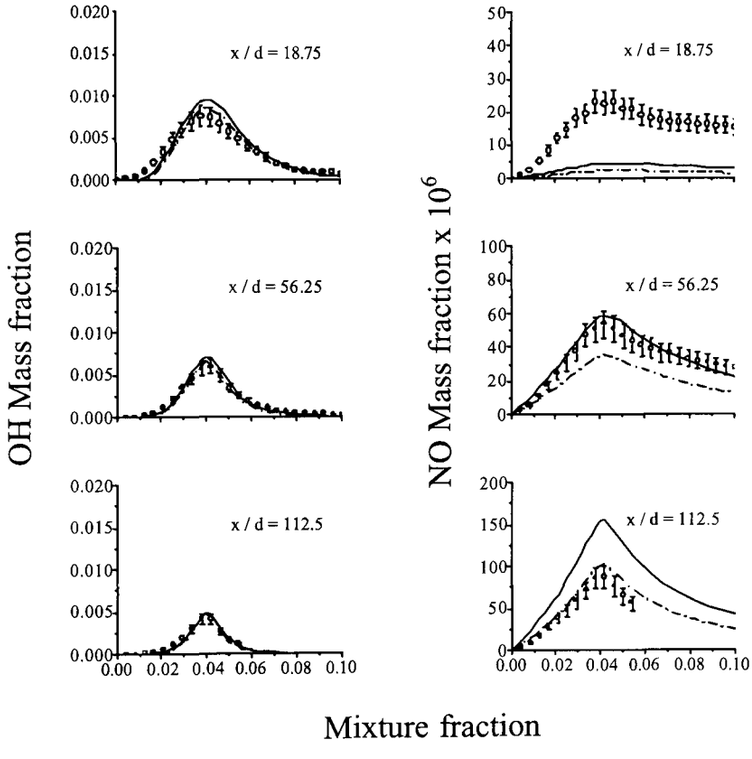

Figure 4.11 – Comparison of measured and predicted conditional OH and NO mass-fractions at three axial stations for hydrogen flame B, derived using kinetics scheme (ii) (o measured, —predicted k-e 1st order, - · - predicted k-ε 2nd order).

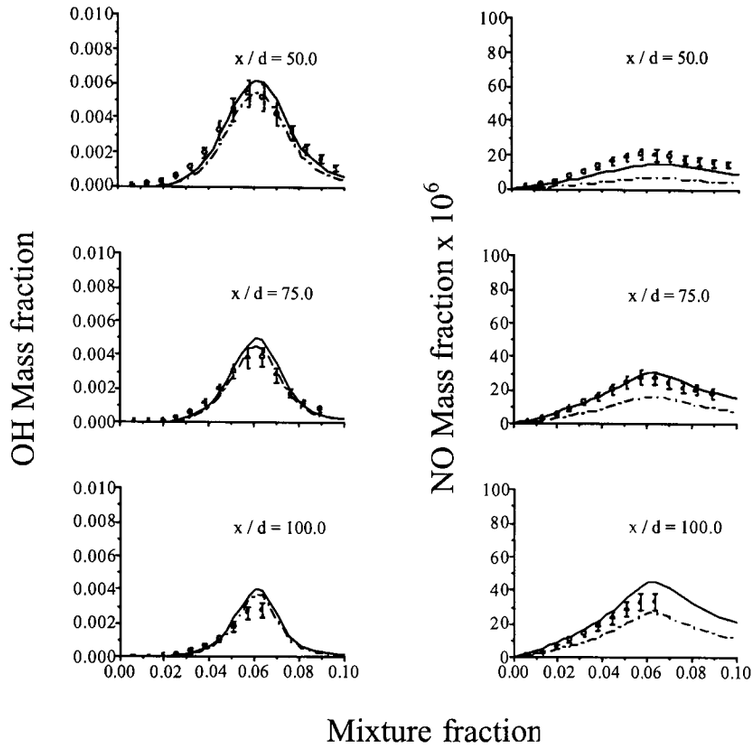

Figure 4.12 – Comparison of measured and predicted conditional OH and NO mass-fractions at three axial stations for hydrogen flame C, derived using kinetics scheme (ii) (o measured, —predicted k-e 1st order, - - predicted k-ε 2nd order).

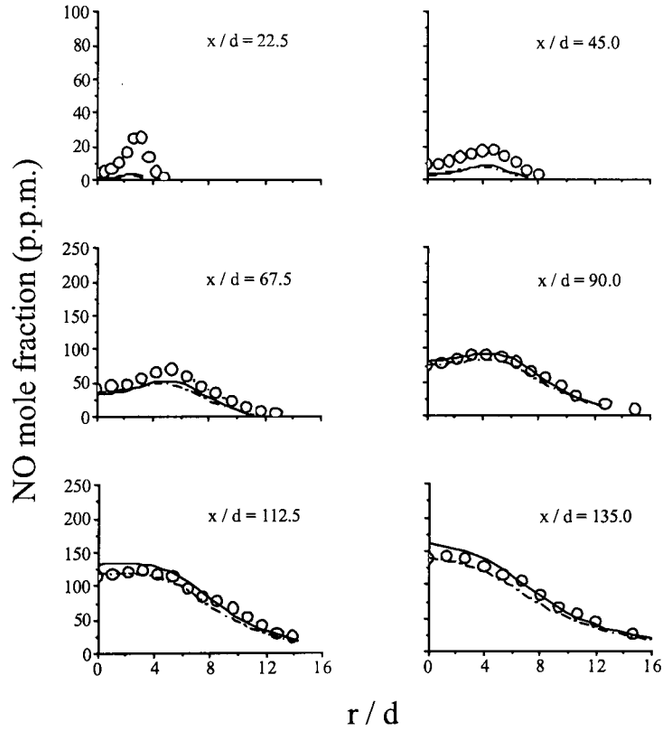

Figure 4.13 – Comparison of measured and predicted radial NO mole-fraction profiles at six axial stations for hydrogen flame A, derived using kinetics scheme (ii) (o measured, —predicted Re stress 1st order, - - predicted Re stress 2nd order).

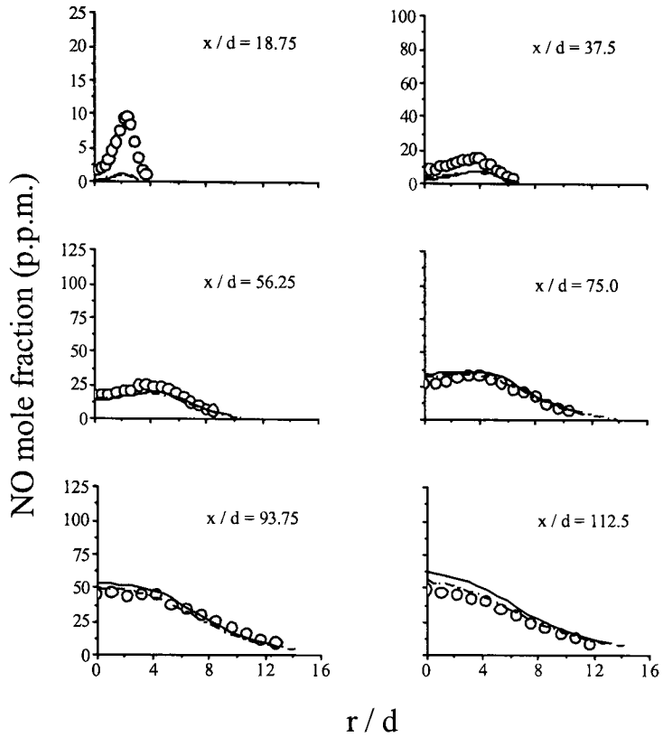

Figure 4.14 – Comparison of measured and predicted radial NO mole-fraction profiles at six axial stations for hydrogen flame B, derived using kinetics scheme (ii) (o measured, —predicted Re stress 1st order, - - predicted Re stress 2nd order).

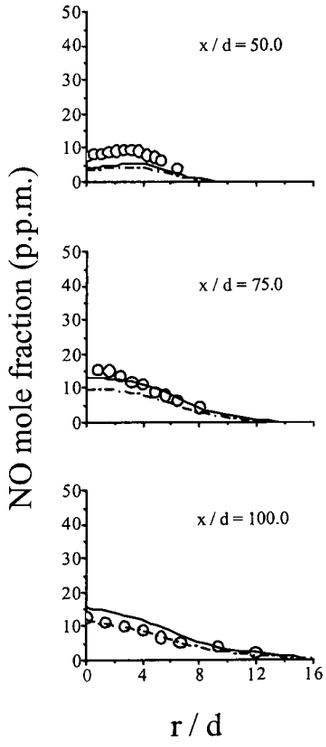

Figure 4.15 – Comparison of measured and predicted radial NO mole-fraction profiles at three axial stations for hydrogen flame C, derived using kinetics scheme (ii) (o measured, —predicted Re stress 1st order, - - predicted Re stress 2nd order).

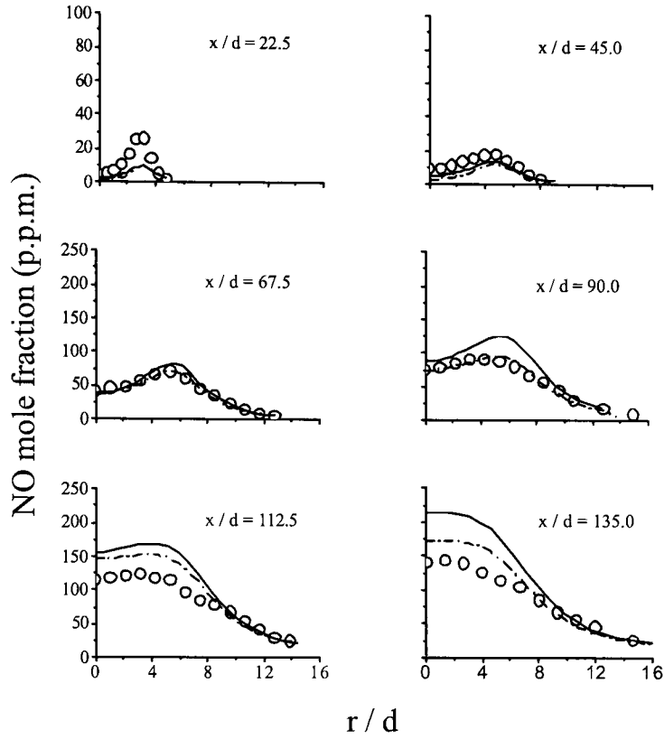

Figure 4.16 – Comparison of measured and predicted radial NO mole-fraction profiles at six axial stations for hydrogen flame A, derived using kinetics scheme (ii) (o measured, —predicted k-e 1st order, - · - predicted k-ε 2nd order).

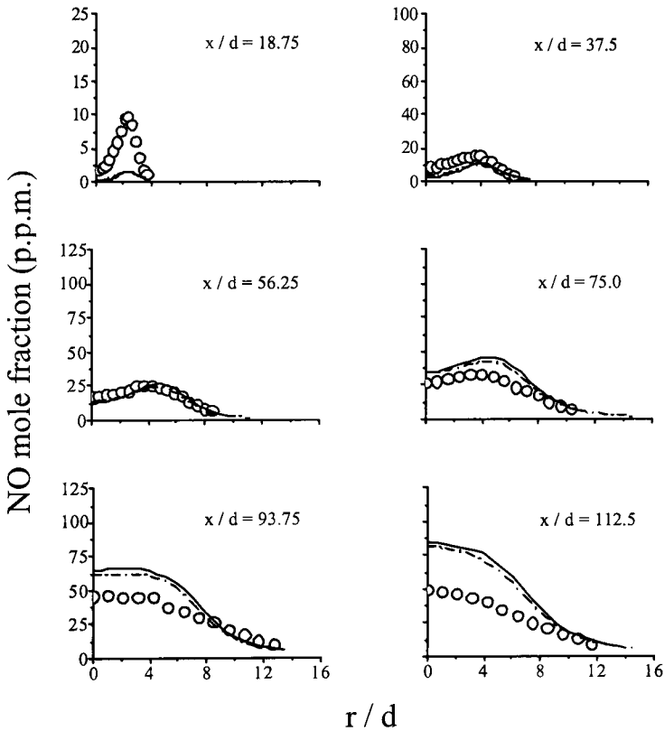

Figure 4.17 – Comparison of measured and predicted radial NO mole-fraction profiles at six axial stations for hydrogen flame B, derived using kinetics scheme (ii) (o measured, —predicted k-e 1st order, - · - predicted k-ε 2nd order).

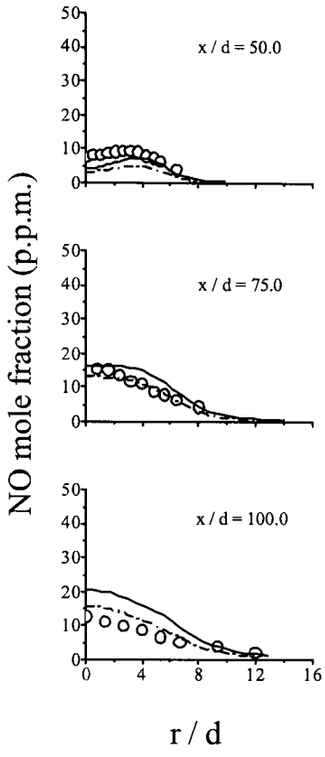

Figure 4.18 – Comparison of measured and predicted radial NO mole-fraction profiles at three axial stations for hydrogen flame C, derived using kinetics scheme (ii) (o measured, —predicted k-e 1st order, - - predicted k-ε 2nd order).

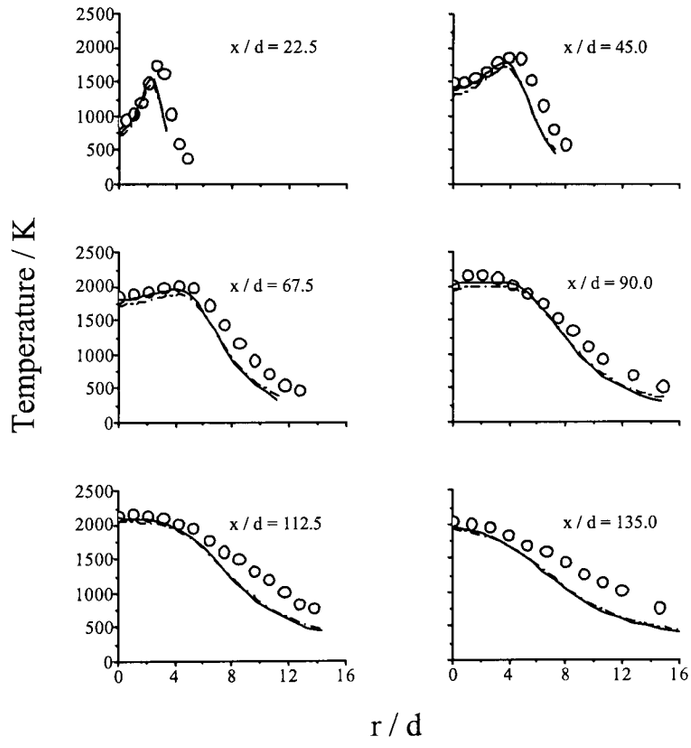

Figure 4.19 – Comparison of measured and predicted radial temperature profiles at six axial stations for hydrogen flame A, derived using kinetics scheme (ii) (o measured, —predicted Re stress 1st order, - - predicted Re stress 2nd order).

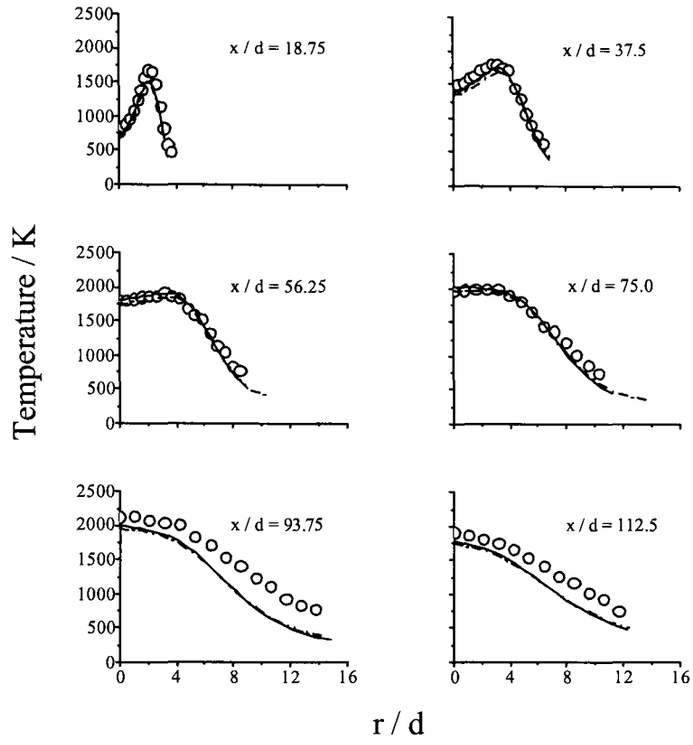

Figure 4.20 – Comparison of measured and predicted radial temperature profiles at six axial stations for hydrogen flame B, derived using kinetics scheme (ii) (o measured, —predicted Re stress 1st order, - - predicted Re stress 2nd order).

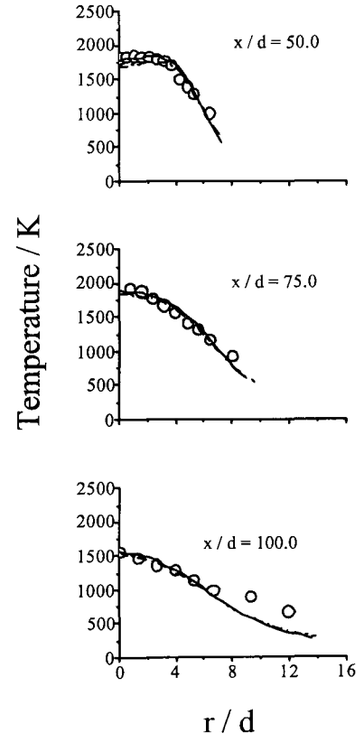

Figure 4.21 – Comparison of measured and predicted radial temperature profiles at three axial stations for hydrogen flame C, derived using kinetics scheme (ii) (o measured, —predicted Re stress 1st order, - - predicted Re stress 2nd order).

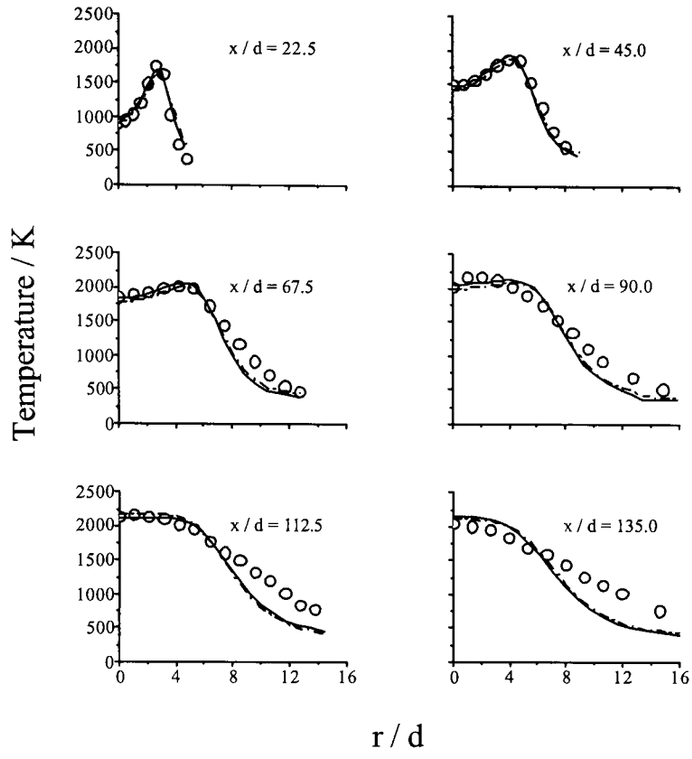

Figure 4.22 – Comparison of measured and predicted radial temperature profiles at six axial stations for hydrogen flame A, derived using kinetics scheme (ii) (o measured, — predicted k-e 1st order, -·- predicted k-ε 2nd order).

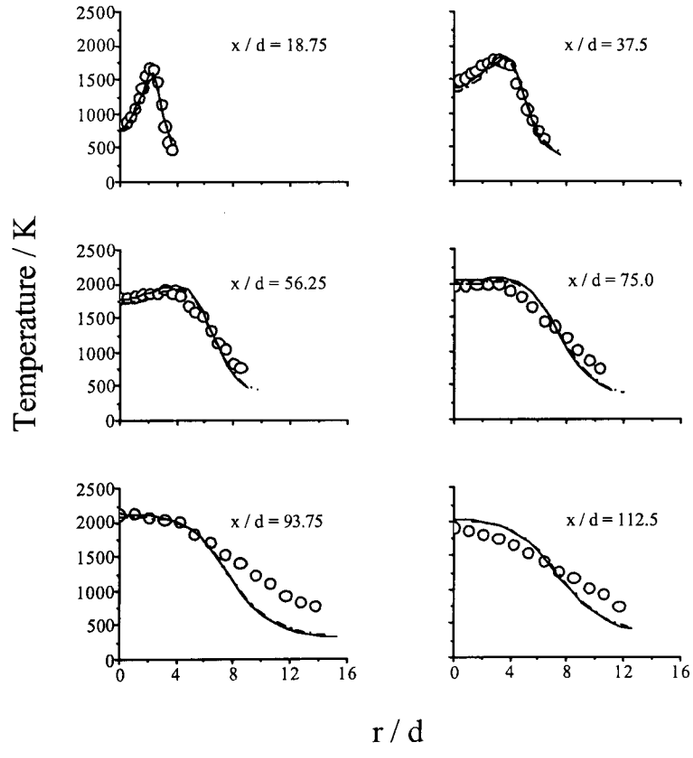

Figure 4.23 – Comparison of measured and predicted radial temperature profiles at six axial stations for hydrogen flame B , derived using kinetics scheme (ii) (o measured, — predicted k-e 1st order, -·- predicted k-ε 2nd order).

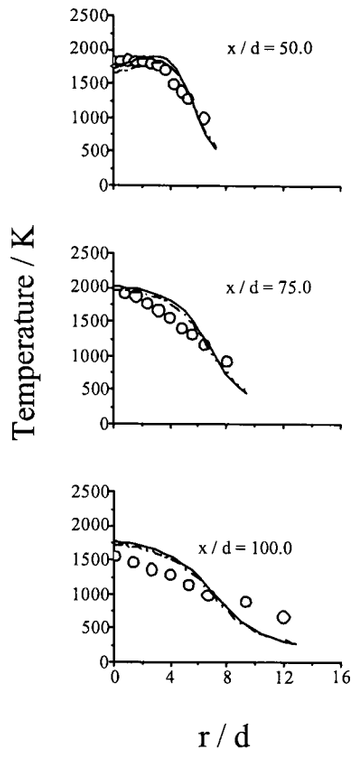

Figure 4.24 – Comparison of measured and predicted radial temperature profiles at three axial stations for hydrogen flame C , derived using kinetics scheme (ii) (o measured, —predicted k-e 1st order, - - predicted k-ε 2nd order).

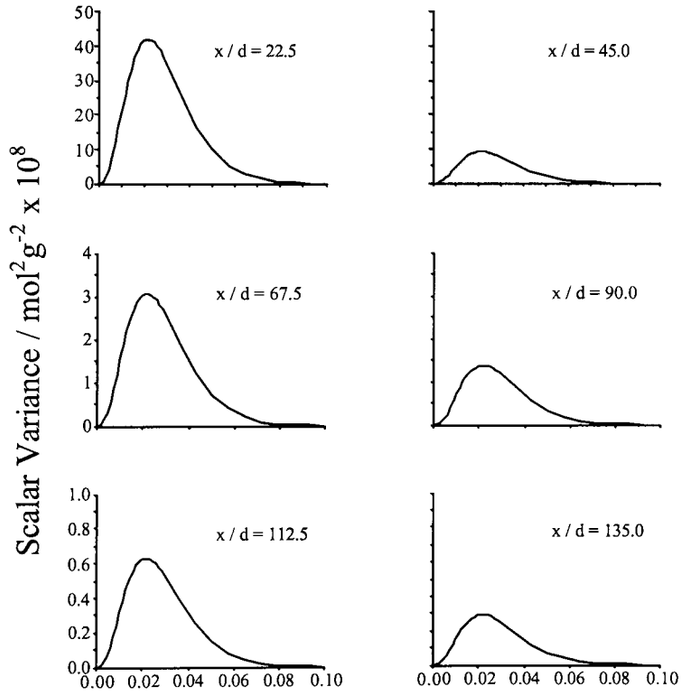

Figure 4.25 – Predicted conditional variance profiles at six axial stations for hydrogen flame A, derived using kinetics scheme (ii) and Re stress turbulence model.

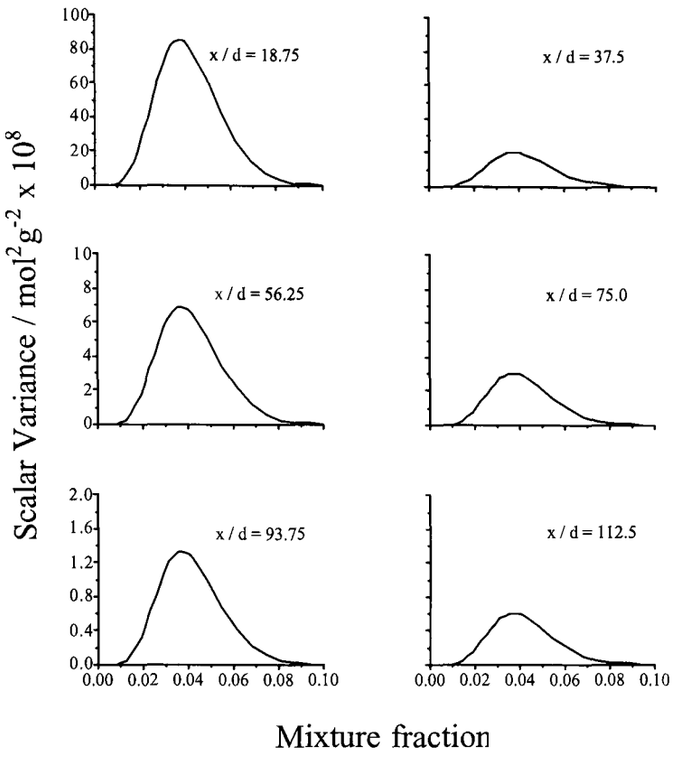

Figure 4.26 – Predicted conditional variance profiles at six axial stations for hydrogen flame B, derived using kinetics scheme (ii) and Re stress turbulence model.

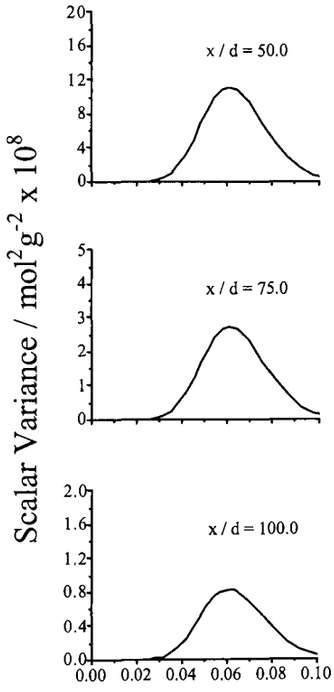

Figure 4.27 – Predicted conditional variance profiles at three axial stations for hydrogen flame C, derived using kinetics scheme (ii) and Re stress turbulence model.

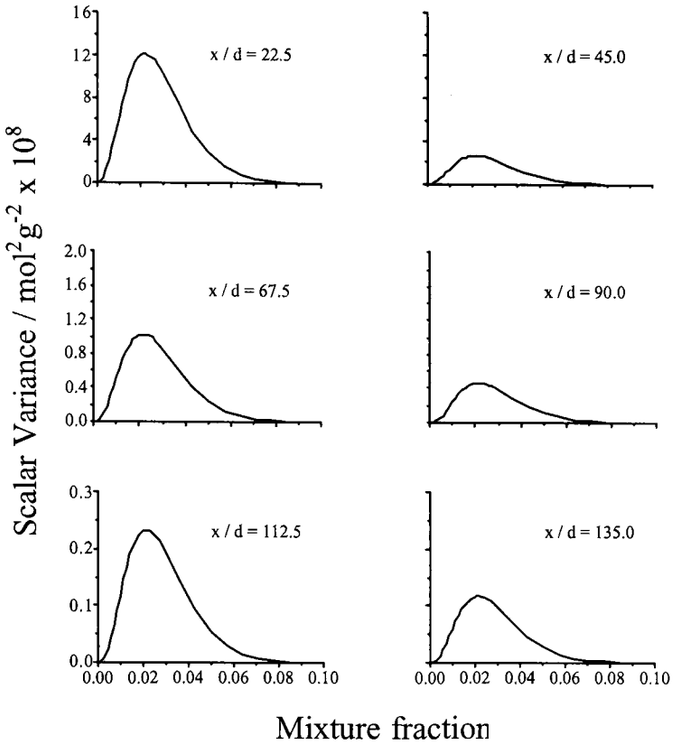

Figure 4.28 – Predicted conditional variance profiles at six axial stations for hydrogen flame A, derived using kinetics scheme (ii) and k-e turbulence model.

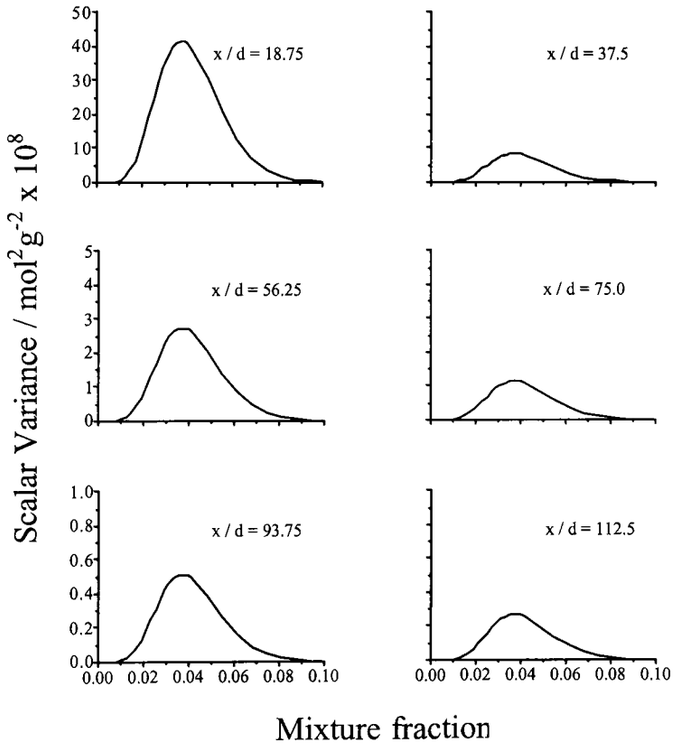

Figure 4.29 – Predicted conditional variance profiles at six axial stations for hydrogen flame B, derived using kinetics scheme (ii) and k-e turbulence model.

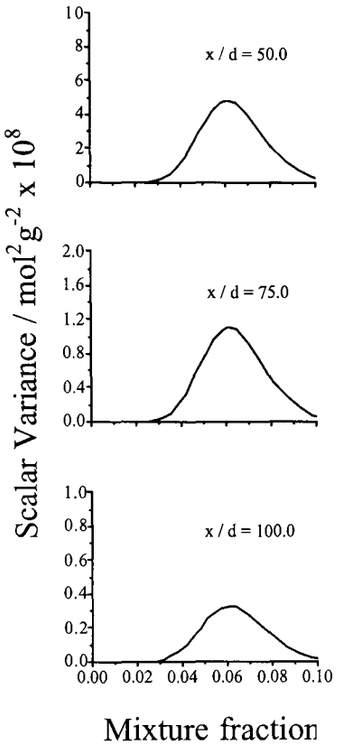

Figure 4.30 – Predicted conditional variance profiles at three axial stations for hydrogen flame C, derived using kinetics scheme (ii) and k-e turbulence model.

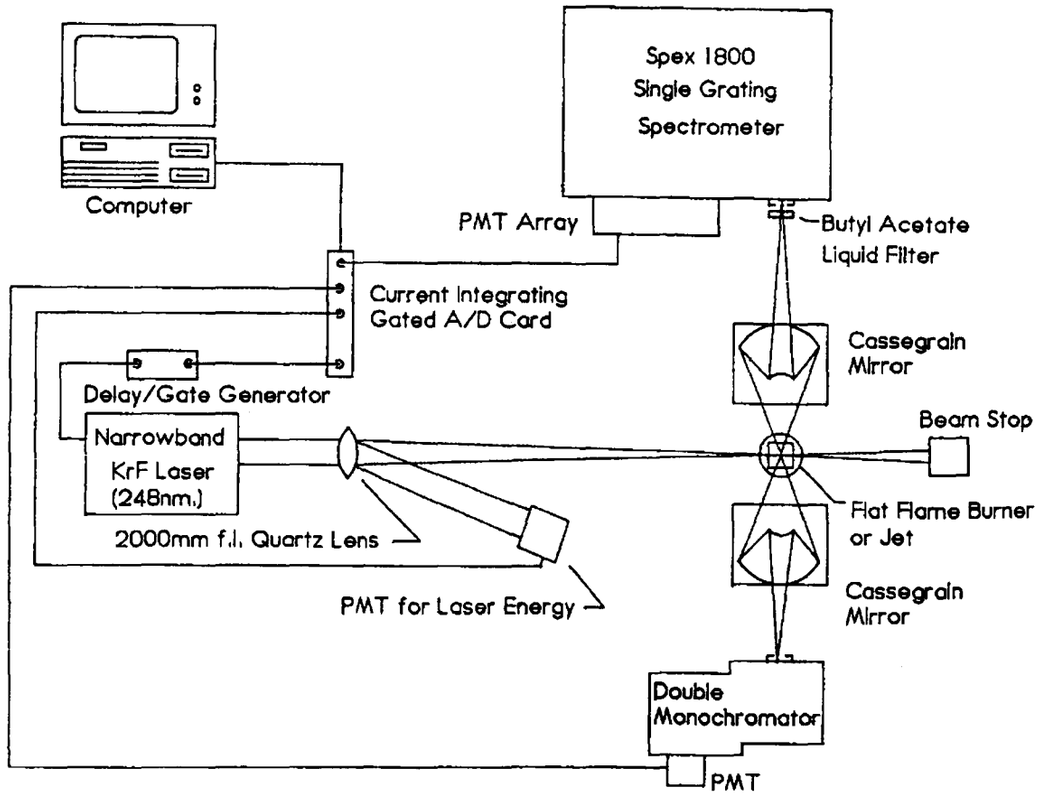

Figure 4.31 – Experimental Setup Used by Cheng et al (1992).

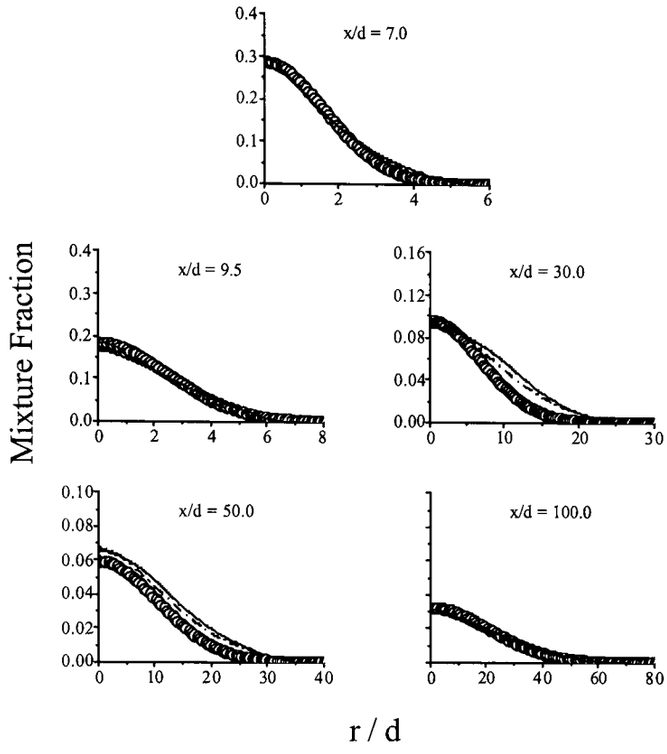

Figure 4.32 – Comparison of measured and predicted radial mean mixture-fraction profiles at five axial stations for the lifted hydrogen flame (o measured, — predicted Re stress, - - predicted k-ε).

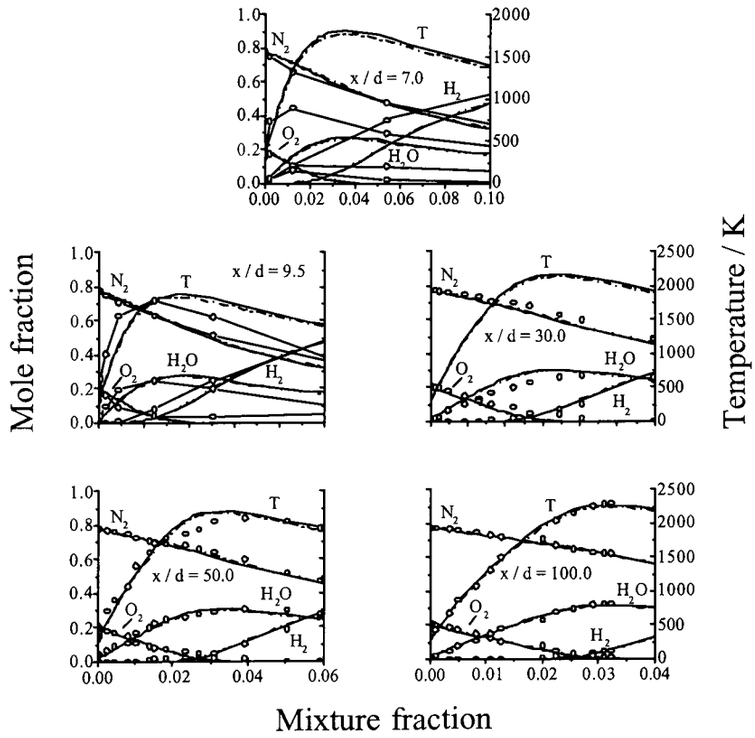

Figure 4.33 – Comparison of measured and predicted conditional species mole-fractions and temperature at five axial stations for the lifted hydrogen flame, derived using kinetics scheme (ii) (o measured, — predicted Re stress 1st order, - - predicted Re stress 2nd order).

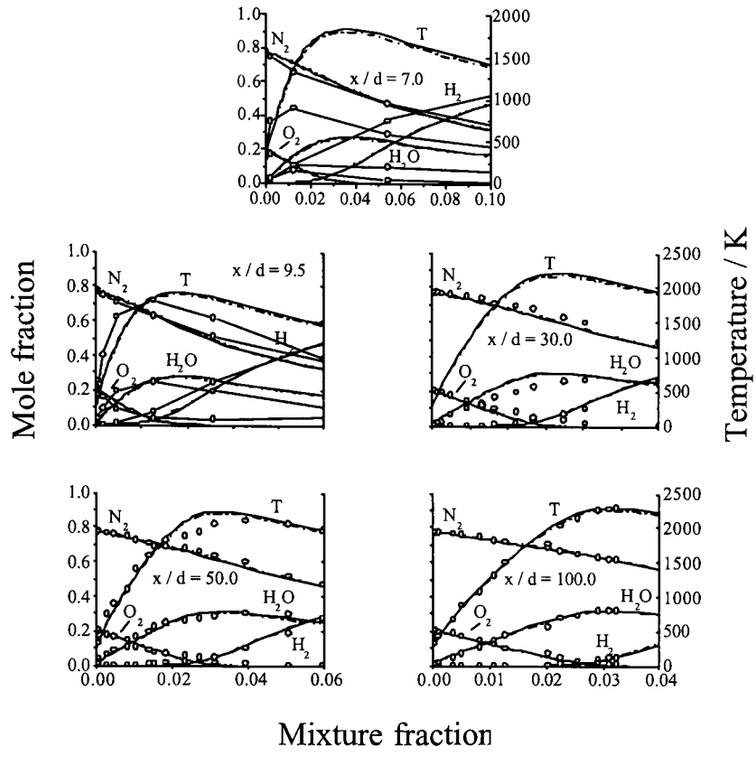

Figure 4.34 – Comparison of measured and predicted conditional species mole-fractions and temperature at five axial stations for the lifted hydrogen flame, derived using kinetics scheme (ii) (o measured, —predicted k-e 1st order, -- predicted k-ε 2nd order).

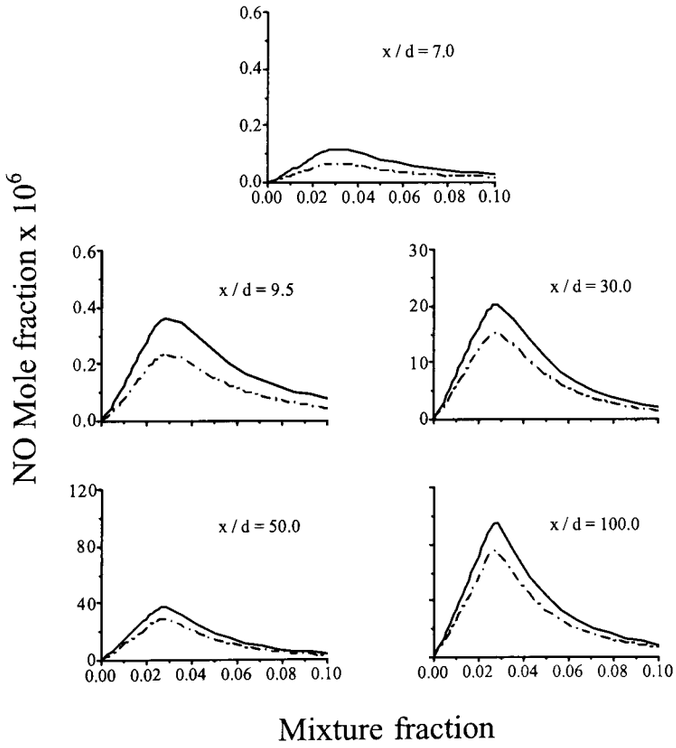

Figure 4.35 – Comparison of predicted conditional NO mole-fractions at five axial stations for the lifted hydrogen flame, derived using kinetics scheme (ii) (o measured, —predicted Re stress 1st order, -- predicted Re stress 2nd order).

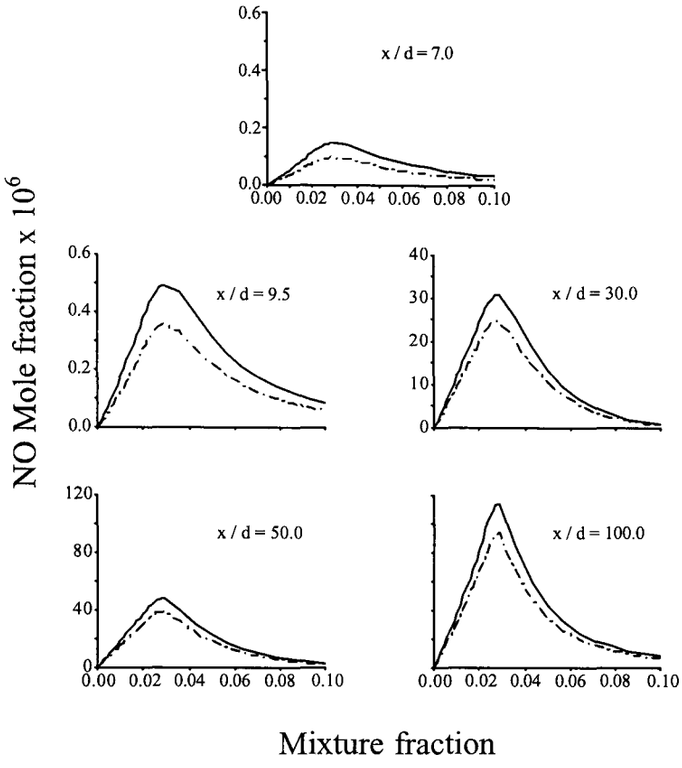

Figure 4.36 – Comparison of predicted conditional NO mole-fractions at five axial stations for the lifted hydrogen flame, derived using kinetics scheme (ii) (o measured, —predicted k-e 1st order, - - predicted k-ε 2nd order).

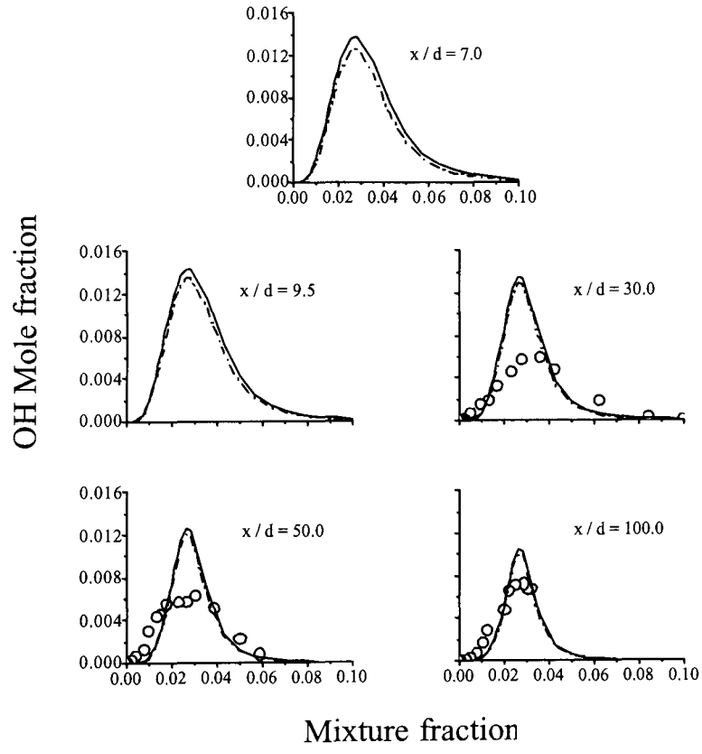

Figure 4.37 – Comparison of measured and predicted conditional OH mole-fractions at five axial stations for the lifted hydrogen flame, derived using kinetics scheme (ii) (o measured, —predicted Re stress 1st order, - - predicted Re stress 2nd order).

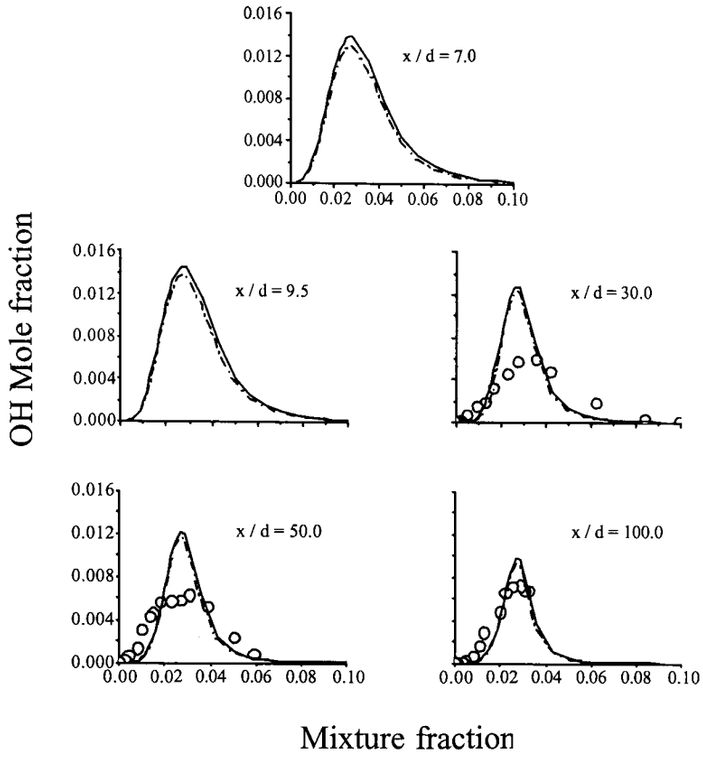

Figure 4.38 – Comparison of measured and predicted conditional OH mole-fractions at five axial stations for the lifted hydrogen flame, derived using kinetics scheme (ii) (o measured, —predicted k-e 1st order, - - predicted k-ε 2nd order)

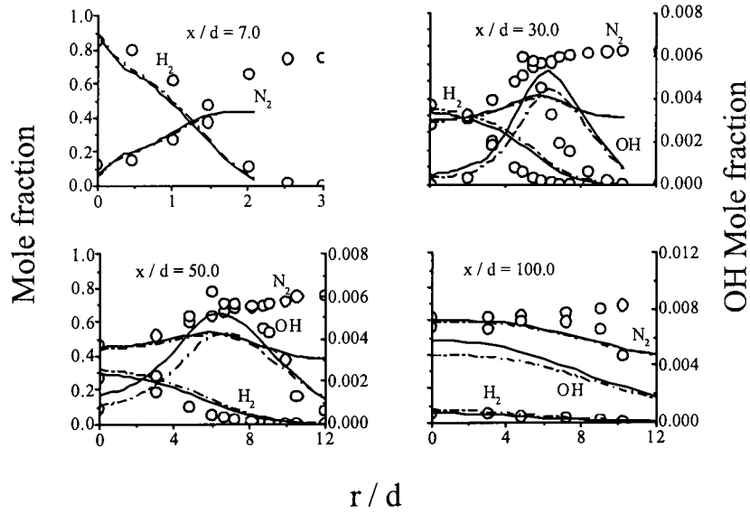

Figure 4.39 – Comparison of measured and predicted radial species mole-fraction profiles at four axial stations for the lifted hydrogen flame, derived using kinetics scheme (ii) (o measured, —predicted Re stress 1st order, - - predicted Re stress 2nd order).

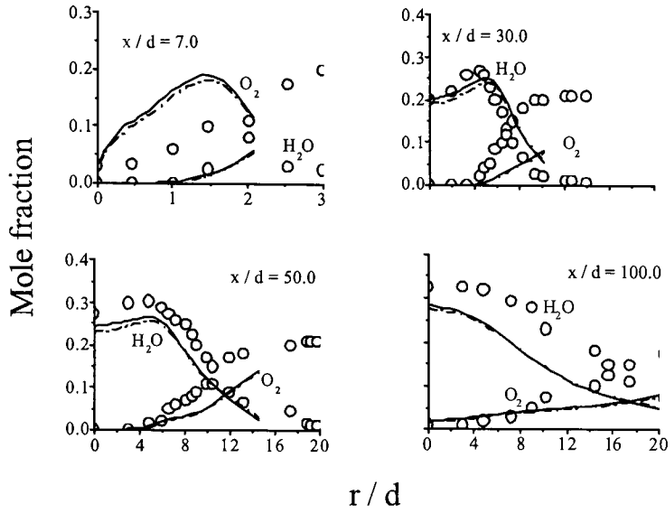

Figure 4.40 – Comparison of measured and predicted radial species mole-fraction profiles at four axial stations for the lifted hydrogen lifted, derived using kinetics scheme (ii) (o measured, —predicted Re stress 1st order, - - predicted Re stress 2nd order).

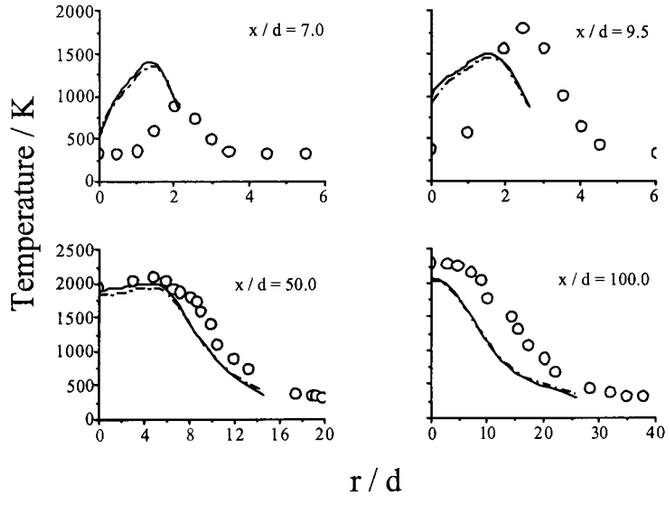

Figure 4.41 – Comparison of measured and predicted radial temperature profiles at four axial stations for the lifted hydrogen flame, derived using kinetics scheme (ii) (o measured, —predicted Re stress 1st order, - - predicted Re stress 2nd order).

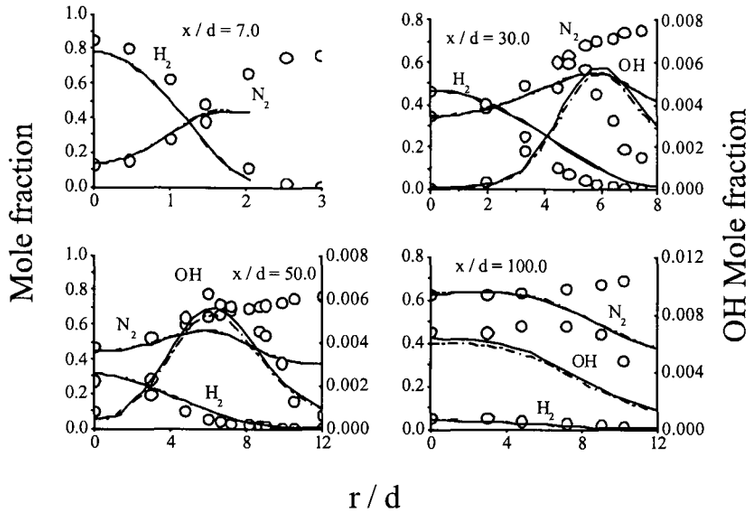

Figure 4.42 – Comparison of measured and predicted radial species mole-fraction profiles at four axial stations for the lifted hydrogen flame, derived using kinetics scheme (ii) (o measured, —predicted k-e 1st order, - - predicted k-ε 2nd order).

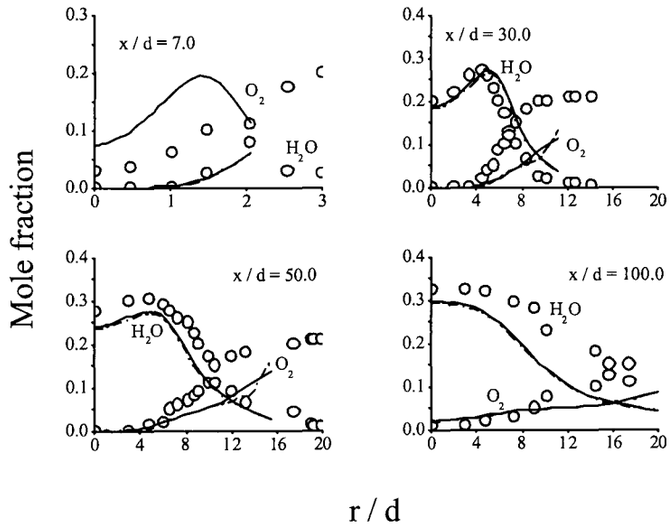

Figure 4.43 – Comparison of measured and predicted radial species mole-fraction profiles at four axial stations for the lifted hydrogen flame, derived using kinetics scheme (ii) (o measured, —predicted k-e 1st order, - - predicted k-ε 2nd order).

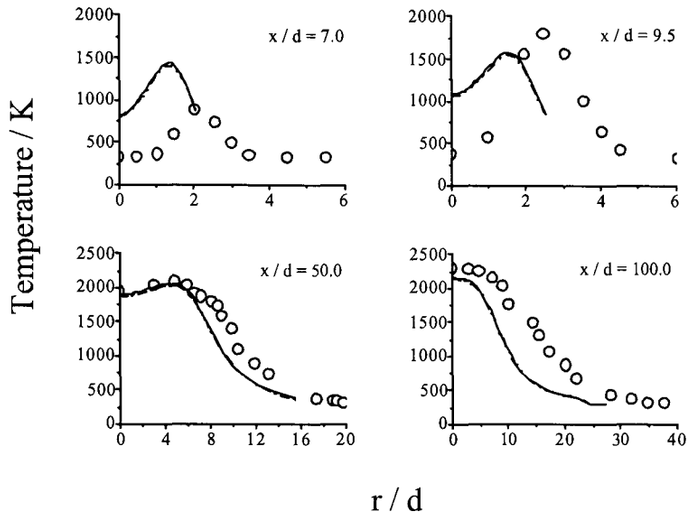

Figure 4.44 – Comparison of measured and predicted radial temperature profiles at four axial stations for the lifted hydrogen flame, derived using kinetics scheme (ii) (o measured, —predicted k-e 1st order, - - predicted k-ε 2nd order).

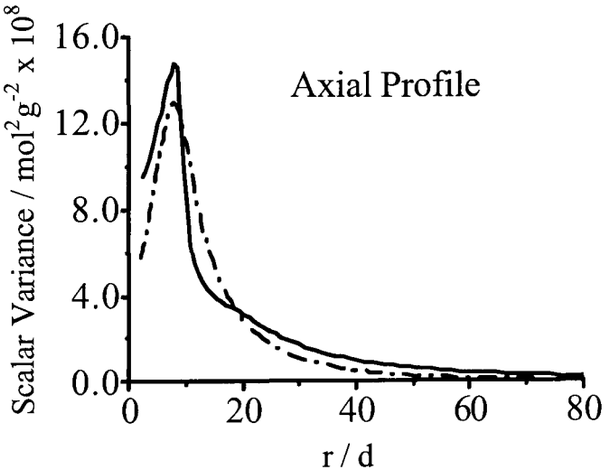

Figure 4.45 – Comparison of axial profiles of conditional scalar variance at stoichiometric mixture fraction in the lifted hydrogen flame, derived using kinetics scheme (ii) (— predicted Re stress, - - predicted k-ε).

5: First Order Conditional Moment Closure Modelling of Methane Jet Diffusion Flames

In this chapter, the application of the first-order Conditional Moment Closure model is further investigated in the assessment of its ability to predict the more complex chemical systems of simple hydrocarbon fuels; namely methane. Once again, both $k-\varepsilon$ and Reynolds stress/scalar flux (RSSF) turbulence models are used to define the flow-fields, and two kinetics schemes are used in the evaluation of the chemistry terms. To provide a comprehensive assessment of the ability of these methods, comparisons are made with experimental data of three piloted and three unpiloted non-premixed methane jets of varying compositions. All of which, exhibit none or little localised extinction effects. This contrasts with earlier studies of a similar model by Roomina and Bilger (2001). Here, the authors asses the behaviour of differing kinetics schemes, including that of the GRI-Mech 2.11 (Bowman et al 1996) scheme applied in the present work, used in conjunction with a simple $k-\varepsilon$ turbulence closure, and applied in the calculation of one flame only.

The following dialogue describes the flames, their methods of calculation, and the subsequent analysis of data. For further details regarding the methodologies,

the reader is referred to Chapter 3, to prevent repetition here on in. Any differences in procedure are outlined where applicable.

5.i Experimental Data And Description of The Flames

5.i.i Unpiloted $CH_4/H_2/N_2$ Jet Flames

The first two flames of the six to be investigated, and henceforth referred to as flames A and B, are simple non-premixed diffusion flames of CH_4, H_2, and N_2, situated in a low-velocity co-flow of air. Table (5.1) can be referred to for their respective parameters. Bergmann et al (1998) present an initial study of the flames using single-shot spontaneous Raman scattering, yielding joint probability density functions of mixture fraction, temperature, and major species concentrations from pointwise measurements. Also applied is planar LIF and planar Rayleigh scattering, to yield two-dimensional qualitative distributions of OH, CH, and NO, and temperature fields of flame A. Meier et al (2000) further this study, extending the data base by measuring simultaneously, in addition to major species and temperature, concentrations of OH, NO, and CO, by laser-induced fluorescence. Also, they proffer a complete data set of a higher Reynolds number flow, being that of flame B. Velocity distributions for these flames have been measured by laser Doppler anemometry by Schneider et al (2003). Both these flows are being considered as part of the International Workshop on Measurement And Computation of Turbulent Non-Premixed Flames (2003).

Experimental Setup:

The initial investigation of flame A (Bergmann et al 1998) applied a 489nm flashlamp-pumped dye laser for the excitation of the vibrational Raman bands of CH_4, H_2, O_2, N_2, H_2O, CO_2, and CO, and the Raman scattering. The collection of scattered light, spectral separation, and signal detection, was similar to that employed by the Sandia Laboratories scheme described in Chapter 3. Meier et al (2000), in fact apply this very Sandia equipment with the only modification made for the LIF of CO, requiring a 230nm radiation wavelength for excitation.

The burners in both investigations consist of a straight stainless-steel tube of length 350 mm, and internal diameter 8mm with a thinned rim at the exit. This is seated at the exit plane of a vertical wind tunnel, which provides a coflow of air at a velocity of 0.3 ms^{-1} in both cases.

5.i.ii Piloted CH_4/Air Jet Flames

The flames to be referred to as C, D, and E, are amongst six such CH_4/Air flames, measured experimentally by Barlow and Frank (1998). Also being considered by the International Workshop on Measurement And Computation of Turbulent Non-Premixed Flames (2003) as target data sets, these three are all fully turbulent flows, with only flame E displaying small amounts of local extinction. The respective flow parameters are described in Table (5.2), and can be seen to be of progressively higher Reynolds number. The effect of locally higher rates-of-strain shall presently be discussed in light of the results from the current calculations. Again, velocity distributions have been made available for

flames D and E, and for Barlow and Frank's (1998) flame F, although the latter not forming part of this study.

Experimental Setup:

Again, the experimental flow facility used was that located at Sandia National Laboratories in Livermore, and the diagnostic systems are described in Chapter 3. The specific burner geometry has been extensively used by combustion research groups at Sydney University, Sandia Laboratories, and at General Electric in Schenectady, New York State. A full description of this, and indeed a number of other burners and associated data sets can be found discussed in Masri et al (1996). The burner has a main jet diameter of 7.2 mm, a pilot diameter of 18.2 mm, and produces a parabolic flow, with the heat source of a set of premixed flames situated in the pilot annulus providing stability to the main jet. The pilot fuel is a mixture of C_2H_2, H_2, air, CO_2, and N_2, having the same enthalpy and equilibrium composition as a stoichiometric mixture of the main jet fuel and air.

5.i.iii CH_4/Oxygen Enriched Air Jet Flame

The final flame to be examined in this study, and consequently designated to be flame F, is that of Howard (1998) and Howard et al (1999). Table 5.3 depicts some of the flow's parameters, which although of relatively low Reynolds number, is ensured fully developed turbulent flow at the pipe exit by the length

of delivery tube employed in the burner's construction. Being a pure CH_4 jet, the flow is delivered through a 1.75 mm aperture at 37 ms^{-1} into a co-flow of air, the latter having been oxygen enriched to 26 per cent, with a velocity of 0.43 ms^{-1}. It is anticipated that, given the Reynolds number involved, that the flame contains no extinction effects.

Experimental Setup:

The axisymmetric, non-premixed turbulent flame in question was generated at atmospheric pressure using a burner issuing methane fuel from a changeable delivery tube into a co-flow of oxygen-enriched air. Low-turbulence shroud flow was established via the implementation of wire meshes, a contraction section, and porous plates, located in the pipe passageways.

Pacified-quartz probes were used, mounted on adjustable platforms for in-flame gas sampling and transference to a gas chromatogram. NO and NO_2 measurements were obtained using chemiluminescence in association with laser-induced fluorescence techniques. Infra-red absorption was implemented to quantify CO and CO_2 concentrations. Paramagnetic techniques were applied to establish O_2 content, and the gas chromatogram was used in the establishment of CH_4, H_2, N_2, O_2, CO, CO_2, and higher hydrocarbon content. Temperatures, corrected for radiation losses were calculated with the use of platinum-rhodium thermocouples. OH detection was carried out using laser-induced fluorescence also, its excitation being produced by a ND:YAG pumped-dye laser with a frequency-doubled beam. Two dichroic mirrors were implemented prior to the

dye laser for the purpose of cleaning the beam. The subsequent dye-laser output was once again frequency doubled, and tuned to 283.55 nm.

The layout of the experimental apparatus, burner, and the LIF facility can be found discussed in more detail in Howard et al (1999).

5.ii Prediction of Flow-Field And Turbulence Quantities

For all subsequent calculations of hydrocarbon fuels, the mixing-field quantities required for the chemistry calculations are derived using an identical method to that described in Chapter 3. This includes the mathematical procedures and numerical methods, and the reader is referred back to the aforementioned prose for additional information.

Again, the same approach is adopted in defining the solution domain and the initial conditions as previously applied. The majority of the inlet boundary conditions for mean velocity and the turbulence quantities are described from experimental data (Bergmann et al 1998, Meier et al 2000, Schneider et al (2003), Barlow and Frank 1998, Howard 1998, Howard et al 1999) for both the fuel and the co-flowing air streams. Where not available, the experimental data are supplemented using that of Hinze (1975) for fully developed turbulent pipe flow. Computations of flames A, B, and F assume the fuel to issue from a straight pipe into a co-flow in line with experimental conditions. Given the geometric complexity of the piloted flames C, D, and E, simplifying assumptions are invoked in their modelling. As indicated by the experimental investigations of Barlow and Frank (1998), these assumptions take the mode of the pilot fuel not being of a composition to interfere with the expected behaviour of the main jet-fuel reaction kinetics, (*id est*, there is negligible difference in the burned gas

composition for the pilot and the fuel mixture) thus reducing the problem complexity. However, in a similar manner to the hydrogen flame calculations, a variety of initial conditions are used. Data (Barlow and Frank 1998) are employed to describe profiled conditions for each of the jet, pilot, and co-flow streams, as applied previously in the works of Roomina and Bilger (2001) and Lindstedt et al (2000), in addition to profiled and flat distributions for the jet and co-flow streams alone. These test demonstrate that closest agreement with data is obtained when flat distributions for the jet and the co-flow are adopted, although the methods display little difference in velocity and mixture fraction results at the first axial station considered at x/d = 15.0. It should also be noted that Lindstedt (2000) finds that variation in composition of the pilot flames has negligible influence upon his calculations of Barlow and Frank's flame B (Barlow and Frank 1998). Results derived using flat profiles are therefore presented in the following discussions. In addition, since the focus of the present study is the evaluation of the first-order CMC model, turbulent flow-field predictions are optimised against velocity and mixture fraction data by adjusting the $C_{\varepsilon 1}$ constant to a value of 1.57; this methodology being previously justified in Chapter 3.

Ignition in the near-field region of all the flames (A to F) is instigated by the use of equilibrium compositions for the reactive scalars down to x/d = 1.5, and obtained via the implementation of the GRI-Mech2.11 (Bowman et al 1996) chemical kinetics scheme. Predictions from x/d = 15.0 for flames C to E show no sensitivity to the extent of the equilibrium region, and hence the simplified initial conditions noted above are considered justified for all the flames concerned.

5.iii Prediction of Species: First Order, One Dimensional, CMC Model

Chapter 3 should be referred to once again for further details regarding the implementation of the CMC model. The only difference between the calculations, excepting the initial conditions, being the representation of the chemistry within the model's formulation. With the introduction of a hydrocarbon fuel, a considerable increase in the complexity of the system's chemistry is effected, and this is introduced into the calculations via two appropriate kinetic mechanisms, being GRI-Mech2.11 (Bowman et al 1996) consisting of 277 elementary reactions and forty-nine species, and GRI-Mech3.0 (Smith et al 1999) consisting of 325 elementary reactions and fifty-three species. These having both been previously implemented in a number of models and applications (Bradley et al (2003), Roomina and Bilger 2001, Kim et al 2000b, Kim and Huh 2002a), are respectively listed in their full form in Tables (5.4, 5.5).

5.iv Results And Discussion

5.iv.i Calculation of Unpiloted $CH_4/H_2/N_2$ Jet Flames

5.iv.i.i Flow Field

Predictions of the radial mixture fraction and the root-mean-square of its fluctuations in flames A and B are compared with data in Figures (5.1-5.4). Figures (5.1, 5.2) display little difference between those obtained with the application of the eddy-viscosity model, and that of the second-moment closure. The RSSF approach does however display a slight over-prediction of mixture fraction in both flames, in line with the results obtained in Chapter 3, and most notable at x/d = 20. With respect to the root-mean-square of the scalar fluctuations depicted in Figures (5.3, 5.4), the RSSF model qualitatively relays a superior predictive ability, although slightly relatively under-performing in quantitative analysis.

Figures (5.5-5.7) show predicted and experimentally derived velocity fields for flame A. A similar data set for flame B is not available, hence no discussion is made. A similar level of agreement is observed between the two turbulence closures in consideration of the radial profiles of axial velocity and Reynolds

shear-stress. The more advanced closure however, can be seen to outperform its counterpart in representation of the axial normal fluctuating component, which is to be expected considering the modelling issues involved.

Overall, this is a lesser-pronounced differential than observed in earlier works (Fairweather and Woolley 2003), and in Chapter 3 of this thesis. In contrast to the present calculations, this leads to closer agreement between CMC predictions based upon the RSSF model for flow temperatures and chemical species concentrations; particularly for NO.

5.iv.i.ii Scalar Field

Measured and predicted conditional major species mass fractions and temperatures are compared for flames A and B in Figures (5.8-5.10). Results for flame A (Figure (5.8)) derived using GRI-Mech2.11 (Bowman et al 1996) demonstrate good agreement with data throughout the flame, although at the near-field stations up to x/d = 40.0, H_2O is under-predicted and CO_2 over-predicted for fuel-rich conditions. A slight over-prediction of temperatures can also be observed up to x/d = 20.0 in the composition space region 0.6 to 0.8. By x/d = 60.0, major species predictions and temperature are in line with experimental observation as the probability of encountering fuel-rich regions is low. The results derived from the two turbulence models display little difference, complimenting the velocity field predictions. Similar observations can also be made of calculations for flame A, represented in Figure (5.9), and derived using GRI-Mech3.0 (Smith at al 1999). Results from flame B (Figure (5.10)) confirm these trends and observations; the only notable difference being that the

temperature predictions in fuel-rich mixtures are now in good agreement with data. However, it can be seen to be over-predicted around stoichiometric near to the flame base.

Figures (5.11-5.14) display experimental and predicted H_2, CO, OH, and NO conditional mass fractions at several locations within flame A. Little difference can be observed between the two turbulence models employed. OH predictions are very good, despite a slightly elevated stoichiometric peak value at all locations, and CO is seen to be slightly over-predicted at the first two measuring stations, and subsequently over-predicted under fuel-rich conditions with furthering downstream distance. H_2 and NO predictions are again very good, but in contrast, NO levels are slightly under-predicted closest to the nozzle, and over-predicted at all other measuring stations. H_2 is also seen to be marginally over-predicted in all observations. Figures (5.15-5.18) respectively depict results of the same four species as just discussed, derived with the application of GRI-Mech3.0. These can be seen to confirm all the trends noted above, with very close agreement to results derived on the basis of GRI-Mech2.11, apart from NO where the absolute levels of this species are approximately doubled at all values of mixture fraction, leading to an over-prediction of data. Figures (5.19-5.22) address the same four species predictions derived using GRI-Mech2.11 and both turbulence closures, but applied to flame B. Again, the conclusions drawn above are confirmed with perhaps the most notable difference being the now over-prediction of NO at all downstream locale, and more significantly so than for flame A.

Turning to real-space data of flame A, figures (5.23-5.32) depict physical space, radial profiles of species mass fractions and temperature, as previously addressed

in composition space, and are obtained from calculations of a fully-coupled flow-field and CMC model. It is found that negligible difference is obtained from the use of density coupling, as opposed to the post-processing technique, but the execution of these calculations were required to ascertain this fact. Although these results cannot be more informative about the level of agreement with data than the conditionally averaged statistics considered so far, they do demonstrate the accuracy that may be expected from a complete model in practical applications. The trends observed in the conditional results are in general reproduced in these subsequent plots. However, predictions of temperature, CO_2, and H_2O tend to be more in line with experiment, whilst the under-estimation of CO and over-prediction of NO and OH remain. The discrepancy between predictions of NO based on the differing kinetics mechanisms can be seen to manifest once again when comparing Figure (5.30) and Figure (5.32). Oxygen is also under-predicted at all axial and radial positions, although the overestimation of H_2 is in line with earlier conditional results. Figure (5.33) shows predictions of NO radial profiles in flame B, derived using GRI-Mech2.11, and can also be seen to be in agreement with their conditional counterparts by more significantly over-predicting levels over the radius of the flame when compared with flame A.

Overall however, the results show good agreement with data, and are certainly of sufficient accuracy for use in the assessment of flame characteristics and emissions for design purposes. Also, at virtually all locations, predictions obtained using the second-moment turbulence closure are superior to the $k-\varepsilon$ based results, despite little difference being apparent between results based on these two models in the equivalent conditional data.

5.iv.ii Calculation of Piloted CH_4/Air Jet Flames

5.iv.ii.i Flow Field

Comparisons between measured and predicted radial mixture-fraction and r.m.s. of mixture-fraction fluctuation profiles for flames C, D, and E are given in Figures (5.34-5.39). These results are generally in line with those for flames A and B, although an improved performance is seen in the Reynolds stress model's prediction of mixture fraction at near-nozzle locale, and conversely, a diminished ability for the $k-\varepsilon$ closure in all three flames. With respect to the previously discussed modelling results, the second-moment closure predictions of r.m.s. scalar fluctuations can now be seen to be quantitatively superior in addition to their qualitative qualities, at the majority of measuring stations in all flames. Lack of experimental data prevents an analysis of the velocity field of flame C, however axial velocities and Reynolds normal and shear stresses of flames D and E are pictorially represented in Figures (5.40-5.47). Although a relatively slight over-prediction at the centreline for axial velocity profiles is noted, in both flames, the RSSF model significantly demonstrates its superiority in prediction of the fluctuating velocity components in nearly all analysis. Compared to the prediction of flame D in the earlier CMC model study of Roomina and Bilger (2001), obtained using an eddy-viscosity based approach, the present RSSF results demonstrate a similar level of agreement for axial and radial profiles of mean and fluctuating axial velocities. The present results for axial and radial mean mixture fraction and its fluctuations are, in general, in closer accord with

data; particularly in the near field up to x/d = 45.0 and in the far field at x/d = 75.0.

5.iv.ii.ii Scalar Field

Measured and predicted conditional major species mass fractions and temperatures, derived using GRI-Mech2.11 and GRI-Mech3.0, are depicted for flame C in Figures (5.48, 5.49). Little difference is observed between the two kinetics schemes, or indeed between the two turbulence closures applied. Compared to the earlier-presented data for flames A and B, these results are less satisfactory, and now show an over-prediction of temperature at all fuel-rich mixture fractions in the near field. In comparison to flames A and B, H_2O is now over-predicted and CO_2 under-predicted in fuel-rich regions, with CH_4 and O_2 significantly under-predicted in these regions. Results do however come more in line with data further downstream, again due to the probability of encountering fuel-rich regions being very low. With increasing Reynolds number (Figures (5.50, 5.51)) and increasing extinction effects, the trends between measured and predicted flame characteristics observed in flame C remain, although deviation between the two sets of results increases at the near-field measurement locations. The only exception is CO_2, where an under-prediction at low Reynolds number turns into an over-prediction at higher values.

Measured and predicted conditional minor species mass fractions of CO, OH, and NO are compared for flame C, using both GRI-Mech2.11 and GRI-Mech3.0 in figures (5.52-5.57). H_2 is omitted from further analysis due to sparse experimental data. OH predictions are in line with previous observations of

flames A and B, and CO can now be seen to be over-predicted in fuel-rich regions in comparison. The previously noted over-prediction of temperatures, coupled with the under-prediction of CH_4 and H_2O under fuel-rich conditions should lead to an over-prediction of CO_2 and H_2O. This is observed for the latter species, but CO_2 is slightly under-predicted due to the over-estimation of the CO concentration. NO levels are also over-predicted more significantly than in previous flames, with deviation from experiment being greatest under fuel-lean and near stoichiometric conditions. With the exception of NO, where significant over-prediction remains, calculations come more into line with observations with farther downstream progression, as noted for the major species. Again, previously noted trends of predicted data are observed with increasing Reynolds number as indicated in Figures (5.58-5.63) for flames D and E, excepting perhaps NO, which is in marginally better agreement for flame D. Results derived for flame C using GRI-Mech3.0 confirm all trends noted above, apart from NO (Figure (5.57)), where once again, absolute levels are approximately doubled at all mixture fractions, leading to significant over-prediction of data at all stoichiometries. Results obtained using the two turbulence closures are in close agreement at all downstream locations, although CO and NO are in marginally closer accord with data for the RSSF model, and OH marginally so for the $k-\varepsilon$ model.

Results for flame D are in good agreement with those obtained by Roomina and Bilger (2001), although differences do occur for NO. In particular, predicted NO trends obtained in the present work over-estimate data in fuel-lean and near stoichiometric region, but come in line with data under very fuel-rich conditions. In contrast, the predictions of Roomina and Bilger (2001), whilst quantitatively

similar to those of Figure (5.60), under-predict NO levels under very fuel-rich conditions. The present results also compare favourably with earlier investigations of this flame that employed probability density function approaches (Lindstedt et al 2000, Xu and Pope 2000) and Eulerian particle flamelet methods (Coelho and Peters 2001a).

Turning to predictions in physical space, major species of H_2O, CH_4, CO_2, and O_2 are depicted in Figures (5.64-5.67) for flame C, derived using both GRI-Mech2.11 and GRI-Mech3.0. Observations fall in line with those made for the conditional data, with H_2O now being over-predicted, and CH_4 and O_2 being under-predicted. CO_2 does however display good agreement with experimental results. Little difference is observed between data derived from the two kinetics schemes, and a similar level of agreement is observed for flames D and E, as indicated by Figures (5.68-5.71). The greatest difference in predictions is observed to be between the two turbulence closures, with the second moment method effecting noticeably superior results for all species and flow conditions considered. These observations can be extended to the minor species of CO, OH, and NO, and temperature for all three flames, which are shown in figures (5.72-5.87). Again, GRI-Mech3.0 is noted to perform similarly to its GRI-Mech2.11 counterpart, excepting predictions of NO, which display an almost two-fold increase of the peak values (Figure (5.78)), as previously observed in flames A and B. The real-space predictions derived using the $k-\varepsilon$ closure and GRI-Mech2.11 favour very well with the results obtained by Roomina and Bilger (2001), but as previously mentioned, underperform in contrast to the second-moment model of the present study.

5.iv.iii Calculation of a CH_4 Jet Flame in Oxygen Enriched Air

5.iv.iii.i Flow Field

Turning to flame F, it being the final flame in this study, although velocity data are not available, predictions of radial profiles of mean mixture fraction shown in Figure (5.88) are observed to be in similar agreement to those observed for the other five flames, excepting that at x/d = 170.0 where the spread of the jet appears to be under-estimated. Previous calculations do not extend this far downstream of the nozzle, and hence no data is available for comparison and comment.

5.iv.iii.ii Scalar Field

Conditional temperatures and major mole fractions of H_2O, CH_4, O_2, and CO_2, derived using two turbulence closures and GRI-Mech2.11 are compared against experimental data in figures (5.89-5.92). Although not as extensive as results for flames A, B, C, D, and E, the level of agreement between measured and predicted results is comparable to that of C, D, and E, with the slight over-predictions of H_2O and under-prediction of CH_4 evident at the near-field locale, noting an improvement in prediction with downstream progression. Again, similarly to flames C, D, and E, predictions of O_2 and CO_2 show good agreement with data, and an over-prediction of CO, although more accentuated in the

present case, is noted in near-field data. With respect to NO however, although an over-prediction is certainly evident, it is not as pronounced as that observed for flames C and E in Figures (5.54, 5.63), which display approximately thirty percent greater deviation from experimental data. Errors in results can however be seen to be of a similar magnitude to those obtained in calculations of flame C. Results obtained from the two turbulence closures can be seen to display little difference.

Figures (5.93-5.95) depict physical space predictions of CO, NO, and mean temperature, derived from both turbulence models, and plotted against experimentally derived data. Results from both models are generally very good, displaying similar levels of agreement. Again, NO predictions are notably superior to those obtained for flames C, D, and E (Figures (5.74, 5.82, 5.86)), and more in line with observations of flames A and B shown in Figures (5.30, 5.33).

5.iv.iv Calculation of a CH_4 Opposed-Flow Laminar Diffusion Flames

Considering the previously discussed modelling results, and in particular the discrepancies observed in NO predictions between the two kinetics schemes applied and over the different flames studied, one-dimensional laminar flame calculations are now presented. The purpose of this study is to isolate the effects of turbulence from the predictions, and present an investigation of the sensitivity of results to the modelling of the complex geometry and fuel composition found in the piloted flames previously discussed. The laminar flame code RUN-1DL

(Rogg and Wang 2001) was chosen to simulate a strained laminar one-dimensional flame, modelled as an opposed-jet counterflow geometry. The choice of flame code was made due to the ease in which CHEMKIN routines can be employed to handle the kinetic effects within the flames. Hence, calculations are made applying the same mechanisms and numerics as employed in the CMC calculations, without incorporating turbulence effects, or geometric complexities. This code adopts boundary-layer equations to describe the variations of density, velocity, pressure, energy, and species mass fractions in a laminar, chemically reacting, low Mach-number, stagnation-point diffusion flame. An ideal gas mixture is considered, and Dufour effects, diffusion caused by pressure gradients, and external forces are neglected. Thus, the equations governing conservation of mass, momentum, energy, and species are constructed and solved over an adaptive grid via the implementation of a modified Newton's method. For a detailed description of the code, including other applications its use is intended for, the reader is referred to Rogg and Wang (2001).

In an attempt to identify a possible cause for the excessively over-predicted NO levels observed in the aforementioned flames, a laminar flame is calculated using the flow parameters of flame D, with results being depicted in Figure (5.96). Presented are predictions of the minor species CO, OH, and NO, calculated using GRI-Mech2.11, with the initial conditions for the fuel composition set to 0%, 1%, 5%, and 10% C_2H_2 dilution. If the presence of un-combusted acetylene in the fuel jet were to be responsible for decreasing the NO levels in the downstream locale, indication should be given through analysis of these results. An increase in acetylene concentration would be expected to effect this reduction in calculated values. As can be observed in Figure (5.96), the introduction of

acetylene has the converse effect, increasing levels of NO production. For reference, this trend is also observed in the predictions of CO and OH, reflected on the same figure.

Figures (5.97-5.99) show minor species predictions of CO, OH, and NO derived using both GRI-Mech2.11 and GRI-Mech3.0 for the fuel and oxidiser compositions of flames B, D, and F. In line with the previous observations, little difference is observed between the two kinetic models with reference to CO and OH, but NO is seen to display a large discrepancy between the two kinetics schemes. Figure (5.100) also confirms previous observations of negligible differences between major species predictions and temperature between the two schemes.

5.v Conclusions

A first-order CMC model has been applied to the calculation of six CH_4 non-premixed jet flames of varying dilutions, with predictions based upon two differing kinetics schemes and both $k-\varepsilon$ and Reynolds stress/scalar flux closures. In contrast to the findings of similar studies conducted of hydrogen fuel jets (Fairweather and Woolley 2003) and Chapter 3 of this present work, little difference is observed between results derived on the basis of the two closures for the majority of flow parameters considered, in conditional space at least. Physical space predictions do however demonstrate the superiority of results derived on the basis of the second-moment turbulence closure.

There is an observed general deterioration in accuracy of results from flames A to B and from flames C to E, pointing to the requirement for second-order CMC modelling, as local extinction effects become more significant. With the increase in conditional fluctuations of species concentrations and temperature, allowance for the variances and covariances of these fluctuations is therefore required within a second-order CMC model for accurate modelling of such flames.

An anomaly remains with regard to predictions of NO in these flames. Whilst results for flames A, B, D, and F are in reasonable accord with measurements, those for flames C and E are not. The present work was performed on the basis of GRI-Mech 2.11 and GRI-Mech 3.0 and, whilst obtaining close agreement between the results of these two schemes for the majority of species and temperature, the NO results exhibit a significant discrepancy. This finding in line

with those of Roomina and Bilger (2001) who used a variety of kinetic schemes to predict Flame D, including GRI-Mech2.11, a skeletal mechanism consisting of 19 species and 36 reactions (Roomina and Bilger 2001), and the Miller-Bowman scheme with 51 species and 259 reactions (Miller and Bowman 1989). As noted above, the GRI-Mech2.11 based results obtained by these authors were similar to those of the present study, although some differences did occur under fuel-rich conditions. Predictions of the skeletal scheme were found to be largely unsatisfactory, with this scheme resulting in an over-prediction of temperatures and both minor and major species in fuel-rich regions, although NO was under-predicted. The Miller-Bowman mechanism led to results similar to those of GRI-Mech2.11, although predictions of the latter mechanism were generally in closer agreement with data, apart from NO where closer agreement under fuel-lean and near stoichiometric conditions was obtained using the Miller-Bowman scheme. Overall, application of GRI-Mech2.11 to Flame D by Roomina and Bilger (2001) showed good predictions of temperature and reactive scalars in fuel-lean regions, but an over-prediction of NO in fuel-lean regions and an under-prediction when fuel-rich. These authors attributed errors on the fuel-lean side to either the use of a first-order approximation for closure on conditional reaction rate terms within the CMC model employed, with the requirement for second-order closure identified, or the need for further work to establish whether the rate constant for the N_2O pathway to NO formation, which is important in fuel-lean regions, is too high. On the fuel-rich side, the comparison of different mechanisms revealed the importance of C_2 chemistry, although the overall adequacy of current mechanisms in fuel-rich regions was questioned, and the need for further model

improvement and wider validation against a range of non-premixed flames identified.

The present work largely confirms these findings in regard of Flames C to E, although reasonable agreement for NO levels is obtained in fuel-rich regions of Flame C, with no under-prediction of NO levels being seen in any of the three flames. Predictions for Flames A, B and F show closer agreement with NO data at all stoichiometries, although over-prediction in both fuel-lean and fuel-rich zones is generally the case in Flames A and B, with predictions for Flame F being in line with observations, apart from in peak temperature zones. Results for NO are therefore conflicting, and demonstrate a need to explore second-order CMC modelling approaches where the inclusion of such terms has been found (Kronenburg et al 1998) to significantly reduce NO levels over all stoichiometries. In addition, however, there is clearly a requirement to further investigate the application of different kinetic schemes in the modelling of turbulent non-premixed flames, including detailed investigations of the mechanisms and rates employed for NO chemistry.

The use of laminar flame calculations in the present study has also confirmed the findings above, with respect to the performance of the two kinetics schemes and the latter comments regarding the further investigation of NO chemistry, although not themselves providing an elucidation of the anomalies observed.

Overall, first-order modelling is found to be capable of yielding reliable predictions for methane flames that have little or no extinction effects, excepting those of NO levels, with results from flame D comparing favourably with earlier investigations that employ CMC, PDF, and particle flamelet methods.

5.vi Tables

Flame	Composition by volume	Re	Axial Velocity (ms^{-1})	Stoic Z
A	22.1:33.2:44.7	15,200	42.2	0.167
B	22.1:33.2:44.7	22,800	63.2	0.167

Table 5.1 – $CH_4/H_2/N_2$ Jet Flame Parameters.

Flame	Composition by volume	Re	Axial Velocity (ms^{-1})	Stoic Z
C	25:75	13,400	29.7	0.351
D	25:75	22,400	49.6	0.351
E	25:75	33,600	74.4	0.351

Table 5.2 – CH_4/air Jet Flame Parameters.

Flame	Composition by volume	Re	Axial Velocity (ms^{-1})	Stoic Z
F	100	4,510	37.0	

Table 5.3 – CH_4/Oxygen Enriched Air Jet Flame Parameters.

Reaction	A	b	E
2O+M<=>O2+M	1.20E+17	-1	0
O+H+M<=>OH+M	5.00E+17	-1	0
O+H2<=>H+OH	5.00E+04	2.7	6290
O+HO2<=>OH+O2	2.00E+13	0	0
O+H2O2<=>OH+HO2	9.63E+06	2	4000
O+CH<=>H+CO	5.70E+13	0	0
O+CH2<=>H+HCO	8.00E+13	0	0
O+CH2(S)<=>H2+CO	1.50E+13	0	0
O+CH2(S)<=>H+HCO	1.50E+13	0	0
O+CH3<=>H+CH2O	8.43E+13	0	0
O+CH4<=>OH+CH3	1.02E+09	1.5	8600
O+CO+M<=>CO2+M	6.02E+14	0	3000
O+HCO<=>OH+CO	3.00E+13	0	0
O+HCO<=>H+CO2	3.00E+13	0	0
O+CH2O<=>OH+HCO	3.90E+13	0	3540
O+CH2OH<=>OH+CH2O	1.00E+13	0	0
O+CH3O<=>OH+CH2O	1.00E+13	0	0
O+CH3OH<=>OH+CH2OH	3.88E+05	2.5	3100
O+CH3OH<=>OH+CH3O	1.30E+05	2.5	5000
O+C2H<=>CH+CO	5.00E+13	0	0
O+C2H2<=>H+HCCO	1.02E+07	2	1900
O+C2H2<=>OH+C2H	4.60E+19	-1.4	28950
O+C2H2<=>CO+CH2	1.02E+07	2	1900
O+C2H3<=>H+CH2CO	3.00E+13	0	0
O+C2H4<=>CH3+HCO	1.92E+07	1.8	220
O+C2H5<=>CH3+CH2O	1.32E+14	0	0
O+C2H6<=>OH+C2H5	8.98E+07	1.9	5690
O+HCCO<=>H+2CO	1.00E+14	0	0
O+CH2CO<=>OH+HCCO	1.00E+13	0	8000
O+CH2CO<=>CH2+CO2	1.75E+12	0	1350
O2+CO<=>O+CO2	2.50E+12	0	47800
O2+CH2O<=>HO2+HCO	1.00E+14	0	40000
H+O2+M<=>HO2+M	2.80E+18	-0.9	0
H+2O2<=>HO2+O2	3.00E+20	-1.7	0
H+O2+H2O<=>HO2+H2O	9.38E+18	-0.8	0
H+O2+N2<=>HO2+N2	3.75E+20	-1.7	0
H+O2+AR<=>HO2+AR	7.00E+17	-0.8	0
H+O2<=>O+OH	8.30E+13	0	14413
2H+M<=>H2+M	1.00E+18	-1	0
2H+H2<=>2H2	9.00E+16	-0.6	0
2H+H2O<=>H2+H2O	6.00E+19	-1.3	0
2H+CO2<=>H2+CO2	5.50E+20	-2	0
H+OH+M<=>H2O+M	2.20E+22	-2	0
H+HO2<=>O+H2O	3.97E+12	0	671
H+HO2<=>O2+H2	2.80E+13	0	1068
H+HO2<=>2OH	1.34E+14	0	635
H+H2O2<=>HO2+H2	1.21E+07	2	5200
H+H2O2<=>OH+H2O	1.00E+13	0	3600
H+CH<=>C+H2	1.10E+14	0	0
H+CH2(+M)<=>CH3(+M)	2.50E+16	-0.8	0
H+CH2(S)<=>CH+H2	3.00E+13	0	0
H+CH3(+M)<=>CH4(+M)	1.27E+16	-0.6	383
H+CH4<=>CH3+H2	6.60E+08	1.6	10840
H+HCO(+M)<=>CH2O(+M)	1.09E+12	0.5	-260
H+HCO<=>H2+CO	7.34E+13	0	0
H+CH2O(+M)<=>CH2OH(+M)	5.40E+11	0.5	3600
H+CH2O(+M)<=>CH3O(+M)	5.40E+11	0.5	2600
H+CH2O<=>HCO+H2	2.30E+10	1.1	3275
H+CH2OH(+M)<=>CH3OH(+M)	1.80E+13	0	0
H+CH2OH<=>H2+CH2O	2.00E+13	0	0
H+CH2OH<=>OH+CH3	1.20E+13	0	0
H+CH2OH<=>CH2(S)+H2O	6.00E+12	0	0
H+CH3O(+M)<=>CH3OH(+M)	5.00E+13	0	0
H+CH3O<=>H+CH2OH	3.40E+06	1.6	0
H+CH3O<=>H2+CH2O	2.00E+13	0	0
H+CH3O<=>OH+CH3	3.20E+13	0	0
H+CH3O<=>CH2(S)+H2O	1.60E+13	0	0
H+CH3OH<=>CH2OH+H2	1.70E+07	2.1	4870
H+CH3OH<=>CH3O+H2	4.20E+06	2.1	4870
H+C2H(+M)<=>C2H2(+M)	1.00E+17	-1	0

H+C2H2(+M)<=>C2H3(+M)	5.60E+12	0	2400
H+C2H3(+M)<=>C2H4(+M)	6.08E+12	0.3	280
H+C2H3<=>H2+C2H2	3.00E+13	0	0
H+C2H4(+M)<=>C2H5(+M)	1.08E+12	0.5	1820
H+C2H4<=>C2H3+H2	1.33E+06	2.5	12240
H+C2H5(+M)<=>C2H6(+M)	5.21E+17	-1	1580
H+C2H5<=>H2+C2H4	2.00E+12	0	0
H+C2H6<=>C2H5+H2	1.15E+08	1.9	7530
H+HCCO<=>CH2(S)+CO	1.00E+14	0	0
H+CH2CO<=>HCCO+H2	5.00E+13	0	8000
H+CH2CO<=>CH3+CO	1.13E+13	0	3428
H+HCCOH<=>H+CH2CO	1.00E+13	0	0
H2+CO(+M)<=>CH2O(+M)	4.30E+07	1.5	79600
OH+H2<=>H+H2O	2.16E+08	1.5	3430
2OH(+M)<=>H2O2(+M)	7.40E+13	-0.4	0
2OH<=>O+H2O	3.57E+04	2.4	-2110
OH+HO2<=>O2+H2O	2.90E+13	0	-500
OH+H2O2<=>HO2+H2O	1.75E+12	0	320
OH+H2O2<=>HO2+H2O	5.80E+14	0	9560
OH+C<=>H+CO	5.00E+13	0	0
OH+CH<=>H+HCO	3.00E+13	0	0
OH+CH2<=>H+CH2O	2.00E+13	0	0
OH+CH2<=>CH+H2O	1.13E+07	2	3000
OH+CH2(S)<=>H+CH2O	3.00E+13	0	0
OH+CH3(+M)<=>CH3OH(+M)	6.30E+13	0	0
OH+CH3<=>CH2+H2O	5.60E+07	1.6	5420
OH+CH3<=>CH2+H2O	5.60E+07	1.6	5420
OH+CH3<=>CH2(S)+H2O	2.50E+13	0	0
OH+CH4<=>CH3+H2O	1.00E+08	1.6	3120
OH+CO<=>H+CO2	4.76E+07	1.2	70
OH+HCO<=>H2O+CO	5.00E+13	0	0
OH+CH2O<=>HCO+H2O	3.43E+09	1.2	-447
OH+CH2OH<=>H2O+CH2O	5.00E+12	0	0
OH+CH3O<=>H2O+CH2O	5.00E+12	0	0
OH+CH3OH<=>CH2OH+H2O	1.44E+06	2	-840
OH+CH3OH<=>CH3O+H2O	6.30E+06	2	1500
OH+C2H<=>H+HCCO	2.00E+13	0	0
OH+C2H2<=>H+CH2CO	2.18E-04	4.5	-1000
OH+C2H2<=>H+HCCOH	5.04E+05	2.3	13500
OH+C2H2<=>C2H+H2O	3.37E+07	2	14000
OH+C2H2<=>CH3+CO	4.83E-04	4	-2000
OH+C2H3<=>H2O+C2H2	5.00E+12	0	0
OH+C2H4<=>C2H3+H2O	3.60E+06	2	2500
OH+C2H6<=>C2H5+H2O	3.54E+06	2.1	870
OH+CH2CO<=>HCCO+H2O	7.50E+12	0	2000
2HO2<=>O2+H2O2	1.30E+11	0	-1630
2HO2<=>O2+H2O2	4.20E+14	0	12000
HO2+CH2<=>OH+CH2O	2.00E+13	0	0
HO2+CH3<=>O2+CH4	1.00E+12	0	0
HO2+CH3<=>OH+CH3O	2.00E+13	0	0
HO2+CO<=>OH+CO2	1.50E+14	0	23600
HO2+CH2O<=>HCO+H2O2	1.00E+12	0	8000
C+O2<=>O+CO	5.80E+13	0	576
C+CH2<=>H+C2H	5.00E+13	0	0
C+CH3<=>H+C2H2	5.00E+13	0	0
CH+O2<=>O+HCO	3.30E+13	0	0
CH+H2<=>H+CH2	1.11E+08	1.8	1670
CH+H2O<=>H+CH2O	1.71E+13	0	-755
CH+CH2<=>H+C2H2	4.00E+13	0	0
CH+CH3<=>H+C2H3	3.00E+13	0	0
CH+CH4<=>H+C2H4	6.00E+13	0	0
CH+CO(+M)<=>HCCO(+M)	5.00E+13	0	0
CH+CO2<=>HCO+CO	3.40E+12	0	690
CH+CH2O<=>H+CH2CO	9.46E+13	0	-515
CH+HCCO<=>CO+C2H2	5.00E+13	0	0
CH2+O2<=>OH+HCO	1.32E+13	0	1500
CH2+H2<=>H+CH3	5.00E+05	2	7230
2CH2<=>H2+C2H2	3.20E+13	0	0
CH2+CH3<=>H+C2H4	4.00E+13	0	0
CH2+CH4<=>2CH3	2.46E+06	2	8270
CH2+CO(+M)<=>CH2CO(+M)	8.10E+11	0.5	4510

CH2+HCCO<=>C2H3+CO	3.00E+13	0	0
CH2(S)+N2<=>CH2+N2	1.50E+13	0	600
CH2(S)+AR<=>CH2+AR	9.00E+12	0	600
CH2(S)+O2<=>H+OH+CO	2.80E+13	0	0
CH2(S)+O2<=>CO+H2O	1.20E+13	0	0
CH2(S)+H2<=>CH3+H	7.00E+13	0	0
CH2(S)+H2O(+M)<=>CH3OH(+M)	2.00E+13	0	0
CH2(S)+H2O<=>CH2+H2O	3.00E+13	0	0
CH2(S)+CH3<=>H+C2H4	1.20E+13	0	-570
CH2(S)+CH4<=>2CH3	1.60E+13	0	-570
CH2(S)+CO<=>CH2+CO	9.00E+12	0	0
CH2(S)+CO2<=>CH2+CO2	7.00E+12	0	0
CH2(S)+CO2<=>CO+CH2O	1.40E+13	0	0
CH2(S)+C2H6<=>CH3+C2H5	4.00E+13	0	-550
CH3+O2<=>O+CH3O	2.68E+13	0	28800
CH3+O2<=>OH+CH2O	3.60E+10	0	8940
CH3+H2O2<=>HO2+CH4	2.45E+04	2.5	5180
2CH3(+M)<=>C2H6(+M)	2.12E+16	-1	620
2CH3<=>H+C2H5	4.99E+12	0.1	10600
CH3+HCO<=>CH4+CO	2.65E+13	0	0
CH3+CH2O<=>HCO+CH4	3.32E+03	2.8	5860
CH3+CH3OH<=>CH2OH+CH4	3.00E+07	1.5	9940
CH3+CH3OH<=>CH3O+CH4	1.00E+07	1.5	9940
CH3+C2H4<=>C2H3+CH4	2.27E+05	2	9200
CH3+C2H6<=>C2H5+CH4	6.14E+06	1.7	10450
HCO+H2O<=>H+CO+H2O	2.24E+18	-1	17000
HCO+M<=>H+CO+M	1.87E+17	-1	17000
HCO+O2<=>HO2+CO	7.60E+12	0	400
CH2OH+O2<=>HO2+CH2O	1.80E+13	0	900
CH3O+O2<=>HO2+CH2O	4.28E-13	7.6	-3530
C2H+O2<=>HCO+CO	5.00E+13	0	1500
C2H+H2<=>H+C2H2	4.07E+05	2.4	200
C2H3+O2<=>HCO+CH2O	3.98E+12	0	-240
C2H4(+M)<=>H2+C2H2(+M)	8.00E+12	0.4	88770
C2H5+O2<=>HO2+C2H4	8.40E+11	0	3875
HCCO+O2<=>OH+2CO	1.60E+12	0	854
2HCCO<=>2CO+C2H2	1.00E+13	0	0
N+NO<=>N2+O	3.50E+13	0	330
N+O2<=>NO+O	2.65E+12	0	6400
N+OH<=>NO+H	7.33E+13	0	1120
N2O+O<=>N2+O2	1.40E+12	0	10810
N2O+O<=>2NO	2.90E+13	0	23150
N2O+H<=>N2+OH	4.40E+14	0	18880
N2O+OH<=>N2+HO2	2.00E+12	0	21060
N2O(+M)<=>N2+O(+M)	1.30E+11	0	59620
HO2+NO<=>NO2+OH	2.11E+12	0	-480
NO+O+M<=>NO2+M	1.06E+20	-1.4	0
NO2+O<=>NO+O2	3.90E+12	0	-240
NO2+H<=>NO+OH	1.32E+14	0	360
NH+O<=>NO+H	5.00E+13	0	0
NH+H<=>N+H2	3.20E+13	0	330
NH+OH<=>HNO+H	2.00E+13	0	0
NH+OH<=>N+H2O	2.00E+09	1.2	0
NH+O2<=>HNO+O	4.61E+05	2	6500
NH+O2<=>NO+OH	1.28E+06	1.5	100
NH+N<=>N2+H	1.50E+13	0	0
NH+H2O<=>HNO+H2	2.00E+13	0	13850
NH+NO<=>N2+OH	2.16E+13	-0.2	0
NH+NO<=>N2O+H	4.16E+14	-0.5	0
NH2+O<=>OH+NH	7.00E+12	0	0
NH2+O<=>H+HNO	4.60E+13	0	0
NH2+H<=>NH+H2	4.00E+13	0	3650
NH2+OH<=>NH+H2O	9.00E+07	1.5	-460
NNH<=>N2+H	3.30E+08	0	0
NNH+M<=>N2+H+M	1.30E+14	-0.1	4980
NNH+O2<=>HO2+N2	5.00E+12	0	0
NNH+O<=>OH+N2	2.50E+13	0	0
NNH+O<=>NH+NO	7.00E+13	0	0
NNH+H<=>H2+N2	5.00E+13	0	0
NNH+OH<=>H2O+N2	2.00E+13	0	0
NNH+CH3<=>CH4+N2	2.50E+13	0	0

H+NO+M<=>HNO+M	8.95E+19	-1.3	740
HNO+O<=>NO+OH	2.50E+13	0	0
HNO+H<=>H2+NO	4.50E+11	0.7	660
HNO+OH<=>NO+H2O	1.30E+07	1.9	-950
HNO+O2<=>HO2+NO	1.00E+13	0	13000
CN+O<=>CO+N	7.70E+13	0	0
CN+OH<=>NCO+H	4.00E+13	0	0
CN+H2O<=>HCN+OH	8.00E+12	0	7460
CN+O2<=>NCO+O	6.14E+12	0	-440
CN+H2<=>HCN+H	2.10E+13	0	4710
NCO+O<=>NO+CO	2.35E+13	0	0
NCO+H<=>NH+CO	5.40E+13	0	0
NCO+OH<=>NO+H+CO	2.50E+12	0	0
NCO+N<=>N2+CO	2.00E+13	0	0
NCO+O2<=>NO+CO2	2.00E+12	0	20000
NCO+M<=>N+CO+M	8.80E+16	-0.5	48000
NCO+NO<=>N2O+CO	2.85E+17	-1.5	740
NCO+NO<=>N2+CO2	5.70E+18	-2	800
HCN+M<=>H+CN+M	1.04E+29	-3.3	126600
HCN+O<=>NCO+H	1.11E+04	2.6	4980
HCN+O<=>NH+CO	2.77E+03	2.6	4980
HCN+O<=>CN+OH	2.13E+09	1.6	26600
HCN+OH<=>HOCN+H	1.10E+06	2	13370
HCN+OH<=>HNCO+H	4.40E+03	2.3	6400
HCN+OH<=>NH2+CO	1.60E+02	2.6	9000
H+HCN+M<=>H2CN+M	1.40E+26	-3.4	1900
H2CN+N<=>N2+CH2	6.00E+13	0	400
C+N2<=>CN+N	6.30E+13	0	46020
CH+N2<=>HCN+N	2.86E+08	1.1	20400
CH+N2(+M)<=>HCNN(+M)	3.10E+12	0.1	0
CH2+N2<=>HCN+NH	1.00E+13	0	74000
CH2(S)+N2<=>NH+HCN	1.00E+11	0	65000
C+NO<=>CN+O	1.90E+13	0	0
C+NO<=>CO+N	2.90E+13	0	0
CH+NO<=>HCN+O	5.00E+13	0	0
CH+NO<=>H+NCO	2.00E+13	0	0
CH+NO<=>N+HCO	3.00E+13	0	0
CH2+NO<=>H+HNCO	3.10E+17	-1.4	1270
CH2+NO<=>OH+HCN	2.90E+14	-0.7	760
CH2+NO<=>H+HCNO	3.80E+13	-0.4	580
CH2(S)+NO<=>H+HNCO	3.10E+17	-1.4	1270
CH2(S)+NO<=>OH+HCN	2.90E+14	-0.7	760
CH2(S)+NO<=>H+HCNO	3.80E+13	-0.4	580
CH3+NO<=>HCN+H2O	9.60E+13	0	28800
CH3+NO<=>H2CN+OH	1.00E+12	0	21750
HCNN+O<=>CO+H+N2	2.20E+13	0	0
HCNN+O<=>HCN+NO	2.00E+12	0	0
HCNN+O2<=>O+HCO+N2	1.20E+13	0	0
HCNN+OH<=>H+HCO+N2	1.20E+13	0	0
HCNN+H<=>CH2+N2	1.00E+14	0	0
HNCO+O<=>NH+CO2	9.80E+07	1.4	8500
HNCO+O<=>HNO+CO	1.50E+08	1.6	44000
HNCO+O<=>NCO+OH	2.20E+06	2.1	11400
HNCO+H<=>NH2+CO	2.25E+07	1.7	3800
HNCO+H<=>H2+NCO	1.05E+05	2.5	13300
HNCO+OH<=>NCO+H2O	4.65E+12	0	6850
HNCO+OH<=>NH2+CO2	1.55E+12	0	6850
HNCO+M<=>NH+CO+M	1.18E+16	0	84720
HCNO+H<=>H+HNCO	2.10E+15	-0.7	2850
HCNO+H<=>OH+HCN	2.70E+11	0.2	2120
HCNO+H<=>NH2+CO	1.70E+14	-0.8	2890
HOCN+H<=>H+HNCO	2.00E+07	2	2000
HCCO+NO<=>HCNO+CO	2.35E+13	0	0
CH3+N<=>H2CN+H	6.10E+14	-0.3	290
CH3+N<=>HCN+H2	3.70E+12	0.1	-90
NH3+H<=>NH2+H2	5.40E+05	2.4	9915
NH3+OH<=>NH2+H2O	5.00E+07	1.6	955
NH3+O<=>NH2+OH	9.40E+06	1.9	6460

Table 5.4 – CH_4/Air Combustion Mechanism Scheme GRI-Mech2.11 (Units: mole, cm, s, K, cal).

2O+M<=>O2+M	1.20E+17	-1	0
O+H+M<=>OH+M	5.00E+17	-1	0
O+H2<=>H+OH	3.87E+04	2.7	6260
O+HO2<=>OH+O2	2.00E+13	0	0
O+H2O2<=>OH+HO2	9.63E+06	2	4000
O+CH<=>H+CO	5.70E+13	0	0
O+CH2<=>H+HCO	8.00E+13	0	0
O+CH2(S)<=>H2+CO	1.50E+13	0	0
O+CH2(S)<=>H+HCO	1.50E+13	0	0
O+CH3<=>H+CH2O	5.06E+13	0	0
O+CH4<=>OH+CH3	1.02E+09	1.5	8600
O+CO(+M)<=>CO2(+M)	1.80E+10	0	2385
O+HCO<=>OH+CO	3.00E+13	0	0
O+HCO<=>H+CO2	3.00E+13	0	0
O+CH2O<=>OH+HCO	3.90E+13	0	3540
O+CH2OH<=>OH+CH2O	1.00E+13	0	0
O+CH3O<=>OH+CH2O	1.00E+13	0	0
O+CH3OH<=>OH+CH2OH	3.88E+05	2.5	3100
O+CH3OH<=>OH+CH3O	1.30E+05	2.5	5000
O+C2H<=>CH+CO	5.00E+13	0	0
O+C2H2<=>H+HCCO	1.35E+07	2	1900
O+C2H2<=>OH+C2H	4.60E+19	-1.4	28950
O+C2H2<=>CO+CH2	6.94E+06	2	1900
O+C2H3<=>H+CH2CO	3.00E+13	0	0
O+C2H4<=>CH3+HCO	1.25E+07	1.8	220
O+C2H5<=>CH3+CH2O	2.24E+13	0	0
O+C2H6<=>OH+C2H5	8.98E+07	1.9	5690
O+HCCO<=>H+2CO	1.00E+14	0	0
O+CH2CO<=>OH+HCCO	1.00E+13	0	8000
O+CH2CO<=>CH2+CO2	1.75E+12	0	1350
O2+CO<=>O+CO2	2.50E+12	0	47800
O2+CH2O<=>HO2+HCO	1.00E+14	0	40000
H+O2+M<=>HO2+M	2.80E+18	-0.9	0
H+2O2<=>HO2+O2	2.08E+19	-1.2	0
H+O2+H2O<=>HO2+H2O	1.13E+19	-0.8	0
H+O2+N2<=>HO2+N2	2.60E+19	-1.2	0
H+O2+AR<=>HO2+AR	7.00E+17	-0.8	0
H+O2<=>O+OH	2.65E+16	-0.7	17041
2H+M<=>H2+M	1.00E+18	-1	0
2H+H2<=>2H2	9.00E+16	-0.6	0
2H+H2O<=>H2+H2O	6.00E+19	-1.2	0
2H+CO2<=>H2+CO2	5.50E+20	-2	0
H+OH+M<=>H2O+M	2.20E+22	-2	0
H+HO2<=>O+H2O	3.97E+12	0	671
H+HO2<=>O2+H2	4.48E+13	0	1068
H+HO2<=>2OH	8.40E+13	0	635
H+H2O2<=>HO2+H2	1.21E+07	2	5200
H+H2O2<=>OH+H2O	1.00E+13	0	3600
H+CH<=>C+H2	1.65E+14	0	0
H+CH2(+M)<=>CH3(+M)	6.00E+14	0	0
H+CH2(S)<=>CH+H2	3.00E+13	0	0
H+CH3(+M)<=>CH4(+M)	1.39E+16	-0.5	536
H+CH4<=>CH3+H2	6.60E+08	1.6	10840
H+HCO(+M)<=>CH2O(+M)	1.09E+12	0.5	-260
H+HCO<=>H2+CO	7.34E+13	0	0
H+CH2O(+M)<=>CH2OH(+M)	5.40E+11	0.5	3600
H+CH2O(+M)<=>CH3O(+M)	5.40E+11	0.5	2600
H+CH2O<=>HCO+H2	5.74E+07	1.9	2742
H+CH2OH(+M)<=>CH3OH(+M)	1.06E+12	0.5	86
H+CH2OH<=>H2+CH2O	2.00E+13	0	0
H+CH2OH<=>OH+CH3	1.65E+11	0.7	-284
H+CH2OH<=>CH2(S)+H2O	3.28E+13	-0.1	610
H+CH3O(+M)<=>CH3OH(+M)	2.43E+12	0.5	50
H+CH3O<=>H+CH2OH	4.15E+07	1.6	1924
H+CH3O<=>H2+CH2O	2.00E+13	0	0
H+CH3O<=>OH+CH3	1.50E+12	0.5	-110
H+CH3O<=>CH2(S)+H2O	2.62E+14	-0.2	1070
H+CH3OH<=>CH2OH+H2	1.70E+07	2.1	4870
H+CH3OH<=>CH3O+H2	4.20E+06	2.1	4870
H+C2H(+M)<=>C2H2(+M)	1.00E+17	-1	0

H+C2H2(+M)<=>C2H3(+M)	5.60E+12	0	2400
H+C2H3(+M)<=>C2H4(+M)	6.08E+12	0.3	280
H+C2H3<=>H2+C2H2	3.00E+13	0	0
H+C2H4(+M)<=>C2H5(+M)	5.40E+11	0.5	1820
H+C2H4<=>C2H3+H2	1.33E+06	2.5	12240
H+C2H5(+M)<=>C2H6(+M)	5.21E+17	-1	1580
H+C2H5<=>H2+C2H4	2.00E+12	0	0
H+C2H6<=>C2H5+H2	1.15E+08	1.9	7530
H+HCCO<=>CH2(S)+CO	1.00E+14	0	0
H+CH2CO<=>HCCO+H2	5.00E+13	0	8000
H+CH2CO<=>CH3+CO	1.13E+13	0	3428
H+HCCOH<=>H+CH2CO	1.00E+13	0	0
H2+CO(+M)<=>CH2O(+M)	4.30E+07	1.5	79600
OH+H2<=>H+H2O	2.16E+08	1.5	3430
2OH(+M)<=>H2O2(+M)	7.40E+13	-0.4	0
2OH<=>O+H2O	3.57E+04	2.4	-2110
OH+HO2<=>O2+H2O	1.45E+13	0	-500
OH+H2O2<=>HO2+H2O	2.00E+12	0	427
OH+H2O2<=>HO2+H2O	1.70E+18	0	29410
OH+C<=>H+CO	5.00E+13	0	0
OH+CH<=>H+HCO	3.00E+13	0	0
OH+CH2<=>H+CH2O	2.00E+13	0	0
OH+CH2<=>CH+H2O	1.13E+07	2	3000
OH+CH2(S)<=>H+CH2O	3.00E+13	0	0
OH+CH3(+M)<=>CH3OH(+M)	2.79E+18	-1.4	1330
OH+CH3<=>CH2+H2O	5.60E+07	1.6	5420
OH+CH3<=>CH2(S)+H2O	6.44E+17	-1.3	1417
OH+CH4<=>CH3+H2O	1.00E+08	1.6	3120
OH+CO<=>H+CO2	4.76E+07	1.2	70
OH+HCO<=>H2O+CO	5.00E+13	0	0
OH+CH2O<=>HCO+H2O	3.43E+09	1.2	-447
OH+CH2OH<=>H2O+CH2O	5.00E+12	0	0
OH+CH3O<=>H2O+CH2O	5.00E+12	0	0
OH+CH3OH<=>CH2OH+H2O	1.44E+06	2	-840
OH+CH3OH<=>CH3O+H2O	6.30E+06	2	1500
OH+C2H<=>H+HCCO	2.00E+13	0	0
OH+C2H2<=>H+CH2CO	2.18E-04	4.5	-1000
OH+C2H2<=>H+HCCOH	5.04E+05	2.3	13500
OH+C2H2<=>C2H+H2O	3.37E+07	2	14000
OH+C2H2<=>CH3+CO	4.83E-04	4	-2000
OH+C2H3<=>H2O+C2H2	5.00E+12	0	0
OH+C2H4<=>C2H3+H2O	3.60E+06	2	2500
OH+C2H6<=>C2H5+H2O	3.54E+06	2.1	870
OH+CH2CO<=>HCCO+H2O	7.50E+12	0	2000
2HO2<=>O2+H2O2	1.30E+11	0	-1630
2HO2<=>O2+H2O2	4.20E+14	0	12000
HO2+CH2<=>OH+CH2O	2.00E+13	0	0
HO2+CH3<=>O2+CH4	1.00E+12	0	0
HO2+CH3<=>OH+CH3O	3.78E+13	0	0
HO2+CO<=>OH+CO2	1.50E+14	0	23600
HO2+CH2O<=>HCO+H2O2	5.60E+06	2	12000
C+O2<=>O+CO	5.80E+13	0	576
C+CH2<=>H+C2H	5.00E+13	0	0
C+CH3<=>H+C2H2	5.00E+13	0	0
CH+O2<=>O+HCO	6.71E+13	0	0
CH+H2<=>H+CH2	1.08E+14	0	3110
CH+H2O<=>H+CH2O	5.71E+12	0	-755
CH+CH2<=>H+C2H2	4.00E+13	0	0
CH+CH3<=>H+C2H3	3.00E+13	0	0
CH+CH4<=>H+C2H4	6.00E+13	0	0
CH+CO(+M)<=>HCCO(+M)	5.00E+13	0	0
CH+CO2<=>HCO+CO	1.90E+14	0	15792
CH+CH2O<=>H+CH2CO	9.46E+13	0	-515
CH+HCCO<=>CO+C2H2	5.00E+13	0	0
CH2+O2=>OH+H+CO	5.00E+12	0	1500
CH2+H2<=>H+CH3	5.00E+05	2	7230
2CH2<=>H2+C2H2	1.60E+15	0	11944
CH2+CH3<=>H+C2H4	4.00E+13	0	0
CH2+CH4<=>2CH3	2.46E+06	2	8270
CH2+CO(+M)<=>CH2CO(+M)	8.10E+11	0.5	4510
CH2+HCCO<=>C2H3+CO	3.00E+13	0	0

CH2(S)+N2<=>CH2+N2	1.50E+13	0	600
CH2(S)+AR<=>CH2+AR	9.00E+12	0	600
CH2(S)+O2<=>H+OH+CO	2.80E+13	0	0
CH2(S)+O2<=>CO+H2O	1.20E+13	0	0
CH2(S)+H2<=>CH3+H	7.00E+13	0	0
CH2(S)+H2O(+M)<=>CH3OH(+M)	4.82E+17	-1.2	1145
CH2(S)+H2O<=>CH2+H2O	3.00E+13	0	0
CH2(S)+CH3<=>H+C2H4	1.20E+13	0	-570
CH2(S)+CH4<=>2CH3	1.60E+13	0	-570
CH2(S)+CO<=>CH2+CO	9.00E+12	0	0
CH2(S)+CO2<=>CH2+CO2	7.00E+12	0	0
CH2(S)+CO2<=>CO+CH2O	1.40E+13	0	0
CH2(S)+C2H6<=>CH3+C2H5	4.00E+13	0	-550
CH3+O2<=>O+CH3O	3.56E+13	0	30480
CH3+O2<=>OH+CH2O	2.31E+12	0	20315
CH3+H2O2<=>HO2+CH4	2.45E+04	2.5	5180
2CH3(+M)<=>C2H6(+M)	6.77E+16	-1.2	654
2CH3<=>H+C2H5	6.84E+12	0.1	10600
CH3+HCO<=>CH4+CO	2.65E+13	0	0
CH3+CH2O<=>HCO+CH4	3.32E+03	2.8	5860
CH3+CH3OH<=>CH2OH+CH4	3.00E+07	1.5	9940
CH3+CH3OH<=>CH3O+CH4	1.00E+07	1.5	9940
CH3+C2H4<=>C2H3+CH4	2.27E+05	2	9200
CH3+C2H6<=>C2H5+CH4	6.14E+06	1.7	10450
HCO+H2O<=>H+CO+H2O	1.50E+18	-1	17000
HCO+M<=>H+CO+M	1.87E+17	-1	17000
HCO+O2<=>HO2+CO	1.34E+13	0	400
H2OH+O2<=>HO2+CH2O	1.80E+13	0	900
H3O+O2<=>HO2+CH2O	4.28E-13	7.6	-3530
C2H+O2<=>HCO+CO	1.00E+13	0	-755
C2H+H2<=>H+C2H2	5.68E+10	0.9	1993
C2H3+O2<=>HCO+CH2O	4.58E+16	-1.4	1015
C2H4(+M)<=>H2+C2H2(+M)	8.00E+12	0.4	86770
C2H5+O2<=>HO2+C2H4	8.40E+11	0	3875
HCCO+O2<=>OH+2CO	3.20E+12	0	854
2HCCO<=>2CO+C2H2	1.00E+13	0	0
N+NO<=>N2+O	2.70E+13	0	355
N+O2<=>NO+O	9.00E+09	1	6500
N+OH<=>NO+H	3.36E+13	0	385
N2O+O<=>N2+O2	1.40E+12	0	10810
N2O+O<=>2NO	2.90E+13	0	23150
N2O+H<=>N2+OH	3.87E+14	0	18880
N2O+OH<=>N2+HO2	2.00E+12	0	21060
N2O(+M)<=>N2+O(+M)	7.91E+10	0	56020
HO2+NO<=>NO2+OH	2.11E+12	0	-480
NO+O+M<=>NO2+M	1.06E+20	-1.4	0
NO2+O<=>NO+O2	3.90E+12	0	-240
NO2+H<=>NO+OH	1.32E+14	0	360
NH+O<=>NO+H	4.00E+13	0	0
NH+H<=>N+H2	3.20E+13	0	330
NH+OH<=>HNO+H	2.00E+13	0	0
NH+OH<=>N+H2O	2.00E+09	1.2	0
NH+O2<=>HNO+O	4.61E+05	2	6500
NH+O2<=>NO+OH	1.28E+06	1.5	100
NH+N<=>N2+H	1.50E+13	0	0
NH+H2O<=>HNO+H2	2.00E+13	0	13850
NH+NO<=>N2+OH	2.16E+13	-0.2	0
NH+NO<=>N2O+H	3.65E+14	-0.5	0
NH2+O<=>OH+NH	3.00E+12	0	0
NH2+O<=>H+HNO	3.90E+13	0	0
NH2+H<=>NH+H2	4.00E+13	0	3650
NH2+OH<=>NH+H2O	9.00E+07	1.5	-460
NNH<=>N2+H	3.30E+08	0	0
NNH+M<=>N2+H+M	1.30E+14	-0.1	4980
NNH+O2<=>HO2+N2	5.00E+12	0	0
NNH+O<=>OH+N2	2.50E+13	0	0
NNH+O<=>NH+NO	7.00E+13	0	0
NNH+H<=>H2+N2	5.00E+13	0	0
NNH+OH<=>H2O+N2	2.00E+13	0	0
NNH+CH3<=>CH4+N2	2.50E+13	0	0
H+NO+M<=>HNO+M	4.48E+19	-1.3	740

HNO+O<=>NO+OH	2.50E+13	0	0
HNO+H<=>H2+NO	9.00E+11	0.7	660
HNO+OH<=>NO+H2O	1.30E+07	1.9	-950
HNO+O2<=>HO2+NO	1.00E+13	0	13000
CN+O<=>CO+N	7.70E+13	0	0
CN+OH<=>NCO+H	4.00E+13	0	0
CN+H2O<=>HCN+OH	8.00E+12	0	7460
CN+O2<=>NCO+O	6.14E+12	0	-440
CN+H2<=>HCN+H	2.95E+05	2.5	2240
NCO+O<=>NO+CO	2.35E+13	0	0
NCO+H<=>NH+CO	5.40E+13	0	0
NCO+OH<=>NO+H+CO	2.50E+12	0	0
NCO+N<=>N2+CO	2.00E+13	0	0
NCO+O2<=>NO+CO2	2.00E+12	0	20000
NCO+M<=>N+CO+M	3.10E+14	0	54050
NCO+NO<=>N2O+CO	1.90E+17	-1.5	740
NCO+NO<=>N2+CO2	3.80E+18	-2	800
HCN+M<=>H+CN+M	1.04E+29	-3.3	126600
HCN+O<=>NCO+H	2.03E+04	2.6	4980
HCN+O<=>NH+CO	5.07E+03	2.6	4980
HCN+O<=>CN+OH	3.91E+09	1.6	26600
HCN+OH<=>HOCN+H	1.10E+06	2	13370
HCN+OH<=>HNCO+H	4.40E+03	2.3	6400
HCN+OH<=>NH2+CO	1.60E+02	2.6	9000
H+HCN(+M)<=>H2CN(+M)	3.30E+13	0	0
H2CN+N<=>N2+CH2	6.00E+13	0	400
C+N2<=>CN+N	6.30E+13	0	46020
CH+N2<=>HCN+N	3.12E+09	0.9	20130
CH+N2(+M)<=>HCNN(+M)	3.10E+12	0.1	0
CH2+N2<=>HCN+NH	1.00E+13	0	74000
CH2(S)+N2<=>NH+HCN	1.00E+11	0	65000
C+NO<=>CN+O	1.90E+13	0	0
C+NO<=>CO+N	2.90E+13	0	0
CH+NO<=>HCN+O	4.10E+13	0	0
CH+NO<=>H+NCO	1.62E+13	0	0
CH+NO<=>N+HCO	2.46E+13	0	0
CH2+NO<=>H+HNCO	3.10E+17	-1.4	1270
CH2+NO<=>OH+HCN	2.90E+14	-0.7	760
CH2+NO<=>H+HCNO	3.80E+13	-0.4	580
CH2(S)+NO<=>H+HNCO	3.10E+17	-1.4	1270
CH2(S)+NO<=>OH+HCN	2.90E+14	-0.7	760
CH2(S)+NO<=>H+HCNO	3.80E+13	-0.4	580
CH3+NO<=>HCN+H2O	9.60E+13	0	28800
CH3+NO<=>H2CN+OH	1.00E+12	0	21750
HCNN+O<=>CO+H+N2	2.20E+13	0	0
HCNN+O<=>HCN+NO	2.00E+12	0	0
HCNN+O2<=>O+HCO+N2	1.20E+13	0	0
HCNN+OH<=>H+HCO+N2	1.20E+13	0	0
HCNN+H<=>CH2+N2	1.00E+14	0	0
HNCO+O<=>NH+CO2	9.80E+07	1.4	8500
HNCO+O<=>HNO+CO	1.50E+08	1.6	44000
HNCO+O<=>NCO+OH	2.20E+06	2.1	11400
HNCO+H<=>NH2+CO	2.25E+07	1.7	3800
HNCO+H<=>H2+NCO	1.05E+05	2.5	13300
HNCO+OH<=>NCO+H2O	3.30E+07	1.5	3600
HNCO+OH<=>NH2+CO2	3.30E+06	1.5	3600
HNCO+M<=>NH+CO+M	1.18E+16	0	84720
HCNO+H<=>H+HNCO	2.10E+15	-0.7	2850
HCNO+H<=>OH+HCN	2.70E+11	0.2	2120
HCNO+H<=>NH2+CO	1.70E+14	-0.8	2890
HOCN+H<=>H+HNCO	2.00E+07	2	2000
HCCO+NO<=>HCNO+CO	9.00E+12	0	0
CH3+N<=>H2CN+H	6.10E+14	-0.3	290
CH3+N<=>HCN+H2	3.70E+12	0.1	-90
NH3+H<=>NH2+H2	5.40E+05	2.4	9915
NH3+OH<=>NH2+H2O	5.00E+07	1.6	955
NH3+O<=>NH2+OH	9.40E+06	1.9	6460
NH+CO2<=>HNO+CO	1.00E+13	0	14350
CN+NO2<=>NCO+NO	6.16E+15	-0.8	345
NCO+NO2<=>N2O+CO2	3.25E+12	0	-705
N+CO2<=>NO+CO	3.00E+12	0	11300

O+CH3<=>H+H2+CO	3.37E+13	0	0
O+C2H4<=>H+CH2CHO	6.70E+06	1.8	220
O+C2H5<=>H+CH3CHO	1.10E+14	0	0
OH+HO2<=>O2+H2O	5.00E+15	0	17330
OH+CH3<=>H2+CH2O	8.00E+09	0.5	-1755
CH+H2(+M)<=>CH3(+M)	1.97E+12	0.4	-370
CH2+O2<=>2H+CO2	5.80E+12	0	1500
CH2+O2<=>O+CH2O	2.40E+12	0	1500
CH2+CH2<=>2H+C2H2	2.00E+14	0	10989
CH2(S)+H2O=>H2+CH2O	6.82E+10	0.2	-935
C2H3+O2<=>O+CH2CHO	3.03E+11	0.3	11
C2H3+O2<=>HO2+C2H2	1.34E+06	1.6	-384
O+CH3CHO<=>OH+CH2CHO	2.92E+12	0	1808
O+CH3CHO<=>OH+CH3+CO	2.92E+12	0	1808
O2+CH3CHO<=>HO2+CH3+CO	3.01E+13	0	39150
H+CH3CHO<=>CH2CHO+H2	2.05E+09	1.2	2405
H+CH3CHO<=>CH3+H2+CO	2.05E+09	1.2	2405
OH+CH3CHO<=>CH3+H2O+CO	2.34E+10	0.7	-1113
HO2+CH3CHO<=>CH3+H2O2+CO	3.01E+12	0	11923
CH3+CH3CHO<=>CH3+CH4+CO	2.72E+06	1.8	5920
H+CH2CO(+M)<=>CH2CHO(+M)	4.87E+11	0.4	-1755
O+CH2CHO<=>H+CH2+CO2	1.50E+14	0	0
O2+CH2CHO<=>OH+CO+CH2O	1.81E+10	0	0
O2+CH2CHO<=>OH+2HCO	2.35E+10	0	0
H+CH2CHO<=>CH3+HCO	2.20E+13	0	0
H+CH2CHO<=>CH2CO+H2	1.10E+13	0	0
OH+CH2CHO<=>H2O+CH2CO	1.20E+13	0	0
OH+CH2CHO<=>HCO+CH2OH	3.01E+13	0	0
CH3+C2H5(+M)<=>C3H8(+M)	9.43E+12	0	0
O+C3H8<=>OH+C3H7	1.93E+05	2.7	3716
H+C3H8<=>C3H7+H2	1.32E+06	2.5	6756
OH+C3H8<=>C3H7+H2O	3.16E+07	1.8	934
C3H7+H2O2<=>HO2+C3H8	3.78E+02	2.7	1500
CH3+C3H8<=>C3H7+CH4	9.03E-01	3.6	7154
CH3+C2H4(+M)<=>C3H7(+M)	2.55E+06	1.6	5700
O+C3H7<=>C2H5+CH2O	9.64E+13	0	0
H+C3H7(+M)<=>C3H8(+M)	3.61E+13	0	0
H+C3H7<=>CH3+C2H5	4.06E+06	2.2	890
OH+C3H7<=>C2H5+CH2OH	2.41E+13	0	0
HO2+C3H7<=>O2+C3H8	2.55E+10	0.3	-943
HO2+C3H7<=>OH+C2H5+CH2O	2.41E+13	0	0
CH3+C3H7<=>2C2H5	1.93E+13	-0.3	0

Table 5.5 – CH_4/Air Combustion Mechanism Scheme GRI-Mech3.0 (Units: mole, cm, s, K, cal).

5.vii Figures

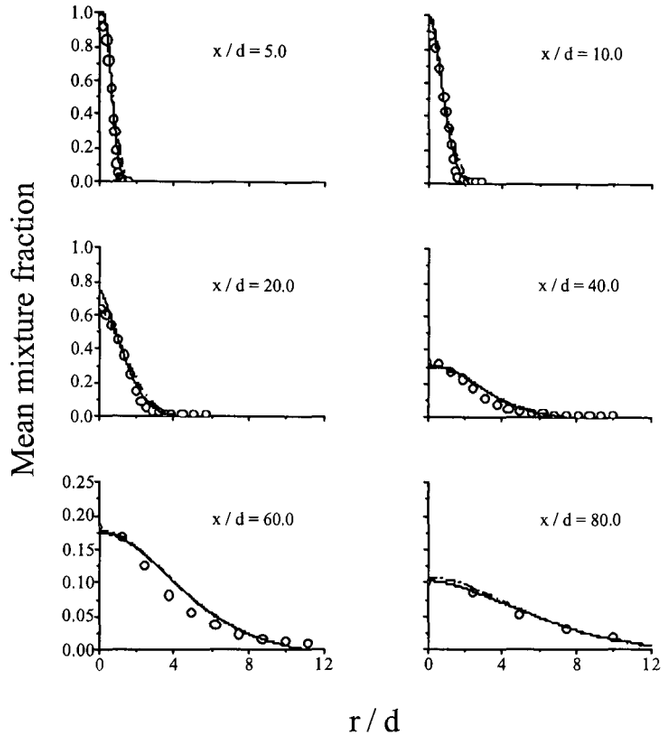

Figure 5.1 – Comparison of measured and predicted radial mean mixture-fraction profiles at six axial stations for methane flame A (o measured, — predicted Re stress, - - predicted k-ε).

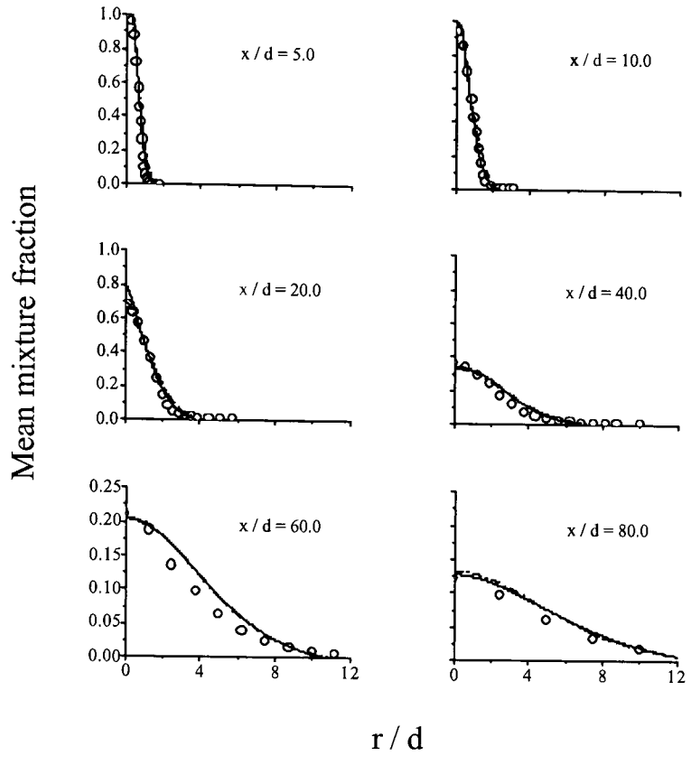

Figure 5.2 – Comparison of measured and predicted radial mean mixture-fraction profiles at six axial stations for methane flame B (o measured, — predicted Re stress, - - predicted k-ε).

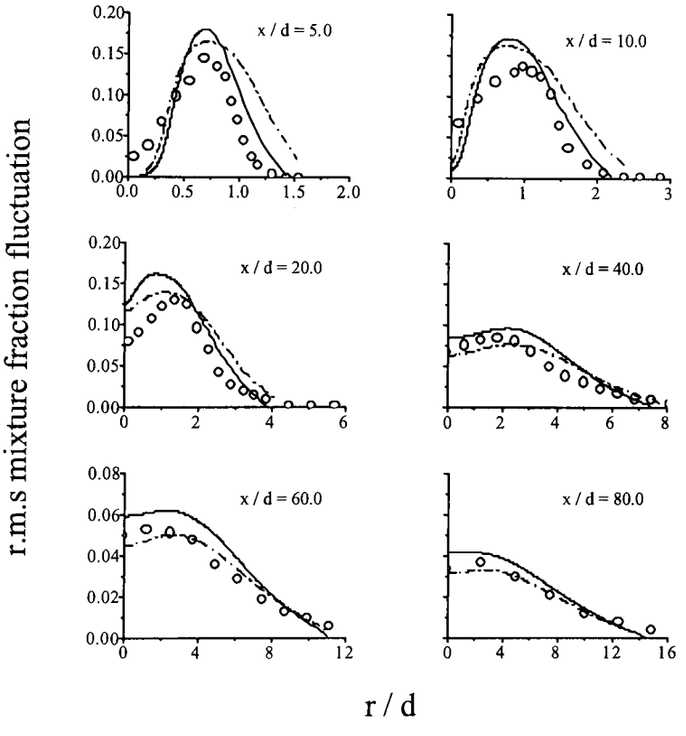

Figure 5.3 – Comparison of measured and predicted radial root-mean-squared mixture-fraction fluctuation profiles at six axial stations for methane flame A (o measured, — predicted Re stress, - - predicted k-ε).

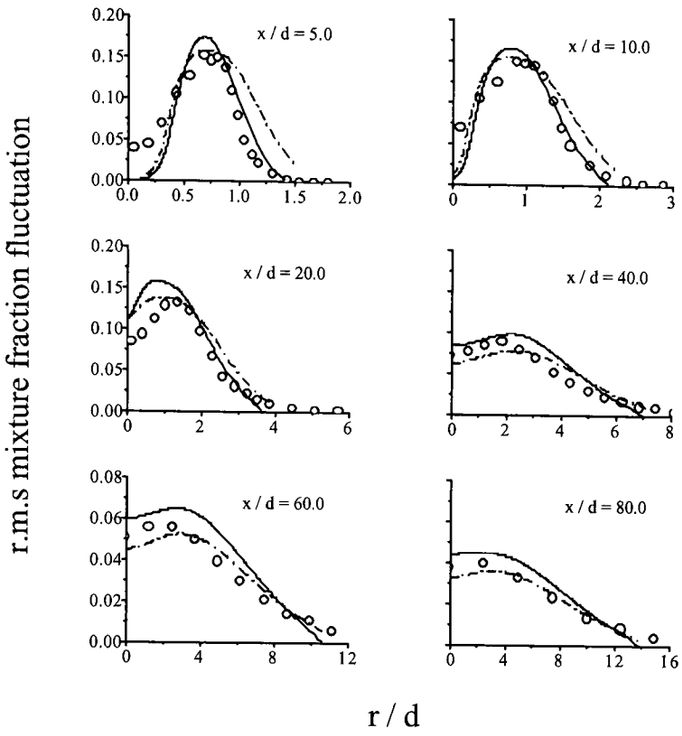

Figure 5.4 – Comparison of measured and predicted radial root-mean-squared mixture-fraction fluctuation profiles at six axial stations for methane flame B (o measured, — predicted Re stress, - - predicted k-ε).

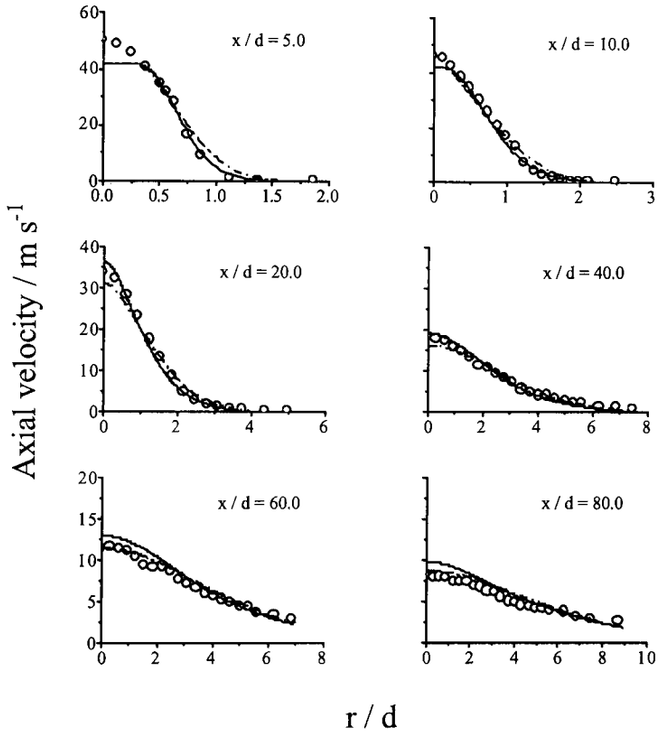

Figure 5.5 – Comparison of measured and predicted radial axial-velocity profiles at six axial stations for methane flame A (o measured, — predicted Re stress, - - predicted k-ε).

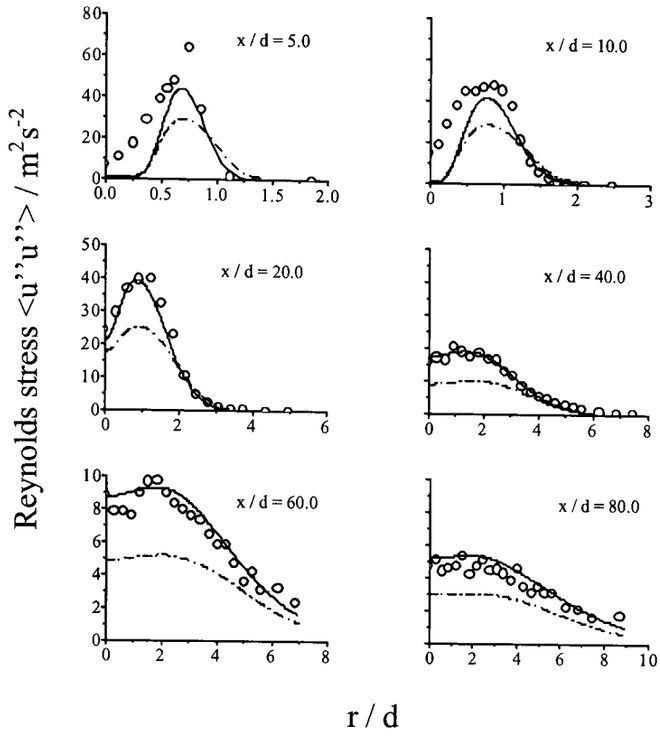

Figure 5.6 – Comparison of measured and predicted radial Reynolds-stress profiles at six axial stations for methane flame A (o measured, — predicted Re stress, - - predicted k-ε).

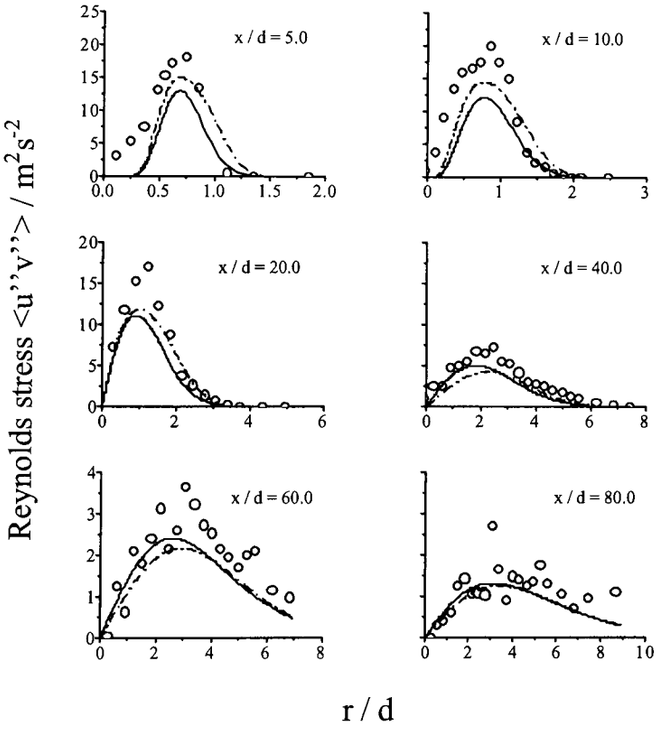

Figure 5.7 – Comparison of measured and predicted radial Reynolds-stress profiles at six axial stations for methane flame A (o measured, — predicted Re stress, - - predicted k-ε).

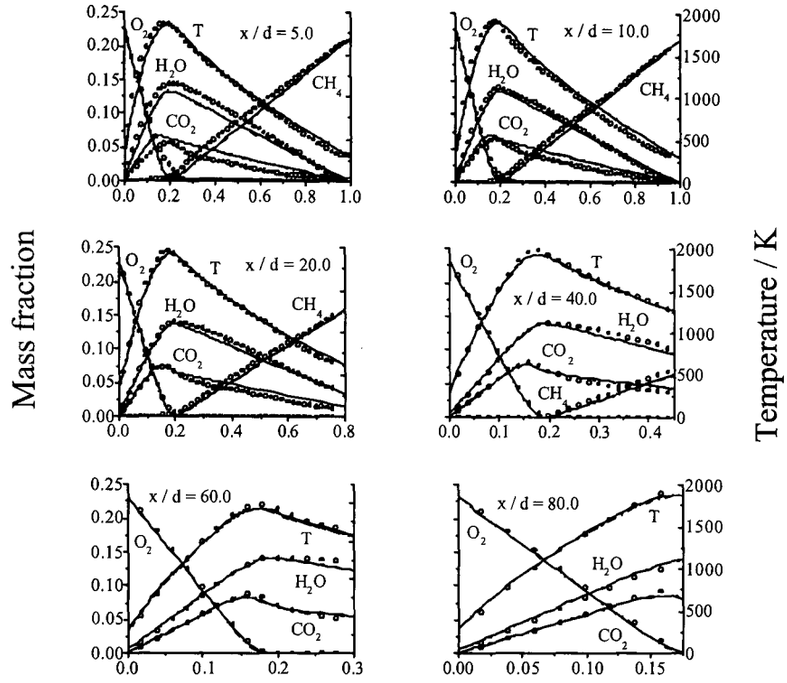

Figure 5.8 – Comparison of measured and predicted conditional species mass-fractions and temperature at six axial stations for methane flame A, derived using GRI-Mech2.11
(o measured, — predicted Re stress, -- predicted k-ε).

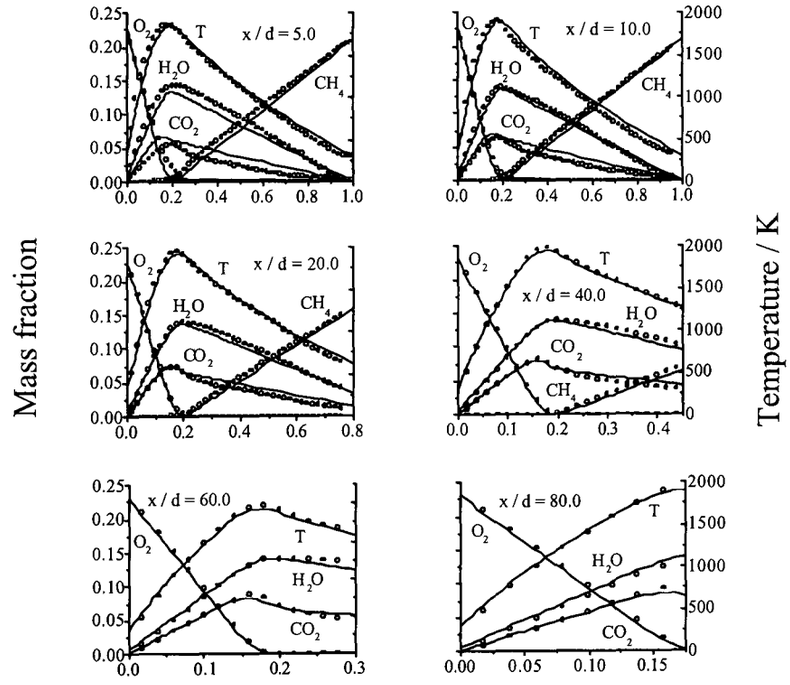

Figure 5.9 – Comparison of measured and predicted conditional species mass-fractions and temperature at six axial stations for methane flame A, derived using GRI-Mech3.00
(o measured, — predicted Re stress).

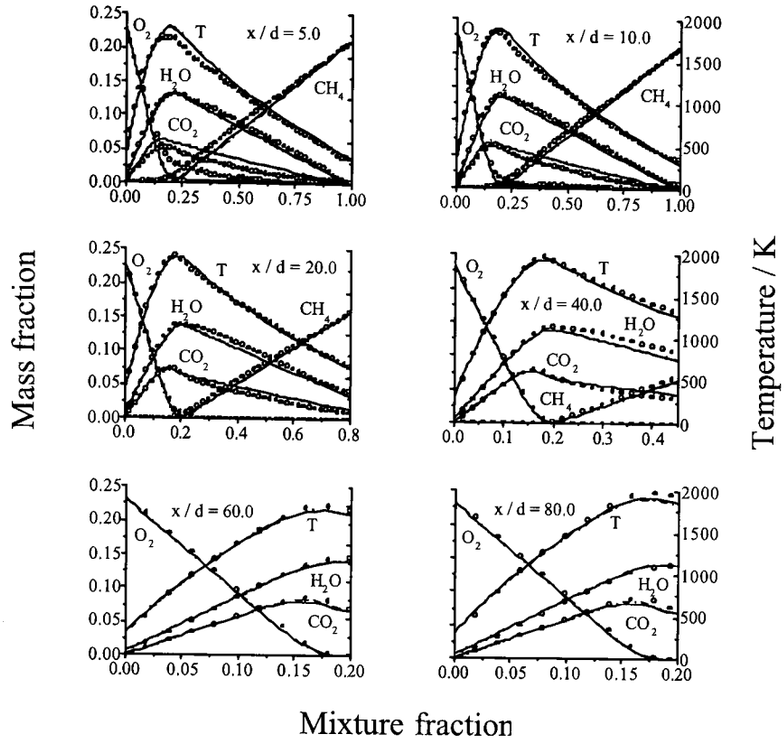

Figure 5.10 – Comparison of measured and predicted conditional species mass-fractions and temperature at six axial stations for methane flame B, derived using GRI-Mech2.11
(o measured, —predicted Re stress, - - predicted k-ε).

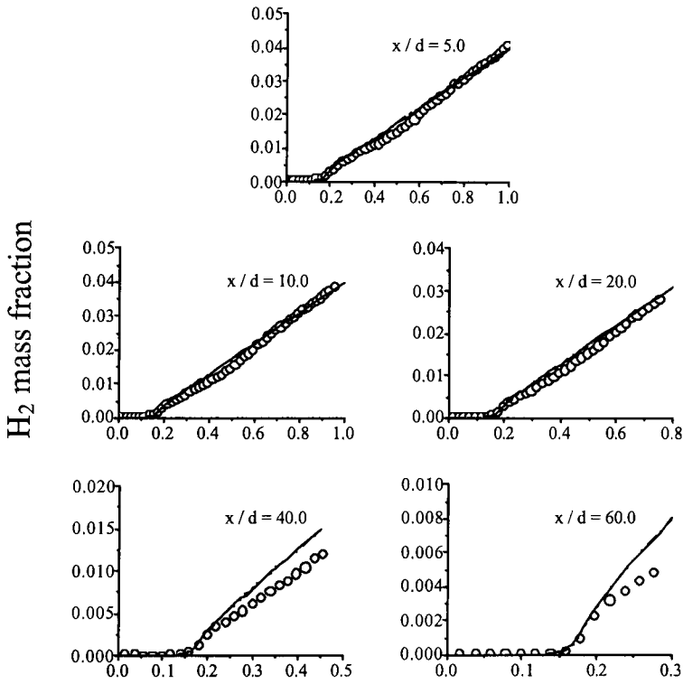

Figure 5.11 – Comparison of measured and predicted conditional H_2 mass-fractions at six axial stations for methane flame A, derived using GRI-Mech2.11
(o measured, —predicted Re stress, - - predicted k-ε).

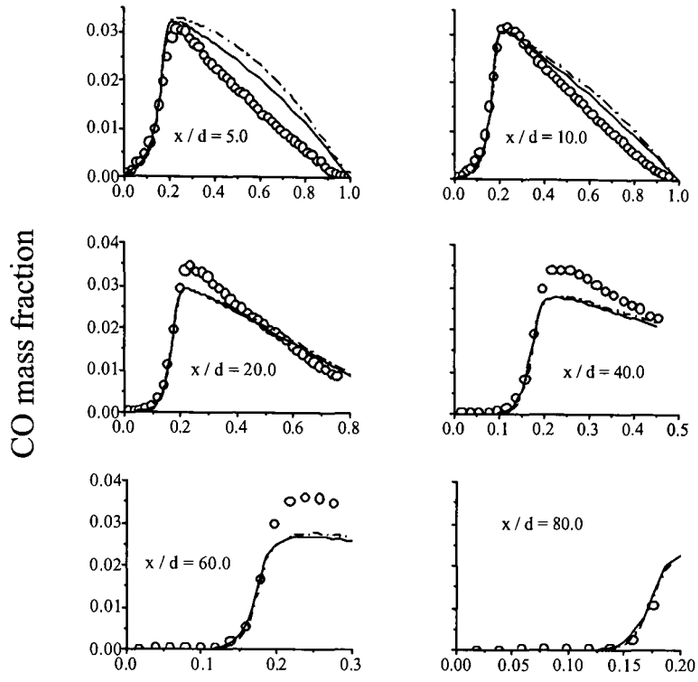

Figure 5.12 – Comparison of measured and predicted conditional CO mass-fractions at six axial stations for methane flame A, derived using GRI-Mech2.11 (o measured, — predicted Re stress, - - predicted k-ε).

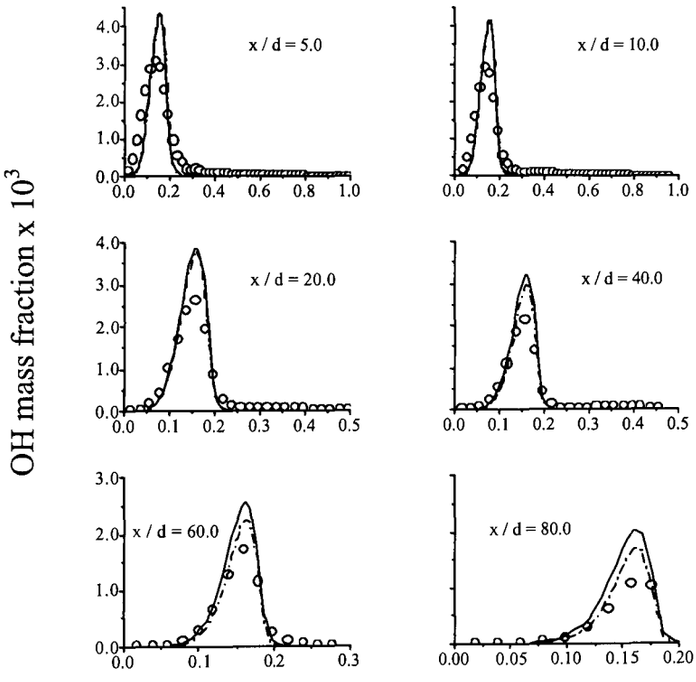

Figure 5.13 – Comparison of measured and predicted conditional OH mass-fractions at six axial stations for methane flame A, derived using GRI-Mech2.11 (o measured, — predicted Re stress, - - predicted k-ε).

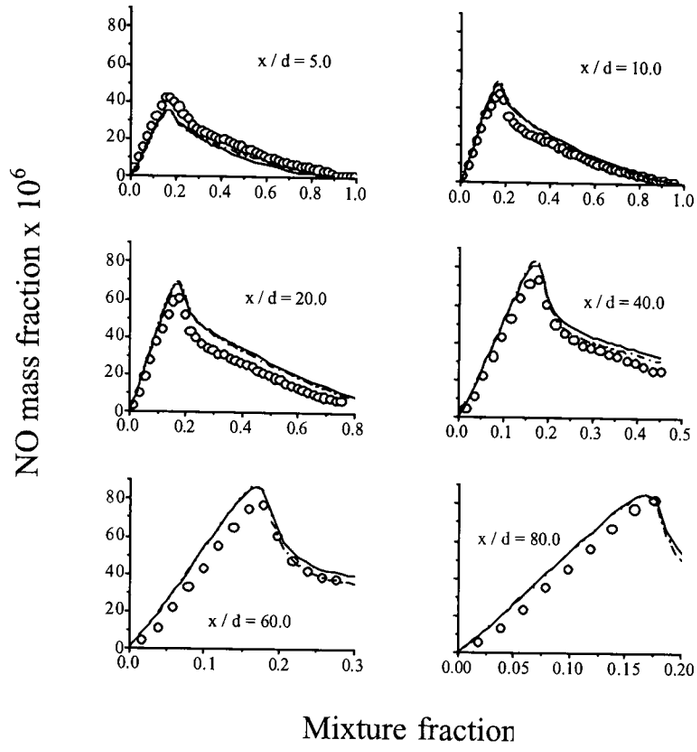

Figure 5.14 – Comparison of measured and predicted conditional NO mass-fractions at six axial stations for methane flame A, derived using GRI-Mech2.11 (o measured, — predicted Re stress, - - predicted k-ε).

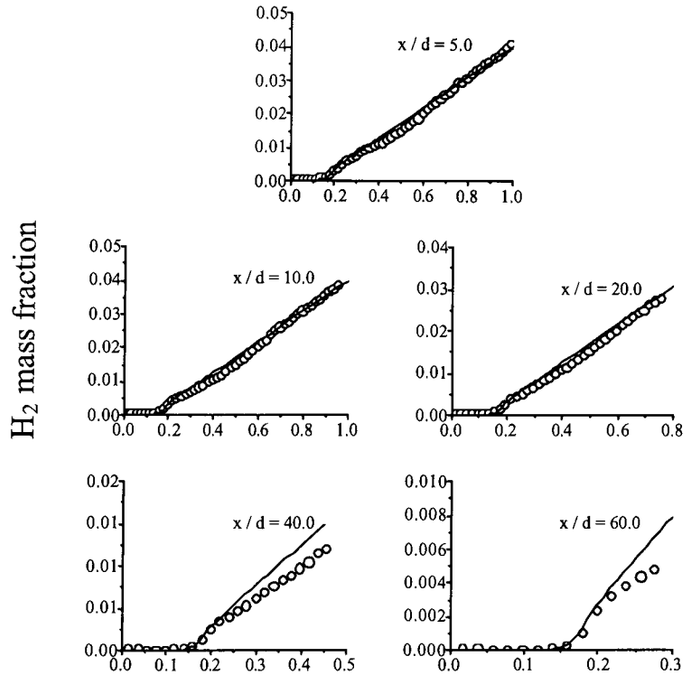

Figure 5.15 – Comparison of measured and predicted conditional H_2 mass-fractions at six axial stations for methane flame A, derived using GRI-Mech3.00 (o measured, — predicted Re stress).

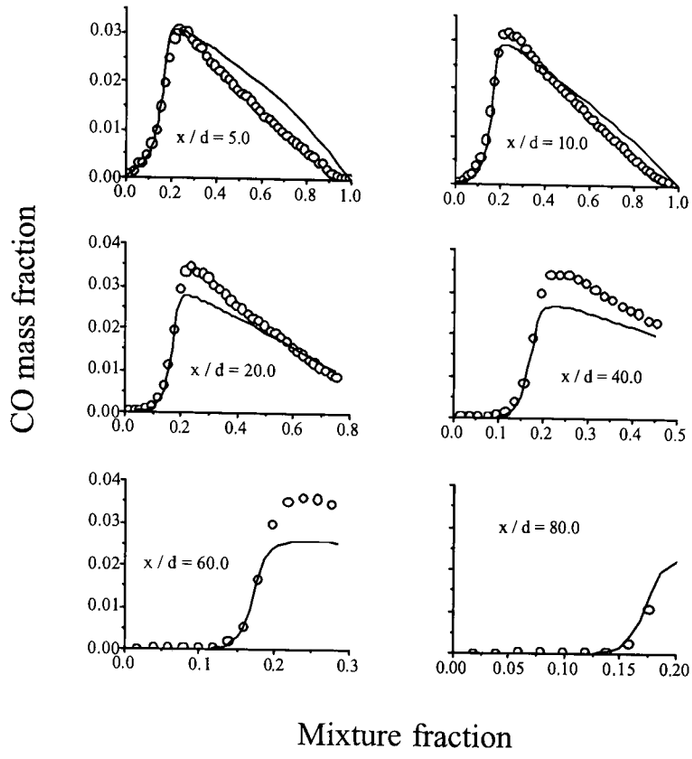

Figure 5.16 – Comparison of measured and predicted conditional CO mass-fractions at six axial stations for methane flame A, derived using GRI-Mech3.00 (o measured, — predicted Re stress).

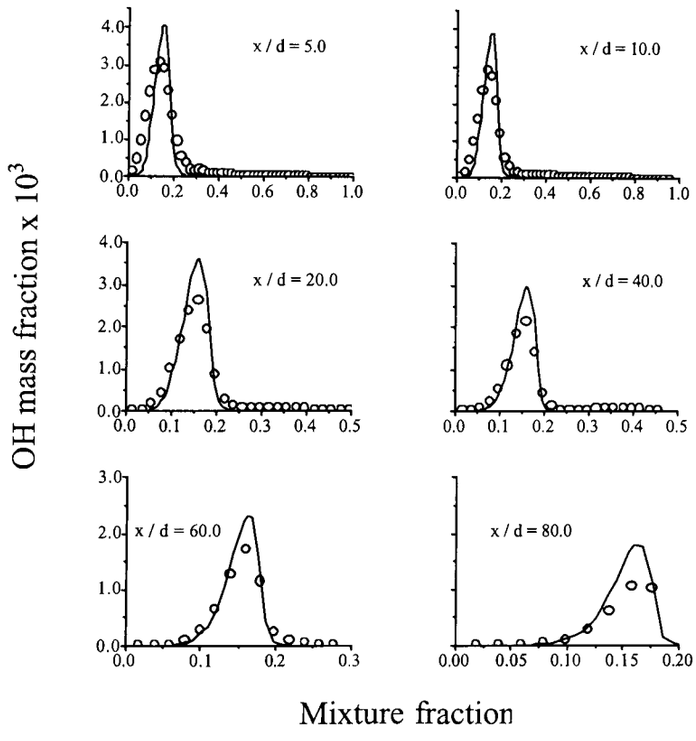

Figure 5.17 – Comparison of measured and predicted conditional OH mass-fractions at six axial stations for methane flame A, derived using GRI-Mech3.00 (o measured, — predicted Re stress).

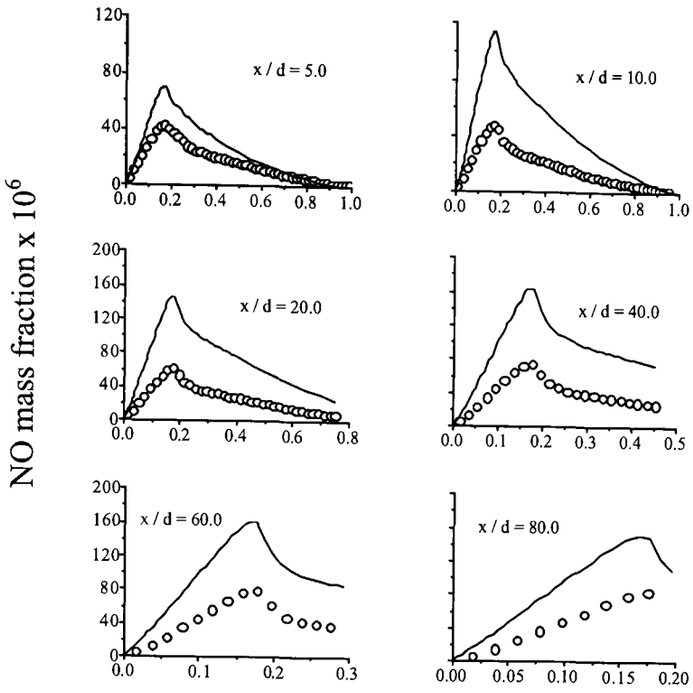

Figure 5.18 – Comparison of measured and predicted conditional NO mass-fractions at six axial stations for methane flame A, derived using GRI-Mech3.00 (o measured, —predicted Re stress).

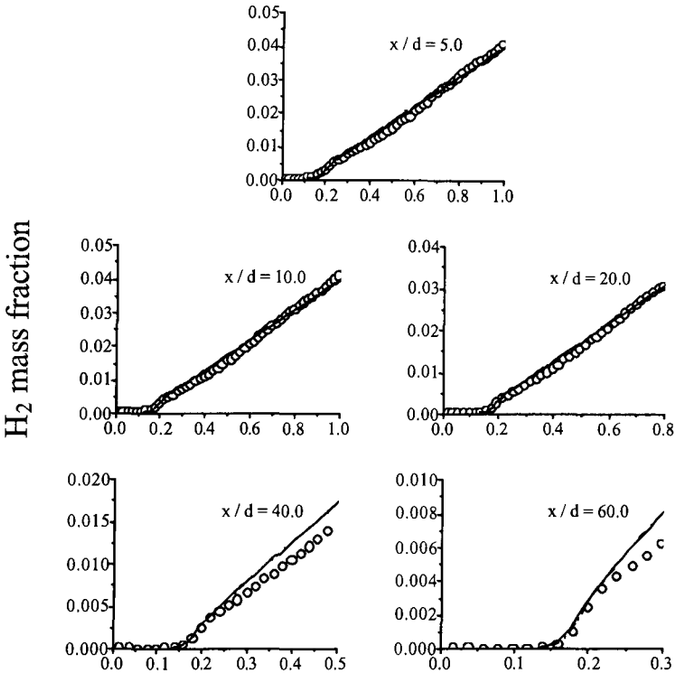

Figure 5.19 – Comparison of measured and predicted conditional H_2 mass-fractions at six axial stations for methane flame B, derived using GRI-Mech2.11 (o measured, —predicted Re stress, - - predicted k-ε).

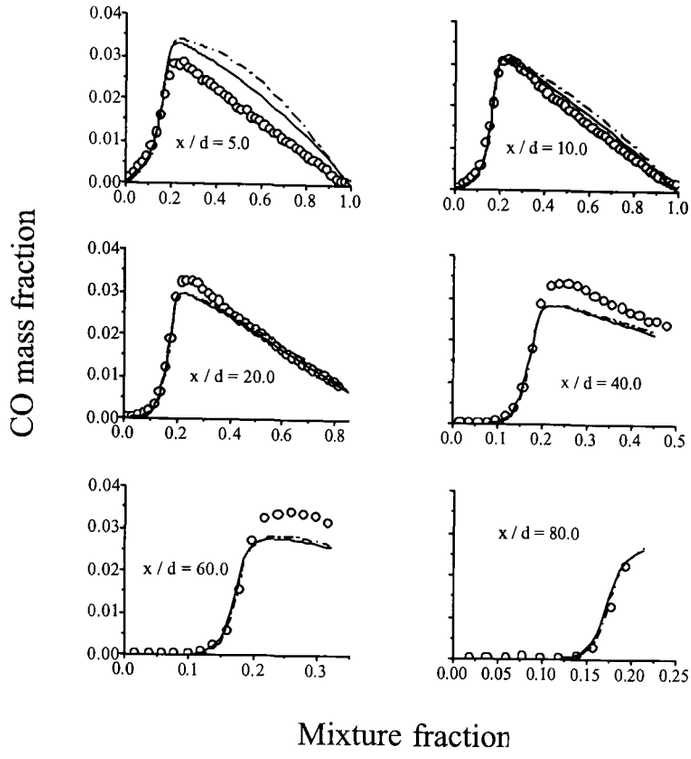

Figure 5.20 – Comparison of measured and predicted conditional CO mass-fractions at six axial stations for methane flame B, derived using GRI-Mech2.11 (o measured, —predicted Re stress, - - predicted k-ε).

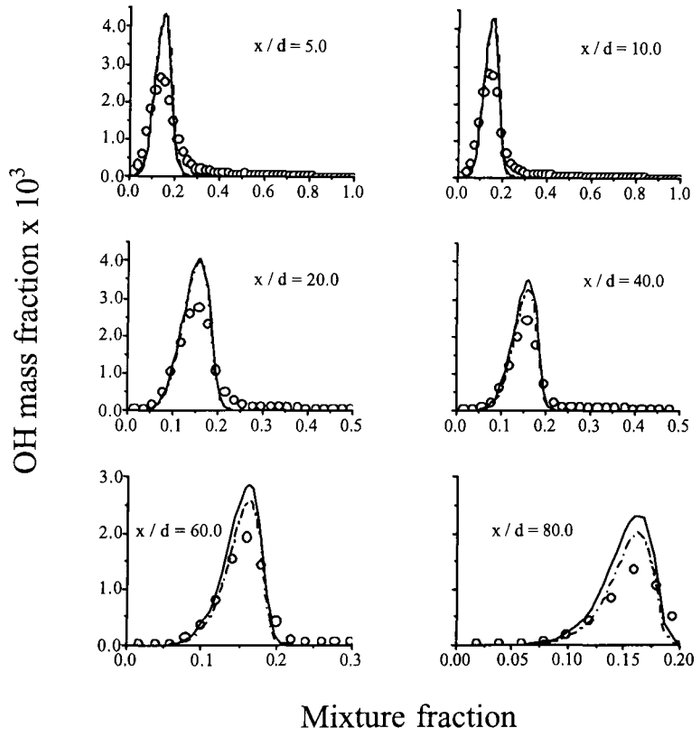

Figure 5.21 – Comparison of measured and predicted conditional OH mass-fractions at six axial stations for methane flame B, derived using GRI-Mech2.11 (o measured, —predicted Re stress, - - predicted k-ε).

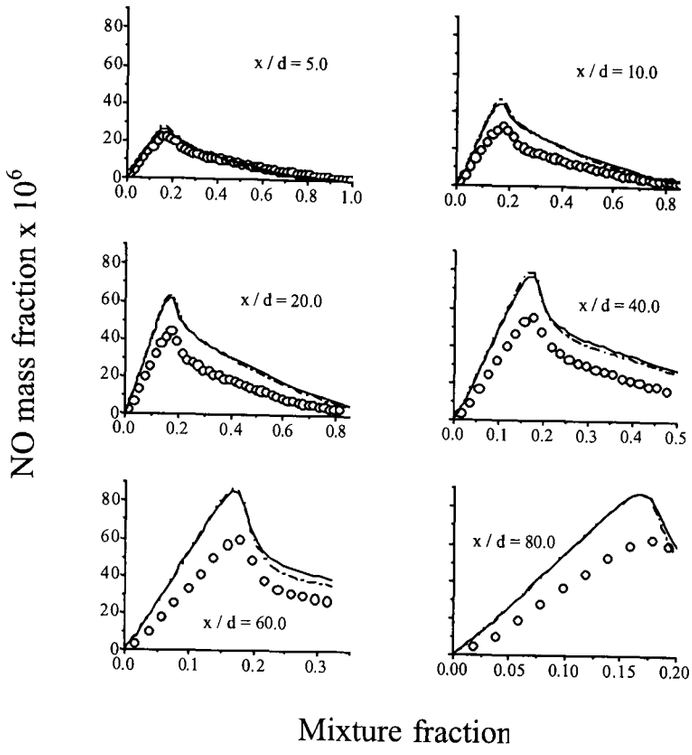

Figure 5.22 – Comparison of measured and predicted conditional NO mass-fractions at six axial stations for methane flame B, derived using GRI-Mech2.11 (o measured, —predicted Re stress, - - predicted k-ε).

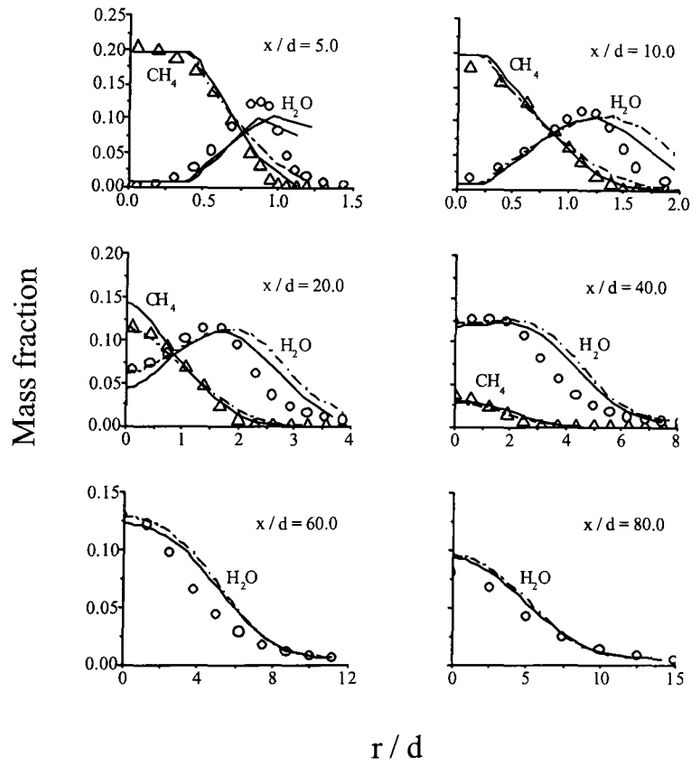

Figure 5.23 – Comparison of measured and predicted radial mean species mass-fractions at six axial stations for methane flame A, derived using GRI-Mech2.11 (o measured, —predicted Re stress, - - predicted k-ε). Density coupled.

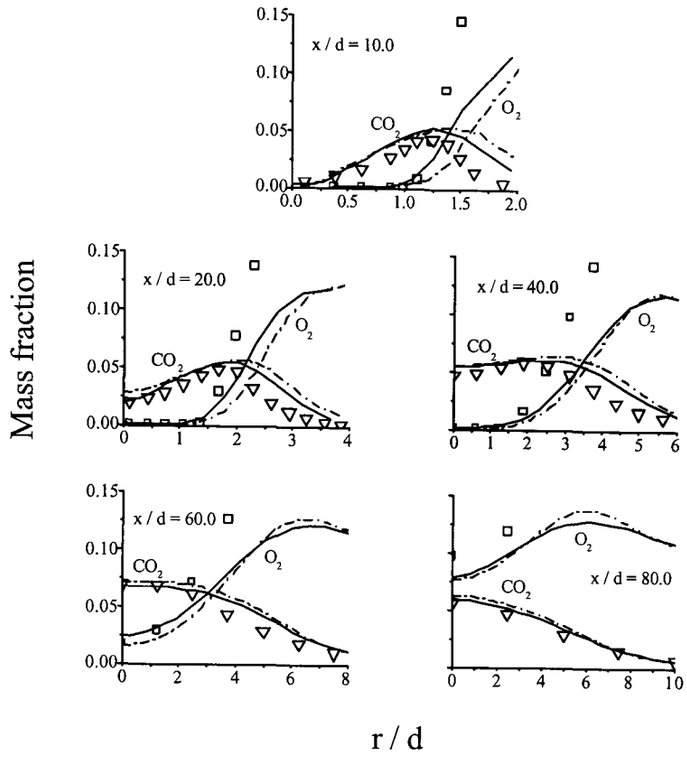

Figure 5.24 – Comparison of measured and predicted radial mean species mass-fractions at five axial stations for methane flame A, derived using GRI-Mech2.11 (o measured, —predicted Re stress, - - predicted k-ε). Density coupled.

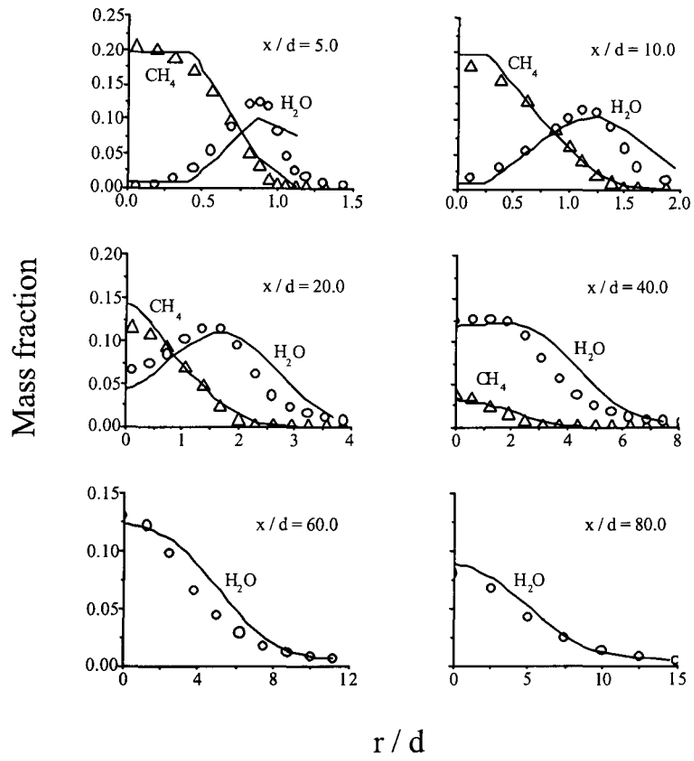

Figure 5.25 – Comparison of measured and predicted radial mean species mass-fractions at six axial stations for methane flame A, derived using GRI-Mech3.00 (o measured, —predicted Re stress). Density coupled.

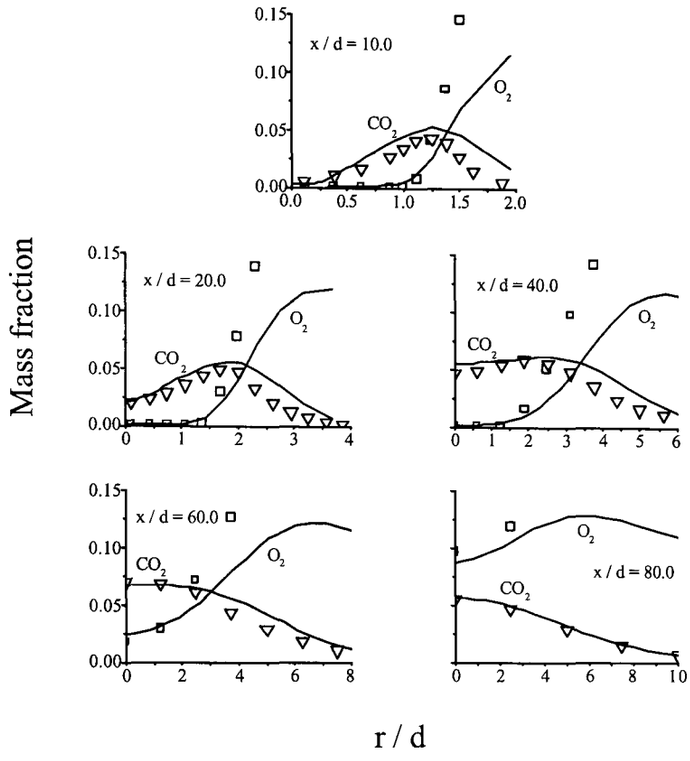

Figure 5.26 – Comparison of measured and predicted radial mean species mass-fractions at five axial stations for methane flame A, derived using GRI-Mech3.00 (o measured, — predicted Re stress). Density coupled.

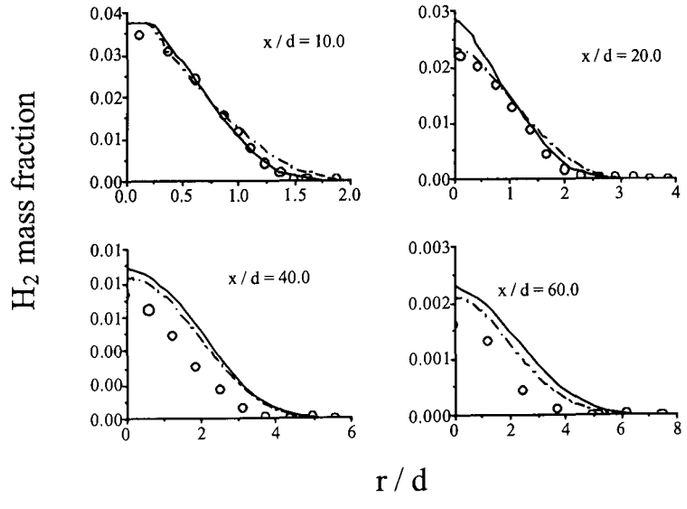

Figure 5.27 – Comparison of measured and predicted radial mean H_2 mass-fractions at four axial stations for methane flame A, derived using GRI-Mech2.11 (o measured, — predicted Re stress, - - predicted k-ε). Density coupled.

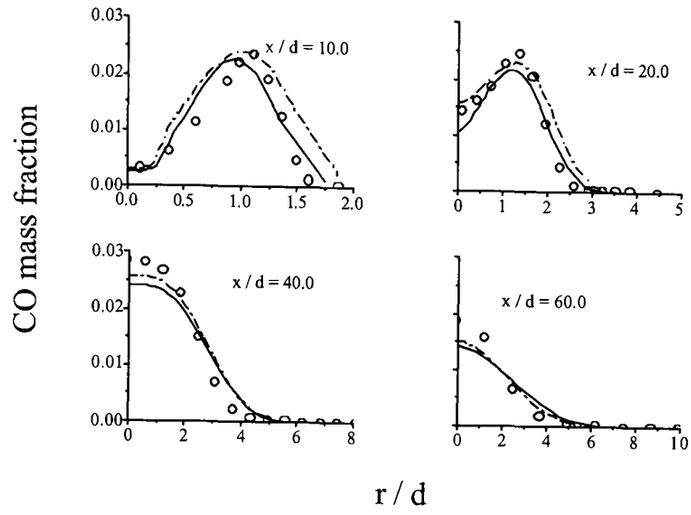

Figure 5.28 – Comparison of measured and predicted radial mean CO mass-fractions at four axial stations for methane flame A, derived using GRI-Mech2.11 (o measured, —predicted Re stress, - - predicted k-ε). Density coupled.

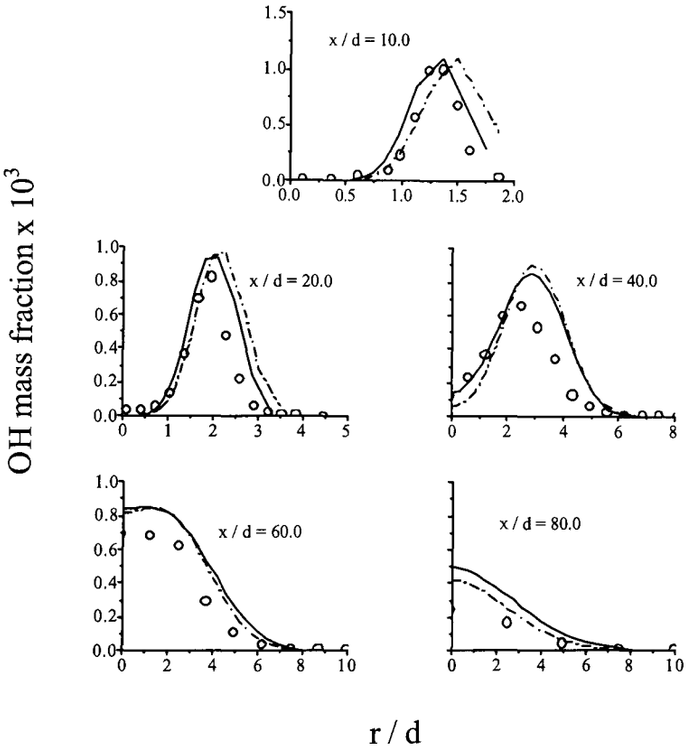

Figure 5.29 – Comparison of measured and predicted radial mean OH mass-fractions at five axial stations for methane flame A, derived using GRI-Mech2.11 (o measured, —predicted Re stress, - - predicted k-ε). Density coupled.

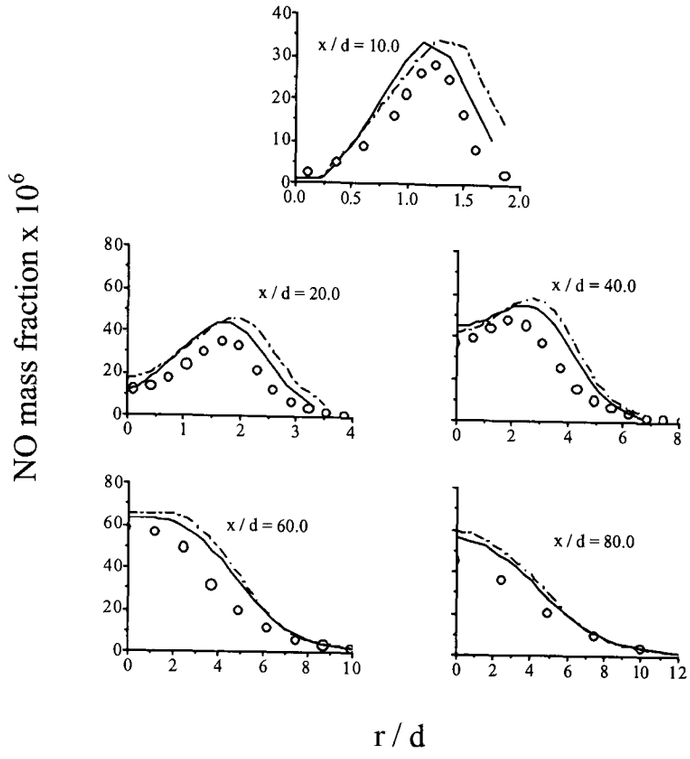

Figure 5.30 – Comparison of measured and predicted radial mean NO mass-fractions at five axial stations for methane flame A, derived using GRI-Mech2.11 (o measured, —predicted Re stress, - - predicted k-ε). Density coupled.

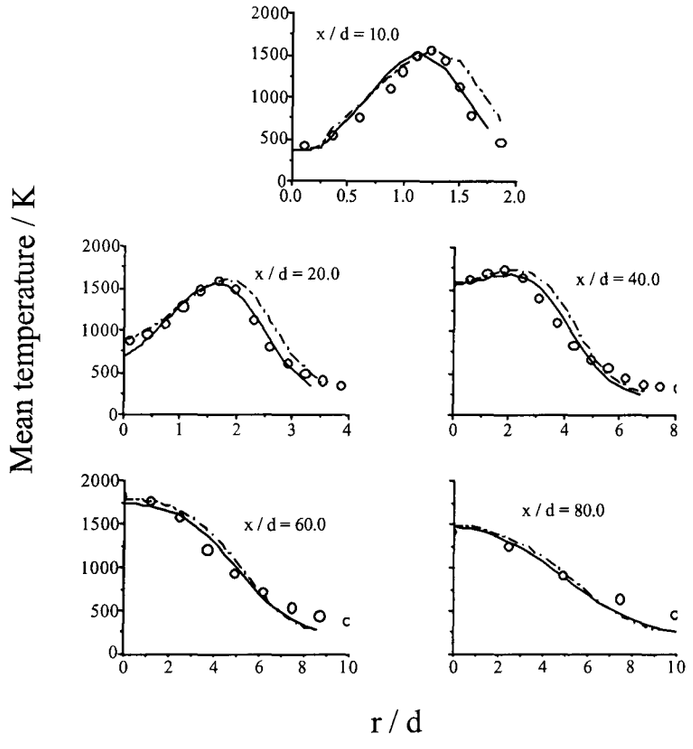

Figure 5.31 – Comparison of measured and predicted radial mean temperature at five axial stations for methane flame A, derived using GRI-Mech2.11 (o measured, —predicted Re stress, - - predicted k-ε). Density coupled.

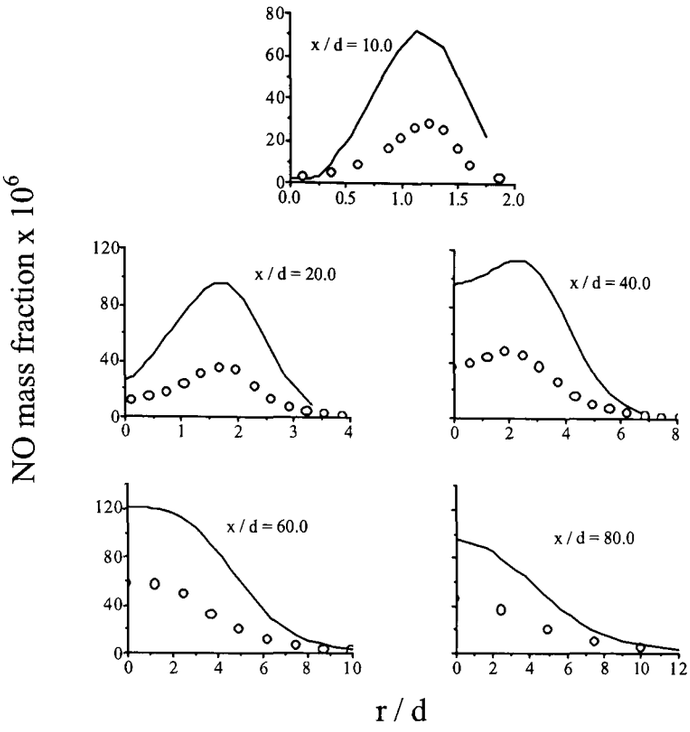

Figure 5.32 – Comparison of measured and predicted radial mean NO mass-fractions at five axial stations for methane flame A, derived using GRI-Mech3.00 (o measured, —predicted Re stress). Density coupled.

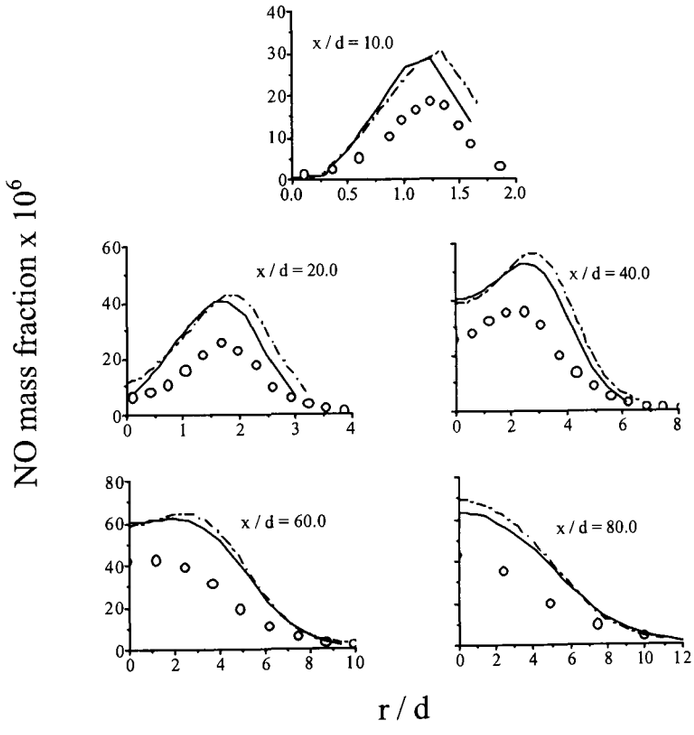

Figure 5.33 – Comparison of measured and predicted radial mean NO mass-fractions at five axial stations for methane flame B, derived using GRI-Mech2.11 (o measured, —predicted Re stress, - - predicted k-ε). Density coupled.

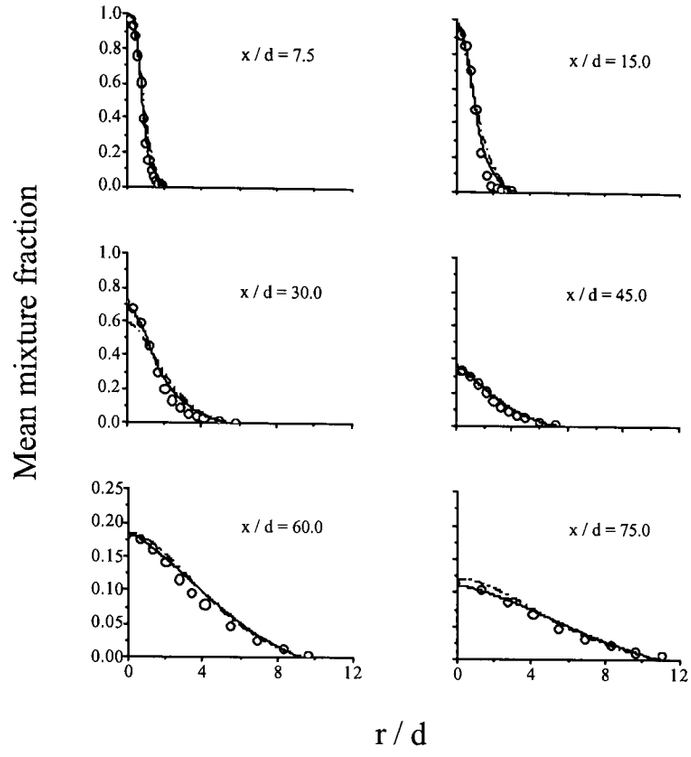

Figure 5.34 – Comparison of measured and predicted radial mean mixture-fraction profiles at six axial stations for methane flame C (o measured, —predicted Re stress, - - predicted k-ε).

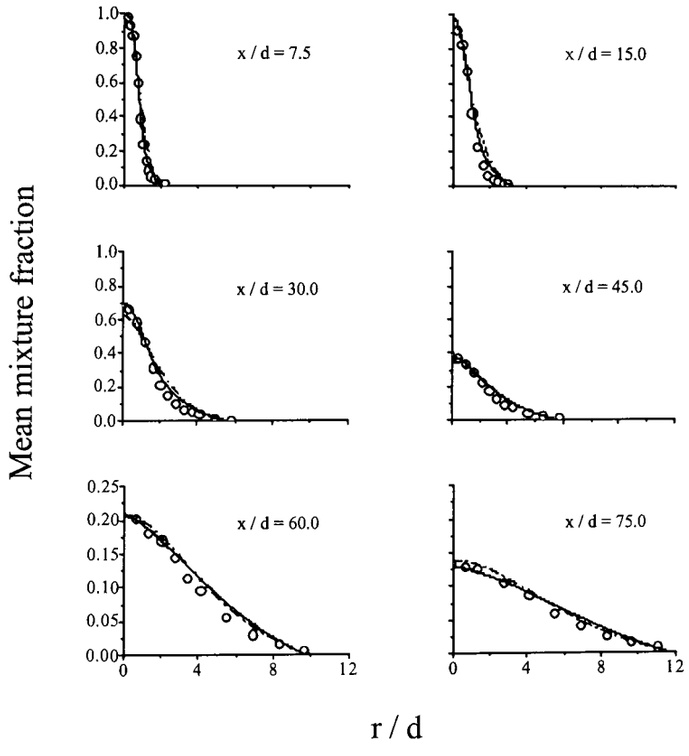

Figure 5.35 – Comparison of measured and predicted radial mean mixture-fraction profiles at six axial stations for methane flame D (o measured, —predicted Re stress, - - predicted k-ε).

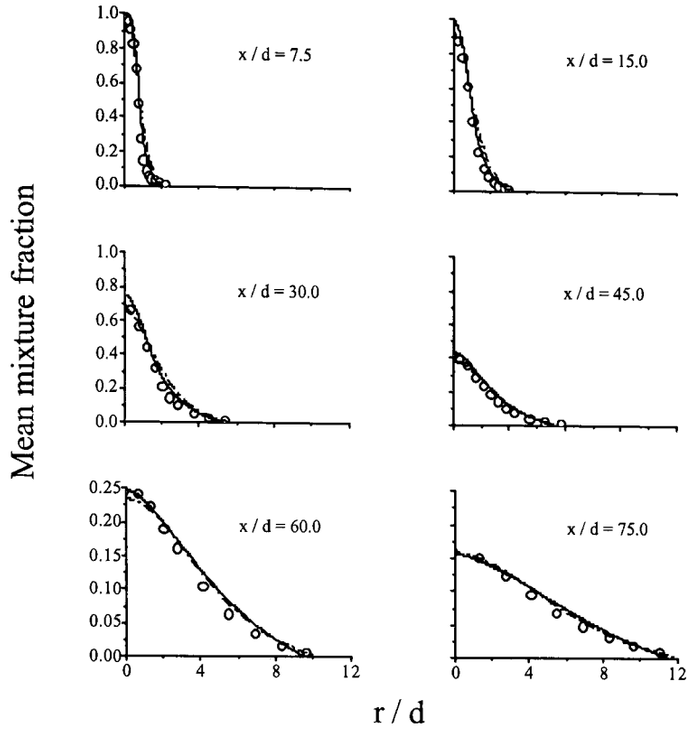

Figure 5.36 – Comparison of measured and predicted radial mean mixture-fraction profiles at six axial stations for methane flame E (o measured, — predicted Re stress, - - predicted k-ε).

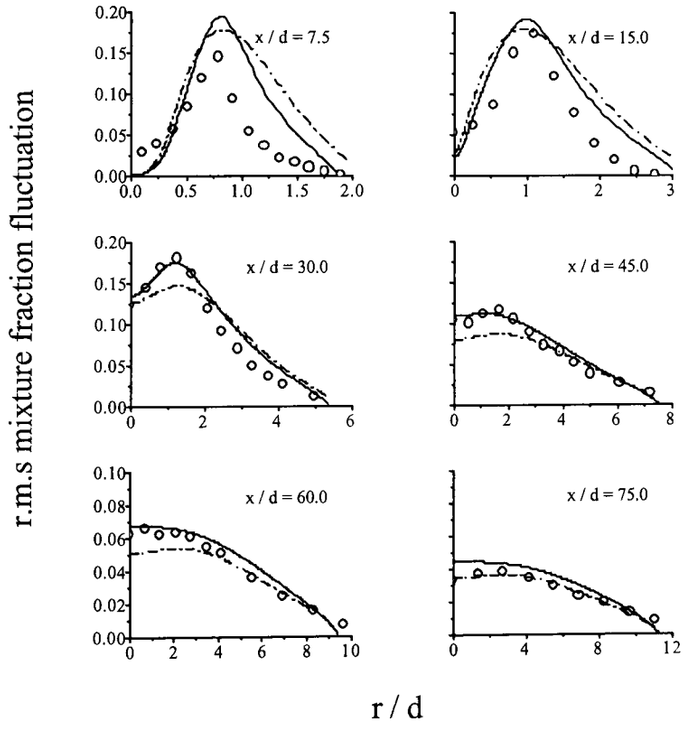

Figure 5.37 – Comparison of measured and predicted radial root-mean-squared mixture-fraction fluctuation profiles at six axial stations for methane flame C (o measured, — predicted Re stress, - - predicted k-ε).

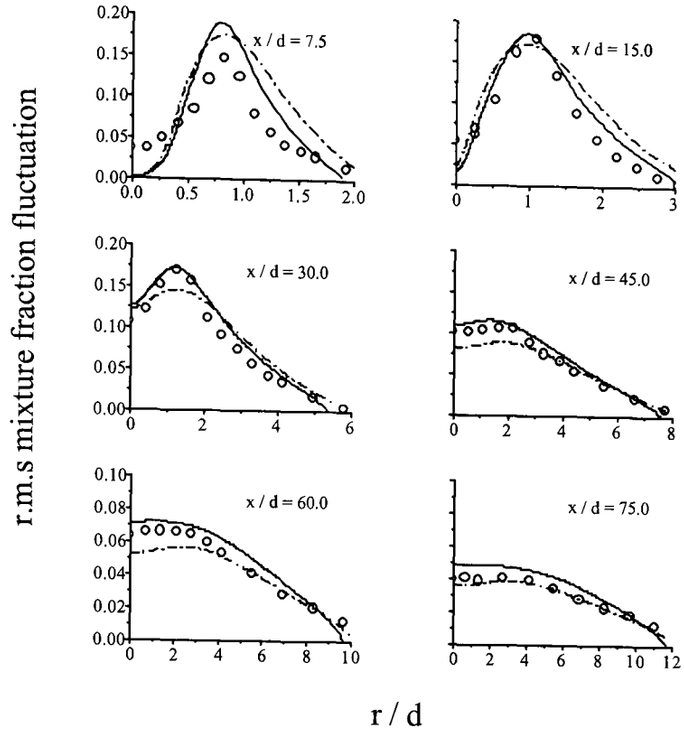

Figure 5.38 – Comparison of measured and predicted radial root-mean-squared mixture-fraction fluctuation profiles at six axial stations for methane flame D (o measured, — predicted Re stress, - - predicted k-ε).

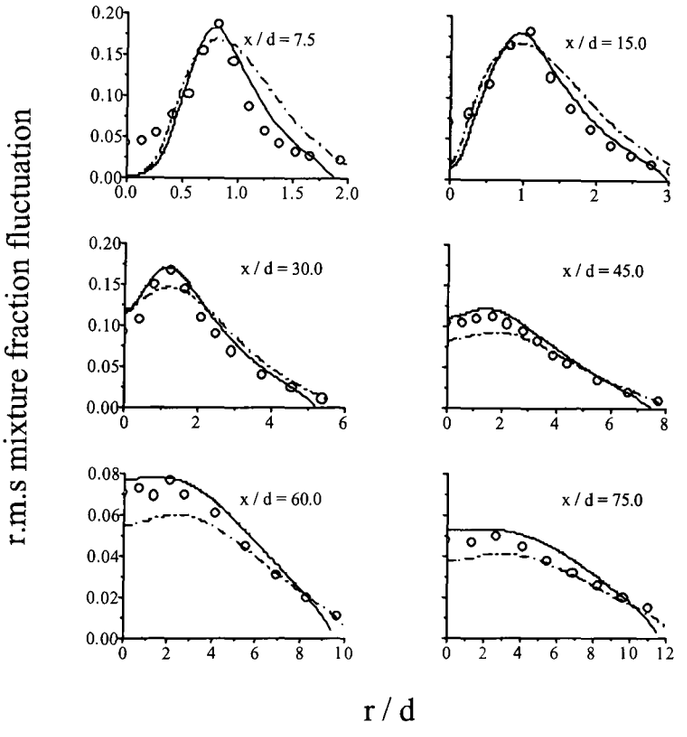

Figure 5.39 – Comparison of measured and predicted radial root-mean-squared mixture-fraction fluctuation profiles at six axial stations for methane flame E (o measured, — predicted Re stress, - - predicted k-ε).

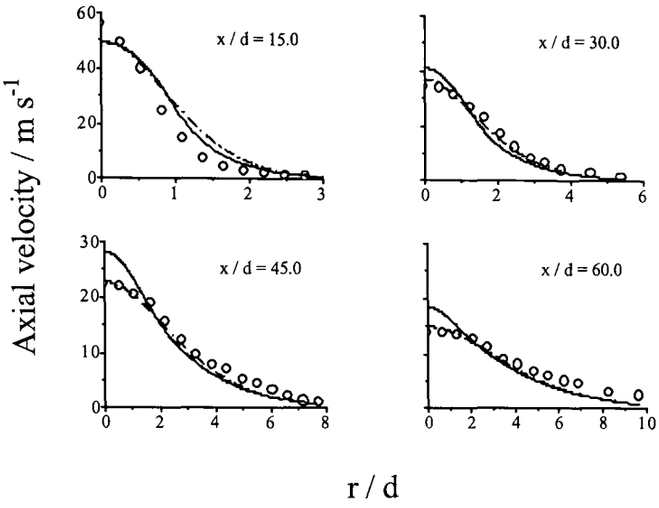

Figure 5.40 – Comparison of measured and predicted radial axial-velocity profiles at four axial stations for methane flame D (o measured, — predicted Re stress, - - predicted k-ε).

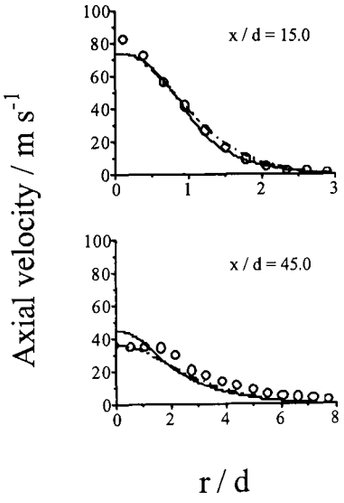

Figure 5.41 – Comparison of measured and predicted radial axial-velocity profiles at two axial stations for methane flame E (o measured, — predicted Re stress, - - predicted k-ε).

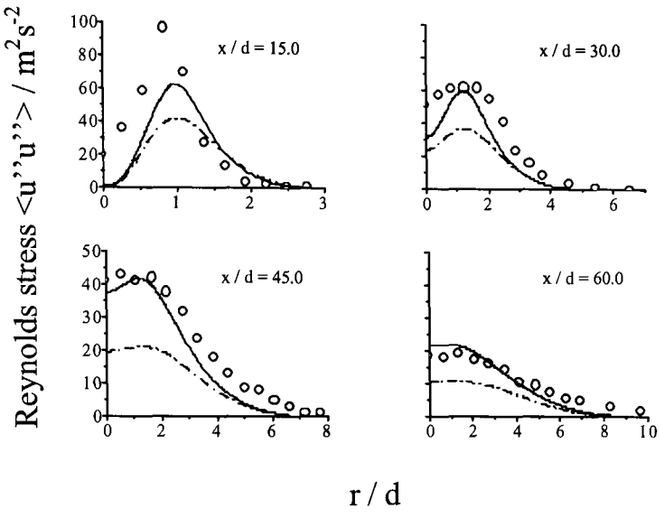

Figure 5.42 – Comparison of measured and predicted radial Reynolds-stress profiles at four axial stations for methane flame D (o measured, — predicted Re stress, -- predicted k-ε).

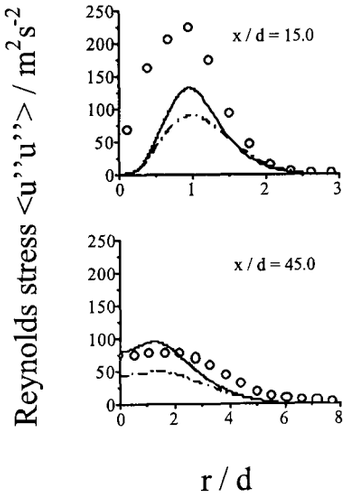

Figure 5.43 – Comparison of measured and predicted radial Reynolds-stress profiles at two axial stations for methane flame E (o measured, — predicted Re stress, -- predicted k-ε).

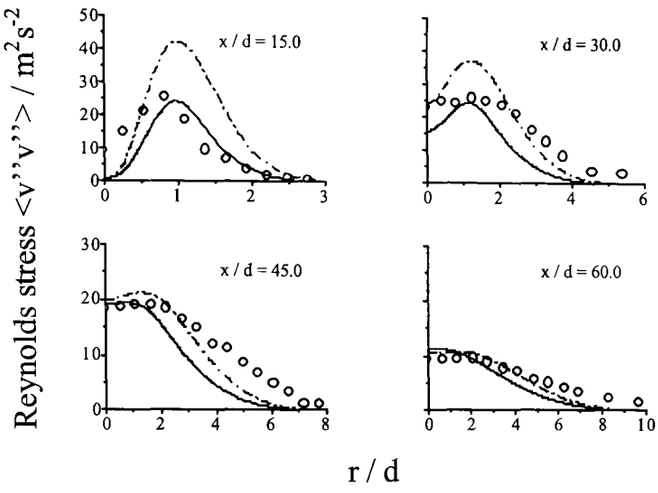

Figure 5.44 – Comparison of measured and predicted radial Reynolds-stress profiles at four axial stations for methane flame D (o measured, — predicted Re stress, - - predicted k-ε).

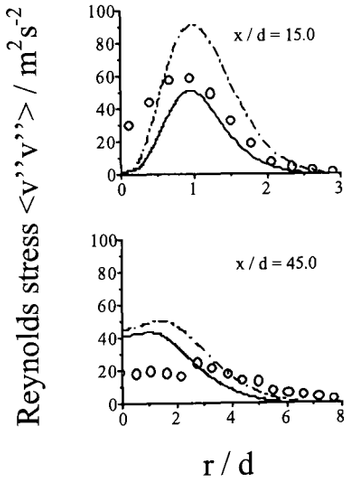

Figure 5.45 – Comparison of measured and predicted radial Reynolds-stress profiles at two axial stations for methane flame E (o measured, — predicted Re stress, - - predicted k-ε).

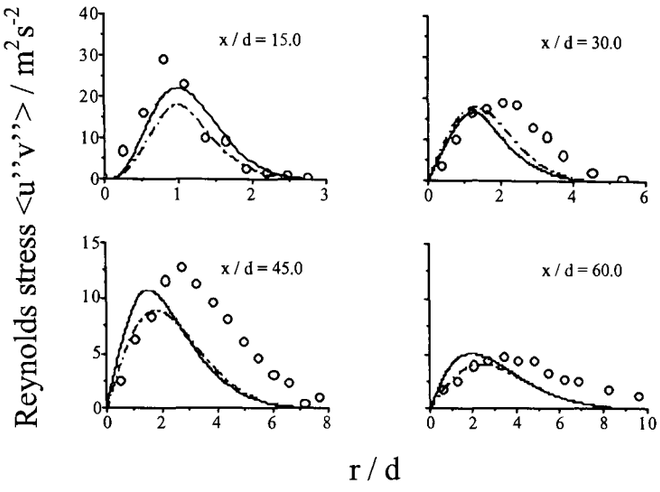

Figure 5.46 – Comparison of measured and predicted radial Reynolds-stress profiles at four axial stations for methane flame D (o measured, —predicted Re stress, - - predicted k-ε).

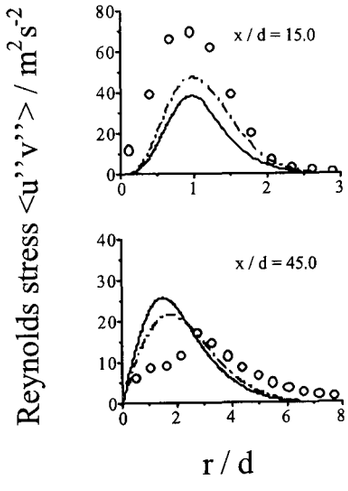

Figure 5.47 – Comparison of measured and predicted radial Reynolds-stress profiles at two axial stations for methane flame E (o measured, —predicted Re stress, - - predicted k-ε).

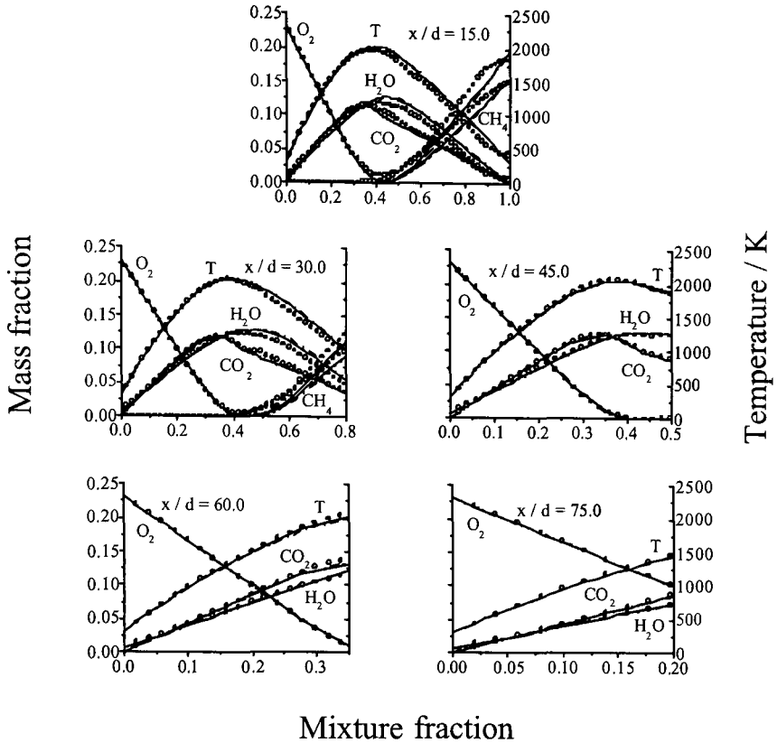

Figure 5.48 – Comparison of measured and predicted conditional species mass-fractions and temperature at five axial stations for methane flame C, derived using GRI-Mech2.11
(o measured, —predicted Re stress, - - predicted k-ε).

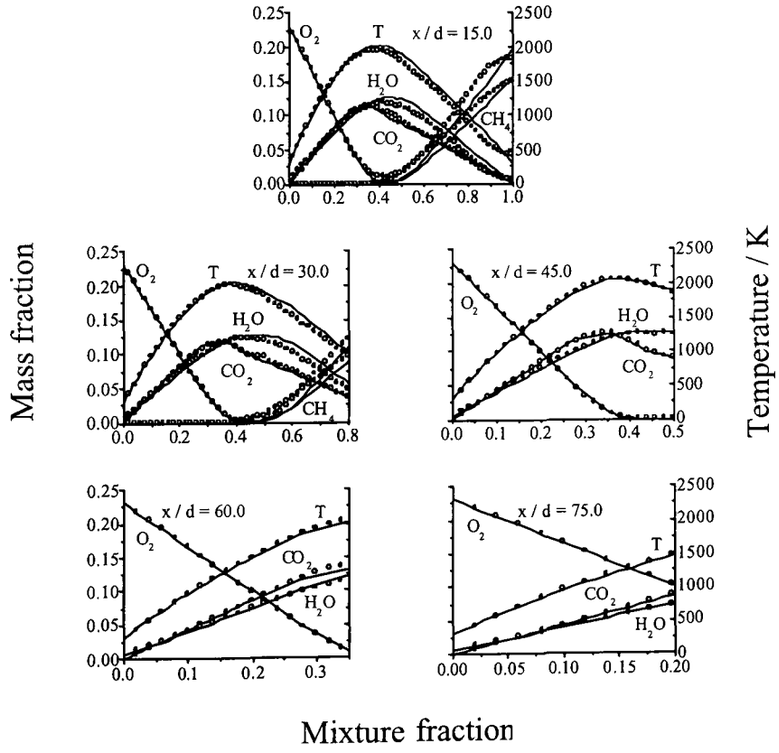

Figure 5.49 – Comparison of measured and predicted conditional species mass-fractions and temperature at five axial stations for methane flame C, derived using GRI-Mech3.00
(o measured, —predicted Re stress).

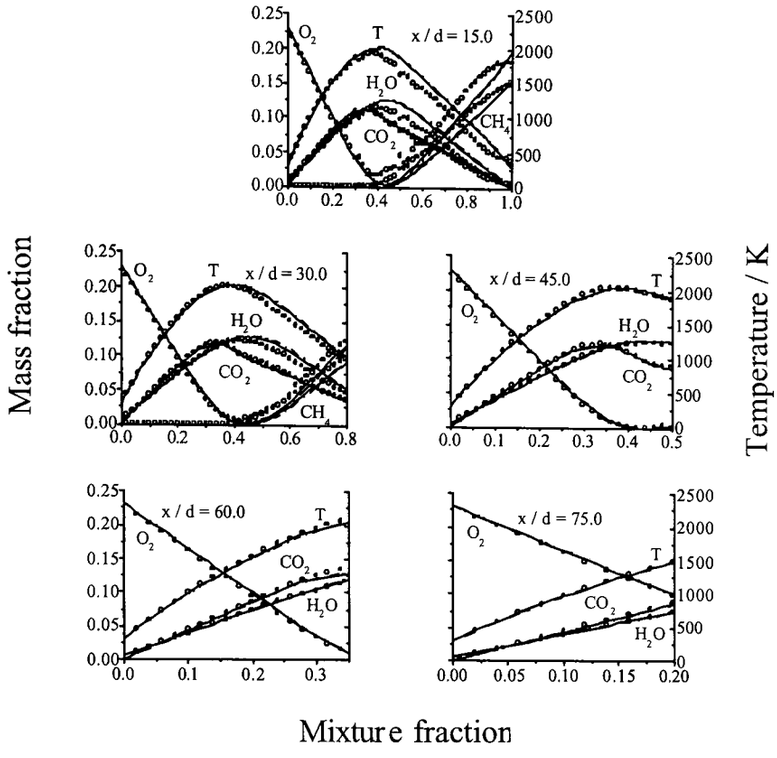

Figure 5.50 – Comparison of measured and predicted conditional species mass-fractions and temperature at five axial stations for methane flame D, derived using GRI-Mech2.11
(o measured, —predicted Re stress, - - predicted k-ε).

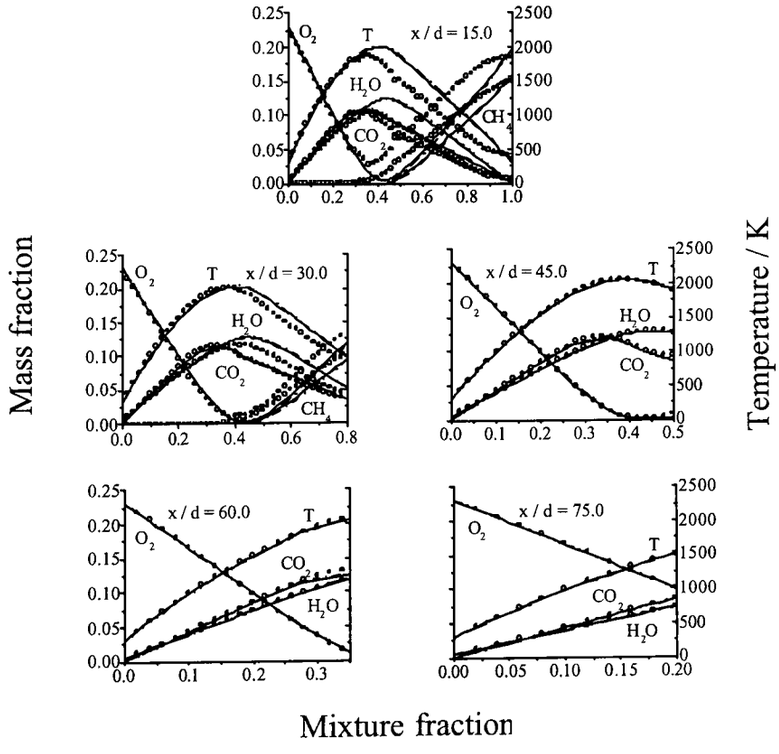

Figure 5.51 – Comparison of measured and predicted conditional species mass-fractions and temperature at five axial stations for methane flame E, derived using GRI-Mech2.11
(o measured, —predicted Re stress, - - predicted k-ε).

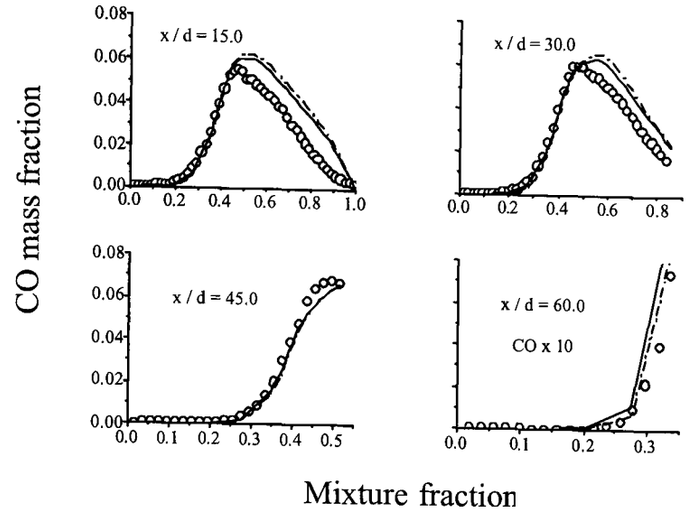

Figure 5.52 – Comparison of measured and predicted conditional CO mass-fractions at four axial stations for methane flame C, derived using GRI-Mech2.11
(o measured, —predicted Re stress, - - predicted k-ε).

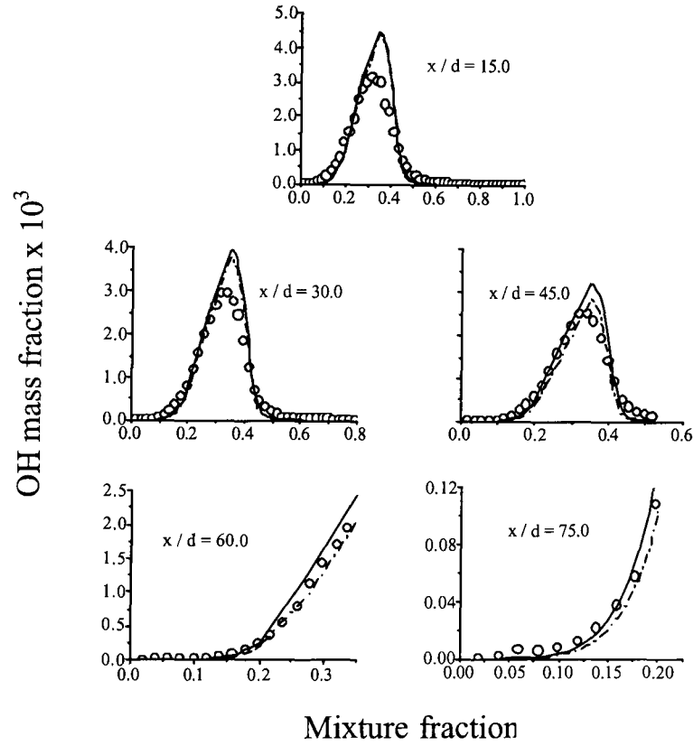

Figure 5.53 – Comparison of measured and predicted conditional OH mass-fractions at five axial stations for methane flame C, derived using GRI-Mech2.11
(o measured, —predicted Re stress, - - predicted k-ε).

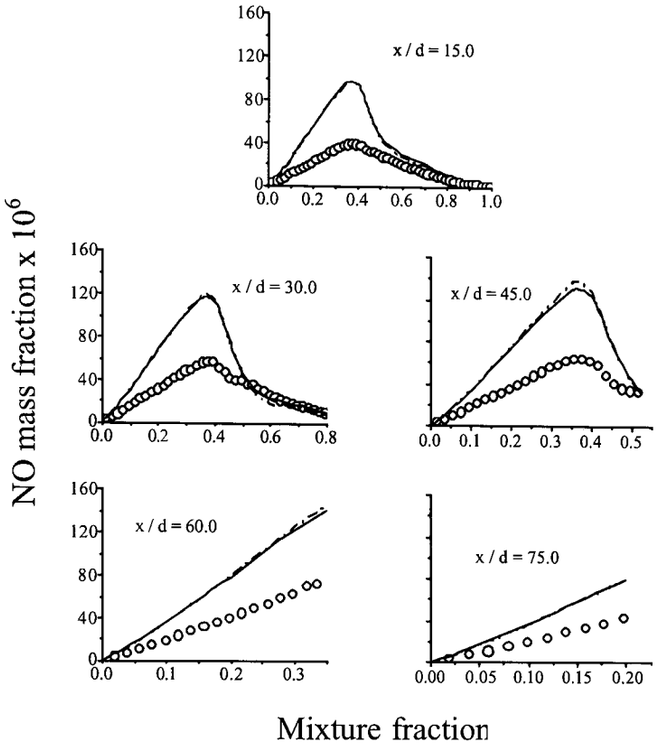

Figure 5.54 – Comparison of measured and predicted conditional NO mass-fractions at five axial stations for methane flame C, derived using GRI-Mech2.11 (o measured, —predicted Re stress, - - predicted k-ε).

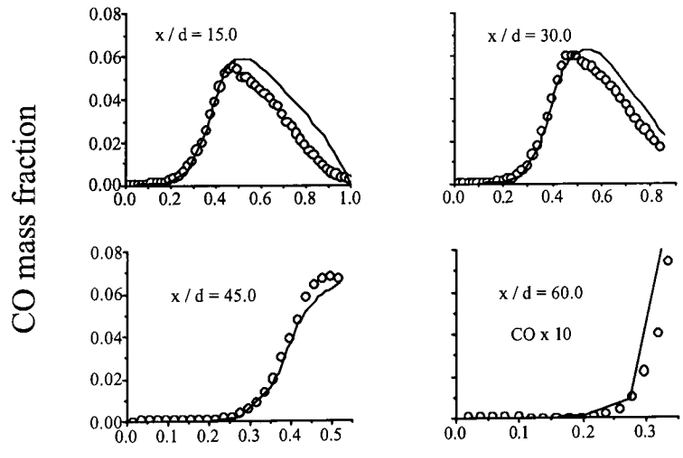

Figure 5.55 – Comparison of measured and predicted conditional CO mass-fractions at four axial stations for methane flame C, derived using GRI-Mech3.00 (o measured, —predicted Re stress).

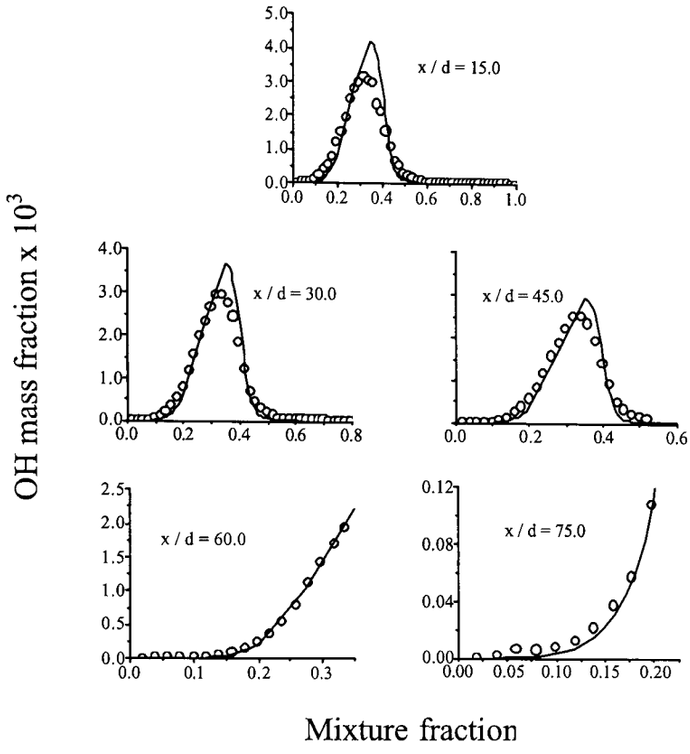

Figure 5.56 – Comparison of measured and predicted conditional OH mass-fractions at five axial stations for methane flame C, derived using GRI-Mech3.00 (o measured, —predicted Re stress).

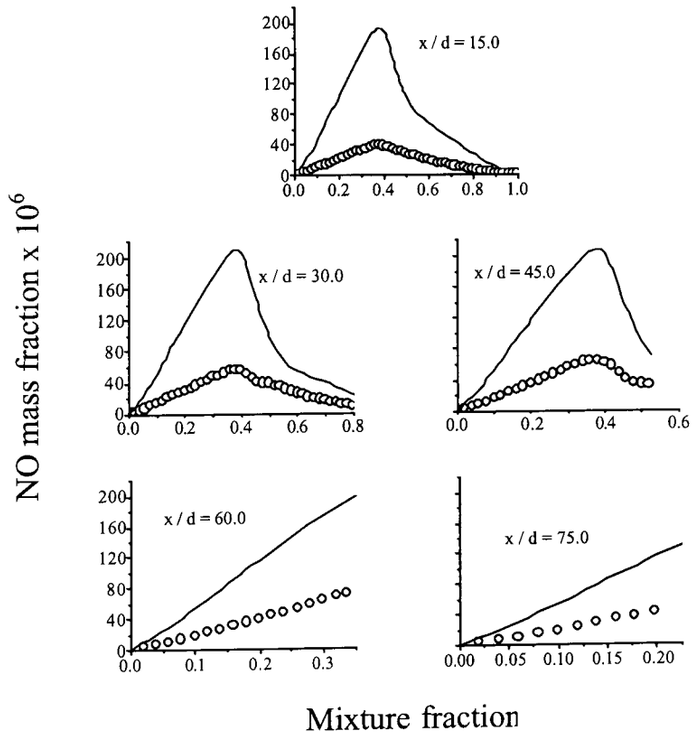

Figure 5.57 – Comparison of measured and predicted conditional NO mass-fractions at five axial stations for methane flame C, derived using GRI-Mech3.00 (o measured, —predicted Re stress).

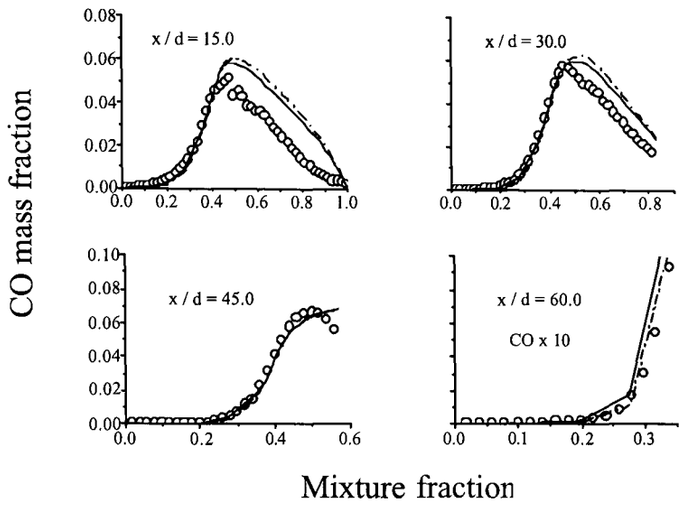

Figure 5.58 – Comparison of measured and predicted conditional CO mass-fractions at four axial stations for methane flame D, derived using GRI-Mech2.11
(o measured, — predicted Re stress, - - predicted k-ε).

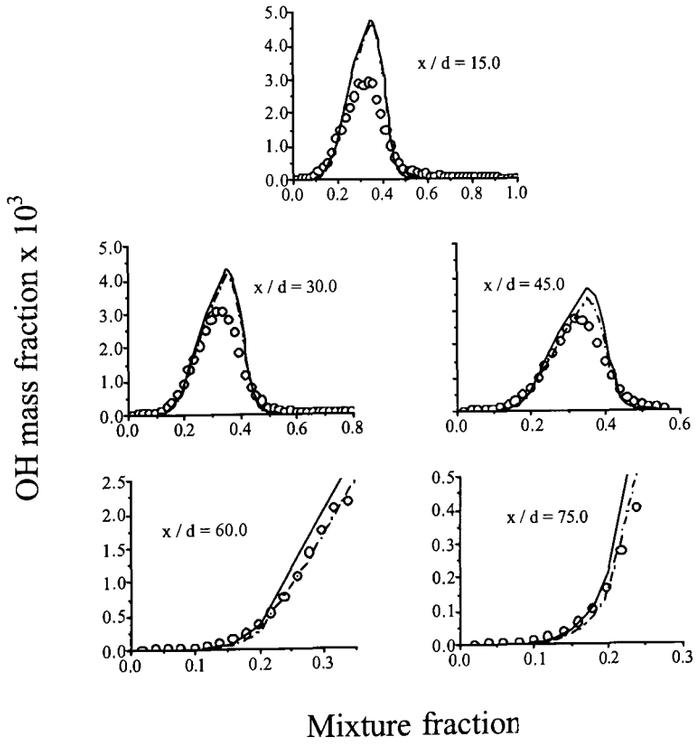

Figure 5.59 – Comparison of measured and predicted conditional OH mass-fractions at five axial stations for methane flame D, derived using GRI-Mech2.11
(o measured, — predicted Re stress, - - predicted k-ε).

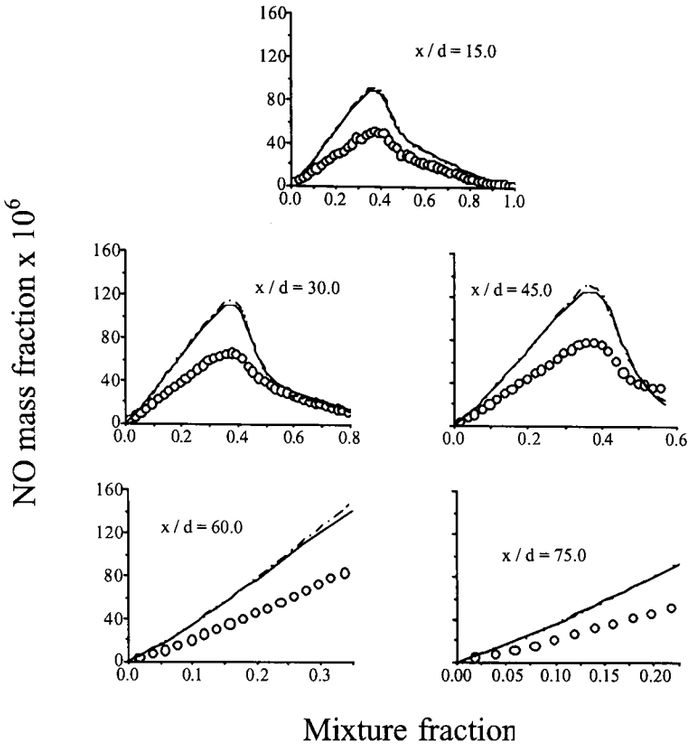

Figure 5.60 – Comparison of measured and predicted conditional NO mass-fractions at five axial stations for methane flame D, derived using GRI-Mech2.11 (o measured, — predicted Re stress, - - predicted k-ε).

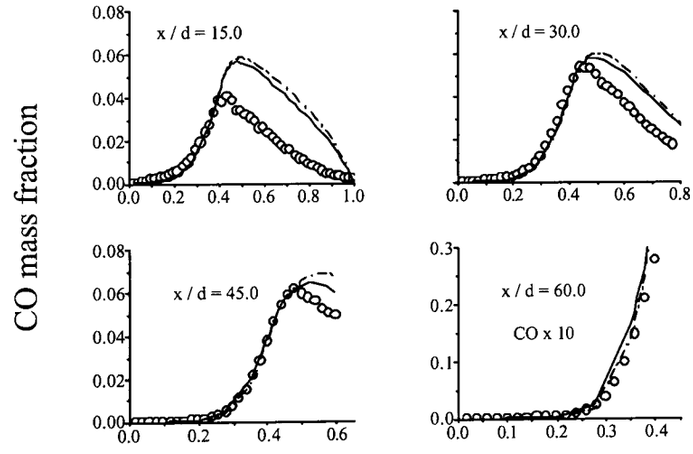

Figure 5.61 – Comparison of measured and predicted conditional CO mass-fractions at four axial stations for methane flame E, derived using GRI-Mech2.11 (o measured, — predicted Re stress, - - predicted k-ε).

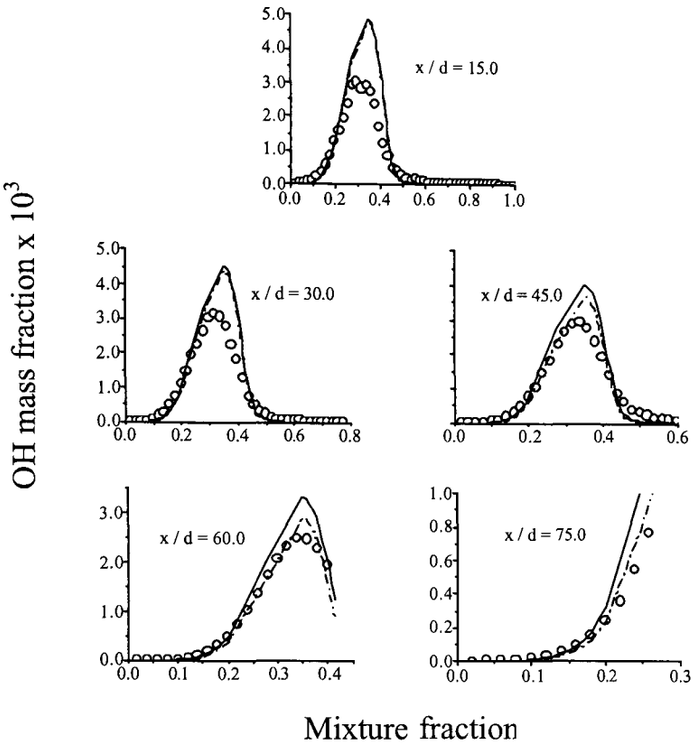

Figure 5.62 – Comparison of measured and predicted conditional OH mass-fractions at five axial stations for methane flame E, derived using GRI-Mech2.11 (o measured, — predicted Re stress, - - predicted k-ε).

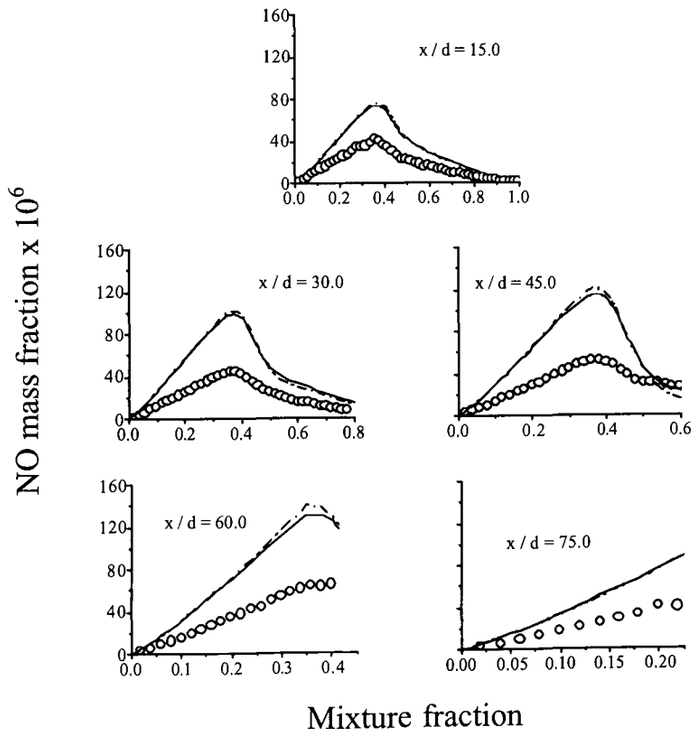

Figure 5.63 – Comparison of measured and predicted conditional NO mass-fractions at five axial stations for methane flame E, derived using GRI-Mech2.11 (o measured, — predicted Re stress, - - predicted k-ε).

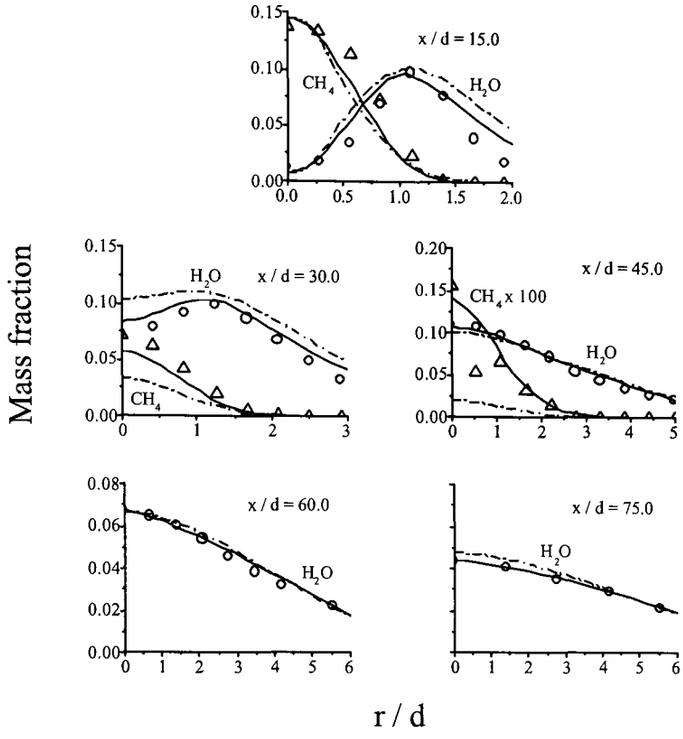

Figure 5.64 – Comparison of measured and predicted radial mean species mass-fractions at five axial stations for methane flame C, derived using GRI-Mech2.11 (o measured, —predicted Re stress, - - predicted k-ε).

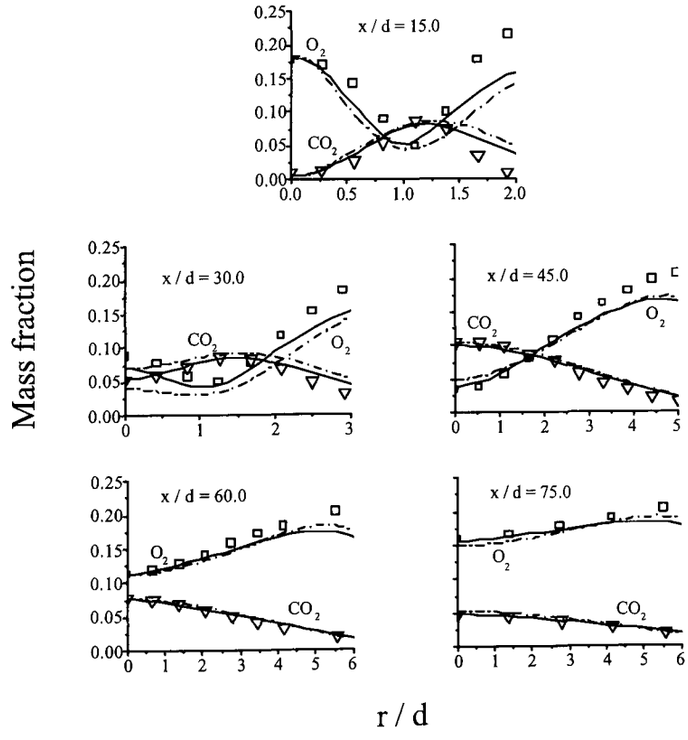

Figure 5.65 – Comparison of measured and predicted radial mean species mass-fractions at five axial stations for methane flame C, derived using GRI-Mech2.11 (o measured, —predicted Re stress, - - predicted k-ε).

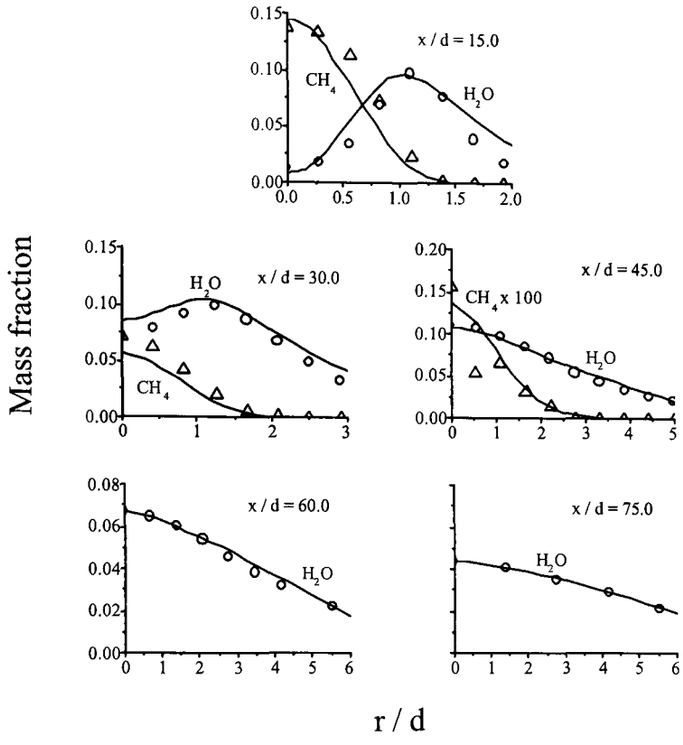

Figure 5.66 – Comparison of measured and predicted species mass-fractions at five axial stations for methane flame C, derived using GRI-Mech3.00 (o measured, — predicted Re stress).

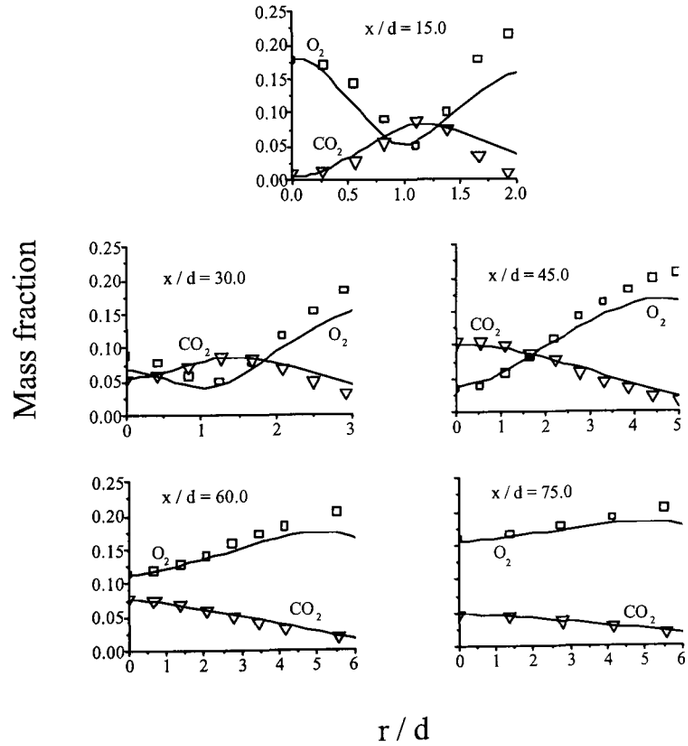

Figure 5.67 – Comparison of measured and predicted radial mean species mass-fractions at five axial stations for methane flame C, derived using GRI-Mech3.00 (o measured, — predicted Re stress).

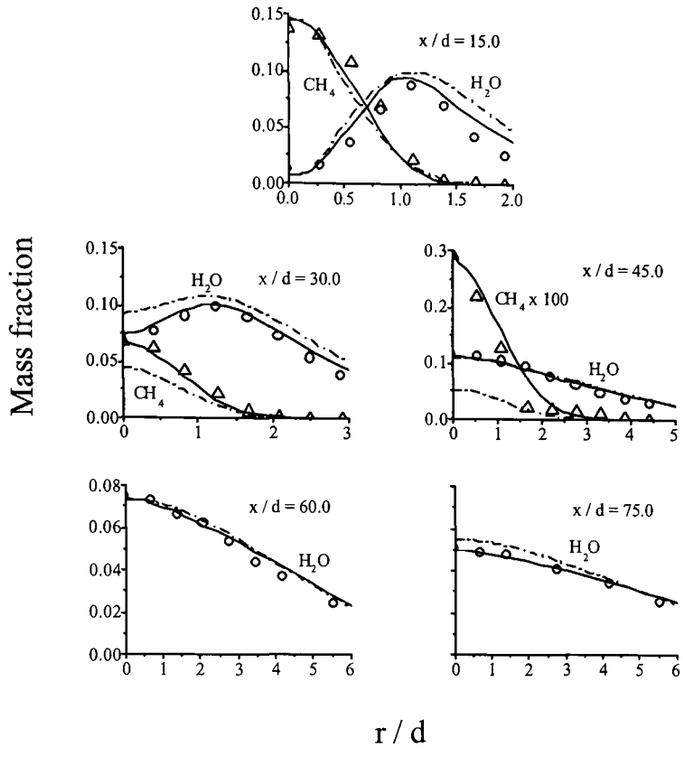

Figure 5.68 – Comparison of measured and predicted radial mean species mass-fractions at five axial stations for methane flame D, derived using GRI-Mech2.11 (o measured, —predicted Re stress, - - predicted k-ε).

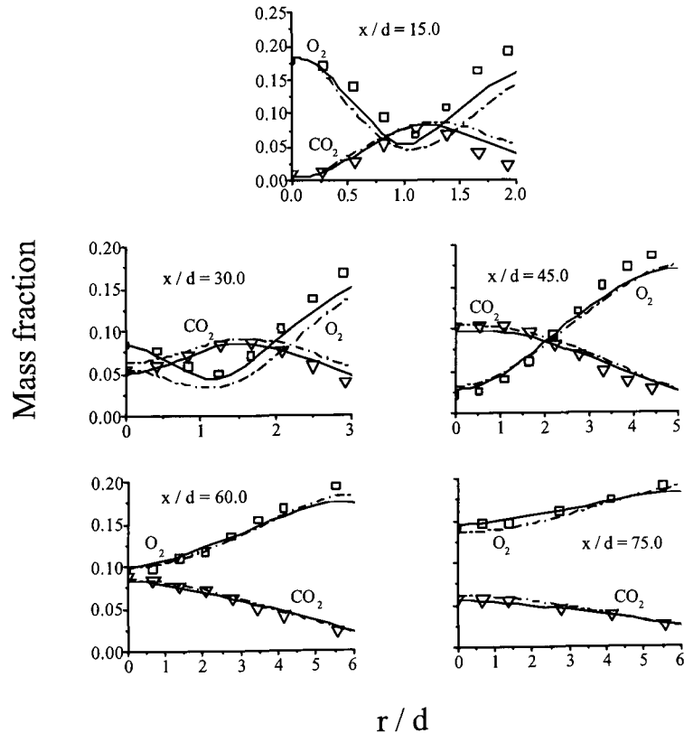

Figure 5.69 – Comparison of measured and predicted radial mean species mass-fractions at five axial stations for methane flame D, derived using GRI-Mech2.11 (o measured, —predicted Re stress, - - predicted k-ε).

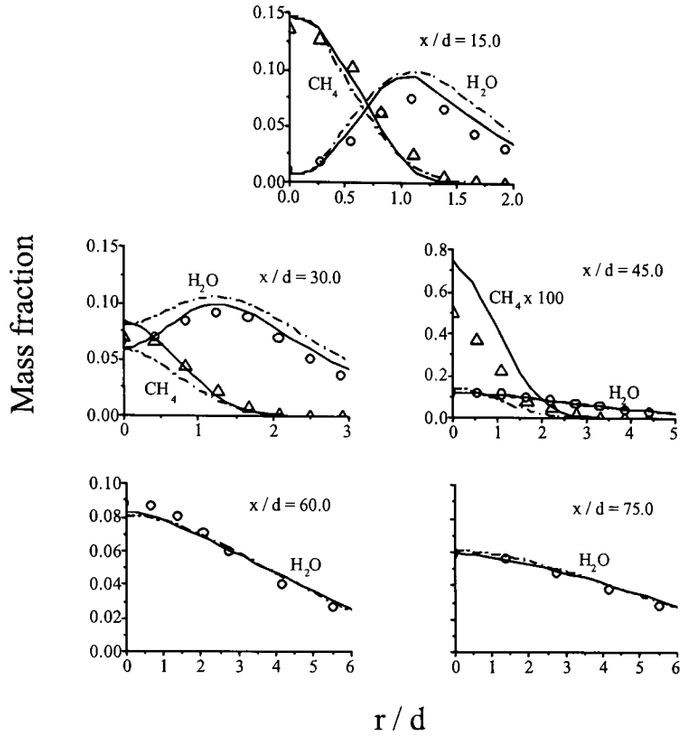

Figure 5.70 – Comparison of measured and predicted radial mean species mass-fractions at five axial stations for methane flame E, derived using GRI-Mech2.11 (o measured, — predicted Re stress, -- predicted k-ε).

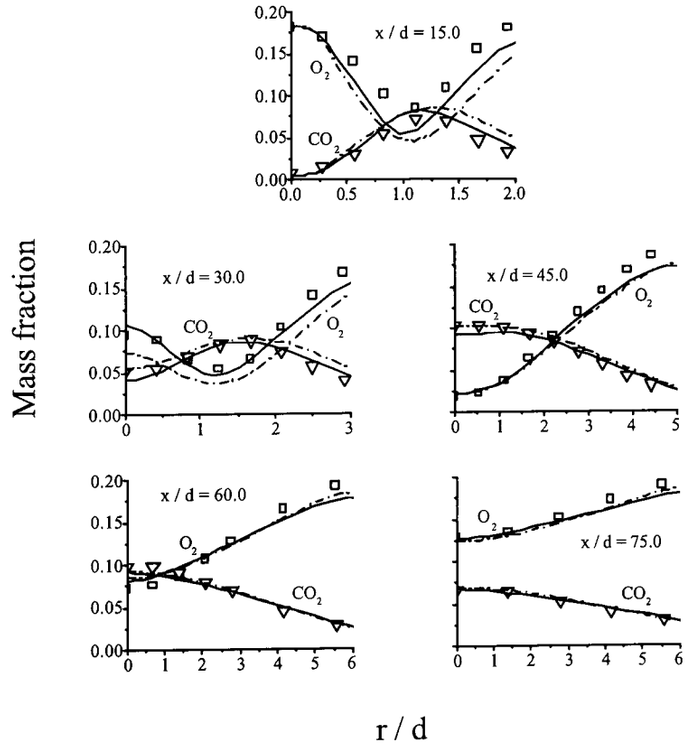

Figure 5.71 – Comparison of measured and predicted radial mean species mass-fractions at five axial stations for methane flame E, derived using GRI-Mech2.11 (o measured, — predicted Re stress, -- predicted k-ε).

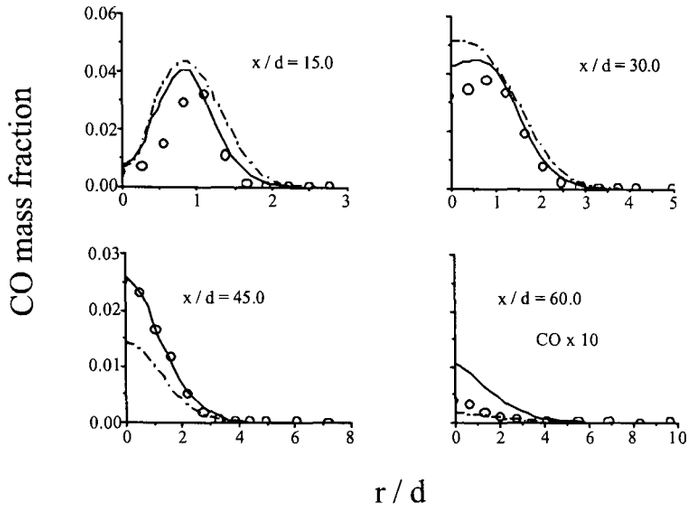

Figure 5.72 – Comparison of measured and predicted radial mean CO mass-fractions at four axial stations for methane flame C, derived using GRI-Mech2.11
(o measured, —predicted Re stress, - - predicted k-ε).

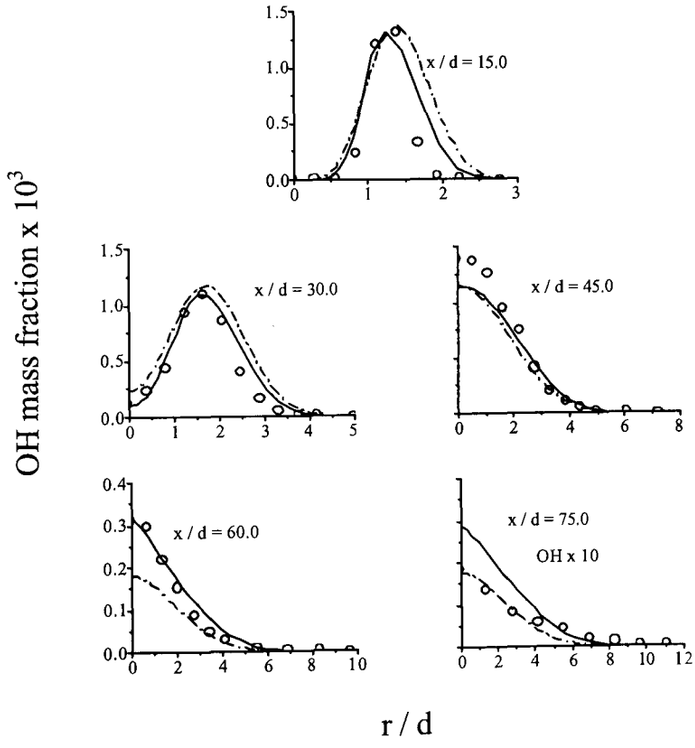

Figure 5.73 – Comparison of measured and predicted radial mean OH mass-fractions at five axial stations for methane flame C, derived using GRI-Mech2.11
(o measured, —predicted Re stress, - - predicted k-ε).

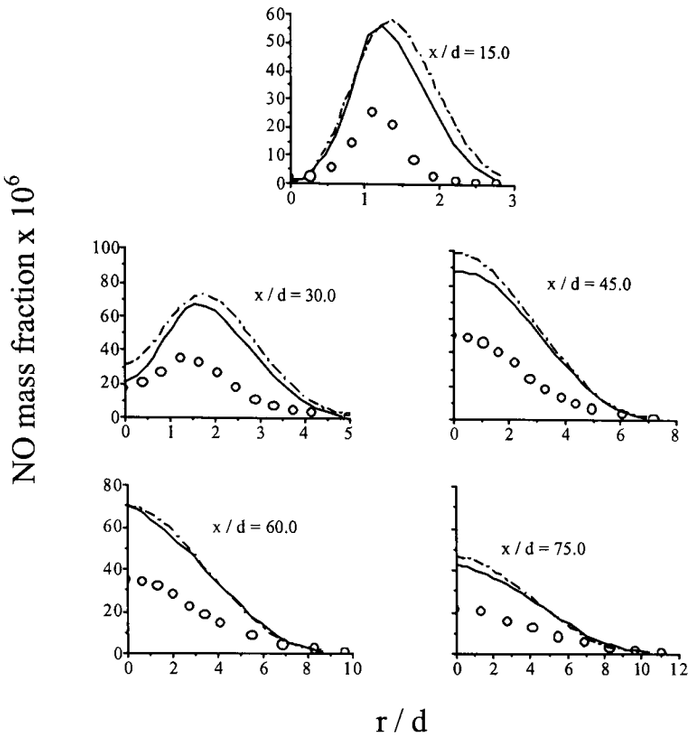

Figure 5.74 – Comparison of measured and predicted radial mean NO mass-fractions at five axial stations for methane flame C, derived using GRI-Mech2.11 (o measured, — predicted Re stress, - - predicted k-ε).

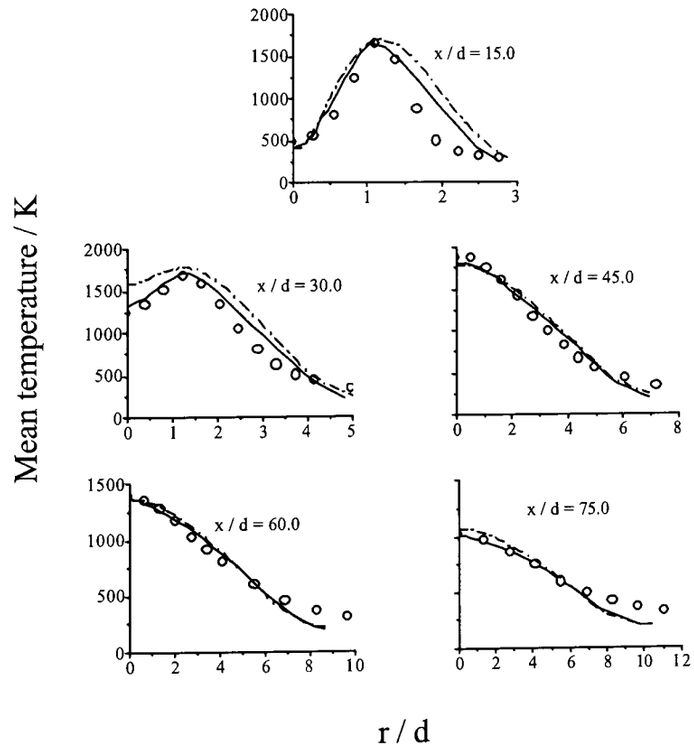

Figure 5.75 – Comparison of measured and predicted radial mean temperature at five axial stations for methane flame C, derived using GRI-Mech2.11 (o measured, — predicted Re stress, - - predicted k-ε).

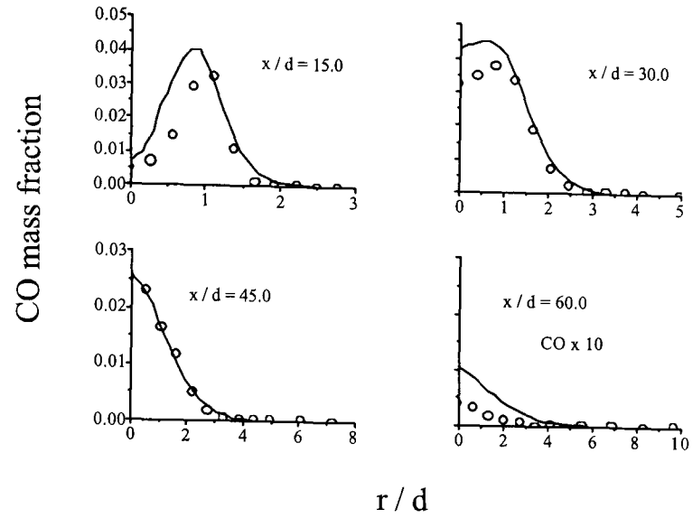

Figure 5.76 – Comparison of measured and predicted radial mean CO mass-fractions at four axial stations for methane flame C, derived using GRI-Mech3.00
(o measured, — predicted Re stress).

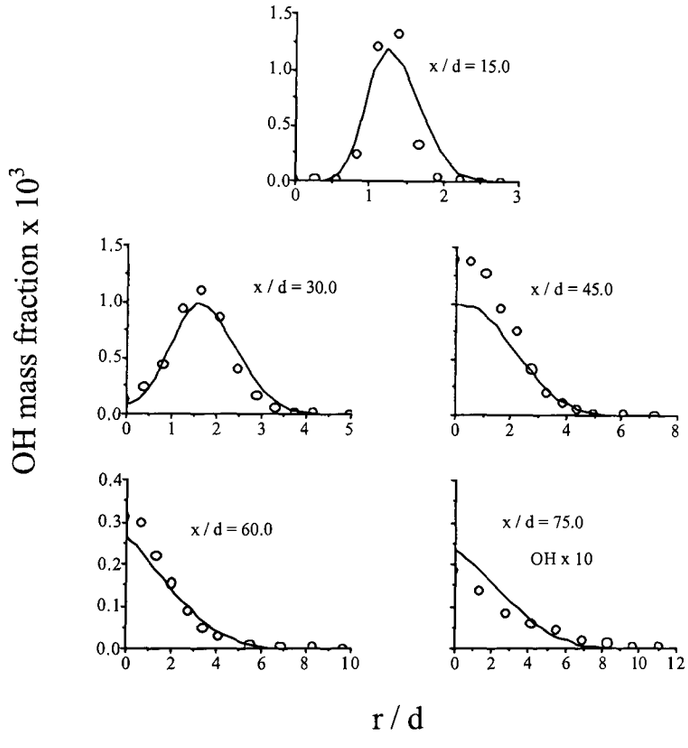

Figure 5.77 – Comparison of measured and predicted radial mean OH mass-fractions at five axial stations for methane flame C, derived using GRI-Mech3.00
(o measured, — predicted Re stress).

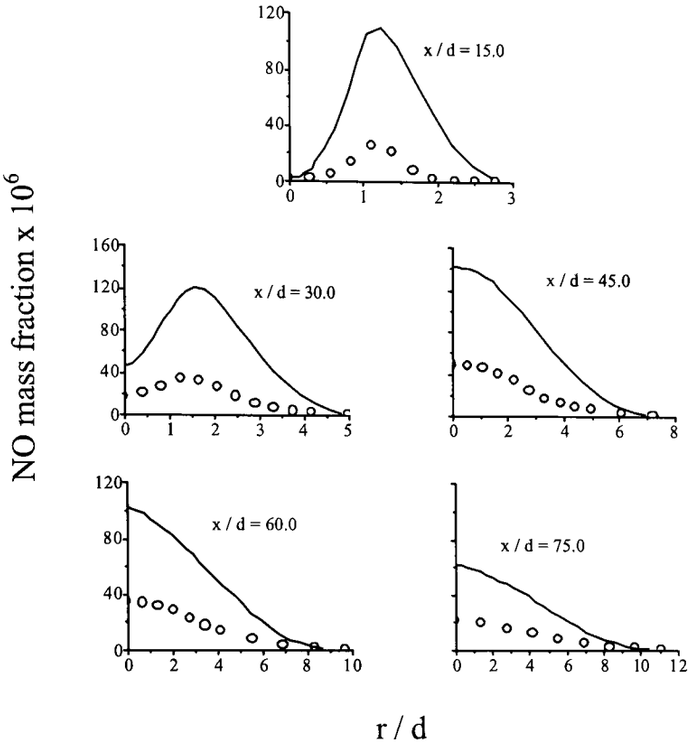

Figure 5.78 – Comparison of measured and predicted radial mean NO mass-fractions at five axial stations for methane flame C, derived using GRI-Mech3.00 (o measured, — predicted Re stress).

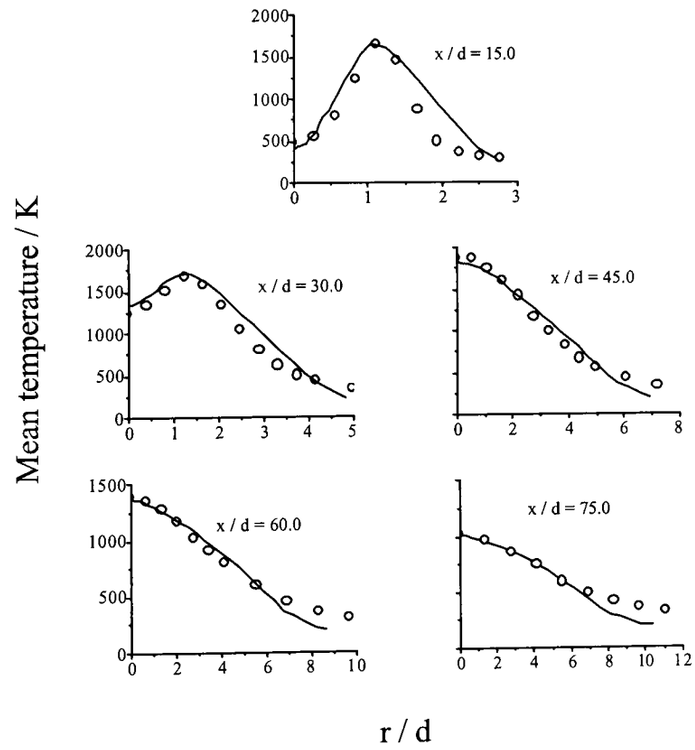

Figure 5.79 – Comparison of measured and predicted radial mean temperature at five axial stations for methane flame C, derived using GRI-Mech3.00 (o measured, — predicted Re stress).

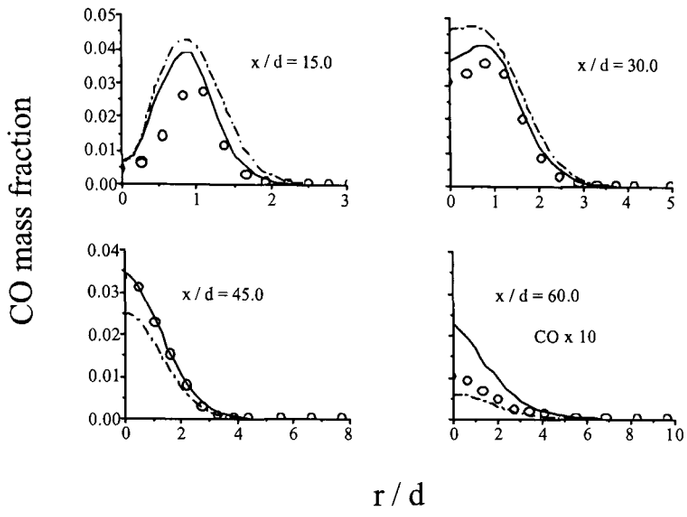

Figure 5.80 – Comparison of measured and predicted radial mean CO mass-fractions at four axial stations for methane flame D, derived using GRI-Mech2.11
(o measured, — predicted Re stress, - - predicted k-ε).

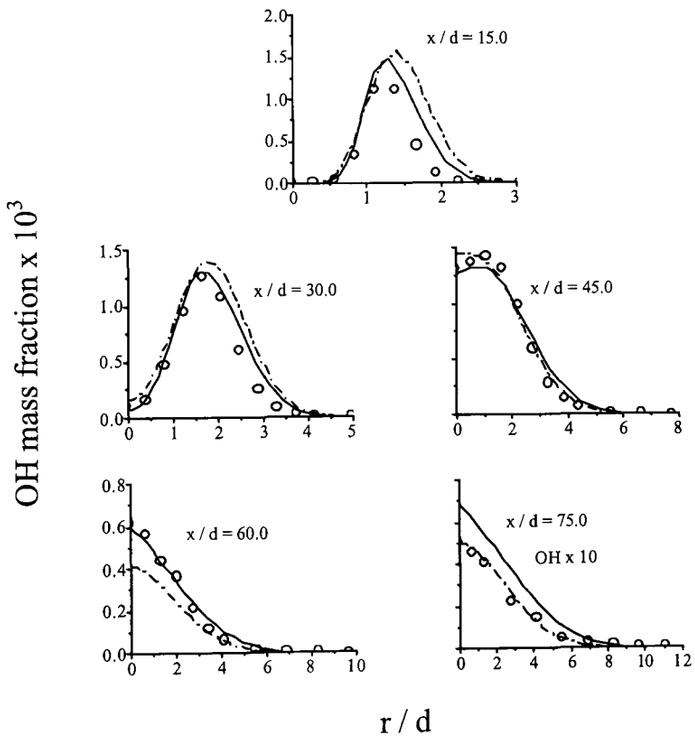

Figure 5.81 – Comparison of measured and predicted radial mean OH mass-fractions at five axial stations for methane flame D, derived using GRI-Mech2.11
(o measured, — predicted Re stress, - - predicted k-ε).

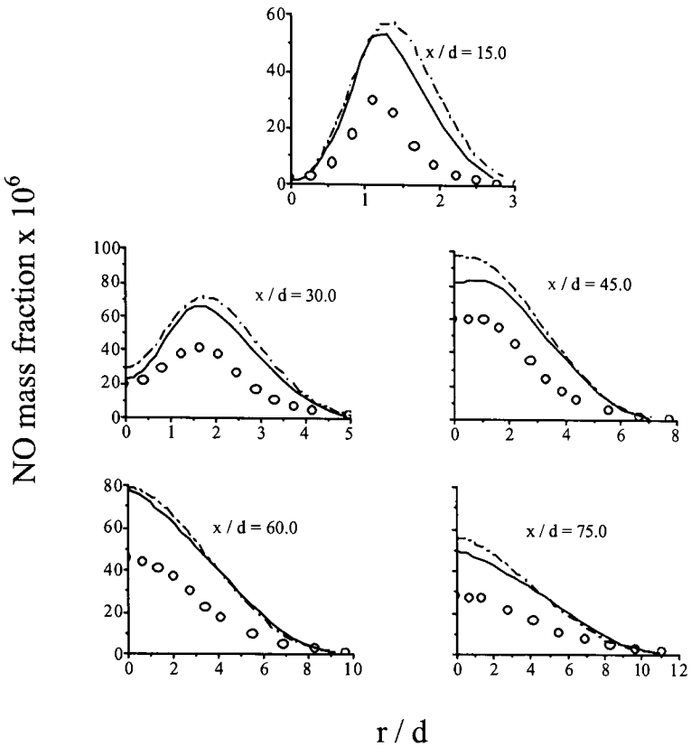

Figure 5.82 – Comparison of measured and predicted radial mean NO mass-fractions at five axial stations for methane flame D, derived using GRI-Mech2.11 (o measured, —predicted Re stress, - - predicted k-ε).

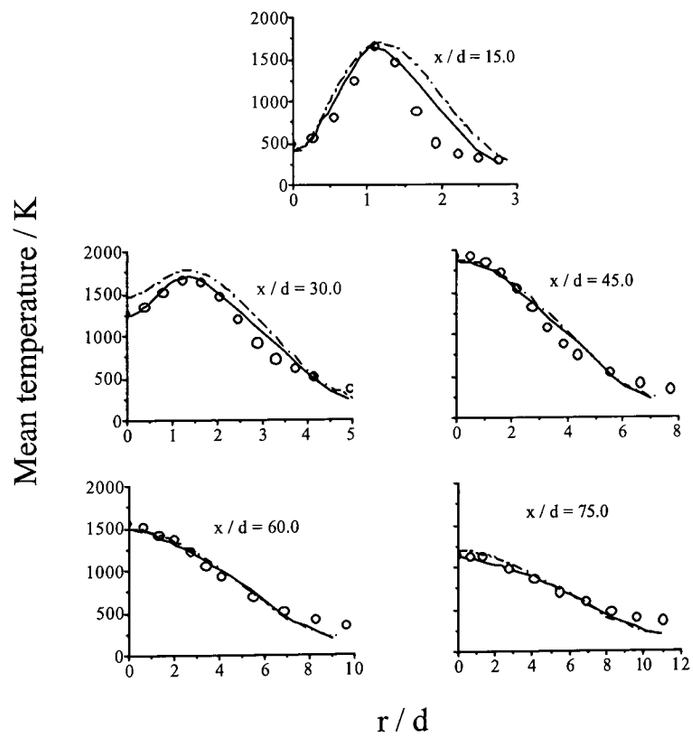

Figure 5.83 – Comparison of measured and predicted radial mean temperature at five axial stations for methane flame D, derived using GRI-Mech2.11 (o measured, —predicted Re stress, - - predicted k-ε).

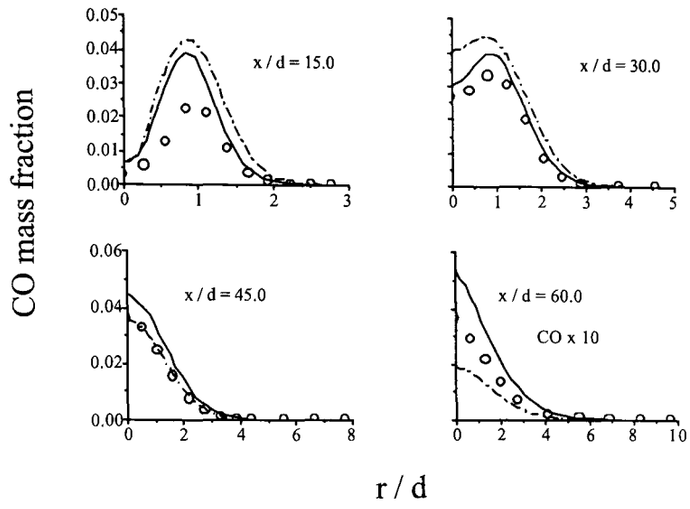

Figure 5.84 – Comparison of measured and predicted radial mean CO mass-fractions at four axial stations for methane flame E, derived using GRI-Mech2.11 (o measured, — predicted Re stress, - - predicted k-ε).

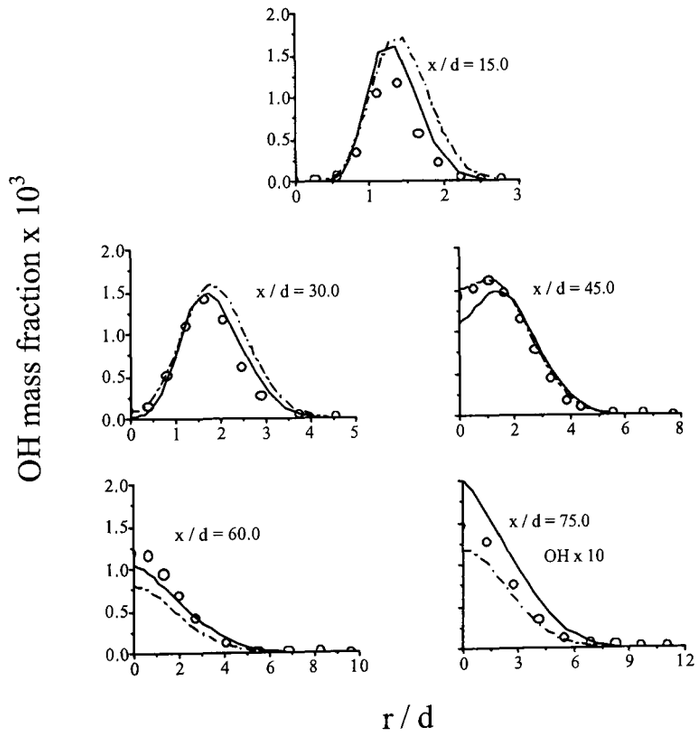

Figure 5.85 – Comparison of measured and predicted radial mean OH mass-fractions at five axial stations for methane flame E, derived using GRI-Mech2.11 (o measured, — predicted Re stress, - - predicted k-ε).

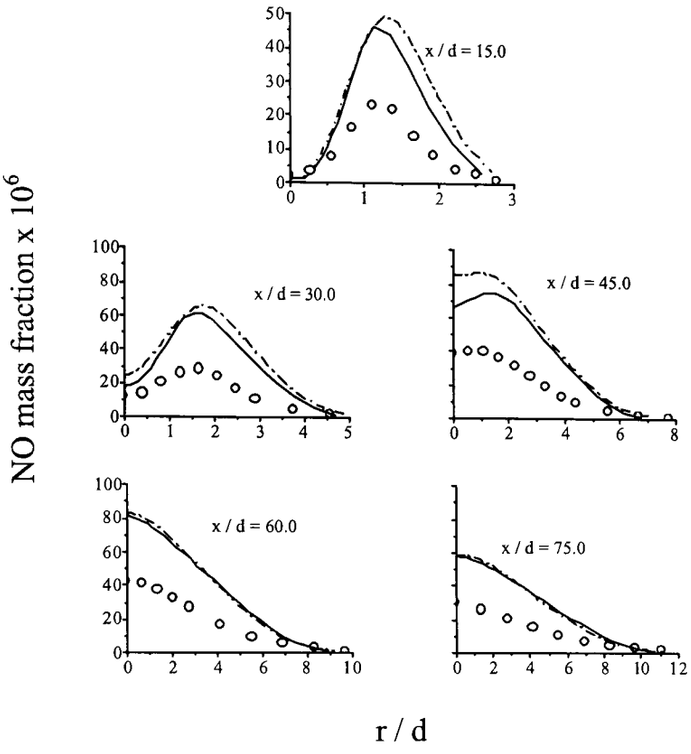

Figure 5.86 – Comparison of measured and predicted radial mean NO mass-fractions at five axial stations for methane flame E, derived using GRI-Mech2.11 (o measured, — predicted Re stress, - - predicted k-ε).

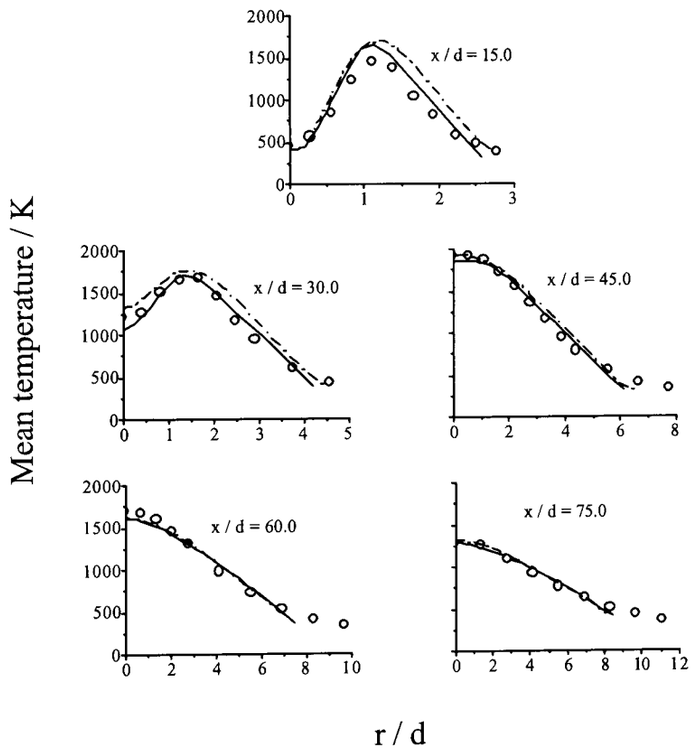

Figure 5.87 – Comparison of measured and predicted radial mean temperature at five axial stations for methane flame E, derived using GRI-Mech2.11 (o measured, — predicted Re stress, - - predicted k-ε).

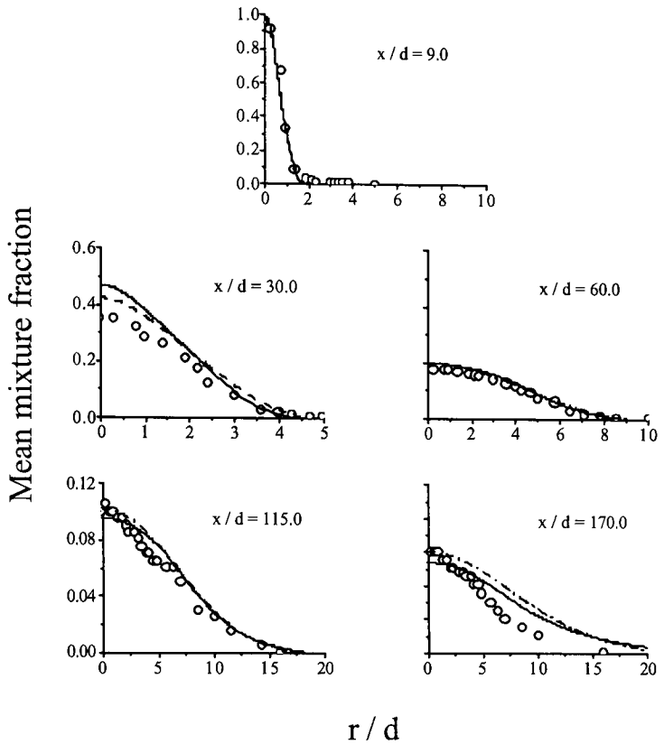

Figure 5.88 – Comparison of measured and predicted radial mean mixture-fraction profiles at five axial stations for methane flame F (o measured, —predicted Re stress, - - predicted k-ε).

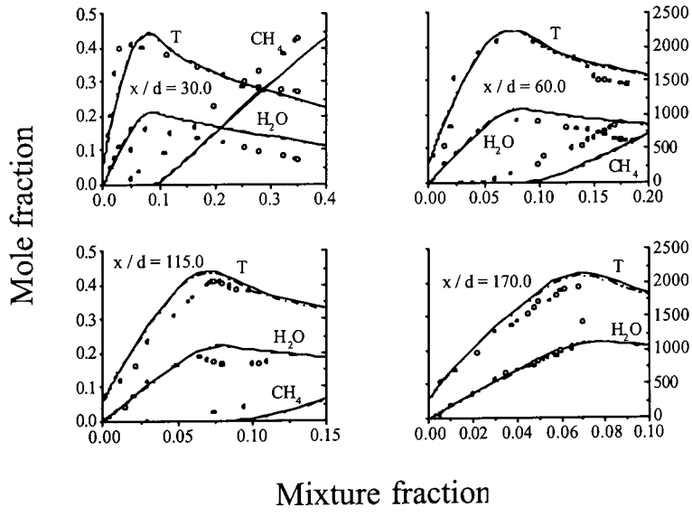

Figure 5.89 – Comparison of measured and predicted conditional species mole-fractions at four axial stations for methane flame F, derived using GRI-Mech2.11 (o measured, —predicted Re stress, - - predicted k-ε).

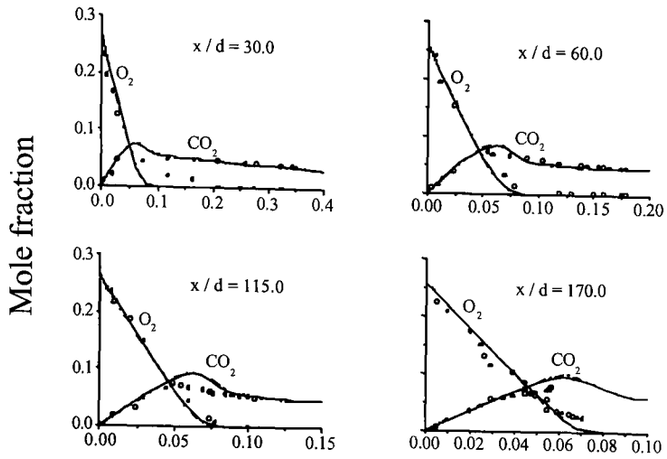

Figure 5.90 – Comparison of measured and predicted conditional species mole-fractions at four axial stations for methane flame F, derived using GRI-Mech2.11 (o measured, —predicted Re stress, - - predicted k-ε).

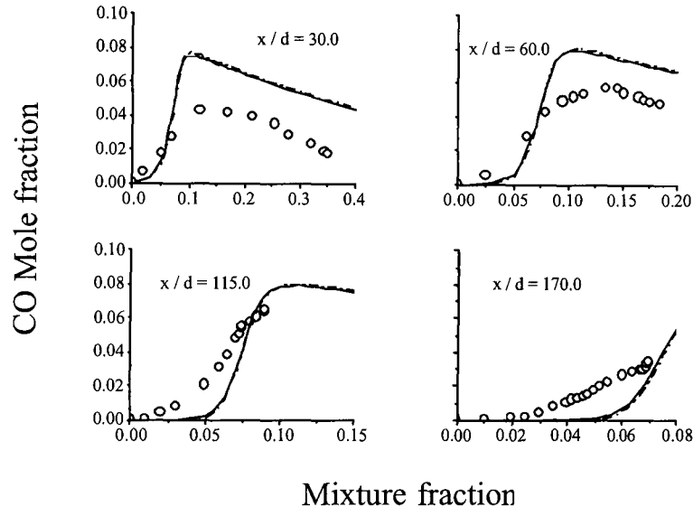

Figure 5.91 – Comparison of measured and predicted conditional CO mole-fractions at four axial stations for methane flame F, derived using GRI-Mech2.11 (o measured, —predicted Re stress, - - predicted k-ε).

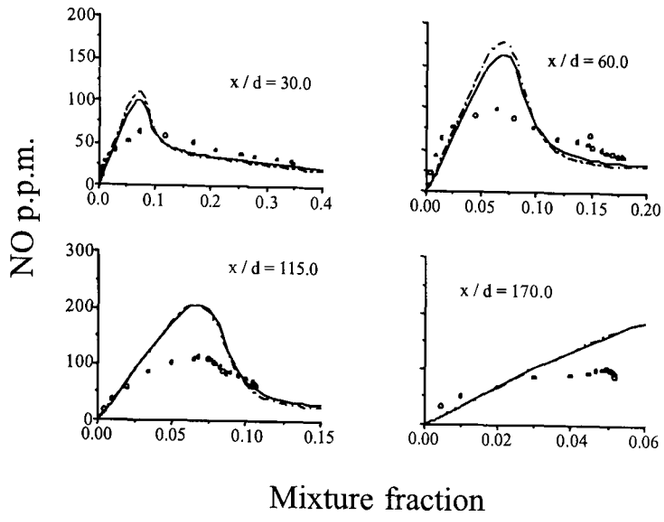

Figure 5.92 – Comparison of measured and predicted conditional NO mole-fractions at four axial stations for methane flame F, derived using GRI-Mech2.11 (o measured, —predicted Re stress, - - predicted k-ε).

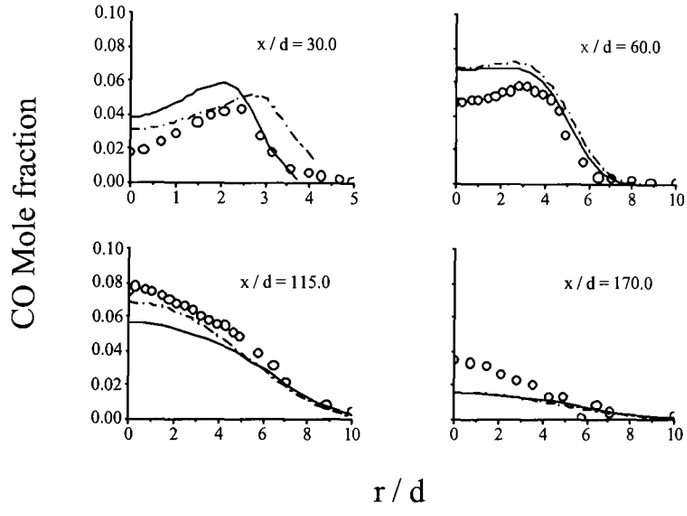

Figure 5.93 – Comparison of measured and predicted radial mean CO mole-fractions at four axial stations for methane flame F, derived using GRI-Mech2.11 (o measured, —predicted Re stress, - - predicted k-ε).

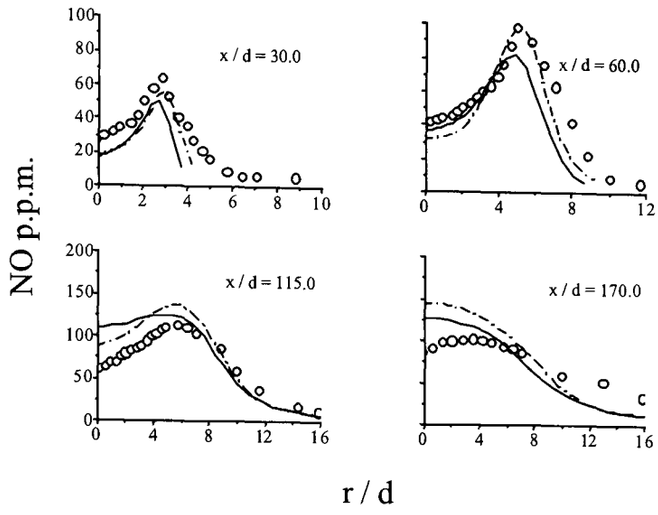

Figure 5.94 – Comparison of measured and predicted radial mean NO mole-fractions at four axial stations for methane flame F, derived using GRI-Mech2.11 (o measured, —predicted Re stress, - - predicted k-ε).

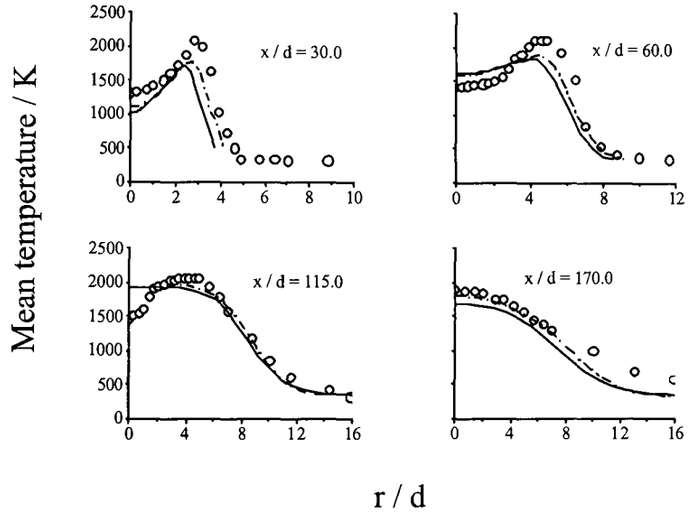

Figure 5.95 – Comparison of measured and predicted radial mean temperature at four axial stations for methane flame F, derived using GRI-Mech2.11 (o measured, —predicted Re stress, - - predicted k-ε).

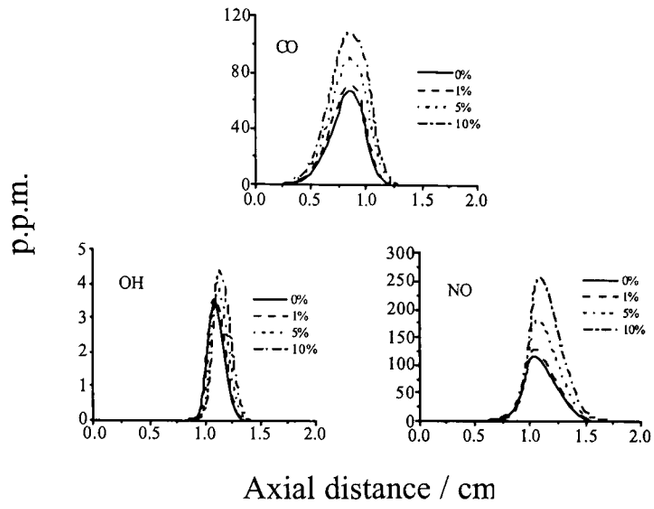

Figure 5.96 – Comparison of predicted minor species mole fractions with varying C_2H_2 fuel dilution in a laminar flame of configuration D, derived using GRI-Mech2.11.

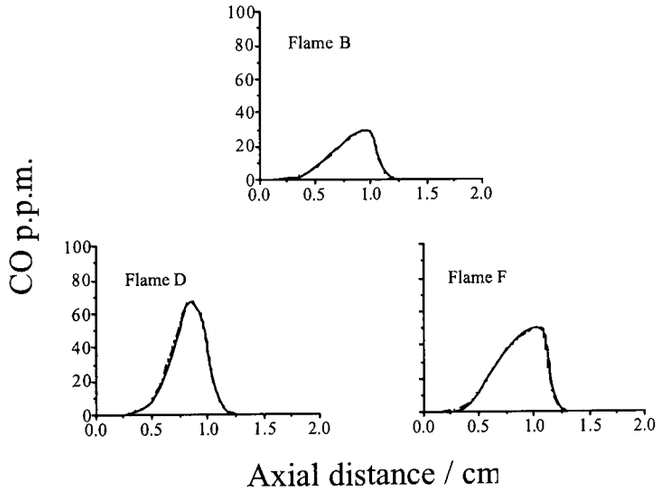

Figure 5.97 – Predicted CO mole fractions in laminar flames of configurations B, D, and F, derived using GRI-Mech2.11 and GRI-Mech3.0.

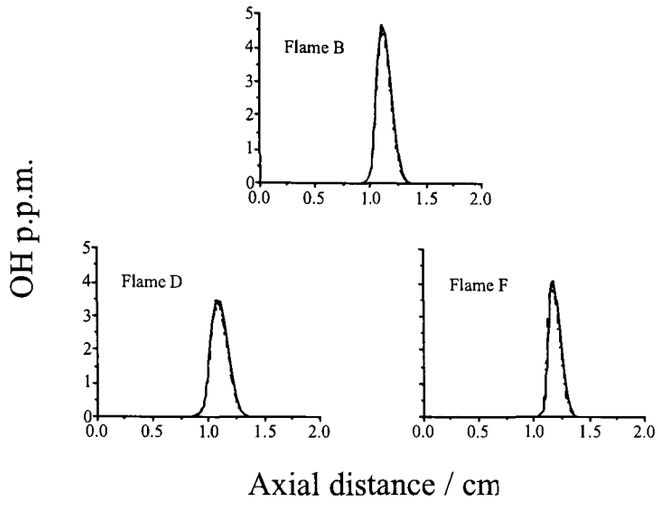

Figure 5.98 – Predicted OH mole fractions in laminar flames of configurations B, D, and F, derived using GRI-Mech2.11 and GRI-Mech3.0.

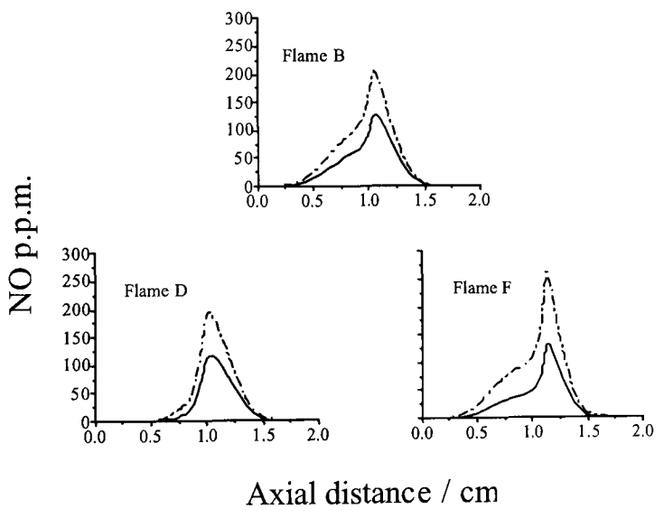

Figure 5.99 – Predicted NO mole fractions in laminar flames of configurations B, D, and F, derived using GRI-Mech2.11 and GRI-Mech3.0.

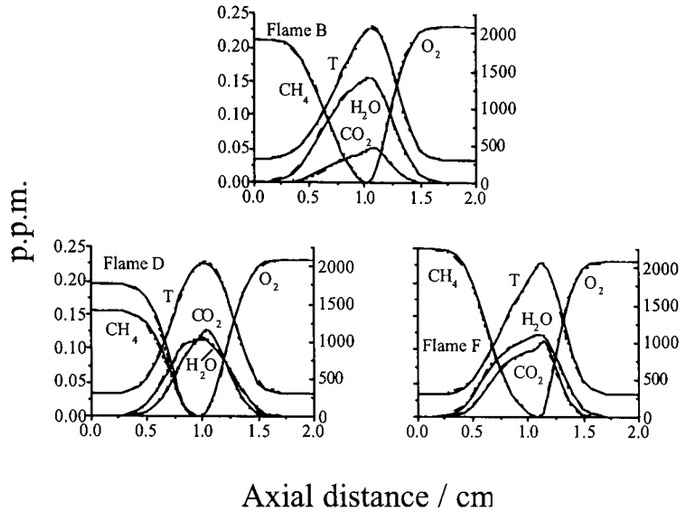

Figure 5.100 – Predicted major species mole fractions in laminar flames of composition B, D, F, derived using GRI-Mech2.11 and GRI-Mech3.0.

6: Discussion, Conclusions, And Suggestion For Further Work

A comprehensive study of the CMC model's application to turbulent jet diffusion flames of hydrogen and methane has been presented. As an embarkation point, this work undertook for the first time, an analysis of the effects of turbulence closure selection upon the performance of the CMC model with respect to predicting flame-structures of hydrogen. The findings of this study lead to such analysis being applied to subsequent works, as the method to which turbulence quantities were represented was found to be important to the performance of the combustion model. In these instances, the Reynolds stress/scalar flux form generally displayed superior results to the $k-\varepsilon$ approach in both mixing and chemistry fields. In addition, three differing kinetics schemes were applied to the calculations in an attempt to elucidate the effects of these closures upon predictions. Findings showed little observable difference in computed values between schemes of different complexity. Shortcomings of the combustion and turbulence models were discussed, although predictions were generally of an excellent level of agreement with experiment. This deliberation lead to the development of a second-order closure model, similar to that applied by previous authors (Kronenburg et al 1998, Devaud 1999), as being the priority area for further development. Other sources of interest were identified as: addressing

differential diffusion; representation of the pdf, representation of scalar dissipation, and the cross-stream averaged formulations.

The second-order chemistry model was successfully applied to three hydrogen flames using, for the first time, two forms of turbulence model. Again, the importance of the model selection was highlighted in both real-space and composition space predictions. These studies subsequently brought to the fore the issue of kinetic mechanism representation, and suggestion for further studies made. The performance of the scalar dissipation model was also questioned, with indications that its abilities may indeed be restricted when addressing certain flame regions, namely near-nozzle locale. This second-order chemistry model, in addition to the first-order model, was further applied to the prediction of a lifted hydrogen jet of relatively high Mach number. Although an expected poor representation of the lift-off region was achieved, both models' performance in predicting conditional data was demonstrated in downstream calculations. Again, both $k-\varepsilon$ and Reynolds-stress models were uniquely applied to describe the flow-field and turbulence quantities, and similar observations were made as those regarding the rim-stable examples. The application of the model to a lifted flame however, succeeded in highlighting the requirements for both elliptic and flow and combustion modelling in this instance. Indeed, the general shortcomings of the models in application to all the flames are indicative that not only a second-moment turbulence closure should be adopted for all future work, but the elliptic solution procedure also. At the time, rather than beginning development of such a method, it was considered more important to extend the investigation of the current modelling strategy to the more complex problems concerned with hydrocarbon combustion to test the validity of previous conclusions. A CMC

model was therefore applied to a wide range of methane turbulent jet diffusion flames, including piloted and unpiloted geometries, and of various fuel compositions although being primarily methogenous in nature. No one study has previously looked at such a comprehensive range of combusting flows, and once again, an original investigation into the effects of turbulence model closure was undertaken, with an analysis of sensitivity of predictions to chemical kinetics schemes carried out. In contrast to the hydrogen flame predictions, the flow-field quantities do not show much variation between the Reynolds stress/scalar flux and $k-\varepsilon$ models, and indeed mixture-fraction space data display little variance. Real space predictions do however serve to highlight the importance of closure once again, with the Reynolds stress model displaying both qualitatively and quantitatively superior results. This study of hydrocarbon chemistry does however indicate a sensitivity of calculations to the chemistry model applied, which leads to the suggestion of further investigation being required for its representation. This is noted particularly for NO pathways, but falls out of the scope of this study. The calculation of flames displaying varying levels of local extinction also leads to the conclusion that the current model is inadequate in respect of its parabolic nature and first-order chemistry representation to describe such phenomena.

Overall, the present work has achieved its intended objectives, by laying of groundwork and subsequent development, of advancing the application of CMC methods to practical application. The study has provided an excellent base of knowledge from which to begin a secondary stage in model development, leading ultimately to a widely applicable modelling strategy implementing CMC methods. The essential findings and suggestions for future work follow, and it is

worth noting that these works are in fact on-going at the University of Leeds as part of an EPSRC funded project with the ultimate aim of providing solution procedures for complex chemistry and complex geometry interaction in practical combustion devices.

In terms of further work, it is recommended that all calculations of both flow-field and chemistry should be carried out in an elliptic framework. To accurately predict phenomena such as lift-off, this is essential, in addition to density coupling being required between the two models. An elliptic CMC model is therefore currently under development, and its coupling with a flow-field and turbulence model providing a body-fitted solution procedure to handle complex geometries is underway. This development of elliptic methods, in addition to enabling the study of more complex physical phenomena, allows for the study of CMC sub-models, and at present, investigation is underway of a transported equation model for the conditional velocity. By its nature, the elliptic form also eliminates the need for cross-stream averaging, and hence any introduced errors from the approximation.

Secondly, all calculations should be carried out in conjunction with a second-moment turbulence closure. The effects of the turbulence model upon the combustion calculations, whether first- or second-order, are of such a scale that they cannot be ignored, and this shall be carried out in future works. Some comparative work with the eddy-viscosity based approach may however still be warranted.

Thirdly, an elliptic second-order chemistry is found to be required to accurately represent such processes in flames displaying extinction effects. Hence, time has been allotted for such a development in the future, for application to hydrocarbon

combustion generally, rather than the case-specific methods described in earlier chapters. This shall be directly incorporated into an elliptic calculation procedure.

The undertaking of such works, and the application of these new strategies to the flames calculated in this thesis should assist the elucidation of a number of anomalous behaviours noted previously. The re-calculation of these flames will aid to answer questions regarding NO prediction and also help in the evaluation of computational sub-models generally used in these methods. In addition, more detailed data sets of the flames would aid in establishing the root causes of experimental and calculated data discrepancies. With the recent developments in Large Eddy Simulation (LES) and Direct Numerical Simulation (DNS) approaches, this is a feasible task to undertake, and consideration shall be made to their application in future works. It is considered that this next step in the research will provide a considerable amount of detailed information which shall go a long way in furthering this study, and the approach to a universally applicable and reliable CMC methodology.

7: References

Andresen, P., Meijer, G., Schlüter, H., Voges, H., Koch, A., Hentschel, W., Oppermann, W., Rothe, E. (1990), Fluorescence Imaging Inside an Internal Combustion Engine Using Tunable Excimer Lasers, *Applied Optics*, 29: 2392-2404, Optical Society of America.

Barlow, R.S., Carter, C.D. (1994), Raman / Rayleigh / LIF Measurements of Nitric Oxide Formation in Turbulent Hydrogen Jet Flames, *Combustion and Flame*, 97: 261-280, Elsevier Science Inc.

Barlow, R.S., Carter, C.D. (1996), Relationships Among Nitric Oxide, Temperature, and Mixture Fraction in Hydrogen Jet Flames, *Combustion and Flame*, 104: 288-299, Elsevier Science Inc.

Barlow, R.S. Frank, J. (1998), Effects of Turbulence on Species Mass Fractions in Methane/Air Jet Flames, *27th Symposium (International) on Combustion*, 1087-1095, Pittsburgh: The Combustion Institute.

Barlow, R.S., Smith, N.S.A., Chen, J.-Y., Bilger, R.W. (1999), Nitric Oxide Formation in Dilute Hydrogen Jet Flames: Isolation of the Effects of Radiation and Turbulence-Chemistry Submodels, *Combustion and Flame*, 117: 4-31, Elsevier Science Inc.

Barths, H., Hasse, C., Bikas, G., Peters, N. (2000), Simulation of Combustion in DI Diesel Engines Using an Eulerian Particle Flamelet Model, *Proceedings of The Combustion Institute*, 28: 1161-1168, Pittsburgh: The Combustion Institute.

Baum, M., Poinsot, T., Hawarth, D., Darabiha, N. (1994), Direct Numerical Simulation of $H_2/O_2/N_2$ Flames With Complex Chemistry in 2-Dimensional Turbulent Flows, *Journal of Fluid Mechanics*, 281: 1-32, Taylor and Francis.

Bédat, B., Fokion, N.E., Poinsot, T. (1999), Direct Numerical Simulation of Heat Release And NO_x Formation in Turbulent Nonpremixed Flames, *Combustion and Flame*, 119: 69-83, Elsevier Science Inc.

Bergmann, V., Meier, W., Wolfe, D., Stricker, W. (1998), Application of Spontaneous Raman and Rayleigh Scattering and 2D LIF For The Characterisation of a Turbulent CH_4/H_2N_2 Jet Diffusion Flame, Applied Physics B, 66: 489-502, Springer-Verlag.

Bilger, R.W. (1975), A Note on Favre Averaging in Variable Density Flows, *Combustion Science and Technology*, 11: 215-217, Gordon and Breach.
Bilger, R.W. (1976), Turbulent Jet Diffusion Flames, *Progress in Energy and Combustion Science*, 1: 87-109, Elsevier Science Inc.

Bilger, R.W. (1993a), Conditional Moment Closure For Turbulent Reacting Flow, *Physics of Fluids A*, 5:2 436-444, American Institute of Physics.

Bilger, R.W. (1993b), Conditional Moment Closure Modelling And Advances Laser Measurements, In Takeno, T. (Ed.), *Turbulence And Molecular Processes in Combustion*, 267-285, Elsevier Science Inc.

Bird, R.B., Stewart, W.E., Lightfoot, E.N. (1960), *Transport Phenomena*, New York: John Wiley & Sons.

Blin, L., Hadjadj, A., Vervisch, L. (2003), Large Eddy Simulation of Turbulent Flows in Reversing Systems, *Journal of Turbulence*, 4: 1-19, Institute of Physics.

Bowman, C.T., Hanson, R.K., Davidson, D.F., Gardiner, W.C., Lissianski, V., Smith, G.P., Golden, D.M., Frenklach, M., Goldneberg, M. (1996), http://www.me.berkeley.edu/gri_mech/, accessed 17th April 2003.

Bradley, D., Emerson, D.R., Gaskell, P.H., Gu, X.J. (2002), Mathematical Modelling of Turbulent Non-Premixed Piloted Jet Flames With Local Extinctions, *Proceedings of The Combustion Institute*, 29: 2155-2162, Pittsburgh: The Combustion Institute.

Branley, N., Jones, W.P. (2001), Large Eddy Simulation of a Turbulent Non-Premixed Flame, *Combustion and Flame*, 127: 1914-1934, Elsevier Science Inc.

Bray, K.N.C., Peters, N. (1994), Laminar Flamelets in Turbulent Flames, In Libby, P.A., Williams, F.A. (Eds.), *Turbulent Reacting Flows*, 2: 63-113, London: Academic Press.

Brethouwer, G., Nieuwstadt, F.T.M. (2001), DNS of Mixing And Reaction of Two Species in a Turbulent Channel Flow: A Validation of Conditional Moment Closure, *Flow, Turbulence, And Combustion*, 66: 209-239.

Brizuela, E.A. (2000), Three-Dimensional Conditional Moment Closure Modelling of The Berl 300kW Burner, Abstracts of Work-in-Progress Poster Presentations, *Proceedings of The Combustion Institute*, 28: 334, Pittsburgh: The Combustion Institute.

Broadwell, J.E., Damm, W.J.A., Mungal, M. (1984), Blowout of Turbulent Diffusion Flames, 20th *Symposium (International) on Combustion*, 303-309, Pittsburgh: The Combustion Institute.

Brown, R.T., Bilger, R.W. (1996), An Experimental Study of a Reactive Plume in Grid Turbulence, *Journal Fluid Mechanics* 312: 373-407, Taylor and Francis.

Brown, R.T., Bilger, R.W. (1998), Experiments on a Reacting Plume: Conventional Concentrations Statistics, *Atmospheric Environment* 32:4 611-628, Pergamon Press.

Brown, P.N., Byrne, G.D., Hindmarsh, A.C. (1989), VODE, a Variable-coefficient ODE Solver, *SIAM Journal on Scientific And Statistical Computing*, 10: 1038-1051, SIAM.

Burcat, A. (2001), Third Millenium Ideal Gas and Condensed Phase Thermochemical Database for Combustion, Report No. TAE-867, Technion Aerospace Engineering.

Burcat, A., McBride, B. (1993), *1994 Ideal Gas Thermodynamic Data for Combustion and Air-Pollution Use*, Report No. TAE-697, Technion Aerospace Engineering.

Burke, S.P., Schumann, T.E.W. (1928a), Diffusion Flames, *Proceedings of The First Symposium on Combustion*, 2-11, Pittsburgh: The Combustion Institute.

Burke, S.P., Schumann, T.E.W. (1928b), Diffusion Flames, *Industrial and Engineering Chemistry*, 20:10 998-1004, American Chemical Society.

Bushe, W.K. (1995), Conditional Moment Closure Methods For Autoignition Problems, *Ph.D. thesis*, Cambridge University.

Bushe, W.K., Steiner, H. (1999), *Conditional Moment Closure For Large Eddy Simulation of Nonpremixed Turbulent Reacting Flows, Physics of Fluids*, 11: 1896-1906, American Institute of Physics.

Bushe, W.K., Bilger, R.W., Ruetsch, G.R. (1999), Direct Numerical Simulation of Nonpremixed Combustion With Realistic Chemistry, *CTR Manuscript*, 173, Centre For Turbulence Research, Stamford University.

Byggstoyl, S., Magnussen, B.F. (1985), *Fourth Symposium on Turbulent Shear Flows*, 381- New York: Springer

Cha, C.M., Pitsch, H. (2002), Higher-order Conditional Moment Closure Modelling of Local Extinction And Reignition in Turbulent Combustion, *Combustion Theory And Modelling*, 6: 425-437, Institute of Physics Publishing Ltd.

Cha, C.M., Kosály, G., Pitsch, H. (2001), Modelling Extinction And Reignition in Turbulent Nonpremixed Combustion Using a Doubly-conditional Moment Closure Approach, *Physics of Fluids*, 13:12 3824-3834, American Institute of Physics.

Chen, J.-Y. (1988), A General Procedure For Constructing Reduced Reaction Mechanisms With Given Independent Relations, *Combustion Science And Technology*, 57: 89-94, Gordon And Breach Science Publishers Inc.

Chen, J.-Y., Kollmann, W. (1990), Chemical Models For Pdf Modelling of Hydrogen-Air Nonpremixed Turbulent Flames, *Combustion and Flame*, 79: 75-99, Elsevier Science Inc.

Chen, J.-Y., Chang, W.-C., Koszykowski, M. (1995), Numerical Simulation And Scaling of NO_x Emissions From Turbulent Hydrogen Jet Flames With Helium Dilution, *Combustion Science And Technology*, 110: 505-529, Gordon And Breach Science Publishers Inc.

Chen, M., Herrmann, M., Peters, N. (2000), Flamelet Modelling of Lifted Turbulent Methane/Air and Propane/Air Jet Diffusion Flames, *Proceedings of The Combustion Institute*, 28: 167-174, Pittsburgh: The Combustion Institute.

Chen, R.H., Driscoll, J.F. (1991), Nitric Oxide Levels of Jet Diffusion Flames: Effects of Coaxial Air And Other Mixing Parameters, *23rd Symposium (International) on Combustion*, 281-288, Pittsburgh: The Combustion Institute.

Cheng, T.S., Wehrmeyer, J.A., Pitz, R.W. (1992), Simultaneous Temperature And Multispecies Measurement in a Lifted Hydrogen Diffusion Flame, *Combustion and Flame*, 91: 323-345, Elsevier Science Inc.

Cleary, M.J., Kent, J.H., Bilger (2002), R.W., Prediction of Carbon Monoxide Fires by Conditional Moment Closure, *Proceedings of The Combustion Institute*, 29: 273-279, Pittsburgh: The Combustion Institute.

Clemens, N.T., Paul, P.H. (1995), The Effects of Heat Release on The Near Field Flow Structure of Hydrogen Jet Diffusion Flames, *Combustion and Flame*, 102: 271-284, Elsevier Science Inc.

Coelho, P.J., Peters, N. (2001a), Unsteady Modelling of a Piloted Methan/Air Jet Flame Based on The Eulerian Particle Flamelet Model, *Combustion and Flame*, 124: 444-465, Elsevier Science Inc.

Coelho, P.J., Peters, N. (2001b), Numerical Simulation of a Mild Combustion Burner, *Combustion and Flame*, 124: 503-518, Elsevier Science Inc.

Combustion Research Facility, Sandia National Laboratories (2002), *International Workshop on Measurement and Computation of Turbulent Nonpremixed Flames*, http://www.ca.sandia.gov/TNF, accessed 26th February 2003.

Curl, R.L. (1963), Dispersed Phase Mixing: I Theory And Effects in Single Reactors, *AIChE Journal*, 9: 175-181, American Institute of Chemical Engineers.

Desjardin, P.E., Frankel, H. (1997), Linear-Eddy Modeling of Nonequilibrium Turbulent Reacting Flows With Nonpremixed Reactants, *Combustion and Flame*, 109: 471-487, Elsevier Science Inc.

Devaud, C. (1999), Conditional Moment Closure Applied to Lifted And Attached Turbulent Jet Flames, *Ph.D. thesis*, University of Cambridge.

Dixon-Lewis, G., Goldsworthy, F.A., Greenberg, J.B. (1975), Flame Structure And Flame Reaction Kinetics, *Proceedings of The Royal Society of London*, A:346 261-278,

Dopazo, C. (1975), Probability Density Function Approach For a Turbulent Axisymmetric Heated Jet. Centreline Evolution, *Physics of Fluids*, 18: 397-404, American Institute of Physics.

Dopazo, C. (1994), "Recent Developments in pdf Methods", In Libby, P.A., Williams, F.A. (Eds.), *Turbulent Reacting Flows*, 7: 375-474, London: Academic Press.

Eickhoff, H., Lenze, B., Leuckel, W. (1984), Experimental Investigation on The Stabilisation Mechanism of Jet Diffusion Flames. *20th Symposium (International) on Combustion*, 311-318, Pittsburgh: The Combustion Institute.

Fairweather, M., Woolley, R.M. (2003 accepted for publication), First-Order Conditional Moment Closure Modelling of Turbulent, Non-Premixed Hydrogen Flames, *Combustion and Flame*, Elsevier Science Inc.

Fairweather, M., Jones, W.P., Ledin, H.S., Lindstedt, R.P. (1992), *24th Symposium (International) on Combustion*, 1067-1074, Pittsburgh: The Combustion Institute.

Favier, V., Vervisch, L. (1998), Investigating the Effects of edge Flames in Liftoff in Non-premixed Turbulent Combustion, *27th Symposium (International) on Combustion*, 1239-1245, Pittsburgh: The Combustion Institute.

Girimaji, S.S. (1991), Assumed β-pdf Model For Turbulent Mixing: Validaton And Extension to Multiple Scalar Mixing, *Combustion Science And Technology*, 78: 177-196, Gordon And Breach Science Publishers Inc.

Girimaji, S.S. (1992), On The Modeling of Scalar Diffusion in Isotropic Turbulence, *Physics of Fluids A*, 4:11 2529-2537, American Institute of Physics.

Günther, R., Horch, K., Lenze, B. (1981), The Stabilisation Mechanism of Free Jet Diffusion Flames, *First Specialist Meeting (International) of The Combustion Institute*, 117-122, Pittsburgh: The Combustion Institute.

Hall, L., Horch, K., Günther, R. (1980), Die Stabilität Von Freistrahl-Diffusionsflammen, *Brennstoff-Wärme-Kraft*, 32: 27-31, Springer

Hanjalic, K., Launder, B.E. (1972), A Reynolds Stress Model of Turbulence And Its Application to Shear Flows, *Journal of Fluid Mechanics*, 52: 609-638, Taylor and Francis.

Hanjalic, K., Launder, B.E. (1976), Contribution Towards a Reynolds Stress Closure For Low-Reynolds-Number Turbulence, *Journal of Fluid Mechanics*, 74: 593-610, Taylor and Francis.

Hawthorne, W.R., Weddell, D.E., Hottel, H.C. (1949), *Mixing And Combustion in Turbulent Jets*, Third Symposium on Combustion, 266-288, Baltimore: Williams and Wilkins.

Hinze, J.O. (1975), *Turbulence*, New York: McGraw-Hill.

Howard, L.M. (1998), An Experimental Investigation of Oxygen-Enriched Methane Turbulent Diffusion Flames, *Ph.D. thesis*, University of Leeds.

Howard, L.M., Patterson, P.M., Pourkashanian, M., Williams, A., Wilson, C.W., Yap, L. (1999), An Experimental Investigation of Oxygen-Enriched Lifted And Attached Turbulent Diffusion Flames, *Proceedings of The Fifth International Conference on Combustion Technologies For a Clean Environment*, 1133-1142.

International Workshop on Measurement And Computation of Turbulent Non-Premixed Flames (2003), http://www.ca.sandia.gov/TNF, accessed 9th April 2003.

Janicka, J., Kollmann, W. (1979), A Two-variables Formalism For The Treatment of Chemical Reactions in Turbulent H_2-Air Diffusion Flames, 17th *Symposium (International) on Combustion*, 421-430, Pittsburgh: The Combustion Institute.

Janicka, J., Kolbe, W., Kollmann, W. (1979), Closure of The Transport Equation For The Probability Density Function of Turbulent Scalar Fields, *Journal of Non-equlibrium Thermodynamics*, 4: 47-66, Walter De Gruyter.

Jones, W.P. (2002), Large Eddy Simulation of Turbulent Combustion Processes, *Computer Physics Communications*, 147: 533-537, Elsevier Science Inc.

Jones, W.P., Launder, B.E. (1972), The Prediction of Laminarisation With a Two-Equation Turbulence Model, *International Journal of Heat And Mass Transfer*, 15: 301-314, Pergamon Press.

Jones, W.P., Musonge, P. (1988), Closure of The Reynolds Stress And Scalar Flux Equations, *Physics of Fluids*, 31:12 3589-3604, American Institute of Physics.

Kalghatgi, G.T. (1984), Lift-off Heights and Visible Length of Vertical Turbulent Jet Diffusion Flames in Still Air, *Combustion Science and Technology*, 41: 17-29, Overseas Publishers Association.

Kee, R.J., Rupley, F.M., and Miller, J.A. (1996), *CHEMKIN II: A FORTRAN Chemical Kinetics Package for the Analysis of Gas-Phase Chemical Kinetics,* Sandia National Laboratories, Report No. SAND89-8009B.

Kim, S.H., Huh, K.Y. (2002a), Use of The Conditional Moment Closure Model to Predict NO Formation in a Turbulent CH_4/H_2 Flame Over a Bluff Body, *Combustion And Flame*, 130: 94-111, Elsevier Science Inc.

Kim, S.H., Huh, K.Y., Tao, L. (2000a), Application of The Elliptic Conditional Moment Closure Model to a Two-dimensional Nonpremixed Methanol Bluff-body Flame, *Combustion And Flame*, 120: 75-90, Elsevier Science Inc.

Kim, S.H., Huh, K.Y., Fraser, R.A. (2000b), Modelling Autoignition of a Turbulent Methane Jet by The Conditional Moment Closure Model, *Proceedings of The Combustion Institute*, 28: 185-193, Pittsburgh: The Combustion Institute.

Kim, S.H., Huh, K.Y., Bilger, R.W. (2002), Second-order Conditional Moment Closure Modelling of Local Extinction And Reignition in Turbulent Nonpremixed Hydrocarbon Flames, *Proceedings of The Combustion Institute*, 29:2131-2137, Pittsburgh: The Combustion Institute.

Kim, W.T., Huh, K.Y. (2002b), Numerical Simulation of Spray Autoignition by The First-order Conditional Moment Closure Model, *Proceedings of The Combustion Institute*, 29: 569-576, Pittsburgh: The Combustion Institute.

Klimenko A.Yu. (1990), Multicomponent Diffusion of Various Admixtures in Turbulent Flow, *Fluid Dynamics*, 25: 328-334, Kluwer Academic.

Klimenko, A.Yu. (1993), Conditional Moment Closure And Fluctuations of Scalar Dissipation, *Fluid Dynamics*, 28: 630-637, Kluwer Academic.

Klimenko, A.Yu. (1995), Note on The Conditional Moment Closure in Turbulent Shear Flows, *Physics of Fluids*, 7:2 446-448, American Institute of Physics.

Klimenko, A.Yu. (2001), On The Relation Between The Conditional Moment Closure And Unsteady Flamelets, *Combustion Theory And Modelling*, 5: 275-294, Institute of Physics Publishing Ltd.

Klimenko, A.Yu., Bilger, R.W. (1999), Conditional Moment Closure for Turbulent Combustion, *Progress in Energy and Combustion Science*, 25: 595-687, Elsevier Science Inc.

Kronenburg, A. (1998), Modelling Pollutant Formation in Turbulent Jet Diffusion Flames, *Ph.D. thesis*, University of Sydney.

Kronenburg, A., Bilger, R.W. (1997), Modelling of Differential Diffusion Effects in Nonpremixed Nonreacting Turbulent Flow, *Physics of Fluids*, 9:5 1435-1447, American Institute of Physics.

Kronenburg, A., Bilger, R.W. (2001a), Modelling Differential Diffusion in Nonpremixed Reacting Turbulent Flow: Application to Turbulent Jet Flames, *Combustion Science And Technology*, 166: 175-194, Overseas Publishers Association.

Kronenburg, A., Bilger, R.W. (2001b), Modelling Differential Diffusion in Nonpremixed Reacting Turbulent Flow: Model Development, *Combustion Science And Technology*, 166: 195-227, Overseas Publishers Association.

Kronenburg, A., Bilger, R.W., Kent, J.H. (1998), Second-Order Conditional Moment Closure For Turbulent Jet Diffusion Flames, *27th Symposium (International) on Combustion*, 1097-1104, Pittsburgh: The Combustion Institute.

Kuo, K.K. (1986), *Principles of Combustion*, New York: John Wiley & Sons.

Launder, B.E., Reece, G.J., Rodi, W. (1975), Progress in The Development of a Reynolds-stress Turbulence Closure, *Journal of Fluid Mechanics*, 68: 537-566, Taylor and Francis.

Lee, J.D., Bilger, R.W. (1995), Conditional Moment Cbsure of Reactive Plumes in Homogeneous Turbulence, *Twelfth Australasian Fluid Mechanics Conference*, 625-628, University of Sydney.

Lee, J., Chung, S.H. (2001), Characteristics of Reattachment And Blowout of Laminar Lifted Flames in a Partially Premixed Propane Jet, *Combustion And Flame*, 127: 2194-2204, Elsevier Science Inc.

Lentini, D., Puri, I.K. (1995), Stretched Laminar Flamelet Modelling of Turbulent Chloromethane-air nonpremixed jet flames, *Combustion and Flame*, 103: 328-338, Elsevier Science Inc.

Leung, K.M., Lindstedt, R.P. (1995), Detailed Kinetic Modelling of C_1-C_3 Alkane Diffusion Flame, *Combustion And Flame*, 102: 129-160, Elsevier Science Inc.

Lewis, B., Von Elbe, G. (1951), *Combustion, Flames, and Explosions of Gases*, New York: Academic Press.

Li, J.D., Bilger, R.W. (1993), Measurement And Prediction of The Conditional Variance in a Turbulent Reactive-Scalar Mixing Layer, *Physics of Fluids A*, 5:12 3255-3264, American Institute of Physics.

Li, J.D., Bilger, R.W. (1994), A Simple Theory of Conditional Mean Velocity in Turbulent Scalar-Mixing Layer, *Physics of Fluids*, 6:2 605-610, American Institute of Physics.

Liew, S.K., Bray, K.N.C., Moss, J.B. (1984), A Stretched Laminar Flamelet Model of Turbulent Nonpremixed Combustion, *Combustion and Flame*, 56: 199-213, Elsevier Science Inc.

Lindstedt, R.P. (2000), The Modelling of Direct Chemical Kinetic Effects in Turbulent Flames, *Proceedings of The Institute of Mechanical Engineers*, 214:G 177-189, Institute of Mechanical Engineers.

Lindstedt, R.P., Selim, M.A. (1994), Reduced Reaction Mechanisms For Ammonia Oxidadtion in Premixed Laminar Flames, *Combustion Science And Technology*, 99: 277-298, Overseas Publishers Association.

Lindstedt, R.P., Skevis, G. (1997), Chemistry of Acetylene Flames, *Combustion Science And Technology*, 125: 73-137, Overseas Publishers Association.

Lindstedt, R.P., Váos, E.M. (2001), The Modelling of CO and NO Formation in Turbulent Jet Flames, In Singh, R. (Ed.), *Gas Turbine Pollutant Emissions – IMechE Seminar*, 75, Professional Engineering Publishing, London.

Lindstedt, R.P., Louloudi, S.A. Váos, E.M. (2000), Joint Scalar PDF Modelling of Pollutant Formation in Piloted Turbulent Jet Diffusion Flames With Comprehensive Chemistry, *Proceedings of The Combustion Institute*, 28: 149-156, Pittsburgh: The Combustion Institute.

Lumley, J.L. (1978), Computational Modelling of Turbulent Flows, *Advances in Applied Mechanics*, 18: 123-176, Academic Press.

Magnussen, B.F., Hjertager, B.H. (1976), On Mathematical Modelling of Turbulent Combustion With Special Emphasis on Soot Formation and Combustion, *16th Symposium (International) on Combustion*, 719-729, Pittsburgh: The Combustion Institute.

Marracino, B., Lentini, D. (1997), Radiation Modelling in Non-luminous Nonpremixed Turbulent Flames, *Combustion Science And Technology*, 128: 23-48, Overseas Publishers Association.

Masri, A.R., Dibble, R.W., Barlow, R.S. (1996), The Structure of Turbulent Non-Premixed Flames Revealed by Raman-Rayleigh-LIF Measurements, *Progress in Energy and Combustion Science*, 22: 307-362, Elsevier Science Inc.

Mastorakos, E., Bilger, R.W. (1998), Second-order Conditional Moment Closure For The Autoignition of Turbulent Flows, *Physics of Fluids*, 10: 1246-1248, American Institute of Physics.

McBride, B.J., Gordon, S., Reno, M.A. (1993), *Coefficients for Calculating Thermodynamic and Transport Properties of Individual Species*, Report No. TM-4513, NASA.

Meier, W., Vyrodov, A.O., Bergmann, V., Stricker, W. (1996), Simultaneous Raman/LIF Measurements of Major Species and NO in Turbulent H_2/Air Diffusion Flames, *Applied Physics B*, 63: 79

Meier, W., Barlow, R.S., Chen, Y.-L., Chen, J.-Y. (2000), Raman/Rayleigh/LIF Measurements in a Turbulent $CH_4/H_2/N_2$ Jet Diffusion Flame: Experimetnal Techniques And Turbulence-Chemistry Interaction, *Combustion and Flame*, 123: 326-343, Elsevier Science Inc.

Mell, W.E., Nilsen, V., Kosály, G., Riley, J.J. (1993), Direct Numerical Simulation Investigation of The Conditional Moment Closure Model For Nonpremixed Turbulent Reacting Flows., *Combustion Science And Technology*, 91: 179-186, Overseas Publishers Association.

Mell, W.E., Nilsen, V., Kosály, G., Riley, J.J. (1994), Investigation of Closure Models For Nonpremixed Turbulent Reacting Flows, Physics of Fluids 6:3 1331-1356, American Institute of Physics.

Miake-Lye, R.C., Hammer, J.A. (1988), Lifted Turbulent Jet Flames: A Stability Criterion Based on The Jet Large-scale Structure, 22nd *Symposium (International) on Combustion*, 817-824, Pittsburgh: The Combustion Institute.

Miller, J.A., Bowman, C.T. (1989), Mechanism And Modelling of Nitrogen Chemistry in Combustion, *Progress in Energy and Combustion Science*, 15: 287-338, Elsevier Science Inc.

Mobini, K., Bilger, R.W., Smith, N.S.A. (1995), Investigation of PDF Shape Effects on Imperfectly Stirred Reactor Modelling, *Australian Symposium on Combustion*, Australian and New Zealand Section of The Combustion Institute.

Mobini, K. (1998), An Investigation of The Imperfectly Stirred Reactor Modelling of Recirculating Combusting Flows, *Ph.D. thesis*, University of Sydney.

Montgomery, C.J., Kosály, G., Riley, J.J. (1997), Direct Numerical Simulation of Turbulent Nonpremixed Combustion with Multistep Hydrogen-Oxygen Kinetics, *Combustion and Flame*, 109: 113-144, Elsevier Science Inc.

Morse, A.P. (1980), Axisymmetric Free Shear Flows With And Without Swirl, *Ph.D. thesis*, University of London.

Müller, C.H., Breitbach, H., Peters, N. (1994), Partially Premixed Turbulent Flame Propagation in Jet Flames, 25th *Symposium (International) on Combustion*, 1099-1106, Pittsburgh: The Combustion Institute.

Numerical Algorithms Group, (2002), http://www.nag.co.uk, accessed 27th February 2003.

O'Brien, E.E., Jiang, T.-L. (1991), The Conditional Dissipation Rate of an Initially Binary Scalar in Homogeneous Turbulence, Physics of Fluids A 3(12): 3121-3123, American Institute of Physics.

Obieglo, A., Gass, J., Poulikakos, D. (2000), Comparative Study of Modelling a Hydrogen Nonpremixed Turbulent Flame, *Combustion and Flame*, 122: 176-194, Elsevier Science Inc.

Peters, N. (1984), Laminar Diffusion Flamelet Models in Non-premixed Turbulent Combustion, *Progress in Energy and Combustion Science*, 10: 319-339, Elsevier Science Inc.

Peters, N. (2000), *Turbulent Combustion*, Cambridge (U.K.): Cambridge University Press.

Peters, N., Williams, F.A. (1983), Lift-off Characteristics of Turbulent Jet Diffusion Flames, *American Institute of Aeronautics And Astronautics Journal*, 21: 423-429, AIAA.

Piesens, R., de Doncker-Kapenga E., Überhuber, C., Kahaner, D (1983), *QUADPACK, A Subroutine Package For Automatic Integration*, Springer-Verlag.

Pitsch, H., Steiner, H. (2000), Large Eddy Simulation of a Turbulent Piloted Methane-Air Diffusion Flame (Sandia flame D), *Physics of Fluids*, 12:10 2541-2554, American Institute of Physics.

Pitsch, H., Riesmeier, E., Peters, N. (2000), Unsteady Flamelet Modelling of Soot Formation in Turbulent Diffusion Flames, *Combustion Science and Technology*, 158: 389-406, Overseas Publishers Association.

Pitts, W.M. (1988), Assessment of Theories For The Behaviour And Blowout of Lifted Turbulent Jet Disffusion Flames, *22nd Symposium (International) on Combustion*, 809-816, Pittsburgh: The Combustion Institute.

Pope, S.B. (1978), An Explanation of The Turbulent Round Jet/Plane Jet Anomaly, *American Institute of Aeronautics And Astronautics Journal*, 16:3 279-281, AIAA.

Pope, S.B. (1981a), A Monte Carlo Method For The pdf Equation of Turbulent Reactive Flow, *Combustion Science and Technology*, 25: 159-174, Overseas Publishers Association.

Pope, S.B. (1981b), Monte Carlo Calculations of Premixed Turbulent Flames, *18th Symposium (International) on Combustion*, 1001-1010, Pittsburgh: The Combustion Institute.

Pope, S.B. (1985), PDF Methods in Turbulent Reacting Flows, *Progress in Energy and Combustion Science*, 11: 119-192, Elsevier Science Inc.

Pope, S.B. (1990), Computations of Turbulent Combustion, Progress and Challenges, 23rd *Symposium (International) on Combustion*, 591-612, Pittsburgh: The Combustion Institute.

Press, W.H., Teukolsky, S.A., Vettering, W.T., Flannery, B.P. (1992), *Numerical Recipes in FORTRAN*, 2nd Edition, Cambridge University Press.

Roache, P.J. (1972), Appendix A Tridiagonal Algorithm, *Computational Fluid Dynamics*, New Mexico: Hermosa.

Roekaerts, D., Teerling, J. (2000), *Proceedings of the 5th International Workshop on Measurement and Computation of Turbulent Non-Premixed Flames*, T. U. Delft, Delft.

Rogg, B., Wang, W. (2001), *RUN-1DL – The Laminar Flame And Flamelet Code*, 9th Revision, http://www.lstm.ruhr-uni-bochum.de/english/home.html, accessed 18th April 2003.

Roomina, M.R. (1998), Conditional Moment Closure Predictions For Piloted Hydrocarbon Jet Flames, *Ph.D. thesis*, University of Sydney.

Roomina, M.R., Bilger, R.W. (1999), Conditional Moment Closure Modelling of Turbulent Methanol Jet Flames, *Combustion Theory And Modelling*, 3: 689-708, Institute of Physics Publishing Ltd.

Roomina, M.R., Bilger, R.W. (2001), Conditional Moment Closure (CMC) Predictions of a Turbulent Methane-Air Jet Flame, *Combustion and Flame*, 125: 1176-1195, Elsevier Science Inc.

Ross, S. (1984), *A First Course in Probability*, 2nd Edition, London: Macmillan.

Ruetsch, G.R., Vervisch, L., Liñán, A. (1995), Effects of Heat Release on Triple Flames, *Physics of Fluids*, 7:6 1447-1454, American Institute of Physics.

Sarkar, S., Erlebacher, G., Hussaini, M.Y., Kreiss, H.O. (1991), The Analysis And Modelling of Dilational Terms in Compressible Turbulence, *Journal of Fluid Mechanics*, 227: 473-493, Taylor and Francis.

Schefer, R.W., Namazian, M., Kelly, J. (1988), Structural Characteristics of Lifted Turbulent Jet Flames, *22nd Symposium (International) on Combustion*, 833-842, Pittsburgh: The Combustion Institute.

Schefer, R.W., Namazian, M., Kelly, J. (1994), Stabilisation of Lifted Turbulent-jet Flames, *Combustion and Flame*, 99: 75-86, Elsevier Science Inc.

Schlatter, M., Ferreira, J.C., Flury, M., Gass, J. (1996), Analysis of Turbulence-Chemistry Interaction With Respect to NO Formation in Turbulent, Nonpremixed Hydrogen-Air Flames, *26th Symposium (International) on Combustion*, 2215-2222 , Pittsburgh: The Combustion Institute.

Schneider, C., Dreizler, A., Janicka, J. (2003 submitted), Flow Field Measurements of Stable And Locally extinguishing Hydrocarbon-Fuelled Jet Flames, *Combustion And Flame*, Elsevier Science Inc.

Sick, V., Hildenbrand, F., Lindstedt, R.P. (1998), Quantitative Laser-based Measurements And Detailed Chemical Kinetic Modelling of NO Concentrations in Methane-Air Counterflow Diffusion Flames, *27th Symposium (International) on Combustion*, 1401-1409 , Pittsburgh: The Combustion Institute.

Smith, G.P., Golden, D.M., Frenklach, M., Moriarty, N.W., Eiteneer, B., Goldenberg, M., Bowman, C.T., Hanson, R.K., Song, S., Gardiner, W.C., Lissianski, V.V., Qin, Z. (1999), http://www.me.berkeley.edu/gri_mech/, accessed 17th April 2003.

Smith, N.S.A. (1994), Development of The CMC Method For Modelling Turbulent Combustion, *Ph.D. thesis*, University of Sydney.

Smith, N.S.A., Bilger, R.W., Chen, J.-Y. (1992), Modelling of nonpremixed hydrogen jet flames using a conditional moment closure method, *Twenty-Forth Symposium (International) on Combustion,* 263-269, The Combustion Institute.

Smith, N.S.A., Bilger, R.W., Carter, C.D., Barlow, R.S., Chen, J.-Y. (1995), A Comparison of CMC and PDF Modelling Predictions with Experimental Nitric Oxide LIF / Raman Measurements in a Turbulent H_2 Jet Flame, *Combustion Science and Technology*, 105: 357-375, Overseas Publishers Association.

Smooke, M.D., and Giovangigli, V. (1990), Formulation of the Premixed and Nonpremixed Test Problems, In Smooke, M.D. (Ed.), *Reduced Kinetic Mechanisms and Asymptotic Approximations For Methane-Air Flames, Lecture Notes in Physics 384*, 1-28, Springer-Verlag, Berlin.

Spalding, D.B. (1971), Mixing And Chemical Reaction in Steady Confined Turbulent Flames, *13th Symposium (International) on Combustion*, 649-657, Pittsburgh: The Combustion Institute.

Spalding, D.B. (1977), *GENMIX: A General Computer Program For Two-dimensional Parabolic Phenomena*, Oxford(England): Pergammon Press.

Sreedhara, S., Laksmisha, K.N. (2002), Assessment of Conditional Moment Closure Models of Turbulent Auto-Ignition Using DNS data, *Proceedings of The Combustion Institute*, 29: 2069-2077, Pittsburgh: The Combustion Institute.

Steiner, H. Bushe, W.K. (2001), Large Eddy Simulation of a Turbulent Reacting Jet With Conditional Source-term Estimation, *Physics of Fluids*, 13:3 754-769, American Institute of Physics.

Swaminathan, N., Bilger, R.W. (1998), Conditional Variance Equation And Its Analysis, *27th Symposium (International) on Combustion*, 833-842, Pittsburgh: The Combustion Institute.

Swaminathan, N., Bilger, R.W. (1999a), Assessment of Combustion Sub-models For Turbulent Nonpremixed Hydrocarbon Flames, *Combustion and Flame*, 116: 519-545, Elsevier Science Inc.

Swaminathan, N., Bilger, R.W. (1999b), Study of The Conditional Variance And Covariance Equations For Second-order CMC Closure, *Physics of Fluids*, 11: 2679-2695, American Institute of Physics.

Swaminathan, N., Bilger, R.W. (2001), Analyses of Conditional Moment Closure For Turbulent Premixed Flames, *Combustion Theory And Modelling*, 5: 241-260, Institute of Physics Publishing Ltd.

Swaminathan, N., Dally, B.B. (1998), Cross-stream Dependence of Conditional Averages in Elliptic Region of Flow Behind a Bluff Body, *Physics of Fluids*, 10: 2424-2426, American Institute of Physics.

Swaminathan, N., Mahalingam, S. (1996), Assessment of Conditional Moment Closure For Single And Multistep Chemistry, *Combustion Science and Technology*, 112: 301-326, Gordon and Breach.

Turns, S.R. (2000), *An Introduction to Combustion, Concepts And Applications*, 2nd Edition, Singapore: McGraw Hill.

United Nations Environment Programme (2000), *Report of the United Nations Conference on the Human Environment*, http://www.unep.org/Documents/Default.asp?DocumentID=97, accessed 9th March 2002.

United Nations Framework Convention on Climate Change (2002), 24th January 2002, *Climate Change Information Sheet 21, The Kyoto Protocol*, http://unfccc.int/text/resource/iuckit/fact21.html, accessed 9th March 2002.

Vanquickenbourne, L., van Tiggelen, A. (1966), The Stabilisation of Lifted Diffusion Flames, *Combustion and Flame*, 10: 59-69, Elsevier Science Inc.

Veynante, D., Vervisch, L., Poinsot, T., Liñán, A., Ruetsch, G. (1994), Triple Flame Structure And Diffusion Flame Stabilisation, *Proceedings of The Summer Program*, 55-73, Centre For Turbulence Research, NASA.

Villermaux, J., Devillon, J.C. (1972), Représentation de la coalescence et de la redispersion des domaines de ségrégation dans un fluide par un modèle d'interaction phénoménologique, *Proceedings of the Second International Symposium on Chemical Reaction Engineering*, 1-13, New York: Elsevier Science Inc.

Warnatz, J., Maas, U., Dibble, R.W. (2001), *Combustion Physical And Chemical Fundamentals, Modeling and Simulation, Experiments, Pollution Formation*, 3rd Edition, Berlin, New York: Springer.

Williams, F.A. (1975), Recent Advances in Theoretical Descriptions of Turbulent Diffusion Flames, In Murthy, S.N.B. (Ed.), *Turbulent Mixing in Nonreactive And Reactive Flows*, 189-208, Plenum Press, New York.

Wohl, K., Kapp, N.M., Gazley, C. (1949), *The Stability of Open Flames*, Third Symposium on Combustion, 3-21, Baltimore: Williams and Wilkins.

Won, S.H., Chung, S.H., Cha, M.S., Lee, B.J. (2000), Lifted Flame Stabilisation in Developing And Developed Regions of Coflow Jets For Highly Diluted Propane, *Proceedings of The Combustion Institute*, 28: 2093-2099, Pittsburgh: The Combustion Institute.

Xu, J., Pope, S.B. (2000), PDF Calculations of Turbulent Nonpremixed Flames With Local Extinction, *Combustion and Flame*, 123: 281-307, Elsevier Science Inc.

Appendix

Equation Sets in Cartesian Tensor Notation:

Continuity:

$$\frac{\partial \bar{\rho}\tilde{u}_i}{\partial x_i} = 0$$

Momentum:

$$\frac{\partial \bar{\rho}\tilde{u}_i\tilde{u}_j}{\partial x_j} = -\frac{\partial \bar{p}}{\partial x_i} - \frac{\partial \bar{\rho}\widetilde{u_i''u_j''}}{\partial x_j} + \bar{\rho}g_i$$

where in terms of an eddy-viscosity approximation:

$$\bar{\rho}\widetilde{u_i''u_j''} = \frac{2}{3}\delta_{ij}\left(\bar{\rho}k + \mu_{eff}\frac{\partial \tilde{u}_l}{\partial x_l}\right) - \mu_{eff}\left(\frac{\partial \tilde{u}_i}{\partial x_j} + \frac{\partial \tilde{u}_j}{\partial x_i}\right)$$

Conserved Scalar (Mixture Fraction/Mixture Fraction Variance):

$$\frac{\partial \bar{\rho}\tilde{u}_i\tilde{\xi}}{\partial x_i} = -\frac{\partial \bar{\rho}\widetilde{u_i''\xi''}}{\partial x_i} + \frac{\partial}{x_i}\left(\frac{\mu_t}{\sigma_{tf}}\frac{\partial \tilde{\xi}}{\partial x_i}\right)$$

where in terms of a gradient-diffusion approximation:

$$\bar{\rho}\widetilde{u_i''\xi''} = -\frac{\mu_t}{\sigma_{tf}}\frac{\partial \tilde{\xi}}{\partial x_i}$$

and

$$\sigma_{tf} = 0.70$$

Turbulence Kinetic Energy:

$$\frac{\partial \bar{\rho}\tilde{u}_i k}{\partial x_i} = \frac{\partial}{\partial x_i}\left(\frac{\mu_t}{\sigma_{tk}}\frac{\partial k}{\partial x_i}\right) + P - \bar{\rho}\varepsilon$$

where:

$$P = -\bar{\rho}\widetilde{u_i'' u_j''}\frac{\partial \tilde{u}_j}{\partial x_i} - \frac{\mu_t}{\bar{\rho}^2}\frac{\partial \bar{\rho}}{\partial x_j}\frac{\partial \bar{p}}{\partial x_j}$$

and

$$\sigma_{tk} = 1.00$$

Dissipation of Turbulence Kinetic Energy:

$$\frac{\partial \bar{\rho}\tilde{u}_i \varepsilon}{\partial x_i} = \frac{\partial}{\partial x_i}\left(\frac{\mu_t}{\sigma_{t\varepsilon}}\frac{\partial \varepsilon}{\partial x_i}\right) + \left(C_{\varepsilon 1}P - C_{\varepsilon 2}\bar{\rho}\varepsilon\right)\frac{\varepsilon}{k}$$

Standard constants being reported (Jones and Launder 1972) as:

$$C_{\varepsilon 1} = 1.40 \qquad C_{\varepsilon 2} = 1.80 \qquad \sigma_{t\varepsilon} = 1.30$$

Reynolds Stress:

$$\frac{\partial \tilde{u}_l \bar{\rho}\widetilde{u_i'' u_j''}}{\partial x_l} =$$

$$-\left(\bar{\rho}\widetilde{u_i'' u_l''}\frac{\partial \tilde{u}_i}{\partial x_l} + \bar{\rho}\widetilde{u_i'' u_l''}\frac{\partial \tilde{u}_j}{\partial x_l}\right) \qquad (i)$$

$$-\left(\widetilde{u_i''\frac{\partial \bar{p}}{\partial x_j}} + \widetilde{u_j''\frac{\partial \bar{p}}{\partial x_i}} - \frac{2}{3}\delta_{ij}\widetilde{u_l''\frac{\partial \bar{p}}{\partial x_l}}\right) \qquad (ii)$$

$$-2\mu_t\widetilde{\frac{\partial u_i''}{\partial x_l}\frac{\partial u_j''}{\partial x_l}} \qquad (iii)$$

$$-\frac{\partial}{\partial x_l}\left(\widetilde{u_i'' u_j'' u_l''}\right) + \frac{2}{3}\delta_{ij}\widetilde{u_l'' p} \qquad (iv)$$

where term (ii) is modelled as:

$$-C_1\frac{\varepsilon}{k}\left(\overline{\rho}\widetilde{u_i''u_j''}-\frac{1}{3}\delta_{ij}2k\right)+C_2\delta_{ij}\overline{\rho}\widetilde{u_l''u_m''}\frac{\partial\tilde{u}_l}{\partial x_m}$$
$$+C_3\left(\overline{\rho}\widetilde{u_l''u_j''}\frac{\partial\tilde{u}_i}{\partial x_l}+\overline{\rho}\widetilde{u_l''u_i''}\frac{\partial\tilde{u}_j}{\partial x_l}\right)$$
$$+C_4\left(\frac{\partial\tilde{u}_i}{\partial x_j}+\frac{\partial\tilde{u}_j}{\partial x_i}\right)k+C_5\overline{\rho}\widetilde{u_i''u_j''}\frac{\partial\tilde{u}_l}{\partial x_l}$$
$$+C_6\left(\overline{\rho}\widetilde{u_l''u_j''}\frac{\partial\tilde{u}_l}{\partial x_i}+\overline{\rho}\widetilde{u_l''u_i''}\frac{\partial\tilde{u}_l}{\partial x_j}\right)+C_7k\delta_{ij}\frac{\partial\tilde{u}_l}{\partial x_l}$$

Standard constants being reported (Jones and Musonge 1988) as:

$$C_1=1.50 \qquad C_2=-0.53 \qquad C_3=0.67 \qquad C_4=-0.12$$
$$C_5=0.67 \qquad C_6=0.125 \qquad C_7=-0.367 \qquad C_s=0.22$$

term (iii) as:

$$-\frac{2}{3}\delta_{ij}\varepsilon$$

and term (iv) as:

$$C_s\frac{\partial}{\partial x_l}\left(\frac{k}{\varepsilon}\overline{\rho}\widetilde{u_l''u_m''}\frac{\partial\widetilde{u_i''u_j''}}{\partial x_m}\right)$$

where ε is obtained from its transport equation:

$$\frac{\partial\overline{\rho}\tilde{u}_i\varepsilon}{\partial x_i}=C_\varepsilon\frac{\partial}{\partial x_l}\left(\frac{k}{\varepsilon}\overline{\rho}\widetilde{u_l''u_m''}\frac{\partial\varepsilon}{\partial x_m}\right)-C_{\varepsilon1}\frac{\varepsilon}{k}\overline{\rho}\widetilde{u_l''u_m''}\frac{\partial\tilde{u}_l}{\partial x_m}-C_{\varepsilon2}\frac{\varepsilon^2}{k}$$

standard constants being:

$$C_\varepsilon=0.18 \qquad C_{\varepsilon1}=1.40 \qquad C_{\varepsilon2}=1.90$$

and k is taken to be:

$$\frac{1}{2}\widetilde{u_i''u_i''}$$

Scalar Flux:

$$\frac{\partial \tilde{u}_l \bar{\rho} \widetilde{u_i'' \xi''}}{\partial x_l} =$$

$$-\left(\bar{\rho} \widetilde{u_j'' \xi''} \frac{\partial \tilde{u}_i}{\partial x_j} + \bar{\rho} \widetilde{u_i'' u_j''} \frac{\partial \tilde{\xi}}{\partial x_j} \right) \qquad (i)$$

$$+ \widetilde{\xi'' \frac{\partial \bar{p}}{\partial x_i}} \qquad (ii)$$

$$- \frac{\partial \bar{\rho} \widetilde{u_i'' u_j'' \xi''}}{\partial x_j} \qquad (iii)$$

where term (ii) is modelled as:

$$-C_{\xi 1} \frac{\varepsilon}{k} \bar{\rho} \widetilde{u_i'' \xi''} + C_{\xi 2} D_{ij} \frac{k}{2} \frac{\partial \tilde{\xi}}{\partial x_j}$$

$$+C_{\xi 3} \bar{\rho} \widetilde{u_j'' \xi''} \frac{\partial \tilde{u}_i}{\partial x_j} + C_{\xi 4} \bar{\rho} \widetilde{u_j'' \xi''} \frac{\partial \tilde{u}_j}{\partial x_i} + C_s \frac{\partial}{\partial x_j} \left(\frac{k}{\varepsilon} \bar{\rho} \widetilde{u_j'' u_l''} \frac{\partial \widetilde{u_i'' \xi''}}{\partial x_l} \right)$$

Standard constants being reported (Jones and Musonge 1988) as:

$$C_{\xi 1} = 3.00 \qquad C_{\xi 2} = 0.12 \qquad C_{\xi 3} = 1.09 \qquad C_{\xi 4} = 0.51$$

where D_{ij} is defined:

$$\bar{\rho} \frac{\widetilde{u_i'' u_i''}}{2k} - \frac{1}{3} \delta_{ij}$$

and term (iii) as:

$$C_s \frac{\partial}{\partial x_j} \left(\frac{k}{\varepsilon} \bar{\rho} \widetilde{u_j'' u_l''} \frac{\partial \widetilde{u_i'' \xi''}}{\partial x_l} \right)$$